PNWD-3551
WTP-RPT-113 Rev 0

Technical Basis for Testing Scaled Pulse Jet Mixing Systems for Non-Newtonian Slurries

J. A. Bamberger
P. A. Meyer
J. R. Bontha
C. W. Enderlin
D. A. Wilson
A. P. Poloski
J. A. Fort
S. T. Yokuda
H. D. Smith
F. Nigl
M. A. Friedrich
D. E. Kurath
G. L. Smith
J. M. Bates
M. A. Gerber

March 2005

Prepared for Bechtel National, Inc.
under Contract 24590-101-TSA-W000-00004

LEGAL NOTICE

This report was prepared by Battelle Memorial Institute (Battelle) as an account of sponsored research activities. Neither Client nor Battelle nor any person acting on behalf of either:

MAKES ANY WARRANTY OR REPRESENTATION, EXPRESS OR IMPLIED, with respect to the accuracy, completeness, or usefulness of the information contained in this report, or that the use of any information, apparatus, process, or composition disclosed in this report may not infringe privately owned rights; or

Assumes any liabilities with respect to the use of, or for damages resulting from the use of, any information, apparatus, process, or composition disclosed in this report.

Reference herein to any specific commercial product, process, or service by trade name, trademark, manufacturer, or otherwise, does not necessarily constitute or imply its endorsement, recommendation, or favoring by Battelle. The views and opinions of authors expressed herein do not necessarily state or reflect those of Battelle.

Technical Basis for Testing Scaled Pulse Jet Mixing Systems for Non-Newtonian Slurries

J. A. Bamberger
P. A. Meyer
J. R. Bontha
C. W. Enderlin
D. A. Wilson[(a)]
A. P. Poloski
J. A. Fort
S. T. Yokuda
H. D. Smith
F. Nigl
M. A. Friedrich
D. E. Kurath
G. L. Smith
J. M. Bates
M. A. Gerber

ACCEPTED FOR
WTP PROJECT USE

March 2005

	PNWD	SRNL
Test Specification	24590-WTP-TSP-RT-03-006 Rev. 0	24590-WTP-TSP-RT-03-007 Rev. 0
Test Plan	TP-RPP-WTP-290 Rev 0	SRT-RPP-2003-00174 Rev 0
Test Exceptions	24590-WTP-TEF-RT-03-052	24590-WTP-TEF-RT-03-059
	24590-WTP-TEF-RT-03-053	24590-WTP-TEF-RT-03-085
	24590-WTP-TEF-RT-03-058	
	24590-WTP-TEF-RT-03-083	
R&T focus area	Pretreatment & Vitrification	Pretreatment & Vitrification
Test Scoping Statement(s)	B-100	

Battelle – Pacific Northwest Division
Richland, Washington 99352

(a) Savannah River National Laboratory

Completeness of Testing

This report describes the results of work and testing specified by Test Specification 24590-WTP-TSP-RT-03-006, Rev. 0 and Test Plan TP-RPP-WTP-290, Rev. 0. The work and any associated testing followed the quality assurance requirements outlined in the Test Specification/Plan. The descriptions provided in this test report are an accurate account of both the conduct of the work and the data collected. Test plan results are reported. Also reported are any unusual or anomalous occurrences that are different from expected results. The test results and this report have been reviewed and verified.

Approved:

Gordon H. Beeman, Manager
WTP R&T Support Project

3/11/05
Date

Summary

This report addresses the research conducted to develop scaling relationships that can be applied to perform scaled tests of pulse jet mixing in non-Newtonian slurry. This research is needed to assess the performance of pulse jet configurations in Hanford Waste Treatment Plant (WTP) vessels. The research incorporates theoretical analysis and data taken at three scales of test fixtures: 336 Building large-scale, Applied Process Engineering Laboratory (APEL) 1/4 scale, and Savannah River National Laboratory (SRNL) 1/9 scale.

Objectives

The scaling investigations were conducted concurrently by Battelle – Pacific Northwest Division (PNWD) and SRNL. The PNWD investigation was conducted according to Test Plan TP-RPP-WTP-290 Rev 0, *Test Plan for Determining Scalability of PJM Performance in Non-Newtonian Fluid*, in response to Test Specification 24590-WTP-TSP-RT-03-006 Rev. 0, *Determination of PJM Design Parameter Scale Laws for Scaled Testing*. The SRNL investigation was conducted according to SRT-RPP-2003-00174 Rev. 0, *Task Technical and Quality Assurance Plan in Support of the RPP One-Eighth Scale Testing for Determination of PJM Design Parameter Scale Laws*, in response to WTP Test Specification 24590-WTP-TSP-RT-03-007 Rev. 0, *Determination of PJM Design Parameter Scale Laws for One-Eighth Scale Testing*. Objectives for both test plans were satisfied. Table S.1 summarizes the test objectives and describes how they were satisfied.

Table S.1. Test Objective Evaluation

Test Objective	Objective Met (Y/N)	Discussion
Identify operating parameters that are critical for scaling PJM systems from full size[(a)] to reduced scale and the type of scale factor to apply to those parameters.	Yes	Section 3 describes critical operating parameters that can be used by WTP engineers to design a PJM system and the scale factors.
Identify and assess regions of mobilization in a non-Newtonian simulant exhibiting rheological characteristics similar to WTP waste streams as a function of PJM operating conditions.	Yes	During scaled PJM testing operations, regions of mobilization were identified and assessed as documented in Section 5 and Appendixes A, B, and C.
Verify scaling factors with geometrically scaled tests.	Yes	Tests were conducted at large scale, at 1/4 scale, and at 1/9 of large scale. These tests are described in Section 4 and Appendixes A, B and C. Scaling results are discussed in Section 5.
Develop a methodology for predicting full-scale WTP behavior from small-scale prototypic testing and validate the scaled testing approach (i.e., demonstrate that PJM tests at small scale adequately represent full-scale mixing performance).	Yes	The PJM Team developed the methodology for scaled testing of WTP mixing vessels with non-Newtonian slurries that is described in Section 3. The scaling relationships and data analysis are described in Section 5.
(a) The term full scale is often used to denote the large-scale test stand in the 336 facility. While large, this test stand is not full scale, though the linear dimensions are within a factor of 2 of the largest tank in the WTP that will contain fluids with non-Newtonian rheology.		

Test Exceptions

Test exceptions applied to these tests are described in Table S.2.

Table S.2. Test Exceptions

List Test Exceptions	Describe Test Exceptions
24590-WTP-TEF-RT-03-052	At PNWD, allow remix of simulant after each constant volume or constant velocity cavern is reached. The set time and fill height over tank diameter ratio after remix are flexible to meet test objectives and schedule.
24590-WTP-TEF-RT-03-053	Determine time to fully mix stagnant Laponite simulant in 336 4PJM test stand.
24590-WTP-TEF-RT-03-058	In APEL 1/4-scale test stand, determine the time to fully mix stagnant Laponite for comparison with the 336 4PJM large-scale test platform data and conduct a test with an increased aspect ratio.
24590-WTP-TEF-RT-03-059	Determine time to fully mix stagnant Laponite in the SRNL 4PJM test stand.
24590-WTP-TEF-RT-03-083	Conduct additional scaling tests in the 336 4PJM large-scale and APEL 4PJM 1/4-scale test stands using a clay simulant.
24590-WTP-TEF-RT-03-085	Conduct additional scaling tests in the SRNL 4PJM test stand using a clay simulant.

Results and Performance Against Success Criteria

The success criteria provided in PNWD Test Specification 24590-WTP-TSP-RT-03-006 Rev. 0, *Determination of PJM Design Parameter Scale Laws for Scaled Testing*, and SRNL Test Specification 24590-WTP-TSP-RT-03-007 Rev. 0, *Determination of PJM Design Parameter Scale Laws for One-Eighth Scale Testing,* are discussed in Table S.3.

Table S.3. Discussion of Test Success Criteria

List Success Criteria	Explain How the Tests Did or Did Not Meet the Success Criteria
Conduct tests in scaled test platforms developed based on geometric scaling and by matching velocity at the three scales. Reduce time scales by the scale factor.	The success criteria were documented as successfully achieved by presentation of experimental data and observations as required by all governing documents, specifically: • Documenting the characteristics of PJM cavern formation and mobilization. • Providing experimental results defining PJM performance using non-Newtonian simulants.
Determine characteristics of PJM cavern formation and mobilization in non-Newtonian simulants in support of the design parameter scale law testing program.	
Obtain experimental data using non-Newtonian simulants exhibiting rheological characteristics similar to WTP waste streams in a scaled test stand to determine the scaling correlation between full-scale and small-scale PJM mixing performance.	

Quality Requirements

PNWD implements the River Protection Project (RPP) WTP quality requirements by performing work in accordance with the PNWD Waste Treatment Plan Support Project Quality Assurance Project Plan (QAPjP) approved by the RPP-WTP Quality Assurance (QA) organization. This work was performed to the quality requirements of NQA-1-1989 Part I, Basic and Supplementary Requirements, and NQA-2a-1990, Part 2.7 and DOE/RW-0333 Rev 13, Quality Assurance Requirements and Description (QARD). These quality requirements were implemented through PNWD's *Waste Treatment Plant Support Project (WTPSP) Quality Assurance Requirements and Description Manual*. The analytical requirements were implemented through WTPSP's Statement of Work (WTPSP-SOW-005) with the Radiochemical Processing Laboratory (RPL) Analytical Service Operations (ASO).

Experiments that were not method-specific were performed in accordance with PNWD's procedures QA-RPP-WTP-1101, "Scientific Investigations," and QA-RPP-WTP-1201, "Calibration Control System," to ensure that sufficient data were taken with properly calibrated measuring and test equipment (M&TE) to obtain quality results.

PNWD addresses internal verification and validation activities by conducting an independent technical review of the final data report in accordance with PNWD's procedure QA-RPP-WTP-604. This review verifies that the reported results are traceable, that inferences and conclusions are soundly based, and that the reported work satisfies the Test Plan objectives. This review procedure is part of PNWD's *WTPSP Quality Assurance Requirements and Description Manual*.

SRNL work was conducted in accordance with the RPP-WTP-QA requirements specified for work conducted by SRNL as identified in DOE IOW M0SRLE60 (Wilson et al. 2004).

R&T Test Conditions

The R&T test conditions provided in the PNWD and SRNL Test Exception are described in Table S.4.

Simulant Use

A clear Laponite simulant was used for the scaling and cavern testing. A kaolin-bentonite clay simulant was used in these tests to duplicate the properties of the non-Newtonian fluids that will be processed in the Hanford WTP. A thorough discussion of the Laponite and kaolin-bentonite simulants can be found in WTP-RPT-111 Rev 0 (Poloski et al. 2004), and a summary is provided in Appendix D of this report.

Discrepancies and Follow-on Tests

No discrepancies were identified or remain unresolved.

Table S.4. R&T Test Conditions

List R&T Test Conditions	Were Test Conditions Followed?
24590-WTP-TEF-RT-03-053	
During the time to fully mix stagnant Laponite in the 336 4PJM large-scale test facility, the Laponite will be allowed to gel at least 18 hours, rheology samples will be taken, and shear strength determined before and after the test. The pulse tubes will be turned on and operated with an 8-ft pulse length at the same cycle time used for current testing. Nominal nozzle velocity will be 8 m/s (26.3 ft/sec). The following points will be noted: 1) time to breakthrough at the Laponite surface 2) time to Laponite movement down the tank wall 3) time for Laponite at the wall to exhibit turbulent motion (fully mixed) 4) if possible, add neutrally buoyant beads near the middle or at the wall and document when they reappear.	Yes
24590-WTP-TEF-RT-03-058	
<u>First replacement test</u> During the time to fully mix stagnant Laponite in the APEL 4PJM 1/4-scale facility, the Laponite will be allowed to gel for at least 18 hours, rheology samples will be taken and shear strength determined before and after the test. The pulse tubes will be turned on and operated with an 8-ft pulse length at the same scaled cycle time being used for 336 large-scale testing. Nominal nozzle velocity will be 8 m/s (26.3 ft/sec). Note the time to the four points listed above.	Yes
<u>Second replacement test</u> In the APEL 1/4-scale 4PJM facility, perform constant volume testing as a function of nozzle velocity using the same Laponite shear strength as during the first replacement test (100 to 110 Pa) and at 336 with an aspect ratio of 1.6. Record and provide to R&T the cavern height versus velocity data.	Yes
24590-WTP-TEF-RT-03-083	
Perform constant drive volume testing as a function of nozzle velocity using the same clay mixture simulant in both platforms. Record and provide the cavern height versus velocity data.	Yes
During constant drive volume testing, use the following measurement methods: 1) colorimetric dye method for determining mixing volume and uniformity, 2) radiofrequency tags to help determine mixing volume and uniformity, 3) polycarbonate beads to help determine mixing volume and uniformity (may be for indication only; determination of use in 336 may be dictated by test engineer), and 4) per availability of equipment, determine velocities using an ultrasonic probe and compare results to previous testing in the same configuration where Laponite was used as the simulant.	Yes

Table S.4 (contd)

List R&T Test Conditions	Were Test Conditions Followed?
Time to fully mix clay mixture simulant. The clay mixture will be mixed before the start of each test to reach the approximate 30-Pa Bingham Plastic yield stress and 30-cP consistency. Rheology samples will be taken and rheological properties determined before and after the test. The pulse tubes will be turned on and operated with an 8-ft pulse length at the same scaled cycle time used for past 336 large-scale testing. Nominal nozzle velocity will be 12 m/s (39.4 ft/sec), or maximum achievable in 336, with the APEL 4PJM test platform nominal velocity matched to that of the 336 4PJM test platform. Note the time to the four points listed above.	Yes
24590-WTP-TEF-RT-03-059 Rev. 0	
Determine the time to fully mix stagnant Laponite in the SRNL 4PJM 1/9-scale test platform for comparison with the 336 4PJM large-scale and APEL 4PJM 1/4-scale test platform data. Data are also needed for a larger aspect ratio (i.e., height of working volume to tank diameter) test using constant pulse tube fill volumes.	Yes
First Replacement Test: The Laponite will be allowed to gel at least 18 hours, and rheology samples will be taken and shear strength determined before and after the test. The pulse tubes will be turned on and operated with an 8-ft pulse length at the same scaled cycle time being used for current 336 large-scale testing. Nominal nozzle velocity will be 8 m/s (26.3 ft/sec). SRNL will note the time to the following points: 1) time to breakthrough at the Laponite surface 2) time to Laponite movement down the tank wall 3) time for the Laponite at the wall to exhibit turbulent motion (fully mixed) 4) if possible, add neutral buoyant beads near the middle or at the wall and document when they reappear.	Yes
Second Replacement Test: Perform constant volume testing as a function of nozzle velocity using the same Laponite shear strength as above (100 to 110 Pa) and at 336 with an aspect ratio of 1.6; record and provide to R&T cavern height versus velocity data.	Yes

References

Poloski AP, PA Meyer, LK Jagoda, and PR Hrma. 2004. *Non-Newtonian Slurry Simulant Development and Selection for Pulse Jet Mixer Testing.* PNWD-3495 (WTP-RPT-111 Rev 0), Battelle – Pacific Northwest Division, Richland, Washington.

Wilson DA, ML Restivo, HN Guerrero, TJ Steeper, RE Eibling, EK Hansen, TM Jones, and KR Eberl. 2004. *One-Eighth Scale Pulse Jet Mixer (PJM) - Design Parameters Scale Law Testing.* SRNL-RPP-2004-00069 Rev. 0 (WSRC-TR-2004-00430 Rev. 0), Westinghouse Savannah River Company, Aiken, South Carolina.

Key Contributors

The results and conclusions presented in this report would not have been possible without the careful work and dedication of many staff at Battelle – Pacific Northwest Division (PNWD) and Savannah River National Laboratory (SRNL). Three groups in particular need to be recognized: the experimental test teams, the simulant team, and the data analysis team. Many staff supported more than one activity and are listed under their area of major contribution.

The large-scale test team at the PNWD 336 Building test facility was led by Carl Enderlin with assistance from Michele Friedrich. Team members included Gary Josephson, Michael McKinnon, Franz Nigl, Bill Combs, Wayne Wilcox, Mike White, Judith Bamberger, Consuelo Guzman-Leong, Brent Barnett, Spiro Tzemos, Don Hartshorn, Mark Gerber, Rich Brown, Jessica Vucelick, Kate Deters, and Jackie Smith.

The 1/4-scale single and 4PJM test team at the PNWD Applied Process Engineering Laboratory (APEL) was led by Jagan Bontha with assistance from Harry Smith. Team members included Jim Bates, Jim Alzheimer, Joe Brothers, Mike Johnson, Dale Wallace, Rich Hallen, and Bill Buchmiller.

The 1/9-scale single and 4PJM test team at SRNL was led by David Wilson and Hector Guerrero. Team members included Michael Restivo, Tim Steeper, Russell Eibling, Erich Hansen, Tim Jones, and Kurt Eberl.

The PNWD simulant team, which was responsible for simulant development, all rheological measurements during testing at 336 and APEL, and dye tracer experiments, was led by Adam Poloski. Team members included Lynette Jagoda, Bob Swoboda, Renee Russell, Brian Cook, and Lanée Snow.

The PNWD data analysis team, which was responsible for nozzle velocity calculations, was led by Jim Fort. Team members included Sato Yokuda, Wassana Yantasee, and Del Lessor.

A special thanks to Art Etchells, Mixing Consultant, DuPont Technology Services for his invaluable input and assistance with this investigation.

Also we would like to acknowledge our editor, Sheila Bennett.

Acronyms and Abbreviations

2-D	two dimensional
3-D	three dimensional
APEL	Applied Process Engineering Laboratory
ASO	Analytical Service Operations
CFD	computational fluid dynamics
CRV	concentrate receipt vessel
DACS	data acquisition system
DOE	U.S. Department of Energy
EDL	engineering development laboratory
EM	electromagnetic
HLW	high-level waste
ID	inner diameter
JPP	jet pump pairs
LAW	low activity waste
LED	light emitting diode
LS	lag storage
M&TE	measuring and test equipment
NPS	nominal pipe size
NPT	nominal pipe thread
NQA	nuclear quality assurance
OD	outer diameter
PC	personal computer
PJM	pulse jet mixer
PNWD	Battelle – Pacific Northwest Division
PVC	polyvinyl chloride
QA	Quality Assurance
QAPjP	Quality Assurance Project Plan
QARD	Quality Assurance Requirements and Description
RF	radio frequency
RPL	Radiochemical Processing Laboratory
RPP	River Protection Project
RW	DOE Office of Civilian Radioactive Waste Management
R&D	research and development
R&T	Research and Technology
SOW	statement of work
SRNL	Savannah River National Laboratory
T/C	thermocouple
UFP	ultrafiltration process
USB	universal serial bus
UVP	ultrasonic velocity probe
WTP	Waste Treatment Plant
WTPSP	Waste Treatment Plant Support Project

Nomenclature

ΔH	fluid level change
ΔL	level change during discharge
ΔL_A	measured level change in pulse tube
K	consistency
δ	local length scale
μ	viscosity
τ_f	turbulent fluid shear stress
τ_s	shear strength
τ_y	yield stress
ρ	slurry density
a	constant coefficient
A_S	scaled area
b	constant
c_1, c_2	constants
C_f	cavern interface friction coefficient
C_L	nozzle loss coefficient
c_J	jet decay constant
c_R	constant
c_{ss}	constant
D_c	diameter of breakthrough region
D_0	Deborah number
d_0	nozzle diameter
d_{0e}	effective nozzle diameter
D_{PT}	pulse tube diameter
D_T	tank diameter
F_0	densimetric Froude number
g	gravitational acceleration
H	operating fill level
H_C	cavern height
He	Hedstrom number
H_{max}	maximum cavern height
H_{VP}	height of velocity probe
J	momentum transport rate
L	subscript referring to large scale
L_L	characteristic linear dimension of large-scale system
L_S	characteristic linear dimension of small-scale system
N	number of PJMs in the tank
N_τ	non-Newtonian stress ratio
p	average hydrostatic pressure
p_a	ambient pressure
p_D	drive pressure
p_e	pressure head at nozzle exit
P_R	pressure ratio
P_0	PJM hydraulic power per pulse
q	exponent
Q_0	PJM flow rate per pulse
Re_0	jet Reynolds number
Re	Reynolds number
Re_τ	yield Reynolds number
Re_ν	viscous Reynolds number
s	geometric scale factor
S	subscript referring to small scale
S_0	Strouhal number
t_C	total cycle time for PJM operation
t_D	drive time
t_{DA}	measured drive time in pulse tube
t_m	time of maximum discharge
t_M	nondimensional mixing time
t_{rel}	slurry relaxation time
t_S	suction time
t_{ss}	time for steady jet to become fully established
t_V	vent time
U	local velocity, nominal discharge velocity
u_a	average PJM velocity
u_c	average maximum velocity at z_c

U_{max}	maximum velocity that does not cause surface breakthrough
u_0	PJM drive velocity
u_p	peak average PJM velocity
u_{ss}	velocity at time of flow establishment
$U_{system\ max}$	maximum discharge velocity achievable at 336
U_{uw}	upwell velocity
$u(z)$	maximum time-averaged velocity at z
V	PJM vessel fluid volume
V_P	pulse volume
V_{PT}	pulse tube volume
V_S	scaled volume
$V_{system\ max}$	maximum discharge volume at 336
V_T	tank volume
V_0	AEA Technology recommended prototypic discharge volume
Y	yield number
z	distance to any point along the primary path the jet travels
z_c	cavern interface

Contents

Figures

Tables

1.0 Introduction

Pulse jet mixer (PJM) technology has been selected for implementation in the Hanford Waste Treatment Plant (WTP). However, the understanding involved in applying this technology to mobilize the non-Newtonian fluids that will be processed through these tanks is not mature. Consequently, an effort has been undertaken to investigate PJM performance in several scaled versions of WTP vessels and develop PJM system configurations that meet WTP requirements. The objectives of this report are to 1) establish the technical basis for performing scaled tests of PJM systems in non-Newtonian slurries and 2) demonstrate that scaled testing produces accurate predictions of full-scale mixing performance.

The results presented in this report are for specific mixing system configurations that were convenient to use in establishing the basis for scaled testing. Specific mixing results obtained from these tests should not be applied directly to WTP process vessels; rather, the scaling laws verified in this work should be implemented when testing scaled versions of plant vessels to ensure meaningful results.

1.1 Background

The Hanford Site contains 177 single- and double-shell tanks holding radioactive waste. The U.S. Department of Energy (DOE) Office of River Protection's WTP is being designed and built to pretreat and then vitrify a large portion of these wastes. The WTP consists of three primary facilities: a pretreatment facility, a low-activity waste (LAW) vitrification facility, and a high-level waste (HLW) vitrification facility. The pretreatment facility receives waste feed from the Hanford tank farms and separates it into 1) a high-volume, low-activity, liquid process stream stripped of most solids and radioisotopes and 2) a much smaller-volume HLW slurry containing most of the solids and most of the radioactivity. In the pretreatment facility, solids and radioisotopes are removed from the waste by precipitation, filtration, and ion exchange processes to produce the LAW streams. The slurry of filtered solids is blended with the ^{137}Cs ion exchange eluate (Sr/TRU precipitate submerged bed scrubber solids) to produce the HLW stream. The HLW and LAW vitrification facilities convert these process streams into glass that is poured directly into stainless steel canisters. The major unit operations of the WTP are shown on the process flow sheet in Figure 1.1.

The process stream significant to this report is identified on the diagram as "HLW pretreated sludge." Several vessels through which the HLW pretreated sludge stream will be processed will be mixed using PJM technology, which has been selected for use in so-called "black cell" regions of the WTP. Within these regions of the plant, maintenance will not be possible for the operating life of the WTP. PJM technology was selected for these regions because there are no moving mechanical parts that require maintenance. While not addressed in this report, PJM-hybrid mixing systems involving air sparging (Poloski et al. 2005), and steady jets produced by a recirculation pump[(a)] are also being implemented in specific vessels.

The concept behind PJM mixing technology involves a pulse tube coupled with a jet nozzle. One end of the tube is immersed in the tank while periodic pressure, vacuum, and venting are supplied to the opposite end. Changing the applied pressure creates three operating modes for the pulse tube:

(a) Johnson MD et al. 2005. *Hybrid Mixing System Test Results for Prototype Ultrafiltration Feed Process and High-Level Waste Lag Storage Vessels*. WTP-RPT-128 Rev. A, PNWD, Richland, Washington.

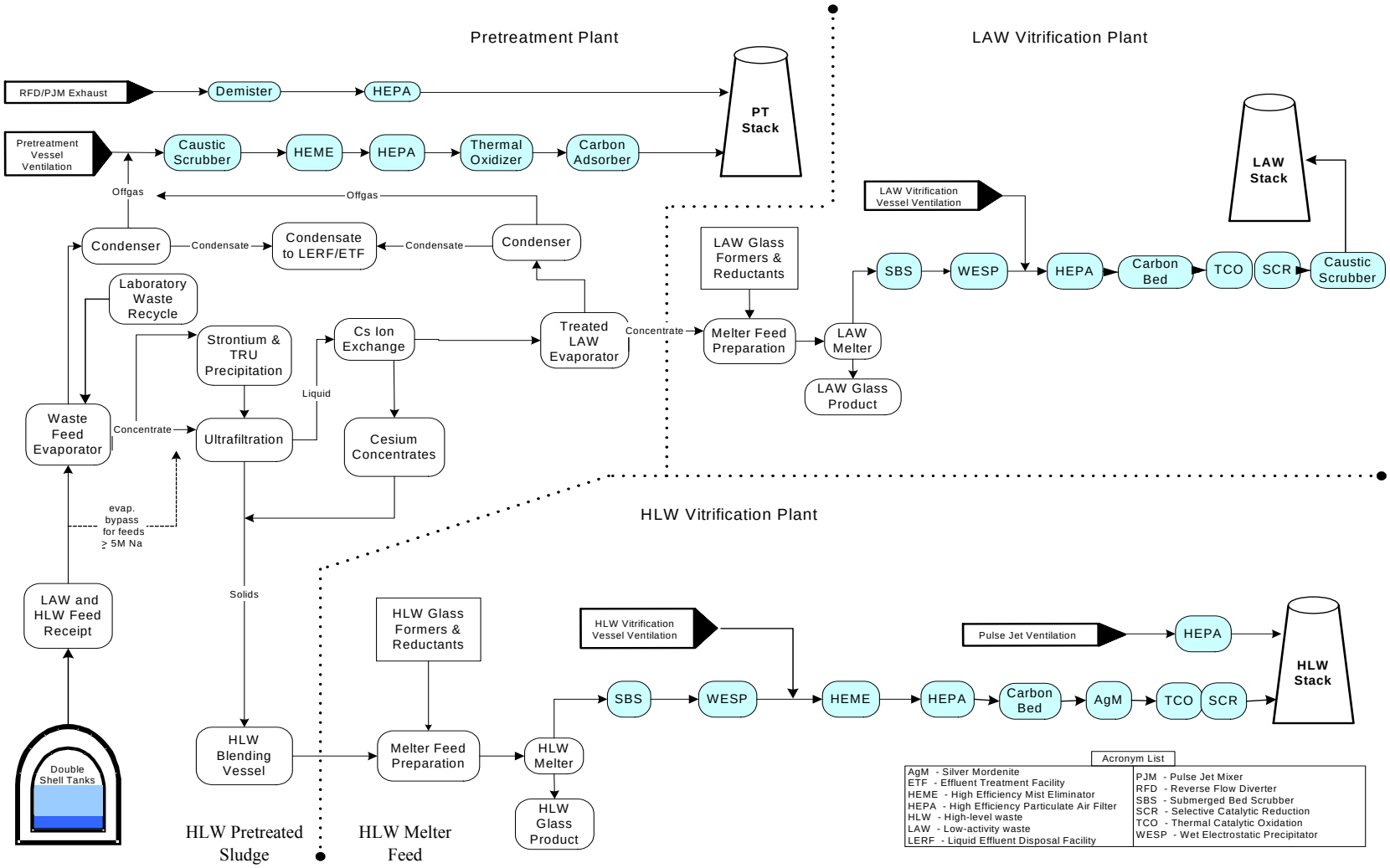

Figure 1.1. RPP-WTP Basic Process Flow Sheet

1) the drive mode, when pressure is applied to discharge the contents of the PJM tube at high velocity through the nozzle; 2) the refill mode, when vacuum is applied to refill the pulse tube; and 3) the equilibration mode, when the pressure is vented to atmosphere and the pulse tube and tank approach the same fill level. The PJM system uses these operating modes to produce a sequence of drive cycles that provide mixing in the vessel. PJM operating parameters—applied pressure, nozzle exit velocity, nozzle diameter, and drive time—along with the rheological properties of the fluid being mixed—all contribute to the effectiveness of mixing within the vessel.

Many of the waste slurries to be received and processed in the WTP exhibit non-Newtonian behavior. In particular, when stationary, these slurries can develop gel-like properties and behave like very weak solids. When an applied force exceeds their shear strength, they behave like a fluid and begin to flow. The majority of knowledge for mixing non-Newtonian fluids is associated with the use of mechanical agitators. The subject of jet mixing in non-Newtonian fluids is a relatively new and developing field, with some theoretical analysis and applied research being pursued in industry and academia. Of the work being done in this area, most is for mixing with continuous or steady jets. The more specialized field of non-steady jet mixing, which is characteristic of PJM mixers, is essentially in its infancy.

One essential phenomenon observed in mixing of non-Newtonian fluids is the formation of a cavern in the mixing zone, as illustrated in Figure 1.2. A cavern is essentially an enclosed region in the non-Newtonian fluid near the mixing jet that is highly agitated and turbulent during portions of the mixing cycle. The cavern is surrounded by material that is essentially stationary, and the transition between the two regions can be very abrupt. The reason for cavern formation is as follows: The fluid velocity in the jet decreases with distance from the nozzle. At some point fluid velocities are so low that the resulting flow-induced fluid stresses are no longer able to overcome the shear strength of the non-Newtonian material. Hence, a force balance occurs that is stable. No flow occurs in this region that is the boundary of the cavern. As the jet discharge increases, fluid velocities increase and the cavern volume grows. As the strength of the non-Newtonian material increases, the cavern becomes smaller.

A successful mixing system design involves placing the PJM jets so there are no regions of stationary material in the desired PJM mixing zone. However, given the absence of established design guidelines for PJM operation in non-Newtonian fluids, demonstration of actual mixing system performance is required.

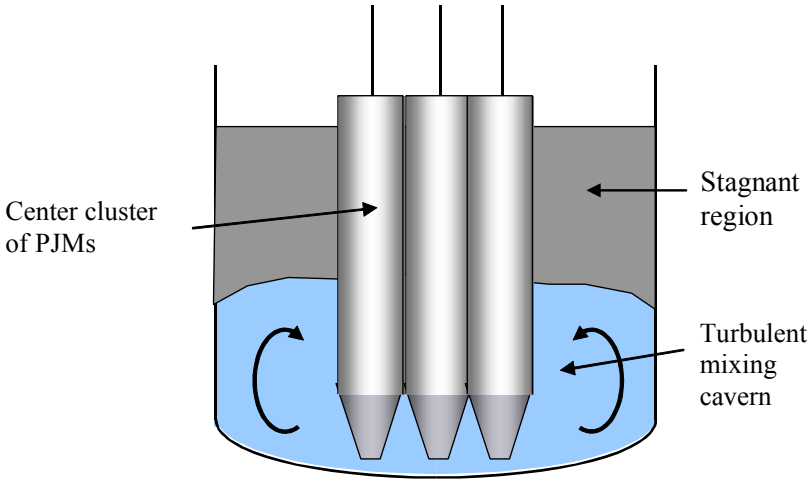

Figure 1.2. Example of Cavern Formation in Non-Newtonian Waste

Computational fluid dynamics (CFD) has been used with some success to model mixing in Newtonian fluids. Using CFD to model mixing in non-Newtonian materials is difficult. Major challenges include modeling yield stress materials, defining minimum velocities that accurately delineate between moving and stationary regions, and modeling turbulent and laminar regions resulting from unsteady-state PJM operation. These challenges would need to be resolved to use CFD to accurately model mixing behavior. Thus, pursuing a CFD approach for non-Newtonian slurries involves the prospect of significant risk requiring development of new computational models, benchmark testing, and protracted analyses.

On the basis of recommendations from the PJM Task Team, which includes representatives from Bechtel R&T, engineering and R&D organizations, fluidics contractor AEA Technology, and mixing consultants, it was agreed to shift the design validation approach to testing non-Newtonian fluid-filled vessels as more efficient in terms of cost, schedule, and assurance of closure of the technical issues. Thus a less analytical, more empirical strategy was developed that included testing at various scales.

1.2 Developing a Scaling Methodology

Small-scale testing is a common approach used successfully in the many varied fields of applied fluid dynamics. The success of the approach depends greatly on the fact that system performance depends on certain nondimensional groupings of physical parameters. If these parameter groupings can be preserved at different geometric scales (large and small), the essential behavior of the system will be the same at both. This principle is referred to as *similarity* in fluid dynamics engineering. In complex fluid dynamic problems, there can be many nondimensional parameter groups; however, often the essential behavior of the phenomenon is dominated by a few key groups. In this situation, small-scale testing can produce results that are very close to large-scale behavior. Understanding the ability to scale the PJM process is complicated because unsteady jet phenomena and jet interactions with non-Newtonian fluids are complex processes in their own right. However, understanding how these processes scale will significantly impact the selection of vessel configuration and operating parameters for the systems to be used in the WTP.

To evaluate the ability to scale these phenomena, tests were conducted at three scales: large scale, 1/4 scale, and 1/9 scale.[(a)] The relationship of these three scales is shown in Figure 1.3. We used dimensional analysis to design the tests and compare the results. Understanding the scaling relationship among results from these tests allowed testing with other PJM mixing systems to be conducted at reduced scale to evaluate mixing performance of actual prototypic mixing systems. These systems were also tested at reduced scale to establish PJM geometries and operating configurations that meet WTP process needs. Understanding how to scale PJM operation for mobilization and mixing of non-Newtonian fluids permits evaluation of the performance of actual system configurations planned for the WTP with the relative ease and lessened cost of a reduced-scale test.

The mixing tests to verify scalability were performed in existing vessels with 4PJM configurations.[(b)] WTP vessels generally differ from the 4PJM mixing systems in height, diameter, number of PJMs, and operating conditions, as well as the rheological properties of slurries. However, the scaling methodology derived from testing the 4PJM systems will be directly applicable to guiding the design of full-scale vessels and testing them at reduced scale.

(a) The scale factors, s, for the three test stands are s = 1 for the 336 Building large scale, s = 4.5 for the APEL ¼ scale, and s = 8.9 for the SRNL 1/9 scale.
(b) Limited testing was also conducted with a single PJM configuration in the 1/4 and 1/9 scale vessels.

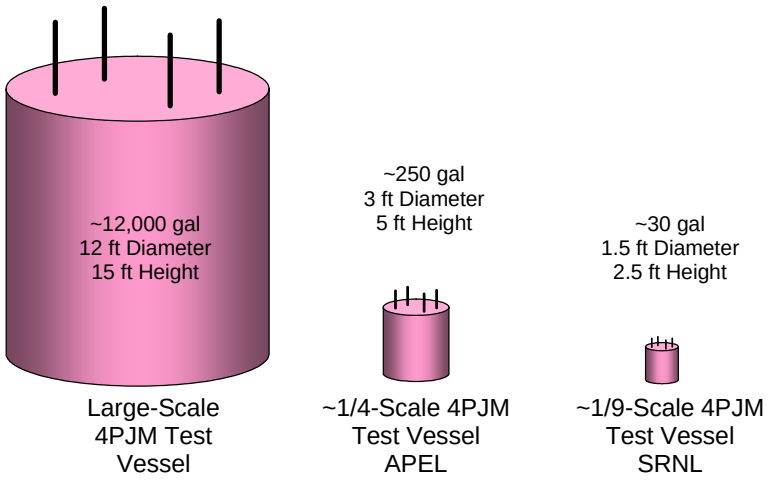

Figure 1.3. Relative Size of 4PJM Mixing System Vessels Used for Validation of Scaling Approach

The WTP will use PJM mixing systems to maintain and mobilize slurries in suspension in the lag storage (LS), ultrafiltration process feed (UFP), and concentrate receipt vessels (CRV).[(a)] Figure 1.4 shows the relative sizes of the full-scale WTP vessels. Also shown are the small-scale versions of the WTP vessels used for scaled prototypic testing, and the 4PJM vessels used for scaling tests. It is advantageous to have a general scaling methodology that can be applied to design PJM systems for all of these

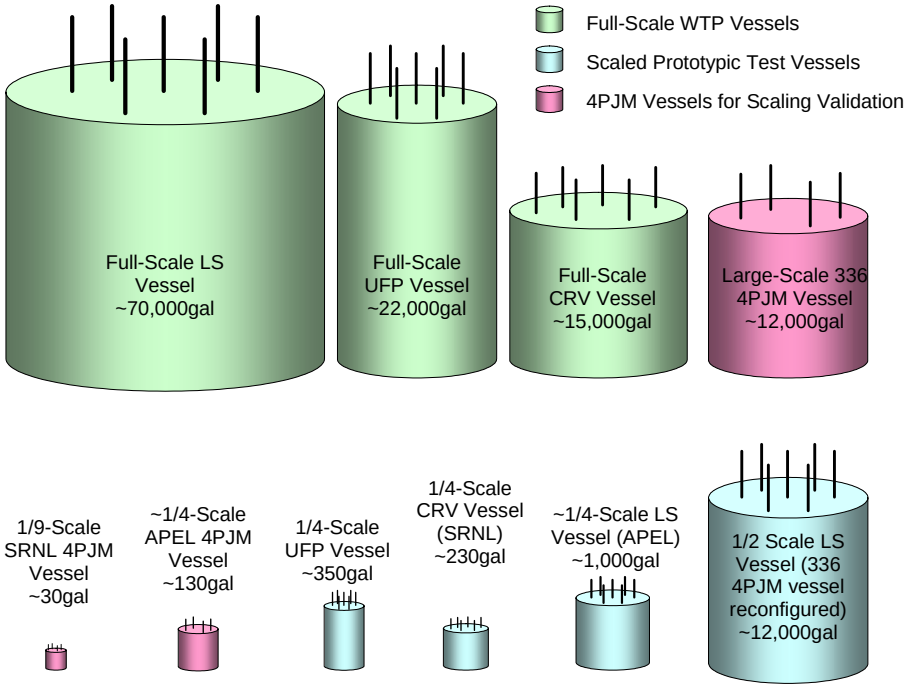

Figure 1.4. Relative Size of 4PJM Mixing System Vessels Used for Validating the Scaling Approach, Scaled Process Test Vessels and Full-Scale Vessels. Volumes shown are nominal batch volumes; actual vessel volumes are somewhat larger.

(a) The concentrate receipt vessel is no longer part of the WTP design.

vessels. With that goal in mind, a series of non-Newtonian mixing experiments was defined to be conducted at three scales to experimentally support the ability to use scaled experiments to define these processes and meet plant mixing system requirements.

1.3 Overview of WTP Non-Newtonian PJM Test Program

In June 2003, the PJM Task Team developed an integrated strategy for scaled testing to demonstrate mixing in WTP vessels containing non-Newtonian fluids. The scaled PJM mixing system tests were intended to provide information on operating parameters critical for uniform movement (total mobilization) of these non-Newtonian slurries. In addition, the WTP project funded work to determine WTP-specific hydrogen generation rate source terms and gas transport characteristics in representative scaled test stand mixing configurations during PJM operation. The gas transport testing included gas retention and release characteristics within non-Newtonian slurries during mixing operations to 1) support development of PJM mixing systems, 2) understand these characteristics within the selected mixing system, and 3) allow for development of normal operation and post-design basis event mixing strategies. The scaled testing strategy incorporated simulant development, scaling tests, and scaled prototypic testing.

Simulant Development: The mixing performance in the PJM test vessels needed to be assessed for non-Newtonian fluids. To realize this objective, non-Newtonian rheological simulants needed to be developed that were nonhazardous and similar in rheological nature to the actual Hanford waste material that will be processed in the WTP. Candidate materials were identified and recipes developed. Both transparent and opaque simulants (described in Appendix D and Poloski et al. 2004) were developed for the testing.

Scaling Methodology: The technical basis for scale-up of non-steady mixing induced by PJMs comprises theoretical modeling, dimensional analysis, and mixing tests. Theoretical modeling produced a physically based model to predict the height of a mixing cavern resulting from pulsed jets in non-Newtonian fluids. Dimensional analysis identified the important dimensionless parameters and guided experimental design. Mixing tests at three physical scales proved that testing at reduced scales was adequate to assess mixing performance. Scales included large-scale (nearly full scale) tests at the 336 Building, ~1/4-scale tests at the Applied Process Engineering Laboratory (APEL), and small-scale (~1/9) tests at Savannah River National Laboratory (SRNL). Each of these geometrically similar vessels had a mixing system comprising four geometrically similar PJMs. Mixing results obtained at these three scales were compared to demonstrate that testing at a reduced scale is a conservative way to predict full-scale mixing performance in WTP vessels. Theoretical analysis and scaling tests were performed on mixing systems and results compared at the three physical scales to demonstrate scale-up laws for gas retention and release behavior. Results of the development and confirmation of a scaling methodology for mixing scaling tests are documented in this report.

Scaled Prototype Testing at Reduced Scale: The final component of the scaled test strategy was to test prototypic vessels at reduced scale. The seven vessels designed to contain and mix non-Newtonian simulants are adequately represented by a subset of three: the UFP vessel, the LS vessel, and the CRV. Reduced-scale models at ~1/4 scale were fabricated that maintained the essential prototypic features, including vessel and PJM geometry, number of PJMs, operational parameters, and major vessel internals. These reduced-scale prototypic vessels allow for performance assessment of the baseline design, obtaining information on key operating parameters and identifying PJM configurations with improved performance. Results of the initial scaled prototypic testing are reported in Bates et al. (2004) while

phase II scaled prototypic testing results are reported in Johnson et al.[(a)] Results of the gas retention and release scaling tests are documented in Rassat et al.[(b)] and Russell et al.[(c)]

1.4 Report Scope

This report addresses the research conducted to develop scaling relationships that can be applied to scaled tests of PJMs in non-Newtonian slurry. This is needed to assess performance of pulse jet configurations in WTP vessels. The research incorporates theoretical analysis and data taken at three scales of test fixtures: 336 large scale, APEL 1/4 scale, and SRNL 1/9 scale.

During these tests and subsequent analysis, the data were evaluated to ensure that the test conditions, data, and observations obtained were appropriate for inclusion in the scaling analysis. Variations in test conditions, simulant preparation, uncertainty associated with measurement techniques, and inconsistent approaches, as well as technical judgment were used to evaluate the data. Data selected for inclusion in the scaling analysis were processed to ensure that variables were all presented consistently for the three test stands. All data presented in the main body of the report (Sections 1 through 6) have been evaluated through the independent technical review process and standardized. Additional observations that may not have been standardized are included in Appendix A to provide insight regarding cavern growth observations from submerged cameras that observed simulant motion in the large-scale test fixture.

- Section 2 lists the quality assurance requirements under which this work was conducted.
- Section 3 develops the scaling relations for pulse-jet mixing and cavern formation.
- Section 4 summarizes the three scales of experiments and test fixtures.
- Section 5 describes the scaling relationships and data analysis.
- Section 6 presents the summary and conclusions.
- Appendixes A, B, and C provide details of the experiments conducted at large-, 1/4-, and 1/9-scale, respectively.
- Appendix D summarizes the simulant selection.

(a) Johnson MD et al. 2005. Hybrid Mixing System Test Results for Prototype Ultrafiltration Feed Process and High-Level Waste Lag Storage Vessels. WTP-RPT-128, PNWD, Richland, Washington.
(b) Rassat SD, CW Stewart, RL Russell, PA Meyer, ST Arm, and CD Johnson. 2004. Interim Report: Gas Retention and Release in Pulsed-Jet Mixed Tanks Containing Non-Newtonian Waste Simulants. WTP-RPT-114 Rev 0, PNWD, Richland, Washington.
(c) Russell RL et al. 2005. Final Report: Gas Retention and Release in Pulse Jet Mixed Tanks Containing Non-Newtonian Waste Simulants. WTP-RPT-114 Rev 1, PNWD, Richland, Washington.

2.0 Quality Requirements

Battelle – Pacific Northwest Division (PNWD) implements the River Protection Project (RPP) WTP quality requirements by performing work in accordance with the PNWD Waste Treatment Plan Support Project Quality Assurance Project Plan (QAPjP) approved by the RPP-WTP Quality Assurance (QA) organization. This work was performed to the quality requirements of NQA-1-1989 Part I, Basic and Supplementary Requirements, and NQA-2a-1990, Part 2.7 and DOE /RW-0333 Rev 13, Quality Assurance Requirements and Description (QARD). These quality requirements were implemented through PNWD's *Waste Treatment Plant Support Project (WTPSP) Quality Assurance Requirements and Description Manual*. The analytical requirements were implemented through WTPSP's Statement of Work (WTPSP-SOW-005) with the Radiochemical Processing Laboratory (RPL) Analytical Service Operations (ASO).

Experiments that were not method-specific were performed in accordance with PNWD's procedures QA-RPP-WTP-1101, "Scientific Investigations," and QA-RPP-WTP-1201, "Calibration Control System," ensuring that sufficient data were taken with properly calibrated measuring and test equipment (M&TE) to obtain quality results.

PNWD addresses internal verification and validation activities by conducting an independent technical review of the final data report in accordance with PNWD's procedure QA-RPP-WTP-604. This review verifies that the reported results are traceable, that inferences and conclusions are soundly based, and that the reported work satisfies the Test Plan objectives. This review procedure is part of PNWD's *WTPSP Quality Assurance Requirements and Description Manual*.

Savannah River National Laboratory (SRNL) work was conducted in accordance with the RPP-WTP-QA requirements specified for work conducted by SRNL as identified in DOE IOW M0SRLE60 (Wilson et al. 2004).

3.0 Technical Basis for Scaled Testing

This section develops the technical basis used by the WTP non-Newtonian Scaled Test Program. It provides an overview of the theory and technical approach to scaled testing of PJM mixing systems in non-Newtonian slurries. It also provides guidance on how the scaling tests at multiple physical scales should be performed to demonstrate that tests performed at reduced scale can adequately represent mixing behavior in full-scale systems.

3.1 Introduction

The WTP project uses PJM technology for tank mixing applications requiring solids mixing, solids suspension, fluid blending, and release of radiolytically and thermolytically generated gases. PJMs are non-steady jet mixing devices that use compressed air as the motive force.

AEA Technology, the WTP fluidics technology contractor, has designed PJMs for WTP mixing applications. The WTP project has evaluated various PJM designs for Newtonian fluids and slurries based on solids lift testing at PNWD and CFD analysis. Applied testing was conducted to produce fluidics code benchmark mixing data (Bontha et al. 2003). This approach has been proven to apply to the large proportion of WTP vessels that contain Newtonian fluids. The approach has not been successful for the seven vessels that contain non-Newtonian fluids due to difficulties in demonstrating that the CFD analysis accurately reflects actual non-Newtonian fluid behavior.

A shift to an emphasis on testing as the design validation approach for PJM in non-Newtonian vessels is seen as a more efficient solution to understanding this application in terms of cost, schedule, and project risk. A less analytical, more empirical strategy, with scaled and full-scale testing included, has accordingly been developed and promoted by the WTP as the design validation approach.

3.1.1 Challenges of Mixing Non-Newtonian Slurries

In Newtonian fluids, the fluid stress is directly proportional to the fluid strain. Newtonian fluids are commonly referred to as constant viscosity fluids. Examples of Newtonian fluids are water, oils, solvents, and, in some cases, slurries. Non-Newtonian fluids are a broad class encompassing all fluids whose rheology deviates from Newtonian.

Many of the Hanford waste slurries to be received and processed in the WTP exhibit non-Newtonian behavior. In particular, when stationary, they can develop gel-like properties where they behave like very weak solids. When an applied force exceeds their *shear strength*, they act like a fluid and begin to flow.

The field of Newtonian fluid mixing is mature and supported by significant theoretical and practical knowledge for designing mixing systems. These systems can be mechanical (impellers or agitators) or hydrodynamic (steady or pulsed fluid jets). For non-Newtonian fluids, the majority of mixing experience is associated with mechanical agitators. The subject of jet mixing in non-Newtonian fluids is a relatively new and developing field, with some theoretical analysis and applied research being pursued in industry and academia. Non-steady jet mixing in non-Newtonian fluids is essentially a new topic of study. Although in its infancy, non-Newtonian fluid jet mixing can derive a great deal of understanding and

guidance from the more mature fields of jet mixing in Newtonian fluids and mechanical mixing in non-Newtonian fluids.

3.1.2 Cavern Formation in Non-Newtonian Mixing

One essential phenomenon observed in mechanical mixing of non-Newtonian fluids is the formation of a cavern, as illustrated in Figure 3.1. A cavern is essentially a bounded region near the impeller that is highly agitated and turbulent. The cavern is surrounded by material that is essentially stationary, and the transition between the two regions can be very abrupt. The reason for the cavern formation is that fluid motion created by the impeller decreases with distance from the impeller. At some point, fluid velocities are so low that the resulting fluid stresses are no longer able to overcome the shear strength of the non-Newtonian material. Hence, a force equilibrium occurs that is stable (illustrated in Figure 3.1). As the impeller speed increases, fluid velocities increase and the cavern grows. As the strength of the non-Newtonian material is increased, the cavern becomes smaller at a given impeller speed. A successful mixing system design involves placing and operating agitators so there are no regions of stationary material in the mixing vessel.

Caverns have also been observed to form when using steady jets. Early testing at PNWD also confirmed that caverns form when fluid is agitated using unsteady jets created by PJMs (Enderlin et al. 2003). This result is to be expected given the similarity between jet mixing and mechanical agitation (both create fluid motion). However, given the absence of established design guidelines for PJM operation in non-Newtonian fluids, a test program is required to establish the design of PJM systems so that the entire vessel contents are mobilized and no caverns are present.

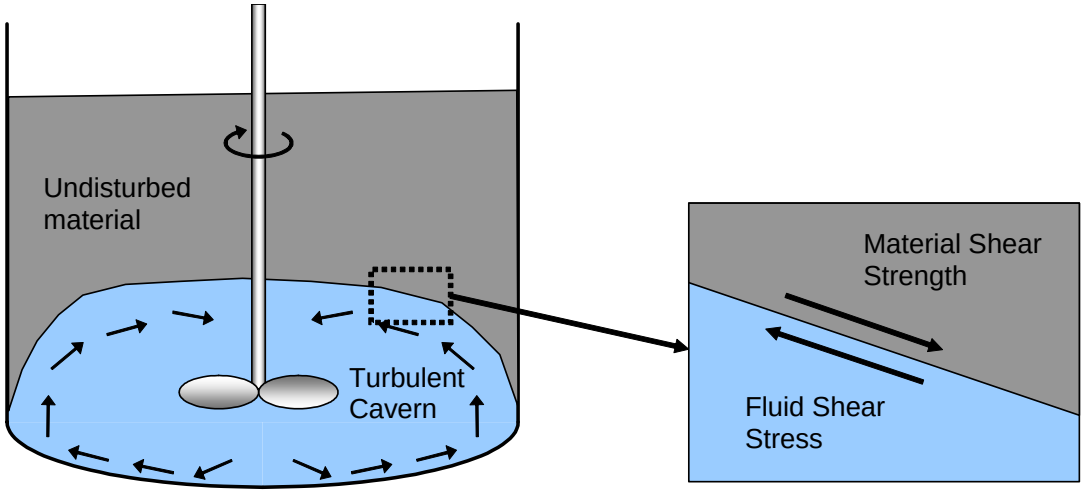

Figure 3.1. Illustration of Cavern Formation During Mechanical Mixing in Non-Newtonian Material

3.1.3 Overview of Technical Basis for Scaled Testing of PJM Systems

This section presents the approach used to establish the technical basis for the scalability of the scaled prototypic mixing tests. The technical basis for scaled testing of PJM mixing systems includes several key elements. The first is the development of a theory of operation for PJM mixing in non-Newtonian slurries. This development includes identifying the key principles of PJM operation, considering rheology, and modeling cavern formation for non-steady jet mixing. The second key element of the

strategy is to perform a scaling analysis on the physical system. Important physical properties, parameters, and nondimensional groups need to be identified. Then scaling laws must be applied to determine how tests at different physical scales should ideally be performed. Finally, scale laws must be verified by actual testing of PJM systems at different physical scales and demonstrating similar results. In establishing this technical basis, the program can have confidence that results of tests in scaled prototypic plant vessels will be valuable and applicable in establishing full scale, actual plant mixing performance.

3.2 Theory of Pulse Jet Mixing in Non-Newtonian Slurries

3.2.1 Principles of PJM Operation

A typical PJM system configuration in a vessel is shown schematically in Figure 3.2.[(a)] The tank has diameter, D_T, volume, V_T, and operating level, H. There are N PJMs in the tank, each with diameter, D_{PT} and volume, V_{PT}. Each PJM has a conical nozzle with diameter, d_0. Typically, the total volume of the pulse tubes $N V_{PT}$ is approximately 10 to 15% of the operating volume of the vessel.

There are three phases to the operation of the PJM—drive, vent, and suction. During the drive phase, the tube is pressurized and a volume of slurry is discharged. The level change in the tube during discharge is ΔL. The corresponding increase in waste level is ΔH, where

$$\Delta H = N\Delta L\left(\frac{D_{PT}^2}{D_T^2 - ND_{PT}^2}\right) \quad \text{(for partially submerged PJMs)} \tag{3.1}$$

or

$$\Delta H = N\Delta L\frac{D_{PT}^2}{D_T^2} \quad \text{(for fully submerged PJMs)} \tag{3.2}$$

Typical values of ΔH are about 8 to 12% of the operating level, H. The average velocity, u_0, discharged during the drive phase is given by

$$u_0 = \frac{D_{PT}^2}{d_0^2}\frac{\Delta L}{t_D} \tag{3.3}$$

where t_D is drive time. The drive pressure, p_D, required to produce the discharge velocity is given by

$$p_D = p_e + \frac{C_L}{2}\rho u_0^2 \tag{3.4}$$

where ρ_e is the pressure head at the nozzle exit, C_L is the nozzle loss coefficient, and ρ is the slurry density.

(a) The PJM configuration used for this analysis is somewhat simplified. Vessels and PJMs are assumed to be cylindrical, and other vessel internals are neglected.

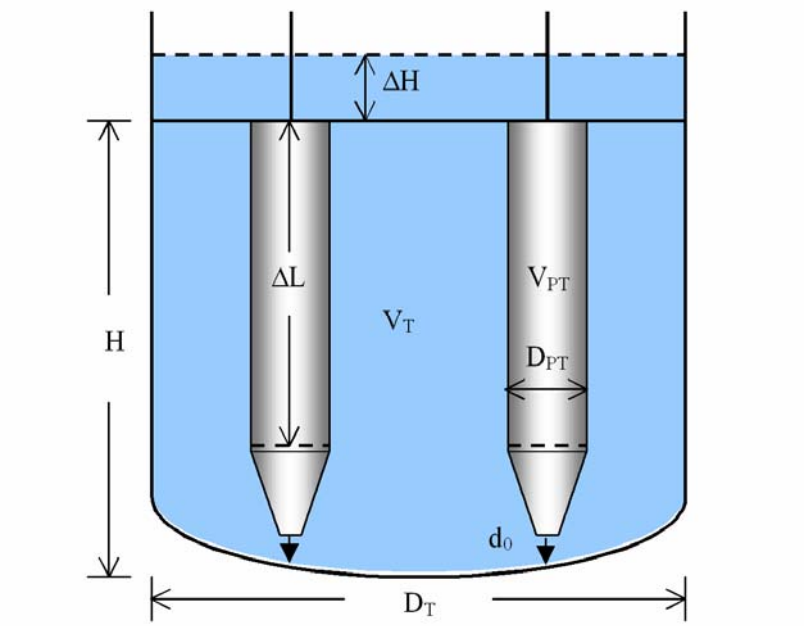

Figure 3.2. Illustration of a Typical PJM System in a WTP Vessel

Immediately after the drive phase, a vent is opened and excess pressure is allowed to vent to atmosphere. During the suction phase, vacuum is applied to the pulse tube, which fills due to a combination of applied vacuum and difference in hydrostatic head between the fluid level and the level in the tube. Vent and suction times are given by t_V and t_S, respectively; total cycle time for PJM operation is given by

$$t_C = t_D + t_V + t_S \tag{3.5}$$

The average drive velocity is both spatially and temporally averaged. Spatially, the velocity varies over the cross section of the nozzle. Temporally, the velocity varies due to inertial effects. At the beginning of the drive phase, the fluid inside the PJM is stationary and must be accelerated. When the drive phase is over, some fluid continues to discharge due to the inertia of the moving column of fluid. The inertial effects depend on the physical size of the system. Hence, the actual velocity varies over the operating cycle. For comparing PJM operation at different scales, various average velocities can be considered. One is the average peak velocity, given by

$$u_P = \frac{1}{t_D - t_m}\int_{t_m}^{t_D} u\,dt \tag{3.6}$$

where u is instantaneous velocity at t_m, time of maximum discharge; another is average velocity, given by

$$u_a = \frac{D_{PT}^2}{d_0^2}\frac{\Delta L_A}{t_{DA}} \tag{3.7}$$

where ΔL_A and t_{DA} are the actual measured level change and drive times in the pulse tube. Figure 3.3 is an illustration of the temporal variation of velocity during one PJM cycle.

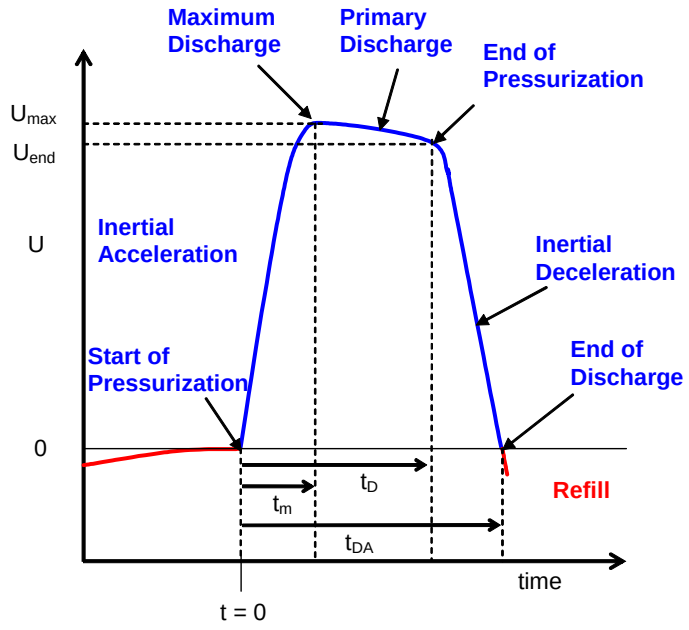

Figure 3.3. Illustration of Temporal Variation of Velocity During PJM Discharge

3.2.2 Rheological Considerations

Cavern formation is highly dependent on the rheological properties of the slurry. Rheological tests with actual waste samples suggest the waste is best represented by the Bingham plastic rheological model. The Bingham plastic model is illustrated in the rheogram shown in Figure 3.4. The rheogram is taken from a rheometer, which measures the shear stress as a function of rate of strain for laminar flow. The model is characterized by yield stress, τ_y, which is the shear stress extrapolated to zero strain rate, and consistency, K, the slope of the linear region. The bounding best-fit parameters of actual waste slurry are τ_y = 30 Pa and K = 30 cP.

While the laminar flow rheogram is useful, it does not adequately describe all the relevant rheology for the cavern formation problem. Before it is disturbed, actual waste slurry will possess shear strength, τ_s. Thus, the actual waste appears to be thixotropic, i.e., the shear stress can decrease while experiencing a strain rate. Specifically, we expect the shear stress of a fluid undisturbed for some time to exhibit one characteristic value, the shear strength, which then decreases asymptotically over time during strain to a smaller value, the yield stress. This is illustrated by the point on the rheogram at zero strain rate in Figure 3.4, as well as in Figure 3.5 in the region entitled "Applied shear." If the fluid remains unstrained for some time, the shear stress extrapolated to zero strain rate will return from the yield stress to the shear strength. This is illustrated in the region entitled "Re-gel period" in Figure 3.5. Apparently, the time to decrease from the shear strength to the yield stress is fast enough, and the time to return from the yield stress to the shear strength is great enough that effectively the fluid behavior divides into one region experiencing strain events repeated quickly enough that the zero-strain shear stress remains at the yield strength, and another region in which the fluid rarely experiences strain such that the zero-strain shear stress remains at the shear strength.

.

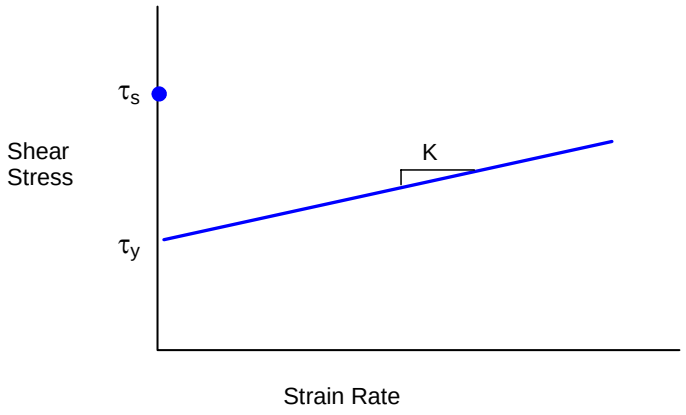

Figure 3.4. Bingham Plastic Rheological Model. Also shown is shear strength of undisturbed slurry.

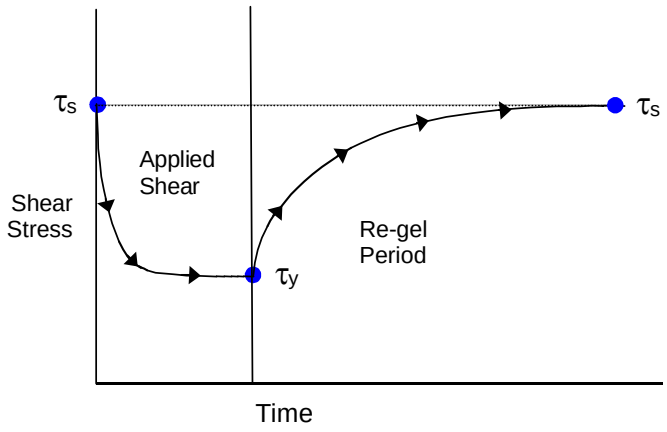

Figure 3.5. Illustration of Thixotropic Behavior of Non-Newtonian Slurry

The shear strength will generally be larger than the yield stress. The ratio of shear strength to yield stress is a useful characterization parameter for a particulate slurry. There is no general relationship between shear strength and yield stress, and the ratio τ_s/τ_y can range from approximately one to many orders of magnitude.

Another limitation of the Bingham plastic model is that turbulent conditions exist inside the cavern. The behavior of Bingham plastic fluids in turbulent flow is not well understood. In some cases, it is believed that the yield stress is not present (or significant) for turbulent flow of a particulate slurry. Rather, the behavior is more Newtonian, with the Newtonian viscosity (μ) approximately equal to Bingham consistency (K). However, the Bingham yield stress may be important in the boundary layer at the cavern interface. As the velocity slows at the interface, it will at some point re-laminarize. Under these conditions the laminar Bingham rheology will apply. It is generally believed that this boundary layer region is quite thin, and that the effects of the yield stress are therefore minor. However, the topic of turbulent to laminar transition in a non-Newtonian slurry is not well understood generally, and the possibility exists that the presence of yield stress in the boundary layer could affect the position of the

cavern. We expect the shear strength, τ_s, yield stress, τ_y, and consistency, K, to be the most important rheological parameters governing cavern formation in a non-Newtonian particulate-laden slurry.

3.2.3 Cavern Formation with Steady Jets

This section presents a simple theory for the position of the cavern resulting from a single, downward oriented, steady turbulent jet. In Figure 3.6, a single PJM system is shown in a vessel with non-Newtonian slurry. The discharging jet impinges on the tank bottom, then moves up the side wall and turns inward. We assume that the flow inside the cavern is fully turbulent and approximately Newtonian.

Three-dimensional Newtonian turbulent jets, whether free (away from boundaries) or impinging on boundaries, are known to follow the law (Rajaratnam 1976):

$$u(z) = c_J \frac{u_0 d_0}{z} \tag{3.8}$$

In Eq. (3.8), z is the distance to any point along the primary path of the jet, u(z) is the maximum time-averaged velocity at point z, and c_J is a constant accounting for the effects of geometry. The value of c_J for Newtonian turbulent circular free jets is ~5 to 6. Other values depend on geometry and flow regime.

A jet is three-dimensional (3-D) if the cross-section of the flow increases as the square of the distance along it, as opposed to a two-dimensional (2-D), "planar" jet, where the cross-section increases only linearly with distance. The jet does not need to be axisymmetric to be 3-D; for example, a jet impinging on a surface, whether perpendicular or at an angle, continues to spread simultaneously in two dimensions and thus is three-dimensional. In Figure 3.6, the descending region of the jet is an ordinary 3-D jet. The jet spreading across the floor is expanding normal to the floor and also the circumference of the jet expands linearly with distance outward. If the jet ascending the wall had perfect radial symmetry it would be 2-D—expanding only normal to the wall but with its circumference no longer expanding, in which case the velocity would decrease inversely with the square root of distance along the jet. However, actual behavior in any real system will not be perfectly radially symmetric, with instead large-scale turbulence tending to divide the flow into a multitude of jets still expanding circumferentially as well as normal to the wall. Thus Eq. (3.8) applies reasonably over the length of the flow from nozzle to cavern boundary.

Eq. (3.8) is observed and theoretically expected from dimensional analysis for Newtonian fluids. For turbulent jets, the diameter of the jet can be a function only of momentum transport rate, J, fluid density, ρ, and distance, z, along the jet. That combination constrains the diameter of the jet to be proportional to z, which, from the conservation of momentum, leads directly to Eq. (3.8). For a jet in a Bingham plastic fluid exhibiting yield stress, τ_y, from dimensional analysis the jet diameter can depend on $(\tau_y z^2/J)^q$, where the exponent q can be other than zero. For this study, we assume that either effectively $q = 0$ or the consequence of $q \neq 0$ is unimportant. In other words, we assume that Eq. (3.8) is approximately true for turbulent non-Newtonian, particulate-laden slurry.

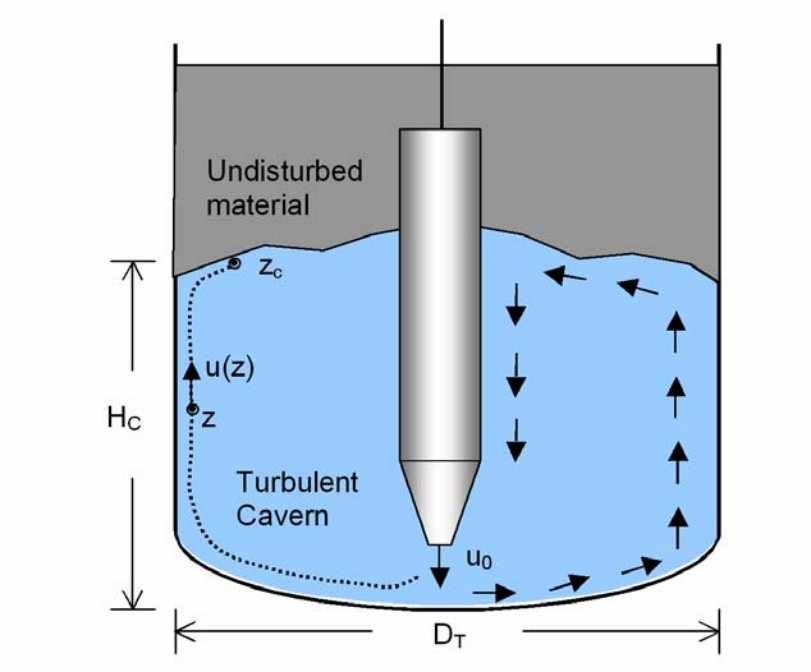

Figure 3.6. A Single Jet in a Vessel with Non-Newtonian Slurry

If the cavern is well established and at steady state, a force balance must exist at the cavern interface. The stress exerted by the turbulent flow at the cavern must equal the shear strength of the undisturbed slurry. We can think of the cavern interface as a solid surface with a turbulent boundary layer.[(a)]

The turbulent fluid shear stress, τ_f, at some point along the interface, z_c, can be expressed as

$$\tau_f = C_f \frac{1}{2} \rho u_c^2 \tag{3.9}$$

where u_c is the average maximum velocity at point z_c, and C_f is a wall frictional coefficient. In both laminar and turbulent flow boundary layers, wall friction coefficients typically depend on the viscous Reynolds number[(b)] according to

$$C_f = c_R \, Re_v^{-1/b} \tag{3.10}$$

where c_R and b are constants and Re_v is the viscous Reynolds number defined by

(a) A boundary layer is normally thought of as the region of decreasing velocity at a solid surface created by a free stream away from the wall. For a turbulent wall jet, little distinction exists between the jet and the boundary layer because the peak mean flow velocity is often very near the wall. We use boundary layer loosely to refer to the turbulent flow right at the cavern interface.

(b) The wall friction coefficient may also depend on the Bingham yield stress to some degree, due to laminar flow in the viscous sublayer of the turbulent boundary layer. It is hypothesized that this dependence of wall friction coefficient on Bingham yield stress is a small effect, but this has not been proven at this time.

$$\mathrm{Re}_v = \frac{\rho U \delta}{\mu} \tag{3.11}$$

Here U is the local velocity, δ is the local length scale (typically the thickness of the boundary layer or distance along the boundary layer to the point of interest), and μ is the viscosity. The viscosity to be used in evaluating the Reynolds number is the consistency, K, from the Bingham plastic rheological model.

To obtain the jet Reynolds number, Re0. , we evaluate Eq. (3.11) at point zc ($U = u_c$ and $\delta = z_c$). Making use of Eq. (3.8) we can write $\mathrm{Re}_v = \mathrm{Re}_0$,

$$\mathrm{Re}_0 = \frac{\rho u_0 d_0}{\mu} \tag{3.12}$$

Hence Eq. (3.10) can be written

$$C_f = c'_R \, \mathrm{Re}_0^{-1/b} \tag{3.13}$$

where $c'_R = c_J^{-1/b} c_R$.

The exponent b in Eq. (3.13) is typically about 4–5 for many turbulent boundary layers. Hence the friction coefficient is not a strong function of jet Reynolds number. The wall shear stress given by Eq. (3.9) is therefore primarily determined by the jet velocity, with only a minor correction for jet Reynolds number. Continuing with the derivation, we write a force balance at the cavern interface by setting $\tau_f = \tau_s$ so that Eq. (3.9) becomes

$$C_f \frac{1}{2} \rho u_c^2 = \tau_s \tag{3.14}$$

If we approximate the point z_c (the distance the jet travels along the floor and up the wall) at the cavern interface by

$$z_c \approx H_C + \frac{D_T}{2} \tag{3.15}$$

then from Eq. (3.8), (3.14), and (3.15) we can write an expression for the height of the cavern:

$$H_C = c_J \sqrt{C_f} \, \frac{u_0 d_0}{\sqrt{2\tau_s / \rho}} - \frac{D_T}{2} \tag{3.16}$$

If we introduce the yield Reynolds number,

$$\mathrm{Re}_\tau = \frac{\rho u_0^2}{\tau_s} \tag{3.17}$$

then Eq. (3.16) combined with Eq. (3.13) gives

$$\frac{H_C}{D_T} = a\frac{d_0}{D_T}\,Re_0^{-1/2b}\,Re_\tau^{1/2} - \frac{1}{2} \tag{3.18}$$

where $a = C_J(C_f/2)^{1/2}$. Because Eq. (3.18) is such a weak function of viscous Reynolds number (with $b \approx 5$ the exponent on Re is approximately 1/10), a simplified expression for the cavern height may be written

$$\frac{H_C}{D_T} = a'\frac{d_0}{D_T}\,Re_\tau^{1/2} - \frac{1}{2} \tag{3.19}$$

where the coefficient a' will be different than the coefficient a in Eq. (3.18).

Figure 3.7 compares the cavern height predicted by Eq. (3.19) and the results of a cavern formation experiment with a steady jet (Enderlin et al. 2003). The simulant used was Laponite[(a)] with shear strength of 44 Pa. Good agreement is seen between the data and the theoretical result when the value of a' in Eq. (3.19) is 1.67, resulting in an R^2 value of 0.976. When the intercept is allowed to be adjusted, the best-fit parameters are $a' = 1.46$ with an intercept of 0.334, resulting in an R^2 value of 0.997. The reduction in the intercept from -1/2 to -1/3 is consistent with the fact the experiment was carried out in a vessel with an elliptical bottom. The distance of travel by the jet to the wall is reduced from that in a flat-bottom tank (which was the basis of the derivation for Eq. 3.19).

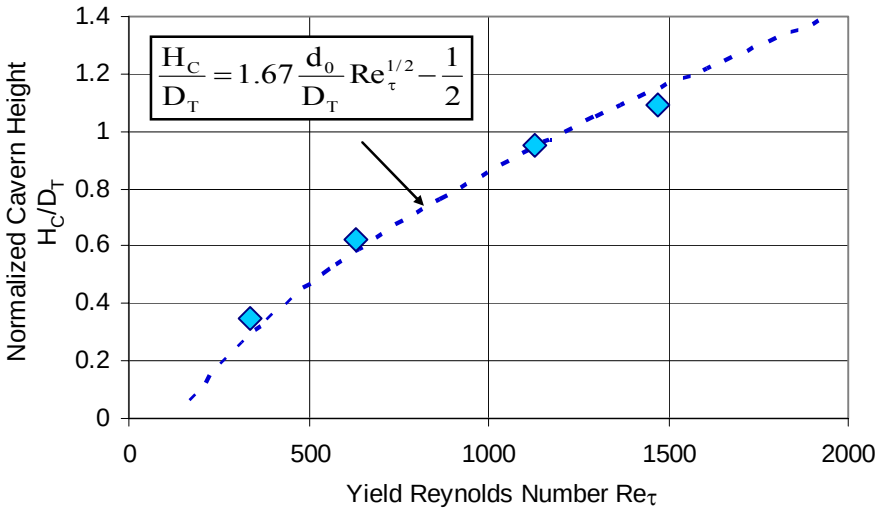

Figure 3.7. Theoretical Prediction of Cavern Height for a Steady Jet Compared with Data in Laponite. Test conditions correspond to τ_s = 44 Pa, d_0 = 0.875 in., D_T = 34 in., ρ = 1000 kg/m^3 with velocities ranging from u_0 = 12 – 27 ft/sec.

(a) Laponite simulant is discussed in detail in Appendix D of this report.

There are some data suggesting that the jet constant, c_J, is a weak function of jet Reynolds number (Zarruk 2002). It is reasonable that lower Reynolds number jets would decay slightly faster than higher Reynolds number jets. It is not known to what extent this effect would interplay with the Reynolds number dependence of the friction coefficient. We generalize Eq. (3.19) to account for all potential Reynolds number effects as well as bottom curvature effects by writing

$$\frac{H_C}{D_T} = c_1 \frac{d_0}{D_T} f(Re_0)\, Re_\tau^{1/2} - c_2 \tag{3.20}$$

Equation (3.20) is the most general form of an expression describing cavern height produced from a single steady jet. Experiments at different Reynolds numbers (geometric scales) would be required to determine the constants c_1 and c_2, as well as the functional form $f(Re_0)$.

3.2.4 Effects of Pulsation

The results presented in the previous section were for the case of a steady turbulent jet. In this section we examine the effects of pulsation on the position of the cavern. There are several potential effects associated with the periodic non-steady discharge of the PJMs. These may be hydrodynamic or rheological.

The primary hydrodynamic issue is that of flow establishment. Any real jet has a finite time required to establish steady flow conditions. If the jet is turned off before this time, the velocity far from the jet will be less than that of the steady jet. The effect of flow establishment is illustrated in Figure 3.8.

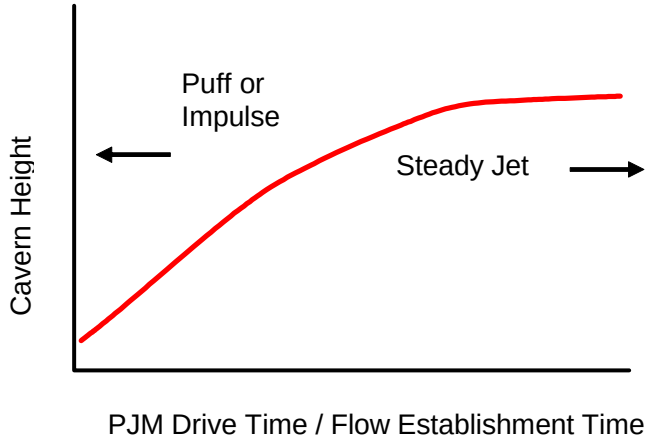

Figure 3.8. Illustration of Potential Range of Behavior for a Pulsed Jet

The time for a steady jet to be fully established (t_{ss}) can be estimated by considering the time it takes a fluid element to travel from the jet to the cavern. By writing u(z) = dz/dt, Eq. (3.8) can be integrated to obtain

$$t_{ss} \approx \frac{(H_C + D_T/2)^2}{u_0 d_0} \tag{3.21}$$

From Eq. (3.21) we see that the flow establishment time increases with the square of the cavern height and is reduced by increasing jet velocity or nozzle size. We can further explore the flow establishment time by writing H_C in terms of its dependent parameters. Combining Eq. (3.21) and (3.19) we have

$$t_{ss} = c_{ss}\, Re_{\tau} \frac{d_0}{u_0} \tag{3.22}$$

The term c_{ss} in Eq. (22) takes into account the constants as well as the friction coefficient, so it therefore may be a weak function of Reynolds number.

The PJM drive time is determined by Eq. (3.23):

$$t_D = \frac{D_{PT}^2}{d_0^2}\frac{\Delta L}{u_0} = \frac{4V_P}{\pi d_0^2 u_0} \tag{3.23}$$

where $V_P = \frac{\pi}{4} D_{PT}^2 \Delta L$ is the volume of a pulse.

The ratio of drive time to flow establishment time is therefore

$$\frac{t_D}{t_{ss}} = \frac{4V_P}{\pi c_{ss} d_0^3 Re_{\tau}} \tag{3.24}$$

From Eq. (3.24) we see that the ratio of drive time to flow establishment depends only on the pulse volume, the nozzle diameter, and the yield Reynolds number.

To obtain an expression for the cavern height for the case of a pulsed jet, we need to understand how the velocity at the cavern interface changes as a function of time. We begin by assuming that the spatial and time dependence of the jet are independent so that

$$u(z,t) = u_{ss}(z) f(t) \tag{3.25}$$

where u_{ss} is given by Eq. (3.8) and f(t) must be determined.

To estimate the function f(t), we assume that the temporal rate of change of the velocity at any point z is proportional to the difference between the velocity and its steady-state value, with the constant of proportionality equal to the time for flow establishment, t_{ss}:

$$\frac{du(z,t)}{dt} = \frac{u_{ss}(z) - u(z,t)}{t_{ss}} \tag{3.26}$$

Solving Eq. (3.26) and evaluating for $t = t_D$ yields

$$u(x,t) = \frac{c_J u_0 d_0}{z}\left(1 - e^{-t_D / t_{ss}}\right) \tag{3.27}$$

Equation (3.27) shows that in the limit of very short drive times the velocity goes to zero. When the drive time is large compared to the flow establishment time, the steady jet solution is recovered.

To obtain an expression for the cavern height, the analysis of the previous section is repeated using Eq. (3.27) instead of Eq. (3.8). The resulting expression is

$$\frac{H_C}{D_T} = a\frac{d_0}{D_T}\mathrm{Re}_\tau^{1/2}\left(1 - e^{t_D / t_{ss}}\right)^{1/2} - \frac{1}{2} \tag{3.28}$$

Substituting the expression for t_D / t_{ss} (Eq. 3.24),

$$\frac{H_C}{D_T} = a\frac{d_0}{D_T}\mathrm{Re}_\tau^{1/2}\left(1 - \exp\left(-c\frac{V_P}{d_0^3\,\mathrm{Re}_\tau}\right)\right)^{1/2} - \frac{1}{2} \tag{3.29}$$

Data shown in Figure 3.9 compare the cavern height predicted by Eq. (3.29) and results of cavern formation experiments with a single pulsed jet. Tests were conducted with a 1-inch nozzle (Laponite, 31 Pa shear strength) and a 2-inch nozzle (Laponite, 44 Pa shear strength). The pulse volume, V_P, was 1090 in.^{3} for the 1-inch nozzle test and 1960 in.^{3} for the 2-inch nozzle test. Excellent agreement is seen between data and theoretical results with the value of $a = 1.64$ and $c = 1.5$. Steady jet data are also shown in Figure 3.9 for comparison.

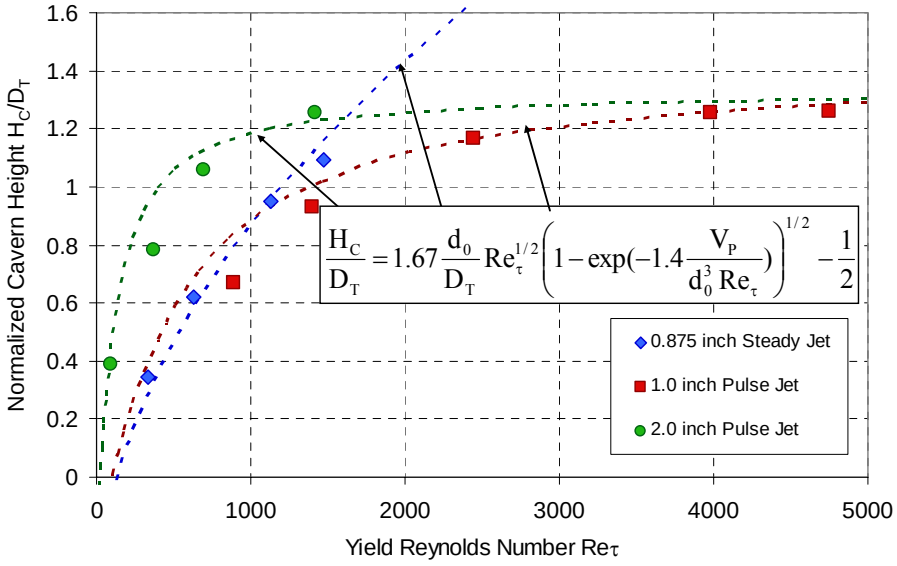

Figure 3.9. Theoretical Prediction of Cavern Height for a Single Pulsed Jet (given by Eq. 3.29) Compared with Data in Laponite. Steady jet data shown for comparison (where pulse volume is taken as infinite in Eq. 3.29 to recover the steady jet result).

The results presented in Figure 3.9 show that a pulsed jet's ability to erode a cavern diminishes significantly if the relative pulse time is short. As the velocity is increased, the relative pulse time diminishes with the inverse square of the velocity, according to Eq. (3.24). Subsequently, there is not enough time to establish steady flow velocity at the cavern, and a reduced cavern height results.

It is clear from examining Figure 3.9 or Eq. (3.29) that a limiting cavern height exists for a given system. By taking the limit of Eq. (3.29) as Re_τ becomes large compared with V_P / d_0^3, the limiting cavern height is found to be

$$H_{max} = a'\left(\frac{cV_P}{d_0}\right)^{1/2} - \frac{D_T}{2} \approx 2\left(\frac{V_P}{d_0}\right)^{1/2} - \frac{D_T}{2} \tag{3.30}$$

Hence the limiting cavern height depends primarily on the ratio of pulse volume to nozzle diameter. Equation (3.30) suggests smaller nozzles produce larger limiting caverns. This suggests that the non-steady effects dominate and that longer pulse times (corresponding to smaller nozzles) result in better jet penetration.

It is also clear from examining Figure 3.9 or Eq. (3.29) that non-steady effects are negligible when the yield Reynolds number is small compared to V_P / d_0^3. By taking the limit of Eq. (3.29) for small Re_τ the limiting expression for cavern height is found:

$$\frac{H_C}{D_T} \approx a' \frac{d_0}{D_T} \mathrm{Re}_\tau^{1/2} - \frac{1}{2} \approx 1.67 \frac{d_0}{D_T} \mathrm{Re}_\tau^{1/2} - \frac{1}{2} \tag{3.31}$$

Equation (3.31) is identical to Eq. (3.19), which gives the cavern height for a steady jet.

In summary, the model for the cavern height resulting from non-steady pulse jet operation suggests that the behavior is highly dependent on the yield Reynolds number. When the yield Reynolds number is small compared to V_P / d_0^3, the effects of pulsation are negligible and the steady jet cavern result is obtained. When the yield Reynolds number is larger than V_P / d_0^3, the limiting cavern depends only on the ratio of pulse volume to nozzle diameter.

3.2.5 Multiple PJMs

The result generated in the previous section applied to a single PJM centered in a cylindrical tank. WTP vessels involve multiple PJMs in cylindrical vessels with elliptical bottoms. Typically six or eight PJMs are arranged in a symmetric fashion. The PJMs can operate in or out of phase. A multi-PJM vessel configuration is illustrated in Figure 3.10.

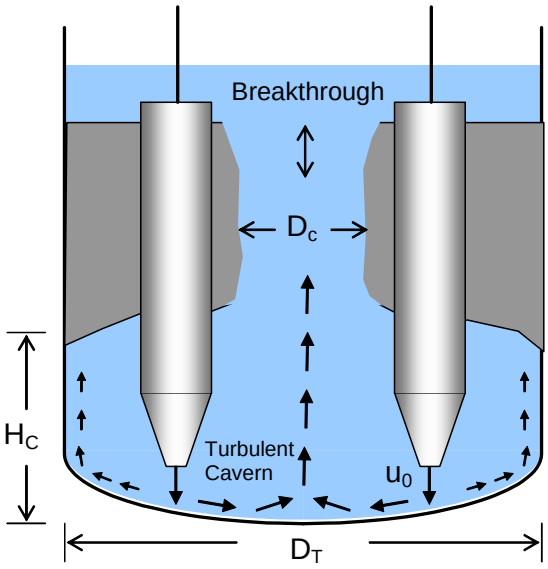

Figure 3.10. Illustration of Potential for Cavern Breakthrough Due to Central Upwelling

One difference between single- and multi-PJM mixing systems is a strong central upwelling flow. As the jets impinge on the elliptical bottom, a significant fraction of the flow moves radially inward and then turns up at the center of the tank. The central upwelling can potentially lead to breakthrough at the surface, leaving an annulus of stationary slurry shown by the gray area in Figure 3.10.

The basic theory developed for single PJMs should apply to the multi-PJM configuration. The dominant upward jet flow should still follow Eq. (3.8), but the nozzle diameter is given by

$$d_{0e} = c\sqrt{N}d_0 \tag{3.34}$$

where N is the number of PJMs and c is a constant determined by geometry.

Because the primary flow is upward, it is likely that the cavern interface will be dictated by the normal stress of the jet as opposed to the shear stress. In this case, the friction coefficient given in Eq. (3.10) is essentially

$$C_f \approx 1 \tag{3.35}$$

Once breakthrough has occurred, the basic model for cavern height will likely fail to predict subsequent cavern behavior because increases in jet velocity may increase the diameter of the breakthrough region, D_c. The dominant flow at this point may be more like pipe flow than a jet. In any event, data from multi-PJM systems exhibiting breakthrough are required to develop and verify the model.

It may not be necessary to directly mobilize all of the material once breakthrough has occurred because some of the fluid brought to the surface during discharge may stay there during the refill stage of the PJM cycle. For mass continuity to be satisfied, this implies that the unmobilized annulus of material

must move downward during refill. After sufficient cycles, this annulus has completely mobilized. If the annulus is able to stick to the vessel wall, the above-mentioned phenomena will not apply.

3.3 Scaling

Small-scale testing is a common approach used successfully in the many varied fields of applied fluid dynamics. The success of the approach depends greatly on the fact that system performance depends on certain nondimensional groupings of physical parameters. If these parameter groupings can be preserved at different geometric scales (i.e., large and small), the essential behavior of the system will be the same at both. This principle is referred to as *similarity* in the theory of fluid dynamics engineering. Limitations of scaled testing are attributed to the inability to match important nondimensional parameter groupings at both scales. In complex fluid dynamic problems, there can be many nondimensional parameter groups; however, often the essential behavior of the phenomenon is dominated by only a few key groups. In this situation, small-scale testing can produce results that are very close to large-scale behavior.

In the previous section, dimensional physical properties were introduced by virtue of physical laws. Nondimensional parameters then appeared by virtue of the mathematics. In this section, potentially relevant physical properties are identified and discussed and ranked by importance. Nondimensional parameters are then formed by virtue of dimensional analysis.

3.3.1 Important Properties, Parameters, and Nondimensional Groups

The following is a list of pertinent waste properties and system parameters to be used in forming nondimensional parameter groups:

- Waste properties
  - ρ slurry density (kg/m^3) (assumes well-mixed slurry with no settling)
  - τ_s slurry shear strength (Pa)
  - τ_y laminar flow yield stress (Pa) (from Bingham plastic fit of waste rheogram)
  - K laminar flow consistency (mPa-s) (assumed to be effective Newtonian viscosity [μ] in turbulent region)
  - t_{rel} slurry relaxation time (s) (characteristic response time of gelled slurry to an impulse)
- Physical parameters
  - u_0 PJM jet velocity (m/s) (may be replaced with an averaged velocity)
  - d_0 PJM nozzle diameter (m)
  - t_D PJM nominal drive time (s) (or actual drive time)
  - t_C cycle time (s)
  - H waste fill level (m)
  - V vessel fluid volume (m^3)
  - V_{PT} pulse tube volume (m^3)
  - p average hydrostatic pressure $\rho gH/2$ (Pa)
  - Q_0 PJM flow rate (per pulse) $(\pi/4)u_0 d_0^2$ (m^3/s)
  - P_0 PJM hydraulic power (per pulse) $(\pi/8)\rho u_0^3 d_0^2$ (W)

The relevant nondimensional parameter groups for the physical system are as follows:

Yield Reynolds number: $$Re_\tau = \frac{\rho u_0^2}{\tau_s}$$

The yield Reynolds number is the ratio of dynamic stress to slurry strength which directly affects the size of the mixing cavern. The yield Reynolds number can also be formed with the Bingham yield stress in the denominator. Re_τ is considered a dominant nondimensional parameter.

Jet Reynolds number: $$Re_0 = \frac{\rho u_0 d_0}{K}$$

The jet Reynolds number is the ratio of dynamic stress to viscous stress. It affects the degree of turbulence in the mixed region as well as weakly affecting stress at the cavern and boundary layers. It is considered a *secondary* nondimensional parameter.

Non-Newtonian stress ratio: $$N_\tau = \frac{\tau_s}{\tau_y}$$

The non-Newtonian stress ratio is the ratio of shear strength to Bingham yield stress. It may affect boundary layer structure and possibly the friction coefficient at the cavern boundary. The importance of this parameter is considered low.

Strouhal number: $$S_0 = \frac{t_D u_0}{d_0}$$

The Strouhal number is the ratio of pulse time to flow time scale. It affects the degree to which flow approaches steady jet behavior and is considered a primary nondimensional parameter. In the limit of steady jet flows, the Strouhal number become infinite, and the effects of pulsation are no longer present. For small Strouhal numbers, the mixing behavior will be highly dominated by pulsation effects.

Deborah number: $$D_0 = \frac{t_D}{t_{rel}}$$

The Deborah number is the ratio of pulse time to material response time. It affects how well non-steady flow at the cavern interface mobilizes gelled slurry and is considered a *secondary nondimensional parameter*.

Pressure ratio: $$P_R = \frac{p_a}{\rho g H}$$

The pressure ratio is the ratio of ambient pressure to static head. It affects the scaling of gravity refill of a PJM but should not affect the discharge flow.

Densimetric Froude Number: $F_0 = \frac{u_0}{\sqrt{\Delta\rho g H/\rho}}$

The Densimetric Froude number is the ratio of the potential energy to kinetic energy of flow. It requires density stratification and affects the ability of a jet to transport material upward. The importance of this parameter is considered low due to minimal solids settling in the turbulent region.

Other parameter groups are sometimes used in the literature that are a combination of the yield Reynolds number and jet Reynolds number. For example,

Yield number: $Y = \frac{\tau_s d_0}{K u_0} = Re_0 / Re_\tau$

Hedstrom number: $He = \frac{\rho \tau_s d_0^2}{K^2} = Re_0^2 / Re_\tau$

An alternative form of the yield Reynolds number exists, which is the ratio of dynamic stress to the total Bingham stress (yield and viscous strain):

Combined Reynolds number: $Re = \frac{\rho u_0^2}{\tau_s + K u_0 / d_0} = \frac{Re_\tau}{1 + Re_\tau / Re_0}$

3.3.2 Geometric Scaling Approach

The non-Newtonian test program uses geometric scaling. We define the geometric scale factor, s, as

$$s = \frac{L_L}{L_S} \tag{3.36}$$

where L_L is any characteristic linear dimension of the large-scale system (such as tank diameter, nozzle diameter, and waste level). At small scale, every linear dimension, L_S, is reduced or *scaled* by s (i.e., $d_{0_S} = d_{0_L}/s$, $D_{T_S} = D_{T_L}/s$, $H_S = H_L/s$). Thus the ideal small-scale test is an exact geometric miniature of the large system, with all areas scaled according to

$$A_S = \frac{1}{s^2} A_L \tag{3.37}$$

and all volumes scaled according to

$$V_S = \frac{1}{s^3} V_L \tag{3.38}$$

Typically in scaled fluid mixing tests, scale factors up to about 10 are considered acceptable; that is, much of the important physics can be captured at small scale. For the non-Newtonian test program,

design of scaled prototypic vessels were limited to conservative scale factors in the range of 4 to 5 due to the relatively new nature of the tests and the importance of the outcome.

When testing at small scale, one must determine how to scale velocity (i.e., PJM drive velocity, u_0). One choice is to scale velocity by the scale factor. This is problematic, however, because it tends to reduce the Reynolds number by $1/s^2$ and introduce further difficulties with the scaling of time. A better choice is to keep jet velocity constant at both scales:

$$u_{0_S} = u_{0_L} \tag{3.39}$$

With geometric and constant velocity scaling, nozzle flow rates per pulse scale according to

$$Q_{0_S} = Q_{0_L} / s^2 \tag{3.40}$$

Jet hydraulic power also scales similarly. However, power per unit volume scales according to

$$\left.\frac{P_0}{V}\right)_S = s\left.\frac{P_0}{V}\right)_L \tag{3.41}$$

For steady jet mixing, time does not come into play. However, PJM operation is a periodic process. Therefore, the scaling of time must be addressed.

If velocity is held constant and the geometry is scaled, then it follows that all imposed time scales must be reduced at small scale. Similarly, to keep the jet discharge velocity the same while scaling pulse volume geometrically, the pulse time will be reduced by the scale factor according to

$$t_{DS} = \frac{1}{s} t_{DL} \tag{3.42}$$

Hence the PJM drive time, refill time, and cycle time are all reduced by s at small scale.

3.3.3 Scaling Nondimensional Parameters

In general, for a given non-Newtonian PJM mixing test, the nondimensional cavern height should depend on all of the nondimensional parameter groups:

$$\frac{H_C}{D_T} = f\left(Re_\tau, Re_0, N_\tau, S_0, D_0, F_0\right) \tag{3.43}$$

Similarly, nondimensional mixing time, t_M, (time to steady cavern formation, time to breakthrough, or time to full mobilization) should depend on the same parameters:

$$\frac{t_M}{t_D} = g\left(Re_\tau, Re_0, N_\tau, S_0, D_0, F_0\right) \tag{3.44}$$

The ideal small-scale test is one in which the measured nondimensional cavern height and mixing time are the same as those at full scale. Hence, the extent to which the nondimensional parameters scale will determine the success of the small scale test approach. To this end, we consider how each of the nondimensional parameters scale with the geometric scale factor, s:

Yield Reynolds number: $Re_{\tau S} = Re_{\tau L}$

The yield Reynolds number will be the same at both scales as long as the simulant used has the same shear strength, τ_s and density, ρ:

Jet Reynolds number: $Re_{0s} = \frac{1}{s} Re_{0L}$

The jet Reynolds number at small scale is reduced by the geometric scale factor. For turbulent conditions, this should introduce only minor differences in test results because the Reynolds numbers in both tests are quite large. The potential need for a minor Reynolds number correction to small-scale results should be evident from the scaling tests. If necessary, the Reynolds number can be matched at small scale by reducing the consistency or viscosity by the factor $1/s$.

Non-Newtonian stress ratio: $N_{\tau S} = N_{\tau L}$

The non-Newtonian stress ratio will be the same at both scales if the same simulant is used.

Strouhal number: $S_{0S} = S_{0L}$

The Strouhal number will be the same at both scales.

Deborah number: $D_{0S} = \frac{1}{s} D_{0L}$

The Deborah number will be smaller in the small-scale tests. If the Deborah number is large overall, the effect will be negligible. If the Deborah number is close to unity, then the small-scale results will be conservative.

Densimetric Froude number: $F_{0S} = sF_{0L}$

The densimetric Froude number will be larger at small scale. This would produce non-conservative results at small scale should the effect be important. As long as simulants with very slow particle settling are used, this effect should be negligible.

3.3.4 Summary of Scaled Test Approach

To summarize, the primary nondimensional parameters required for small-scale testing are the yield Reynolds number, Re_τ, and the Strouhal number, S_0. If these are matched at large and small scale, the nondimensional cavern heights and mixing times should be the same to a first-order approximation:

$$\left.\frac{H_C}{D_T}\right)_S \approx \left.\frac{H_C}{D_T}\right)_L \tag{3.45}$$

and

$$\left.\frac{t_M}{t_D}\right)_S \approx \left.\frac{t_M}{t_D}\right)_L \tag{3.46}$$

Given that full-scale cavern heights are adequately predicted by reduced-scale testing, it follows that specification of PJM operation parameters sufficient to achieve complete mobilization with no stagnant regions at reduced scale will produce designs that also provide complete mobilization at full scale. Further, testing at reduced scale will provide a degree of conservatism so long as the consistency, K, of the simulant is the same as the full-scale bounding value. This is true because the jet Reynolds number will be smaller in the scaled test than in the full-scale system:

$$Re_{0_S} = \frac{1}{s} Re_{0_L} \tag{3.47}$$

If adequate mixing is achieved in a reduced-scale test, then it can be expected that the degree of turbulence will be greater in the full-scale vessel due the associated effect of increased jet Reynolds number.

4.0 Synopsis of Testing

The PJM Task Team developed an integrated approach for scaled testing to validate PJM mixing in WTP vessels containing non-Newtonian fluids. Scaled PJM mixing tests using a 4PJM array were conducted at large scale in the large-tank 336 Building test facility to provide design information on the operating parameters critical for the mixing and mobilization of the tank contents. Experiments conducted using geometrically scaled test stands at 1/4 scale at APEL at 1/9 scale SRNL were conducted under similar conditions to develop test data to support a methodology for predicting large-scale behavior from the small-scale test results. The test data described in this section and Appendixes A, B, and C are coupled with the analysis developed in Section 5 to evaluate the range of applicability for the scaling methodology.

These experiments addressed the following fluid dynamics issues related to PJM operation with non-Newtonian fluids:

- Determine the time to fully mix stagnant Laponite simulant in 336 at large scale, in APEL at 1/4 scale (24590-WTP-TEF-RT-03-053), and at SRNL at 1/9 scale (24590-WTP-TEF-RT-03-058).
- Perform constant drive volume testing as a function of nozzle velocity using clay mixture simulant at three scales (24590-WTP-TEF-RT-03-083).
- Determine the time to fully mix clay simulant at two scales: in 336 at large scale and in APEL at 1/4 scale (24590-WTP-TEF-RT-03-083).

To address these issues, tests were conducted with two non-Newtonian simulants, Laponite (transparent) and a kaolin-bentonite clay mixture (an opaque HLW simulant); these simulants are described in Appendix D.

4.1 Test Stands

The scaled test stands are described in the following sections.

4.1.1 336 Large-Scale 4PJM Test Stand

The large-tank test stand (also referred to as the "supernatant tank") shown in Figure 4.1 is a vertically oriented cylindrical steel vessel of 12.75 ft (3.87 m) internal diameter (ID) and 14.92 ft (179 inches, 4.57 m) depth. The bottom of the tank is elliptically (2:1) shaped and has a radius of 6.4 ft (1.95 m) and a height of 3.2 ft. (0.971 m). The large test tank has a liquid level-to-tank diameter ratio of approximately 0.89. Transfer lines (not shown in the figure) at the top and bottom of the tank allow adding or removing materials during loading or disposal operations. The supernatant tank is positioned on three load cells, which can be used to determine the weight of the tank and its contents.

The PJM system installed in the large tank consists of four pulse tubes, each with a cylindrical section of 10 ft (3.05 m) length, 2 ft (0.610 m) ID, and 0.25 inch (6.35E-03 m) wall thickness. Each tube is elliptically (2:1) rounded at the top end with an opening for a 2-inch (5.10E-02-m) flange connection. The bottom end of the pulse tube is tapered down at an included angle of 60º to a 4-inch (0.102-m) nozzle. The overall height of the pulse tube, shown in Figure 4.2, is approximately 12 ft (3.66 m).

Figure 4.1. Photograph of Large-Tank Test Stand (Supernatant Tank)

Figure 4.2. One of the Pulse Tubes Before Installation in the Large-Tank Test System. The pulse tubes are connected to 2-inch (0.0508-m) pipe couplings that enable insertion of level gauges and attachment of the air/vacuum lines required for PJM operation.

4.1.2 APEL 1/4-Scale 4PJM Test Stand

The APEL 4PJM test stand is a linearly scaled version of the large scale 4PJM test stand in the 336 test facility. The scale factor is 4.53. It consists of four PJMs constructed of a 5-inch (5.29-inch ID) schedule 10 stainless steel pipe tapered to a custom-built nozzle of 0.88-inch ID. The length of the cylindrical section of the PJMs is 48 inches. The height was intentionally set longer than the PJMs in the 336 test facility to enable testing at higher H/D_T ratios than were possible at the large scale. The PJMs are situated around the center of the tank in a square at a pitch diameter of 21.24 inches. The height of the nozzles from the tank floor is 2.1 inches. The schematic in Figure 4.3 shows the placement of the four pulse tubes in the transparent acrylic tank.

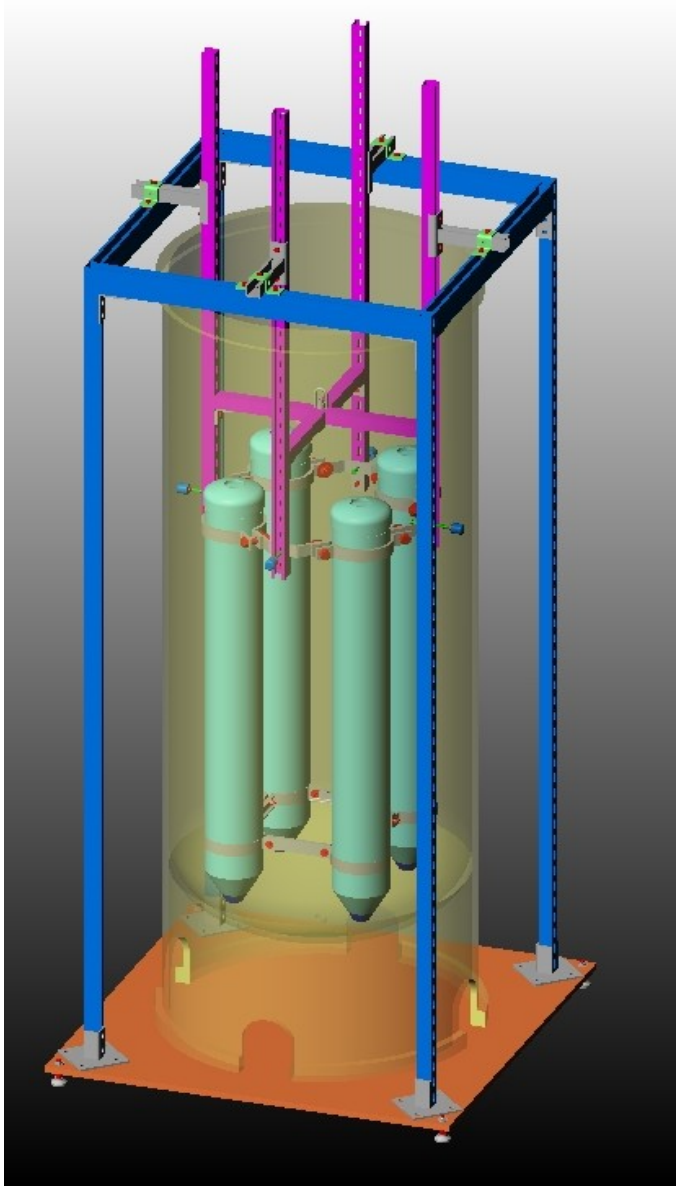

Figure 4.3. Schematic of APEL 4PJM Pulse Tube Square Array in the Tank with Supporting Structure

4.1.3 SRNL 1/9-Scale 4PJM Test Stand

The SRNL 4PJM test stand (Wilson et al. 2004) shown in Figure 4.4 is also a linearly scaled version of the 4PJM setup in the 336 test facility. The SRNL 4PJM test stand is a clear cylindrical shell with a stainless steel 2:1 elliptical head. The test tank's internal diameter is 17.25 inches (average ID) and the internal height is 43 inches. Four PJMs fabricated from 2.5 NPS, schedule 10S stainless steel pipe are spaced at 90-degree intervals on a 10.64-inch pitch diameter and discharge vertically downward. Average internal diameter of the pulse tube is 2.63 inches. The 60-degree nose cone on the outlet of the PJM has a nominal nozzle diameter of 0.45 inch, and the nozzle centerline elevation is 1 inch above the tank head. As-built inspection of the PJM nozzle bores determined that the internal diameter of two PJM nozzles was 0.44 inch, and the internal diameter of the other two was 0.45 inch. A drain/sample valve on the center of the tank head provides a flush interior profile.

Figure 4.4. Photograph of the SRNL 4PJM Test Stand

4.2 Instrumentation

The three test stands all used similar instrumentation and data acquisition systems. The clear 1/4- and 1/9-scale systems required less instrumentation than the steel large-scale systems because engineers could monitor operation through the tank walls. Additional cameras were required for the large-scale tank to provide mechanisms for viewing fluid motion remotely.

4.2.1 Large-Scale Test Stand Instrumentation

Instrumentation for the large-tank test stand is listed in Table 4.1. Each PJM was fitted with a Drexelbrook liquid-level sensor/transmitter and a Cecomp pressure transducer to provide continuous measurement of the slurry level and pressure inside the PJM during operation. Additional sensors are Type K thermocouples (T/C) for measuring the temperature of tank contents and ambient temperature. The data were digitally recorded on a computer using a DASYLab data acquisition and control system (DACS).

Simulant motion was detected visually with cameras and velocity probes, as shown in Figures 4.5 and 4.6. Video systems in camera wells detected the mixed and unmixed regions in transparent simulants by observation of bubbles. A small video camera moved up and down inside the transparent camera well to record the images. Bubbles were always present in the clear simulant, and their motion was used to locate the boundaries between the mixed and unmixed regions.

Table 4.1. Data Acquisition System Resolution for Sensor Input for Large-Tank Test Stand

Sensor	Input Range to DACS	DACS Resolution
Valeport Velocity Sensors	± 5 m/s	7.63E-05 m/s
Drexelbrook Level Sensor	0–140 in.	2.20E-03 in.
Cecomp Pressure Sensor	0–100 psia	1.53E-03 psia
Type K T/C	0–50ºC	7.63E-04ºC
Load Gauges for Tank Weight	0–300 K lb	5 lb

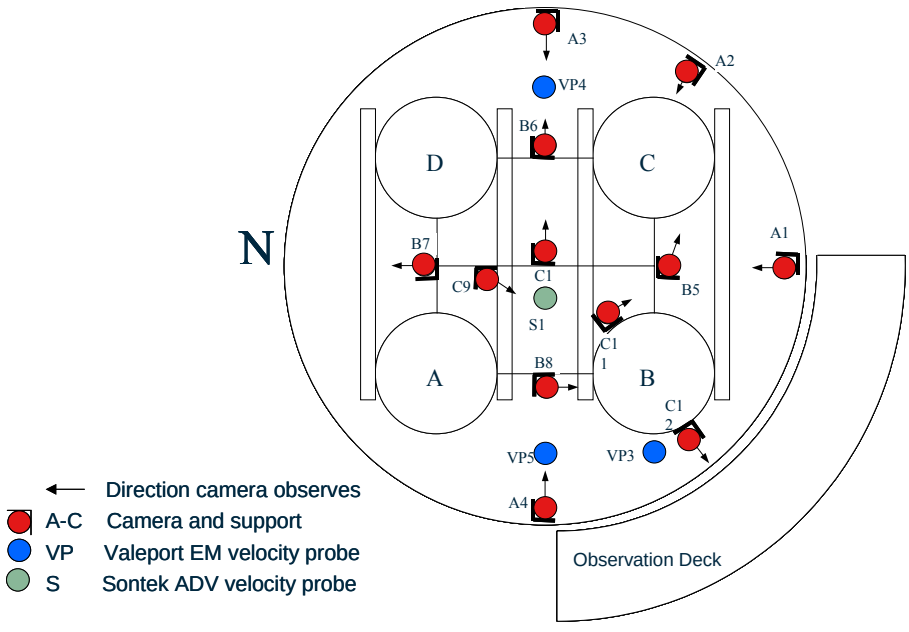

Figure 4.5. Top View of Instrument Locations for the Large-Tank PJM Test Stand

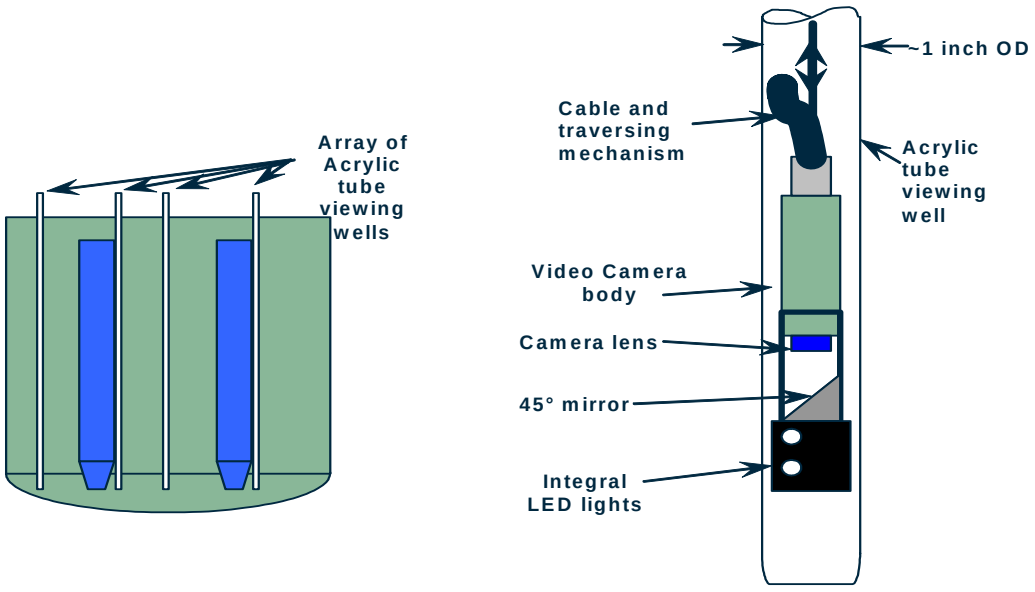

Figure 4.6. Side View of Cameras and Camera Well Configuration Used for Fluid Observation in the Large-Tank PJM Test Stand

Video camera observation wells were used to monitor the tank for the establishment of a repeating, periodic condition indicated by near zero growth in the size of the mobilized (cavern) region. At this periodic condition, the camera wells were used to characterize the extent of the mobilized volume within the tank. Cavern height measurements obtained using camera wells and/or velocity probes were the critical test measurements made during this activity. These measurements were quantifiable to a performance check.

4.2.2 1/4-Scale Test Stand Instrumentation

Instrumentation for the 1/4-scale test stand is listed in Table 4.2. Each PJM was outfitted with a Drexelbrook liquid-level capacitance sensor/transmitter and an Endress+Hauser ceramic pressure transducer, which enabled continuous measurement of the slurry level and pressure inside the PJM during operation. Additional sensors included in the test system are Type K thermocouples that measure the temperature of the tank contents and ambient temperature.

The pressure transducer (Cerabar T PMC 131 from Endress+Hauser) has a capacitive ceramic sensor for absolute and gauge pressure. It is designed to measure absolute pressure for gases, vapors, and liquids. It is extremely stable and resistant to overload. The pressure to be measured causes a small deflection of the ceramic diaphragm of the sensor; a change in capacitance proportional to the pressure is measured by electrodes on the ceramic sensor. This pressure transducer can measure a maximum of 40 bar. The output signal is 4-20 mA.

The ultrasonic velocity probe (UVP) system used to measure the upwelling velocities was a Monitor Model UVP-DUO with Software Version 3 described in Section 4.7. For the upwell velocities measured at APEL and 336, all channels between 25 and 40 mm were averaged to determine velocity.

Table 4.2. Measurement and Test Equipment List for 1/4-Scale Test Stand

Measured Variable	Sensor	Vendor	Accuracy
Level	Capacitance level probe	Drexelbrook	±0.1 in
Pulse tube pressure	Pressure transducer with capacitive ceramic sensor	Endress+Hauser	±0.1 psi
Temperature	Type K T/Cs	Omega	±2°C

4.2.3 1/9-Scale Test Stand Instrumentation

Instrumentation for the 1/9-scale test stand is listed in Table 4.3. The Drexelbrook capacitance level probes were performance checked in situ with the test tank filled with simulant. The level probe transmitter zero and span adjustments were set so that the probe output readings matched the tank level as measured by the adhesive backed tape measure fixed to the clear acrylic tank (±1/8 in.). The level transmitter output signals were input to the DACS for data logging and control during PJM operation. The output signal from PJM1 level probe was used by the DACS to control the system pulse cycle. Output signals from the remaining level probes were used for data acquisition only (i.e., to log the respective level inside the other pulse tubes).

Table 4.3. SRNL 4PJM DACS Instrument Calibration, Range, and Accuracy for 1/9-Scale Test Stand

Component Identification	Manufacturer (model)	Function/Measured Variable	Calibrated or Performance Checked by	Range (accuracy)
LE-001 to LE-004	Drexelbrook (700-002-027-I024.0)	PJM level	Performance Check/User	6.5 to 25.5 inches (±0.25% of span = ±0.05 in.)
PT-001 to PT-004	Rosemount (3051CD3A22)	PJM pressure	Calibrated/SRNL EDL Calibration Services	-5 to 35 psig (±0.25% of span = ±0.1 psig)
PT-005	Rosemount (1144A0200A22)	Compressed air supply pressure	Calibrated/SRNL EDL Calibration Services	0 to 50 psig (±0.25% of span = ±0.13 psig)
TE-001	Omega (Type E T/C)	Slurry/liquid temperature	Calibrated/SRNL EDL Calibration Services	0 to 100°C (±1.7°C)
DACS	National Instruments (NI 6011E)	DACS analog input board	Calibrated/SRNL EDL Calibration Services	All channels (±1.51 mV)

A Drexelbrook capacitance liquid-level sensing element/transmitter and Rosemount pressure transmitter were installed on the PJM to continuously measure the simulant level and pressure inside the PJM during operation. The bulk tank temperature was monitored with a Type E T/C.

The change in liquid height in the pulse tube was measured using a 24-inch-long Drexelbrook capacitance level sensor/transmitter. These transmitters were special ordered with no time delay (20 ms response time) under manufacturer's modification 91-133. Due to spatial constraints in accommodating the pressure/vacuum line, pressure port, and level probe connection, the capacitance probe was mounted 1/4 inch off the pulse tube centerline. This should, however, have a negligible impact on level reading. The 0.84-inch OD probe was threaded into the 1 inch NPT coupling on top of the PJM. The 4-20 mA transmitter output signal was input to the DACS for logging during PJM operation.

4.3 Operation

The operation of the PJMs with any simulant was characterized by stroke length, drive time, pulse tube pressure, and cycle time. The stroke length is the distance the fluid being mixed is driven down the pulse tube in a period of time called the drive time. The pulse tube pressure is the measured gauge pressure in the pulse tube that provides the driving force for expelling the fluid out of the pulse tube. The cycle time is the period of time it takes for the system to pulse (to expel fluid from the pulse tube), refill the pulse tube to the original level, pause if desired, and be ready for the next pulse.

4.3.1 Large-Scale Test Stand Operation

The large-tank PJM cycling was controlled using prototypical components, including a combination of jet pump pairs (JPPs) and solenoid valves to regulate the suction and discharge of the liquid to and from the pulse tubes. The JPPs were connected to the pulse tubes using 2-inch (5.08E-02-m) ID wire reinforced polyvinyl chloride (PVC) tubing.

A compressor/accumulator combination was used to regulate the airflow to the JPPs. The sequence of operation and cycle frequency of the PJMs was controlled by a PJM pressure (PRESCON™) controller, an AEA Technology proprietary control system. The controller monitors pressure signals using pressure transmitters that are a part of the JPP control module. The PJM pressure controller permits various combinations of pulse tube operation (all four at once, two at a time, or one at a time) and cycle times. Before testing started, controller settings were confirmed and the air pressures to the drive/vent sides of the JPPs were adjusted to 1) set cycle times to those required for operation and 2) observe drive/refill cycles for the four PJMs.

To ensure that all the PJMs operate (as closely as possible) in an identical manner, the pressure inside each PJM/JPP was individually measured using pressure transducers mounted on top of the pulse tube and at the air inlets to the drive and suction sides of the JPPs. Although independent pressure measurements within the PJMs and the JPP control module were made during the testing, the PJMs were controlled with the pressure control system. In other words, the drive, vent, and suction times were set in the PJM controller to cycle the PJMs repeatedly at the prescribed period.

4.3.2 1/4-Scale Test Stand Operation

Unlike conventional PJMs, whose operation is regulated by JPPs driven by compressed air, the APEL 4PJM test system used a series of solenoid valves and a combination of an air compressor and vacuum pump to simulate the drive and suction phases of PJM operation. These operations were controlled through a control logic program using DASYLab DACS, which turns the appropriate solenoid valves on and off at specified time intervals. The duration of each phase, the applied pressure, and vacuum are all variables that can be varied independently to simulate the operation of the actual PJMs.

Operation of the APEL 4PJMs is characterized by stroke length, drive time, pulse tube pressure, and cycle time. A cycle for the APEL 4PJM system consisted of a drive phase at which the pulse tube pressure was the highest followed by a brief vent of the pulse tube to release the pressure and then a vacuum condition that caused the pulse tube to refill to the starting level. Hydrostatic head also aided the refilling of the pulse tubes. The cycle time and the physical dimensions of the PJM systems are scaled linearly for 336, APEL, and SRNL. As a result the pulse tube pressure and the resulting pulse tube nozzle velocities are essentially the same for all of the systems under the scaled conditions.

4.3.3 1/9-Scale Test Stand Operation

This 4PJM test stand used a series of solenoid valves with a distribution manifold and the combination of a 125-psig compressed air supply and vacuum pump to produce the drive and suction phases of PJM operation. The compressed air and vacuum were applied to the 4PJM array through a distribution manifold. PJM operations were controlled through a control logic program using LabView software on a Dell OptiPlex GX1p PC running Windows NT Workstation Version 4.0. The duration of each phase and the applied pressure can be varied to simulate the operation of the JPPs. Testing was conducted using four PJMs on a 10.64-in. pitch diameter in the test tank and discharging vertically downward.

There are three solenoid valves, one each for compressed air, vent, and vacuum. The system solenoid valves were controlled to operate the 4PJM array in a time-scaled fashion. A system cycle time consists of a drive time (t_D), a vent time (t_V), and a suction time (t_S). The drive time is entered for a given supply pressure to achieve the desired target nozzle velocity and discharge volume. For a given discharge volume, the vent time is adjusted to obtain the targeted system cycle time. The vacuum cycle ends when the measured level in PJM1 reaches the input starting level for the next drive cycle to begin.

4.4 Test Matrix for the Three-Scales of Experiments

The pertinent parameters that were developed to complete the scaling experiments are vessel scale, fluid rheology, and test condition. Three types of test conditions were evaluated to determine scaling of cavern size, breakthrough, and time to mix.

4.4.1 Vessel Scale

Tests to evaluate the scaling relationships for PJM operation were conducted at the three scales, as shown in Table 4.4. The tank volumes range from 30 to 12,000 gallons.

Table 4.4. Vessels Used for 4PJM Scaling Tests

Vessel	Nominal Volume (gal)	Vessel Diameter (m)	PJM Nozzle Diameter (cm)	Scale Factor (s)
336	12,000	3.88	10.2	1
APEL	250	0.858	2.2	4.53
SRNL	30	0.438	1.1	8.9

4.4.2 Simulant Rheology

The tests were conducted using two simulants, Laponite and a kaolin-bentonite clay mixture. The important physical parameters for the simulants are density, shear strength, yield stress, and consistency. Laponite was used primarily to represent the gelled-state conditions encountered by PJMs upon restart from idle periods. As such, the shear strength was considered the important rheological parameter. For low-strength Laponite (30 Pa shear strength) that has been fully sheared, the yield stress is essentially zero and the material behaves like a Newtonian fluid. For higher-strength Laponite (80–120 Pa), the yield stress was typically in the 10-Pa range. The Laponite used had a density of 1000 kg/m^3, shear strength that ranged from 30 to 120 Pa, and a consistency in the 10 to 20 cP range. The clay used was a non-Newtonian Bingham plastic material designed to rheologically approximate HLW sludge with a yield stress of 30 Pa and a consistency of 30 cP. The density was 1200 kg/m^3, yield stress ranged from about 20 to 45 Pa and consistency from about 10 to 30 cP. The clay also developed shear strength when at rest.

The value of shear strength typically was about 1.5 to 2 times the yield stress and developed over many hours. The shear strength for the clay was not considered important to the test results obtained because the clay was mixed before testing. Simulant properties are described in detail in Appendix D.

4.4.3 Test Matrix

The test types include cavern, breakthrough, and time-to-mix tests.

4.4.3.1 Cavern and Breakthrough Tests

The initial test matrix was formulated to permit evaluation of the maximum range of cavern sizes attainable by the PJM test stand. The test matrix proposed in the test plan is listed in Table 4.5. It incorporated the following parameters:

U	Nominal PJM discharge velocity = V_o/t_D
V_P	PJM pulse volume
V_0	Similar to AEA recommended prototypic discharge volume.
$V_{system\ max}$	Maximum discharge volume that can be achieved with the large-scale (336 Building) air supply system and PRESCON controller.
U_1	Minimum velocity that creates cavern interfaces detectable above the top of the PJM conical nozzles. This velocity was determined during test sequence 1 (refer to Table 4.5)
$U_{system\ max}$	Maximum achievable velocity with large-scale (336 Building) air supply system.
U_4	Similar to AEA's recommendation for prototypic discharge velocity if U_{max} is greater than 110% of AEA's recommendation for prototypic velocity.
U_{max}	Maximum velocity such that PJM operation at U_{max} and V_0 does not cause surface breakthrough. Potentially $U_{max}= U_{system\ max}$

For all the tests, the PJM operation was synchronized, that is, all tubes were filled and discharged simultaneously. The current approach calls for the total cycle time, t_C, to be held constant if the criteria are achievable with the current PJM control systems. The cycle time used was obtained from the sum of the maximum discharge and refill times required to complete the initial test matrix. The cycle times for both large- and small-scale systems were compared and the limiting condition after applying the geometric scale factor determined the cycle times for both large and small-scale test setups.

For specified test conditions listed in Table 4.5, the cavern height was monitored until a repeatable, periodic condition satisfying a specified acceptance criterion was observed with respect to cavern height. The acceptance criterion was specified in the test procedures used to conduct the test operations. Intermediate parameters (such as U_2, U_3, and V_1 through V_4) were estimated with the intent to achieve uniform cavern growth in each test condition. Additional test conditions were evaluated as needed to characterize cavern size over the full range of achievable operating parameters.

4.4.3.2 Time-to-Mix Tests

Time-to-mix tests were conducted with both the Laponite and kaolin-bentonite clay simulants. For the Laponite tests, the Laponite was allowed to gel at least 18 hours; the rheology sample was taken, and shear strength was determined before and after the test. For the clay tests, the target yield stress was 30 Pa with a consistency of 30 cP. All scaled testing done in the APEL and 336 4PJM test platforms used the same clay mixture simulant from the same batch and ensured that the rheological properties were within ±20%. During PJM operation, the time to the following points was noted:

- Time to breakthrough at the surface

- Time to observe fluid movement down the tank wall
- Time for the fluid at the wall to exhibit turbulent motion (fully mixed)

Measurement methods included using

- Colorimetric dye method for determining mixing volume and uniformity
- Radiofrequency (RF) tags to help determine mixing volume and uniformity
- Polycarbonate beads to qualitatively determine mixing volume and uniformity with these results for indication only.
- Velocities measured using a UVP.

Table 4.5. Description of PJM Test Conditions

Test Sequence	Test Description	Test Cases
1	Initial **constant volume tests** to determine at a minimum the minimum and maximum discharge velocities (discharge time) to be used for the test matrix.	1) Velocity ramped up to determine minimum velocity that yields cavern interface heights above the top of the PJM cones. PJMs operated at conditions U_1V_0. 2) Velocity ramped up to maximum achievable velocity that does not result in cavern breakthrough at the simulant surface. PJMs operated at conditions $U_{max}V_0$ 3) PJMs operated at conditions $U_{system\ max}V_o$ - Verify/Determine relative interface position with in-tank camera to best characterize cavern elevation. - Evaluate placement of EM probes. - Additional values of U for $U_1<U<U_{max}$ may be evaluated if time and test conditions allow. - Determine if operating at conditions of $U_{system\ max}$ and $V_{system\ max}$ can mobilize the fluid free surface.
2	**Constant volume tests** at V_0 with caverns measured at increasing values of velocity U.	1) Repeat of U_1V_0 from test sequence 1. 2) U_2V_0 with $U_1<U_2$ 3) U_3V_0 with $U_2<U_3$ 4) U_4V_0 with $U_3<U_4<U_{max}$ 5) Repeat of $U_{max}V_0$ from test sequence 1.
3	**Constant velocity tests** at U_3 with discharge volume, V, incrementally increased.	1) Repeat of U_1V_0 from test sequence 1. 2) U_3V_1 where $V_1<<V_0$ 3) U_3V_2 where $V_1<V_2$ 4) U_3V_3 where $V_2<V_3$ 5) U_3V_4 where $V_3<V_4<V_0$ 6) repeat of U_3V_0 from test sequence 1
4	Optional testing depending on previous test results and available schedule. **Constant velocity tests** at U_{max} with discharge volume, V, incrementally increased.	1) $U_{Max}V_1$ where $V_1<<V_0$ 2) $U_{Max}V_2$ where $V_1<V_2$ 3) $U_{Max}V_3$ where $V_2<V_3$ 4) $U_{Max}V_4$ where $V_3<V_4<V_0$ repeat of $U_{max}V_0$ from test sequence 1
5	**Transient tes**t for U_4V_0 or $U_{max}V_0$	1) Starting with setup (gelled) material in tank record transient for operating conditions of $U_{max}V_0$ 2) If $U_{max}< U_{system\ max}$, velocity ramped up to determine minimum velocity required to mobilize tank surface (fluid free surface)

4.5 Cavern Scaling Tests

Experiments to characterize the development and size of a cavern were conducted at all three scales using well characterized simulant with approximately matching rheological properties. A variety of techniques were used to make a measurement of the cavern size. These ranged from simple visual observations where the cavern height was measured using a tape measure fixed to the side of the mixing vessel, to the use of video cameras in camera wells in the 336 mixing vessel. The 336 vessel is made of stainless steel and is opaque, whereas the APEL and SRNL vessels are transparent. The details describing the tests conducted at the three scales are presented in Appendixes A, B, and C.

Brilliant Blue dye was added to the mixing cavern of some of the Laponite tests to more clearly delineate the cavern. This was done by adding a concentrated dye solution into the bottom portion of the tank. Dye improved the contrast between the mixing and non-mixing portions of the fluid. After each individual test, the tank contents were homogenized by vigorously pulsing the jets. Additional dye or a different dye color could be used to produce good contrast between mixing and non-mixing regions. The dye approach to marking the cavern was also used with the kaolin-bentonite simulant with some success.

Cavern tests were designed to evaluate the size of the mobilized region of a cylindrical tank with an elliptical tank bottom and symmetrically spaced PJM either though the top of one of the pulse tubes discharging vertically downward. Breakthrough occurs when the cavern reaches the fluid surface. During PJM operation the tank surface level goes up and down. For consistency, measurements were made at full PJM discharge when the surface level was at its maximum. Tank fill levels are reported for static conditions. Therefore, reported cavern heights near breakthrough may be slightly higher than static vessel fill levels.

4.5.1 Large-Scale Tests

Data from the specific large-scale tests that have been used to support the scaling analyses for cavern development and breakthrough are summarized in Tables 4.6 through 4.9. These tests represent experiments that met the test conditions useful for inclusion in the scaling analysis presented in Section 5. All of the tests in the large tank were conducted at a nominal H/D_T ratio of 0.9. The tank fill height is shown in Table 4.6. To ensure a common basis for comparison between test stands, velocities were calculated from the level probe measurements as listed in Table 4.7; the velocities are defined in Figure 3.3. The rheological measurements for these tests are summarized in Table 4.8. The tests supporting analysis of cavern height and breakthrough are listed in Table 4.9.

Table 4.6. PJM Test Conditions at Large Scale Used to Support Scaling Analysis

Reference Number	Test Date and Number	Simulant	Tank Diameter D_T (in.)	Nozzle Diameter d_0 (in.)	Liquid Height H (in.)	H/D_T	Number of PJMs
L-1	030831-1-1	Laponite	153	4	138.0	0.902	4
L-2	030831-1-3	Laponite	153	4	138.0	0.902	4
L-3	030902-2-1	Laponite	153	4	133.2	0.871	4
L-4	030902-2-2	Laponite	153	4	133.2	0.871	4
L-5	030911-2-1	Laponite	153	4	133.8	0.874	4
L-6	030911-2-2	Laponite	153	4	133.8	0.874	4
L-7	030911-2-3	Laponite	153	4	133.8	0.874	4
L-8	030911-2-4	Laponite	153	4	133.8	0.874	4
L-9	030915-3-1	Laponite	153	4	133.5	0.873	4
L-10	030915-3-2	Laponite	153	4	133.5	0.873	4
L-11	030917-3-1	Laponite	153	4	132.9	0.869	4
L-12	030917-3-2	Laponite	153	4	132.9	0.869	4
L-13	030917-3-3	Laponite	153	4	132.9	0.869	4
L-14	030917-3-4	Laponite	153	4	132.9	0.869	4
L-15	030917-3-5	Laponite	153	4	132.9	0.869	4
L-16	031028-2-1	Laponite	153	4	131.3	0.858	4
L-17	031118-2-1	Laponite	153	4	133.7	0.874	4
L-18	03121502DD1	Clay	153	4	137.7	0.900	4
L-19	04052510HzDF1	Clay	153	4	137.0	0.895	4
L-20	04052510HzDG1	Clay	153	4	137.0	0.895	4

Table 4.7. Velocity at Large Scale Computed from PJM Level Probe Measurements

Reference Number	Test Date Number	Drive Time		PJM Velocity		Level Probe Correction Factor
		Peak Average (s)	Average (s)	Peak Average (ft/sec)	Average (ft/sec)	
L-1	030831-1-1	29.6	30.2	11.3	10.8	1.04
L-2	030831-1-3	16.9	18.3	20.2	18.2	1.04
L-3	030902-2-1	21.7	22.7	16.0	14.7	1.04
L-4	030902-2-2	20.1	21.4	17.9	16.0	1.04
L-5	030911-2-1	22.6	23.6	13.6	12.6	1.04
L-6	030911-2-2	19.5	20.6	16.0	14.7	1.04
L-7	030911-2-3	17.8	18.8	17.4	15.9	1.04
L-8	030911-2-4	16.8	17.8	18.1	16.5	1.04
L-9	030915-3-1	7.8	9.2	20.4	16.1	1.04
L-10	030915-3-2	10.1	11.4	19.7	16.6	1.04
L-11	030917-3-1	10.4	11.5	16.8	14.0	1.04
L-12	030917-3-2	12.6	13.6	16.4	14.2	1.04
L-13	030917-3-3	15.7	16.6	15.8	14.0	1.04
L-14	030917-3-4	18.0	18.8	15.3	13.9	1.04
L-15	030917-3-5	21.2	22.1	14.7	13.5	1.04
L-16	031028-2-1	17.8	19.2	16.8	15.1	1.00
L-17	031118-2-1	20.2	21.7	15.1	13.6	1.00
L-18	03121502DD1	11.4	15.1	21.6	18.0	1.00
L-19	04052510HzDF1	13.5	15.4	21.6	18.8	1.00
L-20	04052510HzDG1	11.4	13.6	22.8	18.7	1.00

Table 4.8. Summary of Rheological Measurements at Large Scale Used to Support Scaling Analysis

Reference Number	Test Date and Number	Initial Shear Strength (Pa)		Final Shear Strength (Pa)		Yield Stress (Pa)	Consistency (Pa-s)	R
		Average	St. Dev.	Average	St. Dev.			
L-1	030831-1-1	98.4	6.0	102.9	6.3	6.60	0.0129	0.977
L-2	030831-1-3	98.4	6.0	102.9	6.3	9.07	0.0123	0.977
L-3	030902-2-1	108.0	1.6	110.8	2.7	7.92	0.0136	0.977
L-4	030902-2-2	108.0	1.6	110.8	2.7	10.38	0.0129	0.976
L-5	030911-2-1	111.6	1.2	123.3	3.4	12.82	0.0147	0.976
L-6	030911-2-2	111.6	1.2	123.3	3.4	11.81	0.0138	0.977
L-7	030911-2-3	111.6	1.2	123.3	3.4	13.18	0.0146	0.977
L-8	030911-2-4	111.6	1.2	123.3	3.4	6.38	0.0146	0.977
L-9	030915-3-1	111.5	9.7	123.0	1.4	13.65	0.0142	0.977
L-10	030915-3-2	111.5	9.7	123.0	1.4	13.65	0.0142	0.977
L-11	030917-3-1	110.9	2.9	128.0	3.3	10.80	0.0146	0.978
L-12	030917-3-2	110.9	2.9	128.0	3.3	13.79	0.0144	0.977
L-13	030917-3-3	110.9	2.9	128.0	3.3	13.53	0.0152	0.979
L-14	030917-3-4	110.9	2.9	128.0	3.3	13.43	0.0154	0.977
L-15	030917-3-5	110.9	2.9	128.0	3.3	12.05	0.0131	0.976
L-16	031028-2-1	123.5	2.0	123.8	5.1	17.96	0.0153	0.983
L-17	031118-2-1	98.4	2.1	107.2	2.4	13.13	0.0126	0.984
L-18	03121502DD1	48.9	8.4	48.9	8.4	41.31	0.0221	0.998
L-19	04052510HzDF1	NA	NA	NA	NA	28.65	0.0198	NA
L-20	04052510HzDG1	NA	NA	NA	NA	28.65	0.0198	NA

Table 4.9. Summary of Cavern Height and Surface Breakthrough Data at Large Scale Identified Using Camera Measurements at Steady State Referenced to the Bottom of the Tank

Reference Number	Test Date Number	Camera Tank Elevations at Steady State							Status at End
		B5 (in.)	B6 (in.)	B7 (in.)	B8 (in.)	C9 (in.)	C10 (in.)	C11 (in.)	
L-1	030831-1-1						66.3	61.9	
L-2	030831-1-3	133.1			138		138.0	138.0	Surface breakthrough
L-3	030902-2-1				88.6		82.1	87.0	
L-4	030902-2-2						133.2	133.2	Surface breakthrough
L-5	030911-2-1	67.3				75.4	76.8	73.9	
L-6	030911-2-2	76.9				80	78.8	74.7	
L-7	030911-2-3				83	83.3	80.5	76.9	
L-8	030911-2-4				92.9	83.9	82.4	84.9	
L-9	030915-3-1	131		130.0	115.1	124.4	134.3	134.4	
L-10	030915-3-2						133.5	133.5	Surface breakthrough
L-11	030917-3-1				56	76.6	75.2	74.9	
L-12	030917-3-2	60.0	58.2	58.8		79.0	78.0	76.8	
L-13	030917-3-3				74.6		76.8	73.3	
L-14	030917-3-4	76.6			83.6		76.0	75.1	
L-15	030917-3-5						75.6	74.0	
L-16	031028-2-1	78.4				80.6	79.6	81.7	
L-17	031118-2-1	106.5	100.3		108.8	87.9	97.9	97.4	
L-18	03121502DD1	NA	NA	NA	NA	NA	NA	NA	Surface breakthrough
L-19	04052510HzDF1	NA	NA	NA	NA	NA	NA	NA	Surface breakthrough
L-20	04052510HzDG1	NA	NA	NA	NA	NA	NA	NA	Surface breakthrough

4.5.2 1/4-Scale Tests

Data from the specific tests conducted at 1/4 scale that have been used to support the scaling analyses for cavern development and breakthrough are summarized in Tables 4.10 through 4.13. These tests represent those that met the test conditions useful for inclusion in the scaling analysis presented in Section 5. The fluid fill height is shown in Table 4.10. To ensure a common basis for comparison of test stands, velocity averages were calculated from the level probe measurements, as listed in Table 4.11. The rheological measurements for these tests are summarized in Table 4.12. These tests that were conducted at two values of H/D_T represent tests that met test conditions for analysis. H is the fill height for the tank (and pulse tubes) at the beginning of the test. Cavern height and breakthrough data are listed in Table 4.13.

Table 4.10. Test Conditions at 1/4 Scale Used to Support Scaling Analysis

Reference Number	Test Date Number	Simulant	Tank Diameter D_T (in.)	Nozzle Diameter d_0 (in.)	Liquid Height H (in.)	H/D_T	Number of PJMs
M-1	030829R01	Laponite	33.8	0.88	29.9	0.88	4
M-2	030829R02	Laponite	33.8	0.88	29.8	0.88	4
M-3	030903R01	Laponite	33.8	0.88	29.3	0.87	4
M-4	030903R02	Laponite	33.8	0.88	29.3	0.87	4
M-5	030905R01	Laponite	33.8	0.88	29.7	0.88	4
M-6	030908R01	Laponite	33.8	0.88	29.4	0.87	4
M-7	030910R01	Laponite	33.8	0.88	29.8	0.88	4
M-8	030913R01	Laponite	33.8	0.88	29.7	0.88	4
M-9	030915R01	Laponite	33.8	0.88	29.6	0.88	4
M-19	030915R02	Laponite	33.8	0.88	29.6	0.88	4
M-11	030916R01	Laponite	33.8	0.88	29.5	0.87	4
M-12	030918R01	Laponite	33.8	0.88	29.8	0.88	4
M-13	030921R01	Laponite	33.8	0.88	29.7	0.88	4
M-14	030922R01	Laponite	33.8	0.88	29.7	0.88	4
M-15	030930R01	Laponite	33.8	0.88	51.8	1.53	4
M-16	030930R02	Laponite	33.8	0.88	51.4	1.52	4
M-17	030930R03	Laponite	33.8	0.88	51.7	1.53	4
M-18	031003R01	Laponite	33.8	0.88	51.4	1.52	4
M-19	031003R02	Laponite	33.8	0.88	51.4	1.52	4
M-20	031201R04_00	Clay	33.8	0.88	29.4	0.87	4
M-21	031213R05_01	Clay	33.8	0.88	29.8	0.88	4

Table 4.11. PJM Nozzle Velocities at 1/4 Scale Computed from PJM Level Probe Measurements

Reference Number	Test Date Number	Drive Time				PJM Velocity			
		Peak Average		Average		Peak Average		Average	
		Average	St. Dev.	Average	St. Dev.	Average	St. Dev.	Average	St. Dev.
		(s)	(s)	(s)	(s)	(ft/sec)	(ft/sec)	(ft/sec)	(ft/sec)
M-1	030829R01	6.45	0.10	7.25	0.10	10.98	0.11	9.73	0.18
M-2	030829R02	4.10	0.00	4.93	0.05	16.81	0.38	14.29	0.21
M-3	030903R01	5.38	0.05	5.80	0.00	12.49	0.17	11.81	0.26
M-4	030903R02	4.83	0.05	5.25	0.06	14.84	0.31	13.56	0.16
M-5	030905R01	4.40	0.08	5.63	0.10	15.30	0.13	12.31	0.13
M-6	030908R01	3.83	0.17	5.33	0.13	17.35	0.24	13.38	0.38
M-7	030910R01	3.55	0.30	4.48	0.10	19.79	0.69	15.84	0.59
M-8	030913R01	4.68	0.05	5.38	0.05	13.16	0.25	11.31	0.34
M-9	030915R01	4.40	0.08	5.93	0.15	13.98	0.48	10.70	0.27
M-19	030915R02	3.28	0.05	4.83	0.13	18.36	0.38	12.87	0.35
M-11	030916R01	3.80	0.00	5.30	0.00	16.45	0.12	11.82	0.08
M-12	030918R01	4.40	0.08	5.88	0.09	14.45	0.23	10.68	0.13
M-13	030921R01	3.33	0.10	5.00	0.32	17.72	0.07	12.24	0.79
M-14	030922R01	2.95	0.06	4.68	0.13	19.48	0.33	13.06	0.43
M-15	030930R01	4.38	0.05	4.90	0.08	14.85	0.20	13.11	0.53
M-16	030930R02	2.75	0.06	3.53	0.10	23.46	0.24	17.38	0.39
M-17	030930R03	1.93	0.05	2.83	0.05	33.00	0.97	22.10	0.43
M-18	031003R01	3.33	0.05	3.98	0.10	19.46	0.19	15.70	0.26
M-19	031003R02	2.18	0.05	3.05	0.13	29.27	0.13	21.10	0.90
M-20	031201R04_00	2.43	0.13	4.00	0.14	23.87	0.32	15.51	0.64
M-21	031213R05_01	2.13	0.10	3.53	0.15	27.06	0.18	18.85	0.67

Table 4.12. Rheological Measurements at 1/4 Scale Used to Support Scaling Analysis

Reference Number	Test Date Number	Initial Shear Strength (Pa)		Final Shear Strength (Pa)		Bingham Model Parameters		
		Average	St. Dev.	Average	St. Dev.	Yield Stress (Pa)	Consistency (Pa-s)	R
M-1	030829R01	107.5	1.6	112.2	1.1	8.7	0.0121	0.972
M-2	030829R02	107.5	1.6	112.2	1.1	10.1	0.0126	0.973
M-3	030903R01	104.2	3.7	104.5	4.6	6.8	0.0119	0.910
M-4	030903R02	104.2	3.7	104.5	4.6	6.8	0.0119	0.910
M-5	030905R01	118.5	5.3	121.9	2.2	5.9	0.0113	0.947
M-6	030908R01	125.4	2.4	128.3	NA	7.0	0.0117	0.973
M-7	030910R01	101.5	1.5	103.8	1.9	9.5	0.0120	0.977
M-8	030913R01	98.7	3.2	105.0	2.5	10.7	0.0132	0.975
M-9	030915R01	112.4	1.9	119.0	2.4	5.5	0.0126	0.974
M-19	030915R02	112.4	1.9	119.0	2.4	5.5	0.0126	0.974
M-11	030916R01	109.1	3.3	NA	NA	8.7	0.0123	0.950
M-12	030918R01	108.6	4.2	114.0	3.8	6.7	0.0128	0.974
M-13	030921R01	110.9	4.0	112.6	5.4	12.2	0.0133	0.978
M-14	030922R01	113.3	2.0	NA	NA	12.3	0.0130	0.971
M-15	030930R01	116.0	3.0	119.7	1.4	5.1	0.0129	0.975
M-16	030930R02	116.0	3.0	119.7	1.4	13.2	0.0121	0.975
M-17	030930R03	116.0	3.0	119.7	1.4	5.3	0.0092	0.974
M-18	031003R01	113.3	2.4	108.7	NA	9.5	0.0120	0.977
M-19	031003R02	113.3	2.4	108.7	NA	9.5	0.0120	0.977
M-20	031201R04_00	47.6	1.3	NA	NA	21.9	0.0267	0.990
M-21	031213R05_01	75.1	3.8	NA	NA	44.6	0.0191	1.00

Table 4.13. Cavern Height and Surface Breakthrough Data at 1/4 Scale Steady State Referenced to the Bottom of the Tank

Reference Number	Test Date Number	Cavern Height		
		H_C		Status at End
		High (in.)	Low (in.)	
M-1	030829R01	14.8	13.0	
M-2	030829R02	15.6	13.8	
M-3	030903R01	18.3	15.0	
M-4	030903R02	18.5	15.0	
M-5	030905R01	17.6	14.5	
M-6	030908R01	16.2	13.3	
M-7	030910R01	29.8	29.8	Surface breakthrough
M-8	030913R01	16.1	12.9	
M-9	030915R01	10.9	NA	Low not measured
M-19	030915R02	15.8	13.5	
M-11	030916R01	17.7	14.8	
M-12	030918R01	15.8	13.1	
M-13	030921R01	19.4	15.3	
M-14	030922R01	29.7	29.7	Surface breakthrough
M-15	030930R01	17.8	15.2	
M-16	030930R02	30.1	27.2	
M-17	030930R03	51.7	45.2	Surface breakthrough
M-18	031003R01	19.9	17.3	
M-19	031003R02	36.1	33.3	
M-20	031201R04_00	29.8	NA	Surface breakthrough
M-21	031213R05_01	29.8	NA	Surface breakthrough

4.5.3 1/9-Scale Tests

Data from specific tests conducted at 1/9 scale that have been used to support the scaling analyses for cavern development and breakthrough are summarized in Tables 4.14 through 4.17. These tests met the conditions for inclusion in the scaling analysis presented in Section 5. The fluid fill height is shown in Table 4.14. The peak average and measured velocities are listed in Table 4.15. The rheological measurements that support these tests are summarized in Table 4.16. Breakthrough test conditions are shown in Table 4.17. These tests, conducted at two values of $H/D_{T,}$ met the conditions for analysis.

Table 4.14. Test Conditions and Velocities at 1/9 Scale Used to Support the Scaling Analysis

Reference Number	Test Date Number	Simulant	Tank Diameter D_T (in.)	Nozzle Diameter D_0 (in.)	Liquid Height H (in.)	H/D_T	Number of PJM
S-1	031029R3A	Laponite	17.25	0.445	15.5	0.90	4
S-2	031029R4A	Laponite	17.25	0.445	15.5	0.90	4
S-3	031104R1A	Laponite	17.25	0.445	15.5	0.90	4
S-4	031104R2A	Laponite	17.25	0.445	15.5	0.90	4
S-5	031104R3A	Laponite	17.25	0.445	15.5	0.90	4
S-6	031105R2A	Laponite	17.25	0.445	15.5	0.90	4
S-7	031107R1A	Laponite	17.25	0.445	15.5	0.90	4
S-8	031112R1A	Laponite	17.25	0.445	15.5	0.90	4
S-9	031125R1A	Laponite	17.25	0.445	15.5	0.90	4
S-10	031105R3A	Laponite	17.25	0.445	15.5	0.90	4
S-11	031118R1D	Laponite	17.25	0.445	25.0	1.45	4
S-12	031119R1B	Laponite	17.25	0.445	25.0	1.45	4
S-13	031120R1C	Laponite	17.25	0.445	25.0	1.45	4
S-14	031120R2A	Laponite	17.25	0.445	25.0	1.45	4
S-15	031121R1A	Laponite	17.25	0.445	25.0	1.45	4
S-16	031211R1A	Clay	17.25	0.445	15.5	0.90	4

Table 4.15. Velocity at 1/9 Scale Used to Support the Scaling Analysis

Reference Number	Test Date Number	Peak Average Velocity (ft/sec)	Average Velocity (ft/sec)
S-1	031029R3A	13.0	12.0
S-2	031029R4A	20.0	18.0
S-3	031104R1A	15.6	14.6
S-4	031104R2A	20.1	17.9
S-5	031104R3A	22.3	19.6
S-6	031105R2A	15.1	14.3
S-7	031107R1A	17.6	16.0
S-8	031112R1A	19.3	17.4
S-9	031125R1A	22.2	19.0
S-10	031105R3A	38.6	NA
S-11	031118R1D	20.8	20.5
S-12	031119R1B	27.7	24.4
S-13	031120R1C	16.7	17.3
S-14	031120R2A	29.2	26.1
S-15	031121R1A	40.0	34.8
S-16	031211R1A	28.3	22.8

Table 4.16. Rheological Measurements at 1/9 Scale Used to Support the Scaling Analysis

Reference Number	Data File Number	Shear Strength		Yield Stress (Pa)	Consistency (Pa-s)
		Initial (Pa)	Final (Pa)		
S-1	031029R3A	68.2	NA	NA	NA
S-2	031029R4A	NA	71	6.9	9.7
S-3	031104R1A	NA	99.3	7.2	9.6
S-4	031104R2A	99.3	99.5	5.7	9.7
S-5	031104R3A	99.5	99.1	NA	NA
S-6	031105R2A	79.3	83.6	8.1	9.6
S-7	031107R1A	75.9	79.6	8.3	9.2
S-8	031112R1A	79.9	81.6	9	9.9
S-9	031125R1A	96.3	95.8	11.5	9.5
S-10	031105R3A	83.6	NA	NA	NA
S-11	031118R1D	96.1	100.2	9.7	10
S-12	031119R1B	89.1	89.4	10.3	10.2
S-13	031120R1C	86.8	88.4	10.6	10
S-14	031120R2A	88.4	88.5	10.5	9.9
S-15	031121R1A	76.3	83.4	10.8	9.8
S-16	031211R1A	NA	NA	18.3	21.5

Table 4.17. Summary of Cavern Height and Surface Breakthrough Data at 1/9 Scale Steady State

Reference Number	Data File Number	Cavern Height			
		Maximum (in.)	Minimum (in.)	Average (in.)	Status at End
S-1	031029R3A	7.6	6.8	7.2	-
S-2	031029R4A	15.5	15.5	15.5	Breakthrough
S-3	031104R1A	7.3	6.3	6.8	-
S-4	031104R2A	12.9	11.9	12.4	-
S-5	031104R3A	15.5	15.5	15.5	Breakthrough
S-6	031105R2A	8.8	7.9	8.3	-
S-7	031107R1A	10.3	9.3	9.8	-
S-8	031112R1A	12.6	11.6	12.1	-
S-9	031125R1A	10.8	9.8	10.3	-
S-10	031105R3A	15.5	15.5	15.5	Breakthrough
S-11	031118R1D	14.8	13.8	14.3	-
S-12	031119R1B	18.7	17.7	18.2	-
S-13	031120R1C	9.8	8.8	9.3	-
S-14	031120R2A	19.6	18.7	19.1	-
S-15	031121R1A	25.0	25.0	25.0	Breakthrough
S-16	031211R1A	15.5	15.5	15.5	Breakthrough

4.6 Mixing Tests

Specific experiments were conducted at each test facility to evaluate the time to mix the simulant. These tests are summarized in Appendixes A, B, and C. From those tests a subset with more uniform conditions and quantifiable times is summarized in Table 4.18. The comments on these tests show that in some cases the time to mix was measured from the gelled state and at other times it was measured after establishment of a cavern. For two of these tests conducted at large scale, mixing time constants were evaluated based on analysis of dye samples to determine the time to reach 95 and 99% of the steady-state value. The plots of these two time-to-mix cases are included in Appendix A.

4.7 Upwell Velocity Tests

An important scaling parameter is the relationship between the velocities in the vessel that result from jet operation at differing scales. Upwelling in these mixing vessels is the result of the working fluid jet exiting into the tank from the pulse tube. This upwelling causes the mixing caverns to develop in the tank volume. To make this comparison, the upwell velocities were measured at large and 1/4 scale. These data can be used to support nondimensional analysis of this parameter.

4.7.1 Ultrasonic Doppler Velocity Probe

An ultrasonic velocity probe was used to measure the velocity of the jet rising or upwelling in the tank. The probe was a Dantec UVP Monitor Model UVP-DUO with Software Version 3. Sensor operation and nomenclature are illustrated in Figures 4.7 and 4.8. The measurement probe, which is inserted directly into the measurement environment, has a cylindrical geometry about 8 mm in diameter and several centimeters long. It is connected at one end to a cable connecting it to its electronic support hardware. The other end has a flat window designed to emit ultrasonic energy of a known frequency and to detect returning ultrasonic vibrations. By measuring the Doppler shift in the frequency of the returning ultrasonic signal, the system can determine the magnitude of the fluid motion in which the probe is immersed that is parallel to the long axis of the probe, as shown in Figure 4.8.

The UVP measures the velocity in an almost cylindrical cone-shaped volume, as shown in Figure 4.8. The measurement volume may begin very close to the probe face and extend out as far as 100 mm. Knowing the velocity of sound in the medium, the length of the measurement volume can be set and is electronically divided into 100 subvolumes (labeled channels in the data files) based on time of flight. A velocity is determined for each of these subvolumes and in this way a velocity profile is constructed for the length of the measurement volume. What is typically observed for this profile in the kaolin-bentonite simulant is that the measured velocities decrease as the distance to the probe face decreases within about 15 mm. Beyond about 25 mm the measured velocity is constant out to about 50 mm and then the velocity values begin to vary chaotically. For the upwell velocities measured at APEL and at 336 all channels between 25 and 40 mm were averaged to provide a velocity.

Table 4.18. Summary of the Time-to-Mix Test Data for Laponite

Test Stand and Scale	Run Number/ Reference Number	Laponite Shear Strength (Pa)	Aspect Ratio	Break-through	Peak Average Velocity (ft/sec)	Average Velocity (ft/sec)	Mixing Time Constant (min)		Qualitative Observations			Comments
							95%	99%	Break-through (min)	Flow in Annular Region (min)	Time to Full Mobilization (min)	
SRNL 1/9 Scale	031029R4A S-2	71	0.9	yes	20.0	18.1	--	--	4	145	145	Flow rate increased to cause breakthrough after formation of a stable cavern.
	031104R3A S-5	99.1	0.9	yes	22.3	18.9	--	--	3	26	26	Flow rate increased to cause breakthrough after formation of a stable cavern.
	031121R1A S-15	84.2	1.45	yes	40.0	33.6	--	--	5	134	134	Flow rate increased to cause breakthrough after formation of a stable cavern.
APEL 1/4 Scale	030926R01	103.4	0.88	yes	23.7	15.2	--	--	1	17	17	No mixing prior to start of test.
336 Large Scale	030914-RR Run 1	121	0.88	yes	25.2	20.9	--	--	30	120	120	No mixing prior to start of test.
	031106-S5-T2M Run 1	101	0.86	yes	25.3	20.8	23	44	2	15	60	No mixing prior to start of test.
	031106-S5-T2M Run 3	102	0.86	yes	25.5	21.0	31	51	~2	60	60	Tank fully homogenized prior to start of test. Time to breakthrough not recorded; it was assumed to be the same as for Run 1
	031120-S2-1	109	0.87	yes	25.6	21.1	--	--	30	~120	~120	Breakthrough occurred at third PJM condition during the test. The first condition produced a stable cavern; the second condition produced a transient.

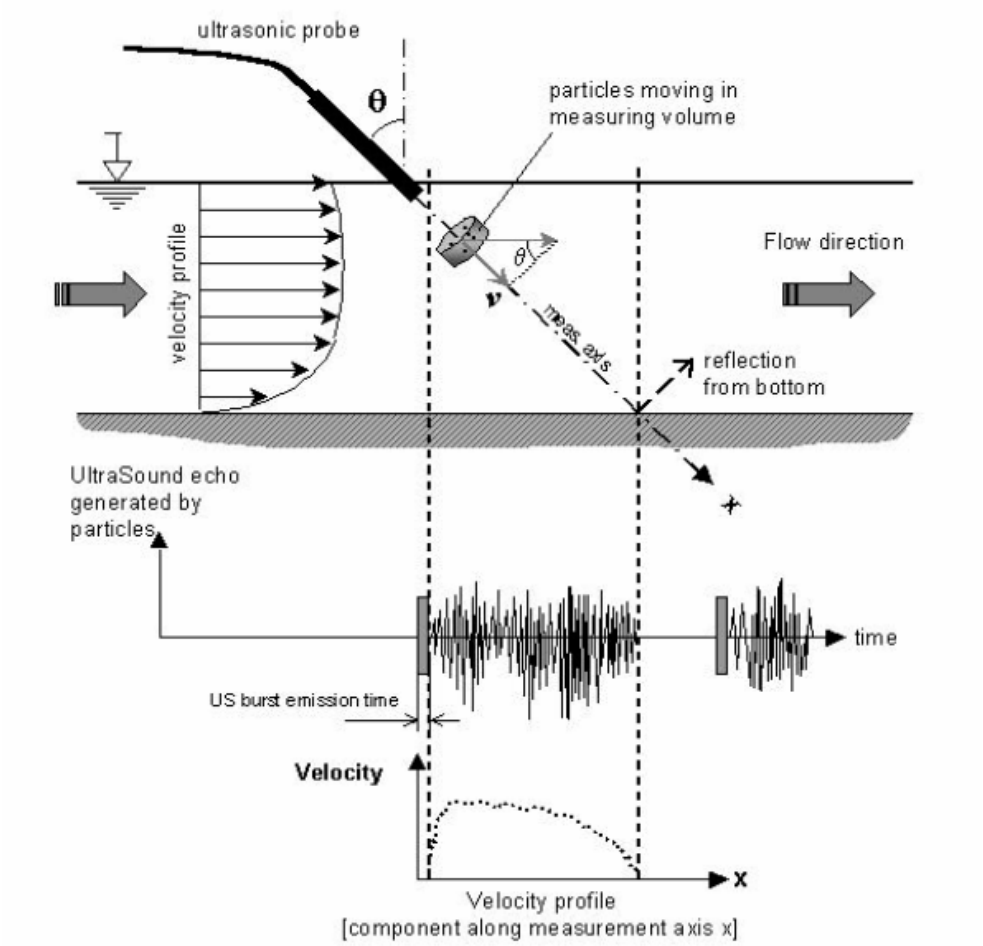

Figure 4.7. Schematic of UVP Velocity Profile Measurement on a Flow with Free Surface

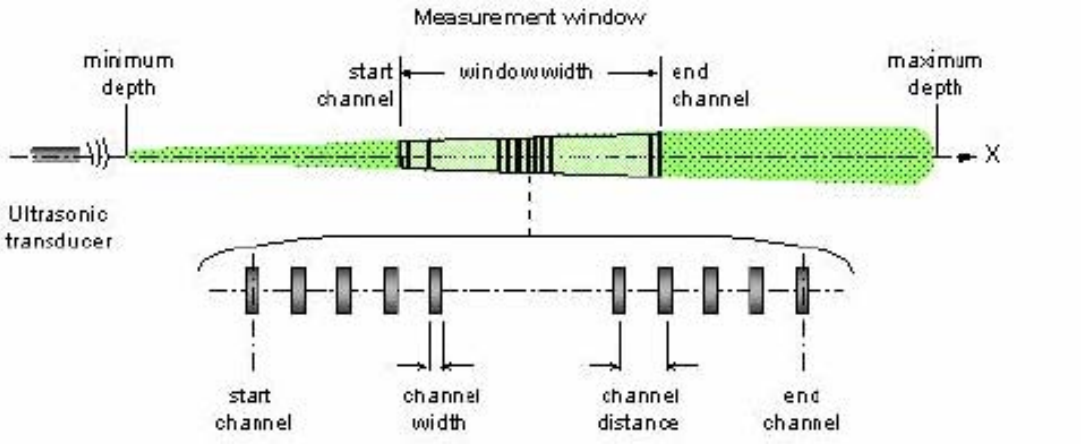

Figure 4.8. Illustration of Terms Connected with UVP Measuring Window

4.7.2 Velocity Measurements

Upwell velocity measurements were taken in the large-scale and 1/4-scale test stands. The rheological properties that support these tests are listed in Table 4.19. During the tests the APEL 4PJMs were operated to produce target nozzle velocities of 8 and 12 m/s with a cycle period of 13.3 seconds while the 336 4PJMs had a 60-second cycle period. Measurements were made at the azimuthal locations and elevations listed in Table 4.20 where H_{VP} is the elevation of the probe. Note that these locations are not the same for the APEL 4PJM configuration as for the 336 4PJM configuration. The APEL 4PJM azimuthal locations are about an axis that is coincident with the center line of the tank; whereas the axis for the 336 4PJM locations is located at a position that coincides with the center line of the upwell plume as expressed at the tank fill surface, which is somewhat off center in both systems. These sets of velocity data were produced every 0.2 second for 5-minute runs, resulting in 1500 data sets for each test condition. For the APEL 4PJM this includes about 23 pulse jet cycles (at 13.3 seconds per cycle) for each test condition. For the 336 4PJM this includes five pulse jet cycles. A summary of the data taken at each test condition as a function of quadrant is provided in Tables 4.21 and 4.22.

Table 4.19. Measured Rheological Properties of the Kaolin-Bentonite Simulant Before and After the Upwelling Test Series

Kaolin-Bentonite Waste Simulant Rheological Properties (Bingham Model)		
Facility	**Yield Stress** (Pa)	**Consistency (viscosity)** (Pa·s)
APEL 4PJM (before)	34.3	0.0223
336 4PJM (before)	29.3	0.0204
336 4PJM (after)	28.4	0.0202

Table 4.20. Test Conditions and Locations for the Velocity Probe Measurements

Facility	**Target Velocity**	**Nominal H_{VP}/D_T**	**Azimuth**
APEL 1/4 Scale	High	0.63	0, 90, 180, 270
	High	0.4	0, 90, 180, 270
	Low	0.8	0, 90, 180, 270
	Low	0.63	0, 90, 180, 270
336 Large Scale	High/Low	0.85	0, 90, 180, 270
	High/Low	0.6	0, 90, 180, 270
	High/Low	0.3	0, 90, 180, 270

Table 4.21. 1/4 Scale 4PJM Upwell Velocity Data Summary

Peak Avg Velocity u_p (m/s)	H_{VP}/D_T	Corrected Upwell Velocities U_{uw} (mm/s)											
		0°			90°			180°			270°		
		Max Avg[a]	St. Dev.[b]	Max[c]	Max Avg[a]	St. Dev.[b]	Max[c]	Max Avg[a]	St. Dev.[b]	Max[c]	Max Avg[a]	St. Dev.[b]	Max[c]
11.3	0.36	1884	206	2209	1427	226	1840	1486	291	2202	1676	281	2198
11.3	0.36	1855	256	2438	no data	no data	no data	1464	293	1942	1757	285	2228
11.3	0.59	1341	232	1751	1021	297	1687	1365	277	2052	1150	220	1481
11.3	0.59	1409	285	1989	1039	228	1333	1424	240	1875	1107	302	1774
11.3	0.76	622	282	1118	452	229	925	719	218	1185	598	211	1047
9.79	0.59	931	273	1584	764	184	1218	1071	186	1459	935	270	1544
9.79	0.76	354	200	738	134	95	379	216	146	522	233	179	629

(a) The average of all peak velocity transients observed.
(b) The standard deviation for the peak average.
(c) The maximum peak measured during five-minute recording period.

Table 4.22. Large-Scale 4PJM Upwell Velocity Data Summary

Peak Average Velocity u_p (m/s)	H_{VP}/D_T	Peak Upwell Velocity							
		Probe Direction							
		East		South		West		North	
		Max[a] (m/s)	Max Avg[b] (m/s)	Max[a] (m/s)	Max Avg[b] (m/s)	Max[a] (m/s)	Max Avg[b] (m/s)	Max[a] (m/s)	Max Avg[b] (m/s)
5.48	0.29	0.99	0.97	0.65	0.50	0.07	0.07	0.69	0.60
8.20	0.29	2.30	2.10	1.63	1.51	NA	--	1.85	1.62
8.53	0.29	2.24	2.16	1.68	1.43	0.20	0.10	1.89	1.46
8.59	0.29	2.29	2.07	1.50	1.42	0.85	0.25	1.39	1.34
5.50	0.59	0.15	0.13	0.23	0.17	0.13	0.10	0.19	0.12
5.50	0.59	NA	NA	0.12	0.11	NA	NA	NA	NA
8.32	0.59	1.24	1.17	1.17	1.03	0.68	0.46	1.26	0.94
8.58	0.59	1.29	1.23	1.43	1.08	0.80	0.40	1.39	1.05
8.67	0.59	1.42	1.30	1.32	1.06	0.79	0.45	1.23	1.02
5.50	0.84	0.07	0.06	0.08	0.07	0.07	0.06	0.09	0.07
8.28	0.84	0.66	0.56	0.81	0.65	0.40	0.30	0.48	0.35
8.60	0.84	NA	NA	0.49	0.48	0.65	0.37	0.69	0.57
8.60	0.84	0.52	0.41	0.84	0.59	0.48	0.40	NA	NA

(a) The maximum peak measured during five-minute recording period.
(b) The average of all peak velocity transients observed.

5.0 Scaling Relationships and Data Analysis

This section presents a comparison of the hydrodynamic data collected from the three geometrically similar 4PJM test stands. The data are compared nondimensionally, using the scaling parameters developed in Section 3, to demonstrate the validity of testing PJM mixing systems at reduced scale.

During these tests and subsequent analysis, the data were evaluated to ensure that the test conditions, data, and observations obtained were appropriate for inclusion in the scaling analysis. Variations in test conditions, simulant preparation, uncertainty associated with measurement techniques, and inconsistent approaches as well as technical judgment were used to evaluate the data. Data selected for inclusion in the scaling analysis were processed to ensure that variables were all presented consistently throughout the three test stands. All data presented in the main body of the report (Sections 1 through 6) have been evaluated through the independent technical review process and standardized. Additional observations that may not have been standardized are included in Appendix A to provide insight regarding cavern growth observations from cameras submerged to observe simulant motion in the large-scale test fixture.

5.1 Introduction

An important component of the test strategy was demonstrating the scalability of the scaled test results. This was done by testing in geometrically similar 4PJM mixing systems at three different scales. Vessel scales are shown in Table 5.1. A 12,000-gallon vessel in the 336 Building was used for large-scale tests; this vessel contains 24-inch-diameter pulse tubes with AEA Technology air/vacuum supply system and controller. A geometrically scaled 250-gallon tank in the APEL was used for the mid-scale tests. This vessel is approximately 1/4.5 scale of the large vessel. Small-scale tests were performed at SRNL in a vessel at approximately 1/9 scale.

Table 5.1. Vessels Used for 4PJM Scaling Tests

Vessel	Nominal Volume (gal)	Vessel Diameter (m)	PJM Nozzle Diameter (cm)	Scale Factor (s)
336	12,000	3.88	10.2	1
APEL	250	0.858	2.2	4.53
SRNL	30	0.438	1.1	8.9

Tests were performed with a Laponite and a kaolin-bentonite clay simulant. PJM mixing systems were operated according to the scaling rules discussed in Section 3. For the purpose of this work, mixing is defined as fluid mobilization within the cavern. No attempt was made to quantify the degree of turbulence within mixing caverns. Generally, PJM velocities varied over a range that provided useful data. Given the geometric similarity (specifically that of the pulse tubes), PJM drive time was reduced by the scale factor "s" for a given PJM velocity. Given the nondimensional nature of the scaling approach, it was not necessary to have simulant rheological properties or PJM velocities be identical in the various test stands. However, generally the properties were relatively close, and velocities were maintained within useful and prototypic ranges.

Different mixing modes can exist in 4PJM systems depending on operating conditions (PJM velocity) and simulant rheology. These modes are illustrated in Figure 5.1. Impingement of the PJM discharge jets on the floor of the vessel creates central upwell flow, as shown in the figure. For low velocities (or high

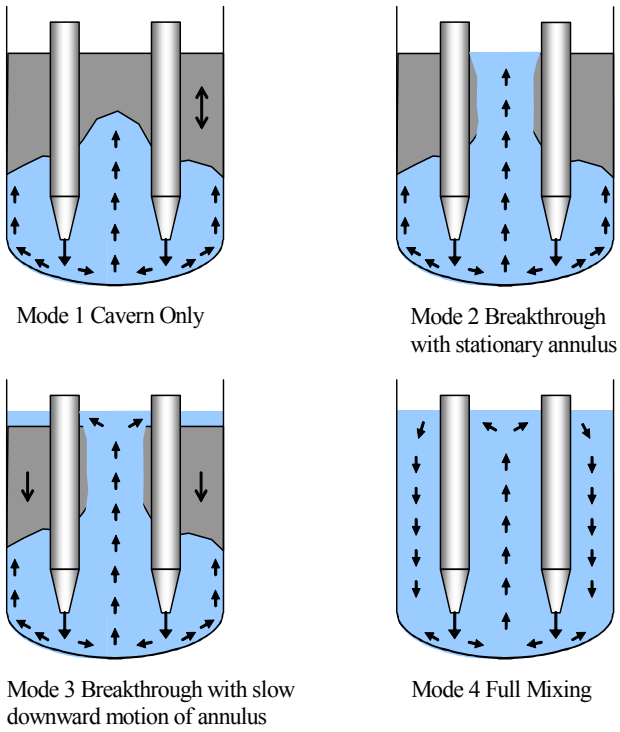

Figure 5.1. Definition of PJM Mixing Modes in Vessels with 4PJM Mixing Configurations

strength simulant), a stationary cavern forms between the PJMs (mode 1 discharge). As velocity increases, at some point the upwell will break through the simulant surface (mode 2). Further increase in velocity will create a weak recirculation in the vessel where fresh material is pushed to the surface via the central upwell, and a slow downward motion results in the outer annulus (mode 3). Finally, if the PJM velocity is high enough and the rheology of sufficiently low strength, turbulent flow will exist everywhere in the vessel.

Given the range of operability of the PJMs and the selected simulants, only modes 1–3 were achievable in the test vessels. Modes 1 and 2 were intentionally created to obtain data to evaluate mixing scaling. If modes 1 and 2 are demonstrated to scale well, it follows that a mixing design which eliminates the cavern altogether (mode 4) will also scale well. Mode 3 operation was not considered a viable mixing mode for prototypic vessels, as the slow downward motion at the vessel wall is highly dependent on the precise amount of material pushed to the surface by the central upwell. Minor changes in rheology or jet velocity may cause a sudden change from mode 3 to mode 2 mixing. Hence demonstration of mode 3 scaling was not attempted as part of this study. The mixing configuration and measured parameters for these tests are illustrated in Figure 5.2.

Generally, the rheology and PJM velocities used during the testing were close to prototypic. However, in some cases higher strength rheologies and velocities were used to fully exercise the range of experimental conditions for a given type of test. In spite of this, however, the yield Reynolds numbers were generally maintained within the prototypic range expected in the WTP.

Three types of data were analyzed to make nondimensional comparisons:

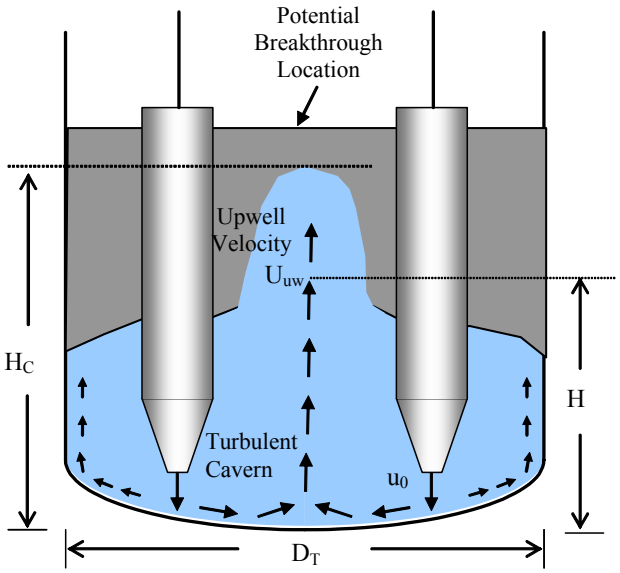

Figure 5.2. Features of Central Cavern for Collecting Data in 4PJM Vessels

- Cavern height measurements with Laponite at three vessel scales (s = 1, s = 4.5, and s = 8.9)
- Breakthrough velocity measurements with Laponite and clay at three vessel scales (s = 1, s = 4.5, and s = 8.9)
- Upwell velocity measurements in clay at two vessel scales (s = 1 and s = 4.5).

Experiments to measure time to mix were conducted using Laponite and clay simulants at three scales. When these data were compared significant differences in experimental conditions, measurement approaches, as well as a limited test matrix, were noted. Therefore, data from these tests did not contribute to the scaling analysis.

5.2 Cavern Height Measurements in Laponite

Cavern heights (H_C) were measured using Laponite in the 336, APEL, and SRNL 4PJM test vessels. Results for these tests are summarized in Table 5.2. Simulant shear strength (τ_s) and PJM velocity (u_p and u_a) were the two primary test variables, with resulting cavern heights being measured. Both peak average (u_p) and average (u_a) PJM velocities are reported in Table 5.2. Also noted in the table are those cases that resulted in a surface breakthrough. The reported results represent only the cases where there was sufficient PJM velocity to *just* achieve breakthrough. Cases that had excess velocity or in which breakthrough had already occurred were not included in this analysis. For Laponite the density is very nearly a constant 1000 kg/m^3. Minor variations in Laponite concentration in the range tested, as well as in temperature, produce negligible change in simulant density.

Table 5.3 presents the data in nondimensional form. The primary independent test variables are the yield Reynolds number (Re_τ), with nondimensional cavern height being the resulting parameter. Yield Reynolds numbers are shown calculated with both peak average (u_p) and average (u_a) PJM velocities. The majority of the tests were performed with a nondimensional simulant fill level of approximately

Table 5.2. Dimensional Data from 4PJM Laponite Cavern Tests at Three Physical Scales

Reference Number	Test Platform	Vessel Diameter, D_T (m)	Simulant Fill Level, H (m)	Shear Strength, τ_s (Pa)	PJM Velocity		Cavern Height, H_C (m)	Surface Breakthrough
					Peak Avg, u_p (m/s)	Avg, u_a (m/s)		
S-1	SRNL	0.438	0.394	68.2	3.96	3.66	0.18	
S-2	SRNL	0.438	0.394	71.0	6.09	5.49	0.39	yes
S-3	SRNL	0.438	0.394	99.3	4.76	4.45	0.17	
S-4	SRNL	0.438	0.394	99.5	6.12	5.46	0.31	
S-5	SRNL	0.438	0.394	99.1	6.80	5.98	0.39	yes
S-6	SRNL	0.438	0.394	79.3	4.60	4.36	0.21	
S-7	SRNL	0.438	0.394	79.6	5.38	4.88	0.25	
S-8	SRNL	0.438	0.394	81.6	5.90	5.30	0.31	
S-9	SRNL	0.438	0.394	96.0	6.75	5.79	0.26	
S-11	SRNL	0.438	0.635	99.4	6.34	6.25	0.36	
S-12	SRNL	0.438	0.635	89.0	8.43	7.44	0.46	
S-13	SRNL	0.438	0.635	87.0	5.10	5.27	0.24	
S-14	SRNL	0.438	0.635	88.0	8.90	7.96	0.49	
S-15	SRNL	0.438	0.635	84.2	12.19	10.61	0.63	yes
M-1	APEL	0.858	0.759	109.9	3.35	2.97	0.38	
M-2	APEL	0.858	0.756	109.9	5.13	4.36	0.40	
M-4	APEL	0.858	0.744	104.4	4.52	4.13	0.47	
M-5	APEL	0.858	0.754	120.2	4.66	3.75	0.45	
M-6	APEL	0.858	0.746	126.9	5.29	4.08	0.41	
M-7	APEL	0.858	0.756	102.6	6.03	4.83	0.76	yes
M-8	APEL	0.858	0.754	101.9	4.01	3.45	0.41	
M-10	APEL	0.858	0.751	115.7	5.60	3.92	0.40	
M-11	APEL	0.858	0.749	109.1	5.01	3.60	0.45	
M-12	APEL	0.858	0.754	111.3	4.41	3.26	0.40	
M-13	APEL	0.858	0.754	111.8	5.40	3.73	0.49	
M-15	APEL	0.858	1.315	117.8	4.53	4.00	0.45	
M-16	APEL	0.858	1.305	117.8	7.15	5.30	0.76	
M-17	APEL	0.858	1.312	117.8	10.06	6.74	1.31	yes
M-18	APEL	0.858	1.305	111.0	5.93	4.79	0.51	
M-19	APEL	0.858	1.305	111.0	8.92	6.43	0.92	
L-1	336	3.88	3.50	100.7	3.46	3.28	1.68	
L-2	336	3.88	3.50	100.7	6.15	5.54	3.50	yes
L-3	336	3.88	3.38	109.4	4.88	4.49	2.25	
L-4	336	3.88	3.38	109.4	5.45	4.88	3.38	yes
L-5	336	3.88	3.39	117.5	4.15	3.85	1.95	
L-6	336	3.88	3.39	117.5	4.88	4.47	2.03	
L-7	336	3.88	3.39	117.5	5.29	4.86	2.11	
L-9	336	3.88	3.39	117.3	6.21	4.91	3.41	
L-14	336	3.88	3.37	119.5	4.66	4.23	2.12	
L-15	336	3.88	3.37	119.5	4.47	4.12	1.92	
L-16	336	3.88	3.33	123.7	5.12	4.61	2.07	
L-17	336	3.88	3.39	102.8	4.60	4.16	2.76	

Table 5.3. Nondimensional Data from 4PJM Laponite Cavern Tests at Three Physical Scales

Reference Number	Test Platform	Test Scale Factor	Nondimensional Fill Level (H/D_T)	Yield Reynolds Number		Nondimensional Cavern Height (H_C/D_T)	Surface Breakthrough
				Peak Average (u_p)	Average (u_a)		
S-1	SRNL	8.87	0.9	2.30E+02	1.96E+02	0.42	
S-2	SRNL	8.87	0.9	5.22E+02	4.24E+02	0.90	yes
S-3	SRNL	8.87	0.9	2.28E+02	2.00E+02	0.39	
S-4	SRNL	8.87	0.9	3.77E+02	2.99E+02	0.72	
S-5	SRNL	8.87	0.9	4.67E+02	3.60E+02	0.90	yes
S-6	SRNL	8.87	0.9	2.67E+02	2.40E+02	0.48	
S-7	SRNL	8.87	0.9	3.63E+02	2.99E+02	0.57	
S-8	SRNL	8.87	0.9	4.26E+02	3.45E+02	0.70	
S-9	SRNL	8.87	0.9	4.75E+02	3.50E+02	0.60	
S-11	SRNL	8.87	1.45	4.05E+02	3.93E+02	0.83	
S-12	SRNL	8.87	1.45	7.98E+02	6.22E+02	1.06	
S-13	SRNL	8.87	1.45	2.99E+02	3.20E+02	0.54	
S-14	SRNL	8.87	1.45	9.00E+02	7.20E+02	1.11	
S-15	SRNL	8.87	1.45	1.77E+03	1.34E+03	1.45	yes
M-1	APEL	4.53	0.88	1.02E+02	8.17E+00	0.44	
M-2	APEL	4.53	0.88	2.39E+02	4.13E+01	0.46	
M-4	APEL	4.53	0.87	1.96E+02	3.21E+01	0.55	
M-5	APEL	4.53	0.88	1.81E+02	2.12E+01	0.52	
M-6	APEL	4.53	0.87	2.21E+02	2.89E+01	0.48	
M-7	APEL	4.53	0.88	3.55E+02	8.06E+01	0.88	yes
M-8	APEL	4.53	0.88	1.58E+02	1.85E+01	0.48	
M-10	APEL	4.53	0.88	2.71E+02	3.60E+01	0.47	
M-11	APEL	4.53	0.87	2.30E+02	2.74E+01	0.52	
M-12	APEL	4.53	0.88	1.74E+02	1.66E+01	0.47	
M-13	APEL	4.53	0.88	2.61E+02	3.25E+01	0.57	
M-15	APEL	4.53	1.53	1.74E+02	2.36E+01	0.53	
M-16	APEL	4.53	1.52	4.34E+02	1.03E+02	0.89	
M-17	APEL	4.53	1.53	8.59E+02	3.31E+02	1.53	yes
M-18	APEL	4.53	1.52	3.17E+02	6.55E+01	0.59	
M-19	APEL	4.53	1.52	7.17E+02	2.67E+02	1.07	
L-1	336	1.0	0.9	1.19E+02	1.07E+02	0.43	
L-2	336	1.0	0.9	3.75E+02	3.05E+02	0.90	yes
L-3	336	1.0	0.9	2.18E+02	1.84E+02	0.58	
L-4	336	1.0	0.9	2.71E+02	2.18E+02	0.87	yes
L-5	336	1.0	0.9	1.47E+02	1.26E+02	0.50	
L-6	336	1.0	0.9	2.03E+02	1.70E+02	0.52	
L-7	336	1.0	0.9	2.38E+02	2.01E+02	0.54	
L-9	336	1.0	0.9	3.29E+02	2.06E+02	0.88	
L-14	336	1.0	0.9	1.82E+02	1.50E+02	0.55	
L-15	336	1.0	0.9	1.67E+02	1.42E+02	0.49	
L-16	336	1.0	0.9	2.12E+02	1.72E+02	0.53	
L-17	336	1.0	0.9	2.06E+02	1.68E+02	0.71	

H/D_T = 0.9; however, some higher fill levels were considered.[(a)] These tests were conducted to examine the effect, at smaller vessel scales, of artificially high caverns and premature surface breakthrough resulting from Laponite bulk fracture.

Nondimensional cavern heights in Laponite are shown plotted versus yield Reynolds number (Re_τ) in Figures 5.3 to 5.6. Linear regressions of the data are also shown on the plot to aid in scale comparison. In Figure 5.3, the yield Reynolds number is calculated using peak average PJM velocity (u_p), and only cases with $H/D_T = 0.9$ are shown. Data for the three scale vessels are plotted separately. In addition, several breakthrough points are included. The data show that nondimensional cavern height increases with increasing yield Reynolds number. While some scatter exists in the data, the linear regression curves demonstrate that cavern heights are generally largest in the 336 vessel and decreased for the smaller vessels.

In Figure 5.4, the yield Reynolds number is calculated using the average PJM velocity. In this case the cavern heights in the 336 and APEL vessels are essentially the same. In Figures 5.5 and 5.6, data from higher fill levels are included. This was done because of the observation that Laponite often failed in discrete chunks. At small scale, as the cavern approaches the surface, a fracture could result in a higher cavern and potentially premature breakthrough. From Figures 5.5 and 5.6, it appears that this was in fact the case because the breakthrough points for the APEL and SRNL tests are shifted considerably to higher yield Reynolds numbers.

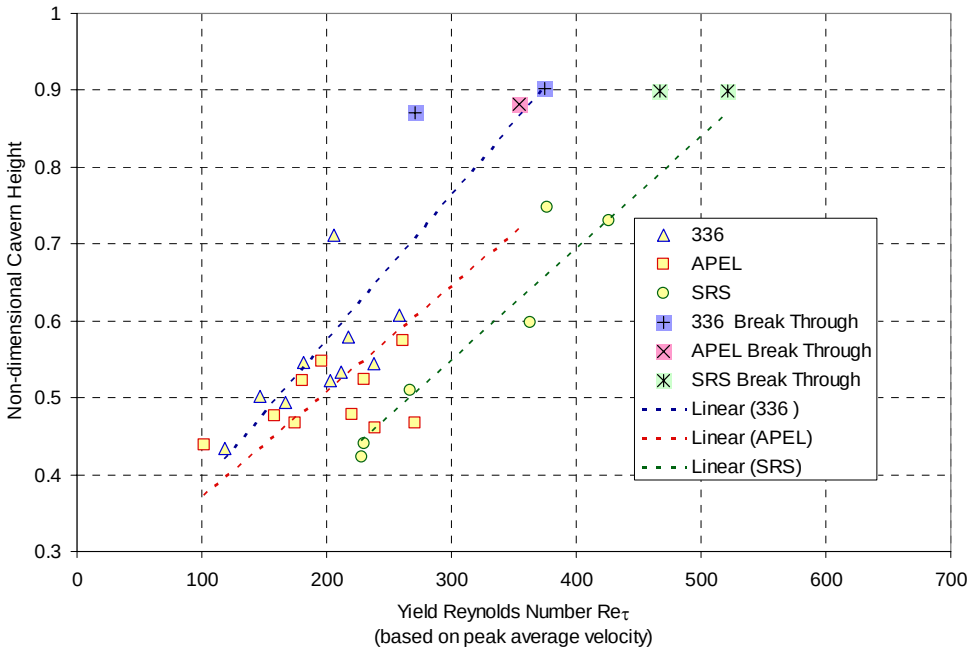

Figure 5.3. Nondimensional Cavern Height (H_C/D_T) Versus Yield Reynolds Number for Laponite. Yield Reynolds number based on peak average PJM velocity; data limited to nondimensional fill level of $H/D_T = 0.9$.

(a) The maximum nondimensional fill level in the 336 test vessel was approximately $H/D_T = 0.9$. The smaller vessels had the capacity to be filled up to approximately $H/D_T = 1.5$.

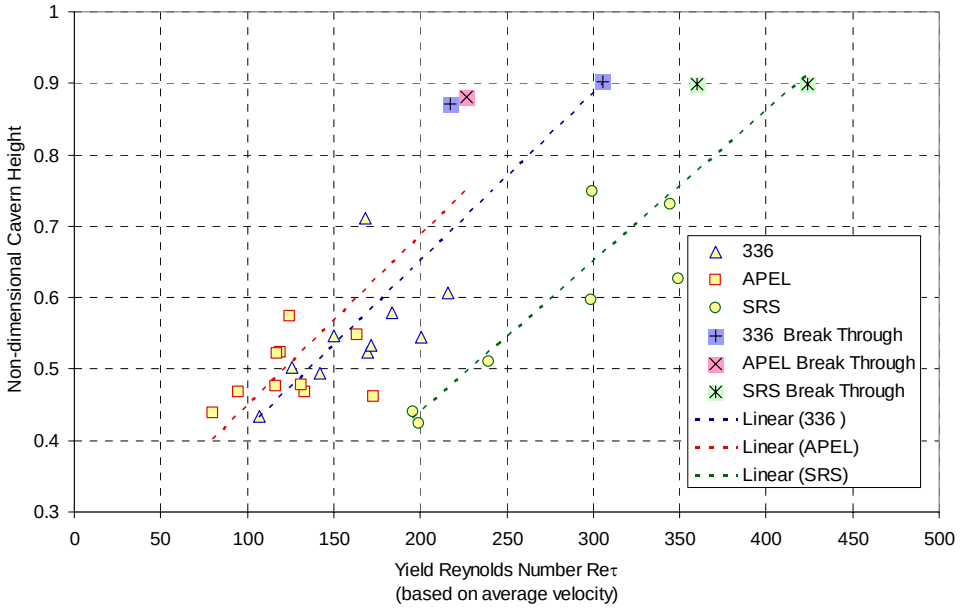

Figure 5.4. Nondimensional Cavern Height (H_C/D_T) Versus Yield Reynolds Number for Laponite. Yield Reynolds number based on average PJM velocity; data limited to nondimensional fill level of $H/D_T = 0.9$.

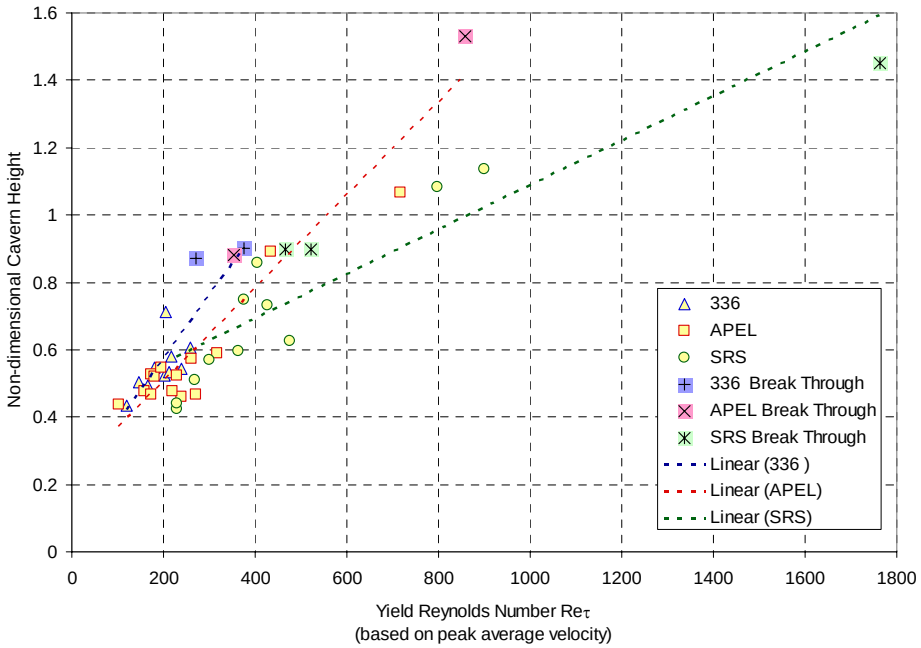

Figure 5.5. Nondimensional Cavern Height (H_C/D_T) Versus Yield Reynolds Number for Laponite. Yield Reynolds number based on peak average PJM velocity; data for higher nondimensional fill levels included.

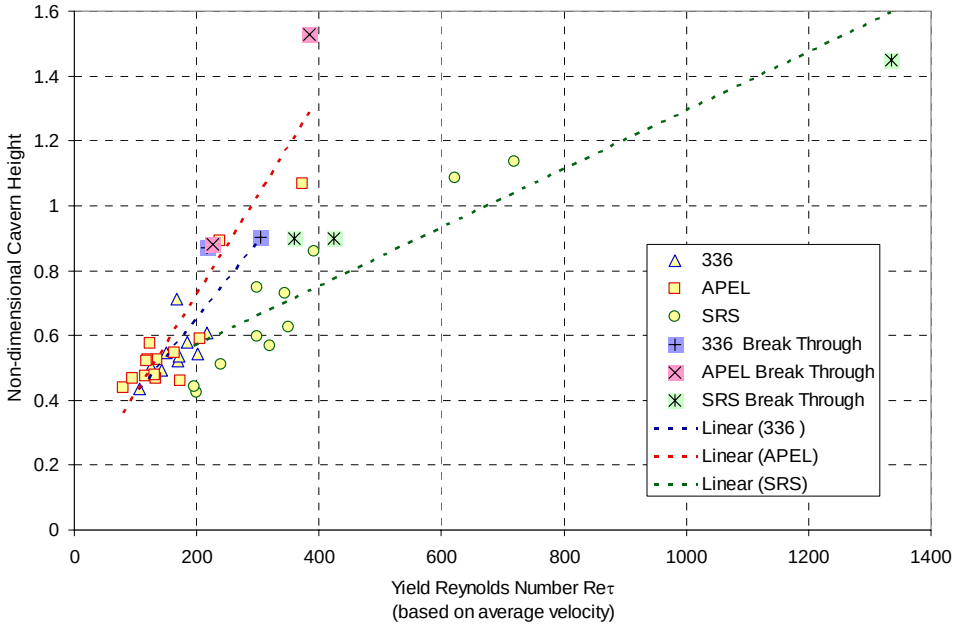

Figure 5.6. Nondimensional Cavern Height (H_C/D_T) Versus Yield Reynolds Number for Laponite. Yield Reynolds number based on average PJM velocity; data for higher nondimensional fill levels included.

The general trend that nondimensional cavern heights are seen to be larger with increasing vessel scale supports the anticipated result that jet Reynolds number effects will produce higher caverns in large vessels. These effects are examined in detail when considering breakthrough data in the next section.

5.3 Surface Breakthrough Measurements in Clay and Laponite Simulants

Surface breakthrough velocities were measured using Laponite and kaolin-bentonite clay simulants in the 336, APEL, and SRNL 4PJM test vessels. In these tests, PJM velocities were increased until the central upwell caused the cavern to reach the surface. The specific velocity at which breakthrough occurs can be compared nondimensionally to examine the scaling relationship between the various vessel scales.

Results for these tests are summarized in Table 5.4. Simulant shear strength (for Laponite) or yield stress (for clay) are the primary test variables, with required PJM breakthrough velocity being measured. Both peak average (u_p) and average (u_a) PJM breakthrough velocities are reported in Table 5.4. The tests were performed with a nondimensional simulant fill level of approximately $H/D_T = 0.9$ for all tests. For Laponite the density is nearly a constant 1000 kg/m^3, while for clay it is approximately 1200 kg/m^3.

Table 5.5 presents the data in nondimensional form. Jet Reynolds number (Re_0), yield Reynolds number (Re_τ), and combined Reynolds number (Re) are all calculated using the measured breakthrough velocities. The jet Reynolds number uses the high shear-rate consistency (K) in place of the commonly used viscosity (μ) for Newtonian fluids. Yield Reynolds number and combined Reynolds number use the shear strength for Laponite and the yield stress (τ_y) for clay. The tests were performed with a nondimensional simulant fill level of approximately $H/D_T = 0.9$.

Table 5.4. Dimensional Data from 4PJM Clay and Laponite Surface Breakthrough Tests at Three Physical Scales

Reference Number	Test Platform	Simulant	Vessel Diameter D_T (m)	Nozzle Diameter d_0 (m)	Shear Strength or Yield Stress[(a)] τ_s τ_y (Pa)	Consistency K (cP)	Fill Level H (m)	Breakthrough Velocity	
								Peak Average u_p (m/s)	Average u_a (m/s)
L-2	336	Laponite	3.88	0.102	100.7	12.3	3.50	6.1	5.5
L-4	336	Laponite	3.88	0.102	109.4	12.9	3.38	5.4	4.9
M-7	APEL	Laponite	0.86	0.022	102.6	12.0	0.76	6.0	4.8
S-2	SRNL	Laponite	0.44	0.011	71.0	9.7	0.39	6.1	5.5
S-5	SRNL	Laponite	0.44	0.011	99.1	9.7	0.39	6.8	6.0
L-18	336	clay	3.88	0.102	41.3	22.1	3.50	6.6	5.5
L-19&L-20	336	clay	3.88	0.102	28.7	19.8	3.50	6.8	5.7
M-20	APEL	clay	0.86	0.022	21.6	26.7	0.76	7.3	4.7
M-21	APEL	clay	0.86	0.022	44.6	19.1	0.76	8.3	5.7
S-15	SRNL	clay	0.44	0.011	18.4	21.5	0.39	8.6	7.0

(a) Laponite is characterized by the shear strength, while yield stress is used for clay.
A density of $\rho = 1200$ kg/m^3 is used for clay and $\rho = 1000$ kg/m^3 for Laponite.

Table 5.5. Nondimensional Data from 4PJM Clay and Laponite Surface Breakthrough Tests at Three Physical Scales

Reference Number	Test Scale Factor s	Simulant	Non-dimensional Fill Level H/D_T	Jet Reynolds Number		Yield Reynolds Number		Combined Reynolds Number	
				Peak Average Re_0	Average Re_0	Peak Average Re_τ	Average Re_τ	Peak Average Re	Average Re
L-2	1.00	Laponite	0.90	5.1E+04	4.6E+04	3.8E+02	3.1E+02	3.7E+02	3.0E+02
L-4	1.00	Laponite	0.87	4.3E+04	3.8E+04	2.7E+02	2.2E+02	2.7E+02	2.2E+02
M-7	4.53	Laponite	0.88	1.1E+04	9.1E+03	3.5E+02	2.3E+02	3.4E+02	2.2E+02
S-2	8.87	Laponite	0.90	7.2E+03	6.5E+03	5.2E+02	4.2E+02	4.9E+02	4.0E+02
S-5	8.87	Laponite	0.90	8.0E+03	7.1E+03	4.7E+02	3.6E+02	4.4E+02	3.4E+02
L-18	1.00	clay	0.90	3.6E+04	3.0E+04	1.3E+03	8.8E+02	1.2E+03	8.5E+02
L-19&L-20	1.00	clay	0.90	4.2E+04	3.5E+04	1.9E+03	1.4E+03	1.8E+03	1.3E+03
M-20	4.53	clay	0.88	7.3E+03	4.8E+03	2.9E+03	1.2E+03	2.1E+03	9.9E+02
M-21	4.53	clay	0.88	1.2E+04	8.1E+03	1.8E+03	8.7E+02	1.6E+03	7.9E+02
S-15	8.87	clay	0.90	5.5E+03	4.4E+03	4.9E+03	3.2E+03	2.6E+03	1.8E+03

Yield Reynolds numbers at breakthrough for clay and Laponite tests are plotted versus vessel scale factor in Figure 5.7. When peak average velocities (u_P) are used, the data clearly suggest that large vessels require a lower yield Reynolds number for breakthrough. The same trend is seen when the average PJM velocity (u_a) is used to correlate the data, only here it could be argued that no real difference is seen between the large-scale 336 vessel (s = 1) and the APEL vessel (s = 4.53). Yield Reynolds numbers for breakthrough with clay are significantly larger than for Laponite. Part of this difference is attributed to the fact that the shear strength in clay is about 50% higher than the yield stress. However, a

factor of ~5 would be required to explain the difference. This suggests that clay exhibits non-Newtonian effects on the flow structure, not just on the flow boundary, as is believed for Laponite. Hence larger yield Reynolds numbers are required for breakthrough in clay than in Laponite at the same conditions.

In Figure 5.8, the combined Reynolds number is plotted versus vessel scale factor. Recall the combined Reynolds number is the ratio of inertial force to the total Bingham stress, which includes yield stress as well as viscous stress and is given by $\mathrm{Re} = \mathrm{Re}_\tau/(1+\mathrm{Re}_\tau/\mathrm{Re}_0)$. This correlation variable produces similar results to the yield Reynolds number but with reduced values for large s.

In Figure 5.9, the yield Reynolds number (Re_τ) is plotted versus jet Reynolds number (Re_0). In Figure 5.10 the combined Reynolds number (Re) is plotted versus jet Reynolds number. While there is some scatter in the data, these correlations suggest that the yield or combined Reynolds number required for breakthrough is reduced as the jet Reynolds number is increased. In physical terms this implies, for equal simulant rheology, that breakthrough velocities will be smaller at larger test scales.

Data presented in Figure 5.9 suggest a correlation for cavern height in the form $\mathrm{H_C}/\mathrm{D_T} = \mathrm{A}\,\mathrm{Re}_\tau^{a}\,\mathrm{Re}_0^{b}$. It is evident from Figure 5.9 that the exponent b is significantly smaller than a, consistent with the general finding that jet Reynolds number effects are secondary to yield Reynolds number effects.

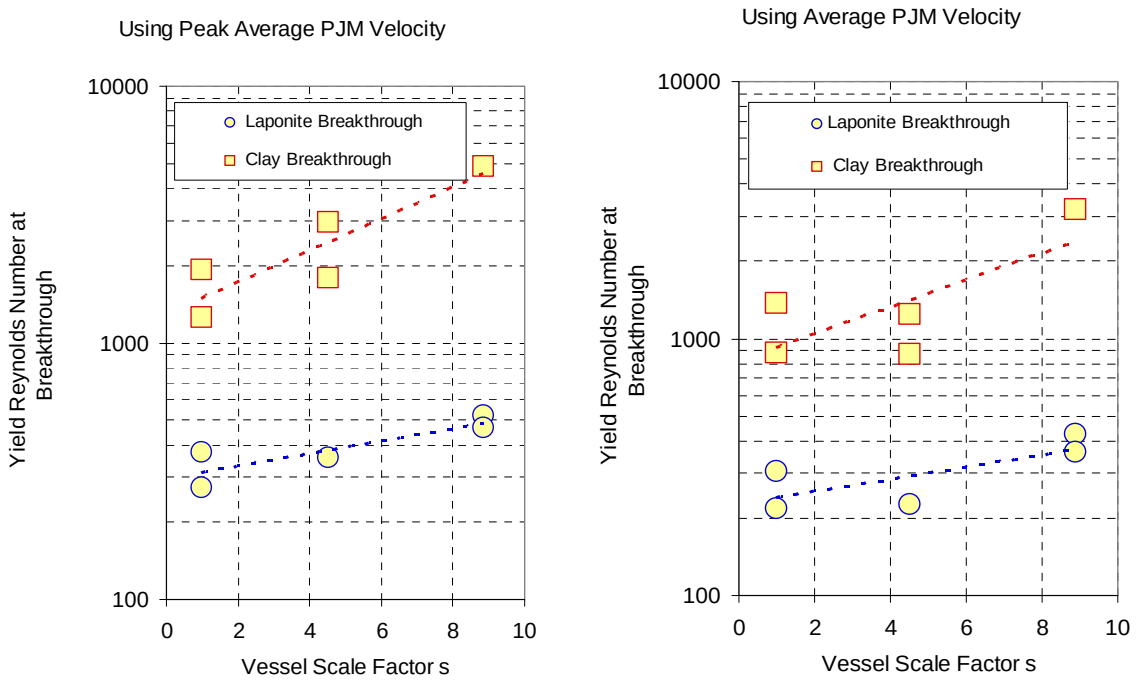

Figure 5.7. Yield Reynolds Number (Re_τ) at Breakthrough Versus Vessel Scale Factor for Breakthrough Tests in Clay and Laponite. Parameters are calculated using peak average PJM velocity (u_p) (left) and average PJM velocity (u_a) (right).

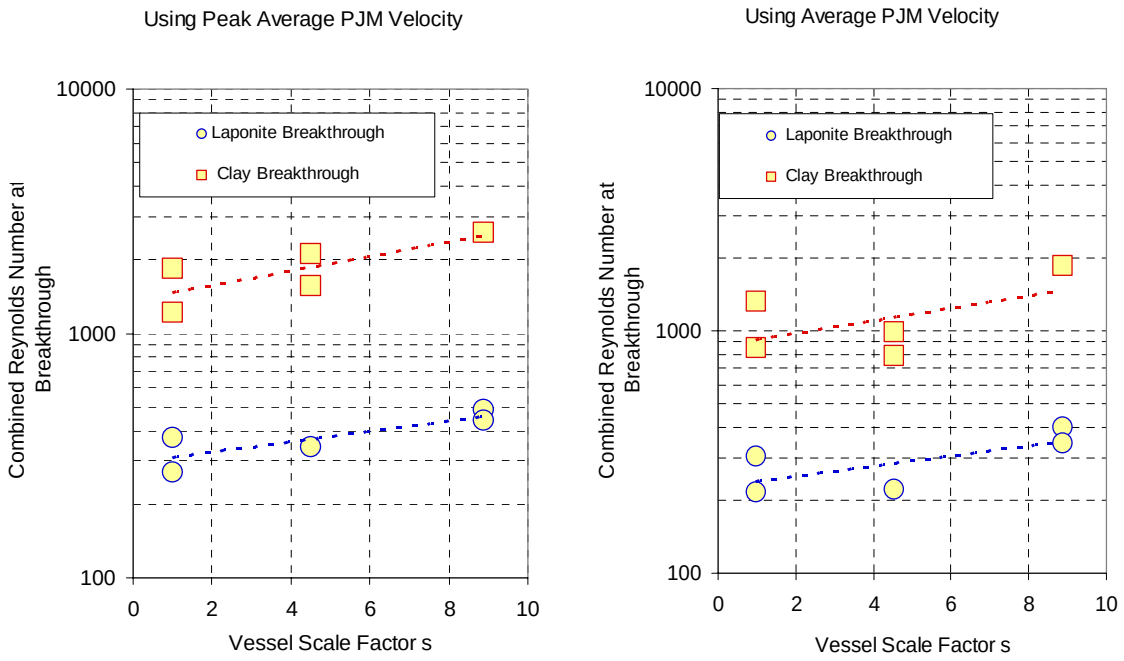

Figure 5.8. Combined Reynolds Number (Re) at Breakthrough Versus Vessel Scale Factor for Breakthrough Tests in Clay and Laponite. Parameters are calculated using peak average PJM velocity (u_p) (left) and average PJM velocity (u_a) (right).

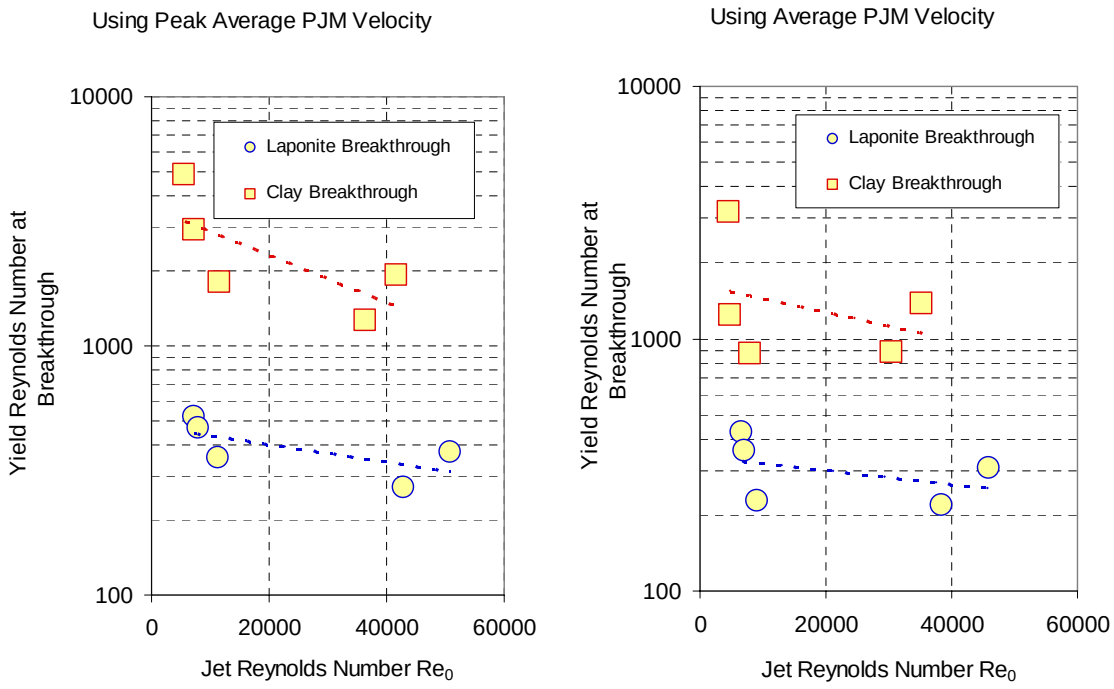

Figure 5.9. Yield Reynolds Number (Re_τ) at Breakthrough Versus Jet Reynolds Number (Re_0) for Breakthrough Tests in Clay and Laponite. Parameters are calculated using peak average PJM velocity (u_p) (left) and average PJM velocity (u_a) (right).

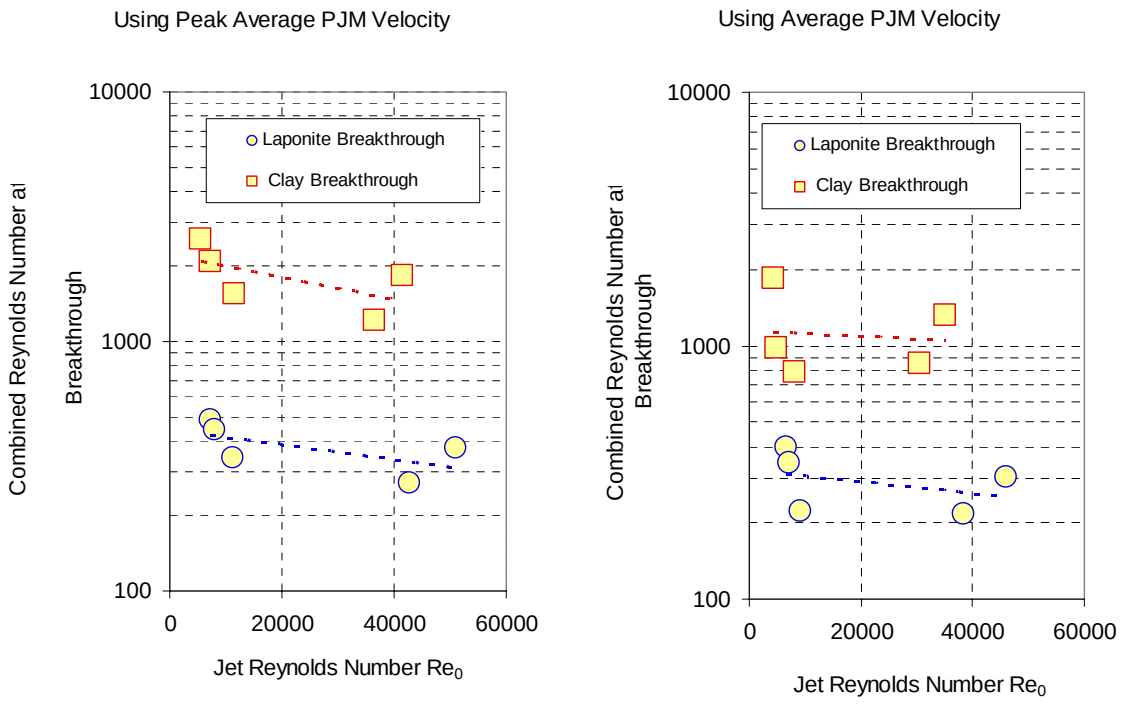

Figure 5.10. Combined Reynolds Number (Re) at Breakthrough Versus Jet Reynolds Number (Re_0) for Breakthrough Tests in Clay and Laponite. Parameters are calculated using peak average PJM velocity (u_p) (left) and average PJM velocity (u_a) (right).

5.4 Upwell Velocity Measurements in Clay Simulant at Two Physical Scales

Velocities in the central upwell of the cavern were measured using clay simulant in the 336 and APEL test vessels. In these tests, the upwell velocity was measured at various elevations for a given PJM velocity. This allows a direct comparison of actual velocities between the two vessels.

Results for these tests are summarized in Table 5.6. Clay rheology, PJM velocity, and vertical elevation are the primary test variables, with upwell velocity a measured dependent variable. Both peak average and average PJM velocities are reported in Table 5.6. The tests were performed with a non-dimensional simulant fill level of approximately $H/D_T = 0.9$ for all tests. The upwell velocities reported in Table 5.6 are the average of the maximum measured velocities. As the PJMs were operating, upwell velocities oscillated between low and high values as the pulse formed, stabilized, and then diminished. The maximum velocity for each PJM drive was determined, and the average over many cycles is shown in the table. The standard deviation in measured upwell velocity is also shown.

Table 5.7 presents the data in nondimensional form. Jet Reynolds number, yield Reynolds number, and combined Reynolds number are all calculated using the peak average and average PJM velocities. The elevation of the measured upwell velocity is nondimensionalized by the vessel diameter, and the upwell velocity is nondimensionalized by the peak average or average PJM velocity.

Table 5.6. Dimensional Data from 4PJM Clay[a] Velocity Upwell Tests at Two Physical Scales

Test Platform	Nozzle Diameter d_0 (m)	Vessel Diameter D_T (m)	Yield Stress τ_y (Pa)	Consistency K (cP)	PJM Velocity		Probe Elevation H_{VP} (m)	Measured Upwell Velocity[b]	
					Peak Average u_p (m/s)	Average u_a (m/s)		U_{uw} (m/s)	St. Dev.
336	0.102	3.89	28.8	20.3	8.2	6.8	1.13	2.10	0.13
336	0.102	3.89	28.8	20.3	5.5	4.9	1.13	0.97	0.03
336	0.102	3.89	28.8	20.3	8.6	6.7	1.13	2.07	0.13
336	0.102	3.89	28.8	20.3	8.5	7.0	1.13	2.16	0.09
336	0.102	3.89	28.8	20.3	5.5	4.9	2.30	0.17	0.05
336	0.102	3.89	28.8	20.3	8.3	6.9	2.30	1.17	0.07
336	0.102	3.89	28.8	20.3	8.7	6.8	2.30	1.30	0.10
336	0.102	3.89	28.8	20.3	8.6	6.9	2.30	1.23	0.06
336	0.102	3.89	28.8	20.3	8.6	6.8	3.27	0.59	0.16
336	0.102	3.89	28.8	20.3	8.3	6.8	3.27	0.65	0.12
336	0.102	3.89	28.8	20.3	5.5	4.9	3.27	0.07	0.01
APEL	0.022	0.86	34.3	22.3	11.3	7.2	0.31	1.88	0.21
APEL	0.022	0.86	34.3	22.3	11.3	7.0	0.31	1.86	0.26
APEL	0.022	0.86	34.3	22.3	11.3	7.5	0.51	1.36	0.28
APEL	0.022	0.86	34.3	22.3	11.3	7.5	0.51	1.42	0.25
APEL	0.022	0.86	34.3	22.3	9.8	6.3	0.51	0.72	0.19
APEL	0.022	0.86	34.3	22.3	11.3	7.4	0.65	1.07	0.22
APEL	0.022	0.86	34.3	22.3	9.8	6.3	0.65	0.35	0.21

(a) Density $\rho = 1200$ kg/m^3 used for all tests.
(b) Average of all observed transient peaks.

In Figure 5.11, normalized upwell velocity is plotted versus normalized elevation for both APEL and 336 clay tests. It is clear from the plots that upwell velocity generally decreases with elevation. It is not clear, however, that the velocities from the 336 results bound the APEL velocities. In fact, several of the 336 data points are clearly lower than the APEL velocities at the same vertical elevation, a trend that appears inconsistent with jet Reynolds number scaling.

Figure 5.12 explores the effect of jet Reynolds number on upwell velocity. Again, it is not clear that the data follow simple jet Reynolds number scaling because some of the upwell velocities decrease with increasing Jet Reynolds number.

In Figure 5.13, the normalized upwell velocities are correlated with yield Reynolds number. These data indicate a general trend that upwell velocity increases with increasing yield Reynolds number. Also, the APEL data generally fall below the 336 data (or at least the apparent trend of the 336 data). The same trend is seen when plotting against the combined Reynolds number, as shown in Figure 5.14, where the data become a little more tightly grouped. Evidently the dominant parameter affecting upwell velocity is the yield Reynolds number (or the similar combined Reynolds number). Jet Reynolds number effects are secondary. If one carefully examines Figures 5.13 and 5.14, however, it is clear that the upwell velocities measured in APEL are equal to or less than those measured in 336. Also, because upwell velocity appears to be an increasing function of the combined Reynolds number, an additional conservatism exists— for similar rheology and PJM velocity, the combined Reynolds number is larger at large scale.

Table 5.7. Nondimensional Data from 4PJM Clay Velocity Upwell Tests at Two Physical Scales

Vessel Scale Factor (s)	Non-dimensional Elevation (H_{VP}/D_T)	Jet Reynolds Number		Yield Reynolds Number		Combined Reynolds Number		Nondimensional Upwell Velocity	
		Peak Average (Re_0)	Average (Re_0)	Peak Average (Re_τ)	Average (Re_τ)	Peak Average (Re)	Average (Re)	Peak Average (U_{uw}/u_p)	Average (U_{uw}/u_a)
1	0.29	4.9E+04	4.1E+04	2.8E+03	1.9E+03	2.6E+03	1.8E+03	0.26	0.31
1	0.29	3.3E+04	2.9E+04	1.2E+03	1.0E+03	1.2E+03	9.7E+02	0.18	0.20
1	0.29	5.2E+04	4.0E+04	3.1E+03	1.9E+03	2.9E+03	1.8E+03	0.24	0.31
1	0.29	5.1E+04	4.2E+04	3.0E+03	2.0E+03	2.9E+03	1.9E+03	0.25	0.31
1	0.59	3.3E+04	2.9E+04	1.3E+03	1.0E+03	1.2E+03	9.7E+02	0.03	0.03
1	0.59	5.0E+04	4.1E+04	2.9E+03	2.0E+03	2.7E+03	1.9E+03	0.14	0.17
1	0.59	5.2E+04	4.1E+04	3.1E+03	1.9E+03	3.0E+03	1.8E+03	0.15	0.19
1	0.59	5.2E+04	4.1E+04	3.1E+03	2.0E+03	2.9E+03	1.9E+03	0.14	0.18
1	0.84	5.2E+04	4.1E+04	3.1E+03	1.9E+03	2.9E+03	1.8E+03	0.07	0.09
1	0.84	5.0E+04	4.1E+04	2.9E+03	1.9E+03	2.7E+03	1.8E+03	0.08	0.10
1	0.84	3.3E+04	2.9E+04	1.3E+03	1.0E+03	1.2E+03	9.7E+02	0.01	0.01
4.53	0.36	1.4E+04	8.7E+03	4.5E+03	1.8E+03	3.4E+03	1.5E+03	0.17	0.26
4.53	0.36	1.4E+04	8.5E+03	4.5E+03	1.7E+03	3.4E+03	1.4E+03	0.16	0.26
4.53	0.59	1.4E+04	9.1E+03	4.5E+03	2.0E+03	3.4E+03	1.6E+03	0.12	0.18
4.53	0.59	1.4E+04	9.1E+03	4.5E+03	2.0E+03	3.4E+03	1.6E+03	0.13	0.19
4.53	0.59	1.2E+04	7.6E+03	3.4E+03	1.4E+03	2.6E+03	1.2E+03	0.07	0.11
4.53	0.76	1.4E+04	9.0E+03	4.5E+03	1.9E+03	3.4E+03	1.6E+03	0.09	0.14
4.53	0.76	1.2E+04	7.6E+03	3.4E+03	1.4E+03	2.6E+03	1.2E+03	0.04	0.06

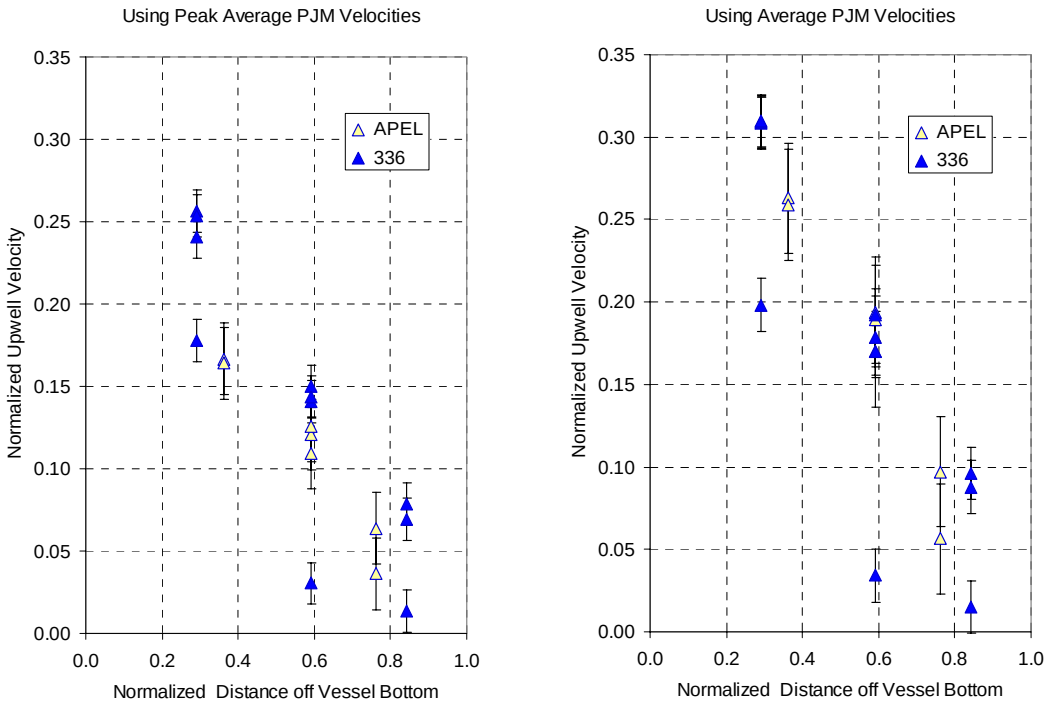

Figure 5.11. Normalized Upwell Velocity Versus Normalized Elevation (H_{VP}/D_T) in Clay Compared at Two Vessel Scales. Upwell velocity (U_{uw}) is normalized by the peak average PJM velocity (u_p) (left) and the average PJM velocity (u_a) (right).

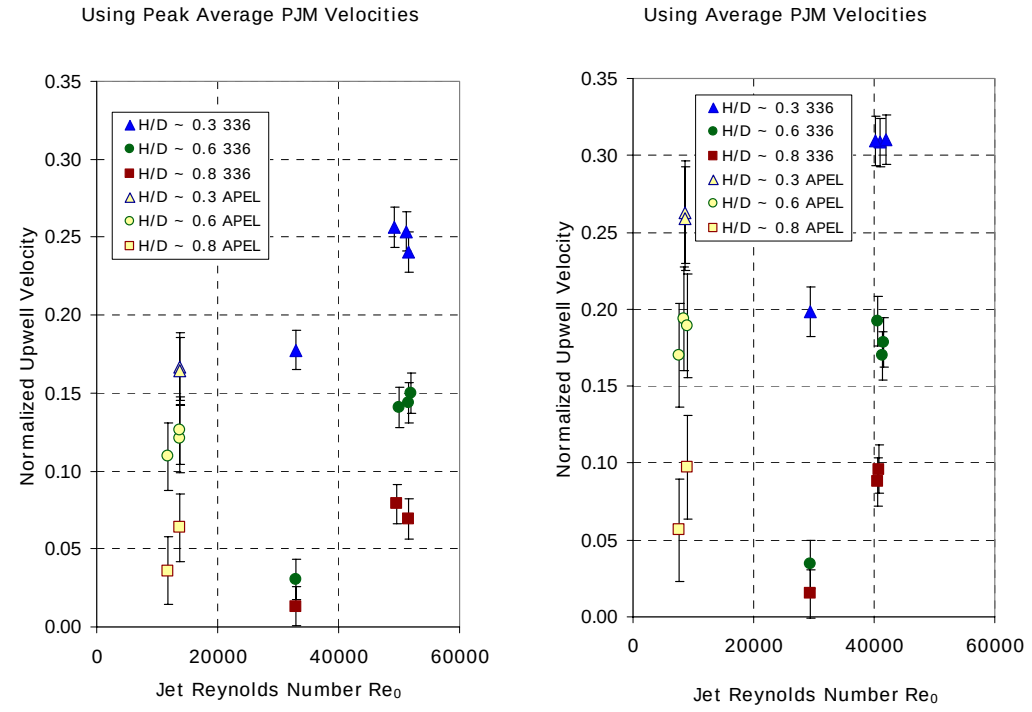

Figure 5.12. Normalized Upwell Velocity Versus Jet Reynolds Number in Clay Compared at Two Vessel Scales. Upwell velocity (U_{uw}) is normalized by the peak average PJM velocity (u_p) (left) and the average PJM velocity (u_a) (right).

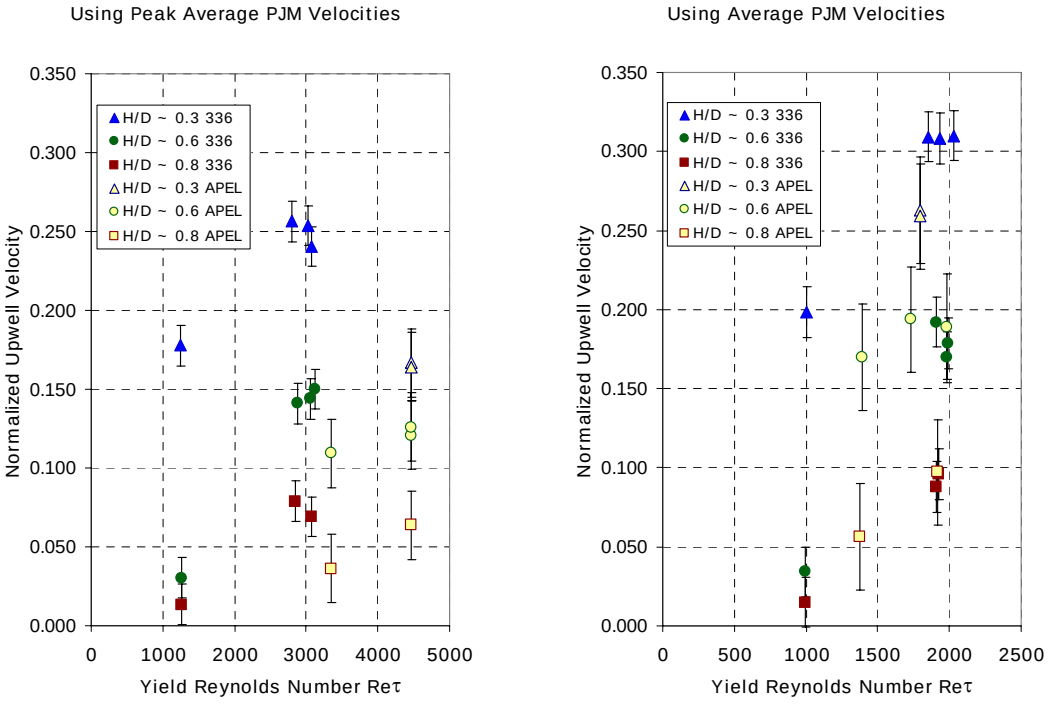

Figure 5.13. Normalized Upwell Velocity Versus Yield Reynolds Number in Clay Compared at Two Vessel Scales. Upwell velocity (U_{uw}) is normalized by the peak average PJM velocity (u_p) (left) and the average PJM velocity (u_a) (right).

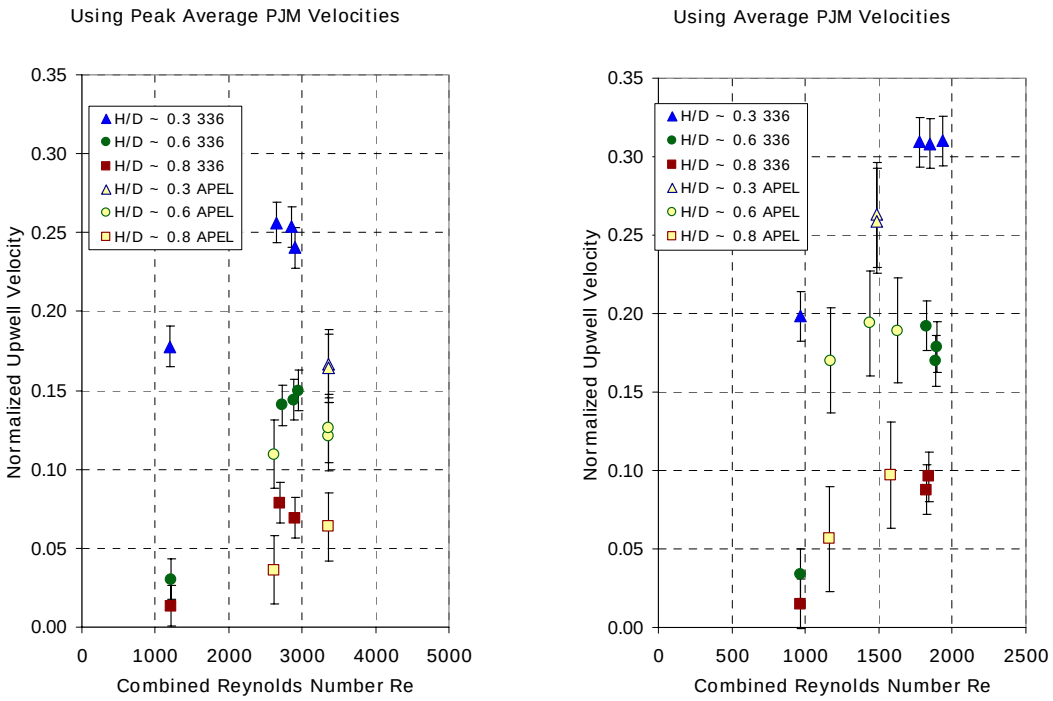

Figure 5.14. Normalized Upwell Velocity Versus Combined Reynolds Number in Clay Compared at Two Vessel Scales. Upwell velocity (U_{uw}) is normalized by the peak average PJM velocity (u_p) (left) and the average PJM velocity (u_a) (right).

6.0 Summary and Conclusions

6.1 Overall Conclusion

The analysis and experimental test results obtained from this study demonstrate that the mixing performance of PJM mixing systems in non-Newtonian slurries can be conservatively assessed at small scale for the following reasons:

- The three most important nondimensional parameter groups were found to be the Strouhal number, the yield Reynolds number, and the jet Reynolds number. If these parameters are preserved at small scale, the essential behavior of the mixing phenomena will be the same as at full scale.
- The Strouhal number, which takes into account non-steady PJM operation, is the same at small and full scale when the PJM cycling is reduced by the geometric scale factor.
- The yield Reynolds number, which determines cavern formation due to non-Newtonian fluid behavior, is the same at small and full scale when rheology and PJM velocities are the same at both scales.
- The jet Reynolds number, which determines the flow regime (laminar or turbulent) and the degree of turbulence, will be reduced by the geometric scale factor at small scale when rheology and PJM velocities are the same at both scales. This is conservative because full-scale mixing will always occur at higher jet Reynolds number and hence have a higher degree of turbulence.

The actual mixing results obtained from the 4PJM scaling tests are not to be directly applied to full-scale WTP vessels. Rather, the results were obtained to prove that PJM mixing systems for WTP vessels can be adequately assessed at small scale. If prototypic systems are tested at small scale, according to the scale laws and approach outlined in this report (Section 6.5.1), PJM geometries and operational scenarios that meet plant needs can be determined with confidence.

6.2 Objectives and Technical Approach

The central purpose of this work was to establish the technical basis for performing scaled testing of PJM systems. This scaling approach was required to design, conduct, and apply results of tests in reduced-scale prototypic Hanford WTP PJM mixing systems (Bates et al. 2004).[(a)] The scaling approach consisted of two key components: theoretical analysis and experimental confirmation.

6.2.1 Theoretical Analysis and Scaling Laws

Theoretical analysis included developing a physical model for the cavern position resulting from a single, downward-oriented, steady jet operating in a non-Newtonian slurry. This model used heuristic arguments involving elemental turbulent Newtonian jet theory coupled with a static force balance between the impinging jet and slurry cavern boundary. The model was extended to accommodate non-

(a) Johnson MD et al. 2005. *Hybrid Mixing System Test Results for Prototype Ultrafiltration Feed Process and High-Level Waste Lag Storage Vessels.* WPT-RPT-128 Rev. A, PNWD, Richland, Washington.

steady jet operation characteristic of PJMs as well as multiple PJMs. As a natural consequence of the physical model, the dependence of cavern position on various physical parameters was evident.

Normalized cavern height (cavern height divided by vessel diameter) was found to depend on the yield Reynolds number, the jet Reynolds number, the ratio of PJM nozzle diameter to vessel diameter, and the nondimensional pulse time (ratio of PJM volume to nozzle diameter cubed). Cavern heights predicted by the single PJM model were found to be in good agreement with measured cavern heights in Laponite and clay simulant. As an added benefit, the physical model demonstrates the relative importance of various parameters affecting cavern height and provides insight into the optimal operation of PJMs.

In addition to the development of the physical model, dimensional analysis, and physical insight were used to identify the important nondimensional parameters affecting the performance of PJM mixing systems. The relative importance of the various parameters was analyzed, and those considered dominant were identified. Evaluating how these nondimensional parameters changed with physical test scale led to the scaled testing approach.

6.2.2 Experimental Confirmation of Scaling Approach

The scaling laws and the nondimensional parameters determined to be most important to the non-Newtonian mixing problem required experimental validation. Therefore, an experimental test strategy was developed that involved performing mixing tests using 4PJM arrays at three different scales, including a large-scale vessel in the 336 Building at PNWD that had a capacity of about 12,000 gallons, PJM diameter of 24 inches, and PJM nozzle diameter of 4 inches; a 1/4.5-scale version of the 4PJM vessel in the APEL building at PNWD with a capacity of about 250 gallons, PJM diameter of 5.3 inches, and PJM nozzle diameter of 0.9 inches; and a 1/8.9-scale vessel at SRNL with a capacity of about 18 gallons, PJM diameter of 2.63 inches, and PJM nozzle diameter of 0.45 inches. The tests used two non-Newtonian simulants, a kaolin-bentonite clay mixture and Laponite. Experimental data collected from the geometrically scaled test stands were compared at similar conditions to confirm and demonstrate the methodology for predicting large-scale behavior from the small-scale test results.

6.3 Scaled Testing Approach

6.3.1 Designing Scaled 4PJM Tests

The scaling approach used in the design and operation of the 4PJM tests employed the following:

- *Geometry*. With geometric scaling, a small-scale mixing system is an exact geometric miniature of a large-scale system. This is accomplished by reducing all linear dimensions by a scale factor, s. This method was employed in the 4PJM test program. Taking the 336 vessel as full scale, the APEL test stand had a scale factor of 4.5, and the SRNL test stand had a scale factor of 8.9. This scaling was applied to all significant features such as tank diameter, PJM diameter, and nozzle diameter (in some cases, supporting structures could not be geometrically scaled). With this scaling, all areas are reduced by s^2 and all volumes are reduced by s^3.

- *Rheology*. The scaled test program used a constant rheology approach. That is, the simulant yield stress and consistency were not adjusted to take into account different test scales. The rheology was allowed to vary in the tests, however, to explore the effect on mixing behavior.
- *PJM Velocity*. The scaled test program used a constant PJM velocity approach. That is, the PJM velocity was not adjusted to take into account different test scales. The PJM velocity was allowed to vary in the tests, however, to explore the effect on mixing behavior.
- *PJM Discharge Volume*. The volume of slurry discharged during a PJM drive cycle scales according $1/s^3$, consistent with the geometric scaling approach.
- *PJM Drive Time*. The PJM drive time was scaled by 1/s for all tests. This is a consequence of geometric and constant volume scaling. Other characteristic times (such as PJM cycle time) also followed this scaling.

6.3.2 Results from Dimensional Analysis

The results of dimensional analysis indicate that the primary nondimensional parameters required for small-scale testing are the yield Reynolds number, Re_τ, and Strouhal number, S_0. If these are matched at large and small scale, the nondimensional cavern heights and mixing times should be the same at a first-order approximation. The scaled test strategy outlined above preserved both of these parameters.

The jet Reynolds number, Re_0, is considered to be of secondary importance relative to the yield Reynolds number. Scaling of this parameter is not preserved by the test strategy. When constant yield Reynolds number is preserved at different test scales, the jet Reynolds number will always be reduced at smaller scale. However, the testing approach was conservative since testing at reduced jet Reynolds numbers results in generally reduced mixing phenomena (such as cavern heights, magnitude of velocities, and degree of turbulence).

6.4 Summary of Experimental Results

6.4.1 Types of Data Collected

The specific data used for comparison consisted of both cavern and velocity measurements collected at the three test scales. The logic behind using cavern measurements for comparison was as follows: If normalized cavern heights are shown to agree at different test scales for similarly operated PJMs, operation of PJMs such that the caverns are eliminated in small-scale PJM mixing systems (i.e., complete mobilization of non-Newtonian material) guarantees complete mobilization in full-scale systems when the PJMs are operated similarly.

In addition to cavern height, two types of velocity measurements were found to be useful for comparison: breakthrough velocities and upwell velocities. For the breakthrough velocities, the PJM velocity was increased until cavern breakthrough was achieved. The nondimensional yield Reynolds number at breakthrough was then compared at different scales. The upwell velocities were directly measured in the central upwell in between the four PJMs. The upwell velocity was normalized by the PJM velocity and compared. In addition, limited data were obtained to evaluate mixing time.

6.4.2 Test Conditions

The range of test conditions was selected to provide enough variation to establish a wide range of comparable data and to span full-scale plant operating conditions where possible. The approximate range of test conditions, including dimensional and nondimensional parameters, is listed in Table 6.1.

Table 6.1. Range of Conditions Tested in 4PJM Experiments Compared with Full-Scale WTP Bounding Conditions

Parameter	Symbol	Units	WTP Bounding	Test Range
Average PJM drive velocity	u_a	m/s	9	3.0–10.2
Peak average PJM drive velocity	u_p	m/s	12	3.3–12.2
PJM drive time	t_D	s	15–60	2–20
Nominal vessel batch volume	V_T	gal	12,000–70,000	30–12,000
PJM nozzle diameter	d_0	cm	10	1–10
Slurry density	ρ	kg/m^3	1300	1000–1200
Slurry consistency	K	cP	30	10–27
Slurry yield stress	τ_y	Pa	30	18–46
Slurry shear strength	τ_s	Pa	75 (est.)	30–125
Yield Reynolds number (based on u_p)	Re_τ		6,200	120–4,900
Jet Reynolds number (based on u_p)	Re_0		52,000	5,500–52,000
Strouhal number (based on u_p)	S_0		1800–7200	900–2400

6.4.3 Summary of Test Results

Normalized cavern heights in Laponite were found to be an increasing function of the yield Reynolds number. Although significant scatter exists in the data, cavern heights were generally found to decrease at smaller scales. This behavior is consistent with the reduction in jet Reynolds number associated with smaller test scales.

Surface breakthrough velocity tests performed in both clay and Laponite also showed that the yield Reynolds number associated with surface breakthrough increased with the test scale factor. Equivalently, breakthrough yield Reynolds number decreased with jet Reynolds number.

Upwell velocity measurements indicated that normalized velocities generally decreased with yield Reynolds number. While it was difficult to conclusively observe jet Reynolds number effects, the data suggest that upwell velocities are a weak, decreasing function of jet Reynolds number.

The role of Strouhal number was not explicitly examined in the tests. However, at equivalent operating conditions, the Strouhal number was constant at the different test scales and thus not affected by test scale factor.

Differences in the details of the PJM drive function are expected at different scales. In general, using the peak average PJM velocity appeared to correlate the data slightly better than using average velocity. However, the differences are small and may be within the experimental uncertainty.

Experiments to measure time to mix were conducted using Laponite and kaolin-bentonite simulants at three scales. When these data were compared significant differences in experimental conditions, measurement approaches, as well as a limited test matrix were noted. Therefore, these results did not contribute to the scaling analysis.

In summary, data from the 4PJM tests at three scales clearly indicate that the yield Reynolds number is the dominant nondimensional parameter governing mixing in non-Newtonian slurries. The jet Reynolds number has a secondary effect, which is to generally reduce velocities and cavern heights at smaller test scales due to the effectively high consistency of the simulant.

6.5 Application to Scaled Prototype Testing

6.5.1 Recommended Scaling Approach

It is recommended that scaled testing of prototypic PJM systems in non-Newtonian slurries adhere to the following guidelines:

- Use geometric scaling with a scale factor no greater than 4–5 since the testing was performed within this range
- Use the bounding WTP non-Newtonian rheology (30 Pa yield strength, 30 cP consistency)
- Use the design peak average PJM velocity (12 m/s)
- Use PJM drive times and cycle time reduced by the scale factor, s.

If these guidelines are followed, the yield Reynolds and Strouhal numbers (the two most important nondimensional parameters affecting mixing in non-steady, non-Newtonian slurries) will be matched at small scale. In addition, the jet Reynolds number will be smaller in the small scale test, and the result will thus be conservative. As an alternative, the slurry consistency may be reduced by the scale factor for the simulant in the small scale test. This will have the effect of matching jet Reynolds number. However, adjusting the consistency independent of the yield stress for a non-Newtonian slurry is challenging.

6.5.2 Insights on Optimizing PJM Systems

While not the central purpose of this study, the analysis and experiments conducted led to a number of insights into the behavior of PJM mixing systems and approaches to achieve optimal mixing. A summary of useful findings is presented:

- Quantifying the “goodness” of non-Newtonian mixing systems is difficult. However, with yield stress materials, it is obvious that the presence of stagnant regions represents poor mixing. Thus, performing tests where the PJMs are adjusted in design or operation until complete slurry mobilization occurs is an effective way to guarantee at least one essential feature of adequate mixing. The scaled test approach ensures that the full-scale system will exhibit mixing performance at least as good as the small-scale results indicate.
- Downward-firing PJMs in dished-bottom tanks are not an optimal configuration. The presence of a strong central upwell in these configurations results in poor mixing in the outer annulus and excess mixing in the center. Approaches that spread jet momentum more uniformly are a more

efficient means of mixing vessel contents. Angling the nozzles outward so they have normal or nearly normal impingement with the vessel bottom will likely improve mixing performance.

- For a given total PJM operating volume, it appears beneficial to have fewer, larger PJMs rather than many smaller ones (from a slurry mobilization point of view) because smaller PJMs have shorter drive times and result in jets that are not as well established. Evidently, for a given total PJM volume, an optimum number exists. This benefit needs to be balanced against other potential functions not addressed in this study, such as solids suspension and uniformity.

6.5.3 Limitations of Findings

Nonsteady mixing of radioactive non-Newtonian slurries is a complex problem. This study has attempted to capture certain essential aspects of the problem to provide a means to evaluate and improve PJM mixing systems at reduced scale with nonhazardous simulants. Therefore, certain limitations that are summarized below apply regarding the applicability of the results:

- The scaling approach presented in this report is limited to non-Newtonian slurries that possess Bingham plastic-like rheological behavior. That is, they are characterized by a yield stress and a constant consistency. The results may also be applicable to other non-Newtonian rheologies; however, caution must be exercised. Slurries with strong hysteretic effects or that rapidly develop shear strength on a time scale consistent with the PJM refill time could be problematic.
- The results are limited to mobilization of non-Newtonian slurries. Other mixing functions such as solids suspension and uniformity are not addressed by the scaling analysis and experiments conducted. At high solids concentrations, the slurry is gel-like, and solids settling or separation is unlikely on the time scales associated with PJM operation. However, at lower concentration (or with slurries that behave more Newtonian) solids settling, resuspension, and uniformity may be issues. Separate analysis and/or testing are required to address these aspects of mixing.
- Gas retention is a normal aspect of radioactive slurries because radiolysis and thermolysis produce hydrogen and other gases that take the form of bubbles. The scaling laws presented here did not specifically consider gas retention and release in PJM mixing systems. However, the basic scaling concepts regarding PJM mixing are thought to be applicable when performing scaled mixing tests of non-Newtonian slurries with gas retention and release. The scaling of these phenomena was also a part of the PJM test program and specifically addressed by Rassat et al.[(a)] and Russell et al.[(b)]

(a) Rassat SD, CW Stewart, RL Russell, PA Meyer, ST Arm, and CD Johnson. 2004. *Interim Report: Gas Retention and Release in Pulsed-Jet Mixed Tanks Containing Non-Newtonian Waste Simulants.* WTP-RPT-114, PNWD, Richland, Washington.
(b) Russell RL et al. 2005. *Final Report : Gas Retention and Release in Pulse Jet Mixed Tanks Containing Non-Newtonian Waste Simulants*. WTP-RPT-114, Rev. 1. PNWD, Richland, Washington.

7.0 References

Bates JM, JW Brothers, JM Alzheimer, and DE Wallace. 2004. *Test Results for Pulse Jet Mixers in Prototypic Ultrafiltration Process Feed Process and High-Level Waste Lag Storage Vessels.* PNWD-3496, Battelle – Pacific Northwest Division, Richland, Washington.

Bontha JR, JM Bates, CW Enderlin, and MG Dodson. 2003. *Large Tank Experimental Data for Validation of the FLUENT CFD Model of Pulsed Jet Mixers.* PNWD-3303, Battelle – Pacific Northwest Division, Richland, Washington.

Enderlin CW, MG Dodson, F Nigl, JR Bontha, JM Bates. 2003. *Results of Small-Scale Particle Cloud Tests and Non-Newtonian Fluid Cavern Tests.* PNWD-3360, Battelle – Pacific Northwest Division, Richland, Washington.

Poloski AP, PA Meyer, LK Jagoda, and PR Hrma. 2004. *Non-Newtonian Slurry Simulant Development and Selection for Pulse Jet Mixer Testing*. PNWD-3495, Battelle – Pacific Northwest Division, Richland, Washington.

Poloski AP, ST Arm, JA Bamberger, B Barnett, R Brown, BJ Cook, CW Enderlin, MS Fountain, M Friedrich, BG Fritz, RP Mueller, F Nigl, Y Onishi, LA Schienbein, LA Snow, S Tzemos, M White, JA Vucelick. 2005. *Technical Basis for Scaling of Air Sparging Systems for Mixing in Non Newtonian Slurries.* WTP-RPT-129 Rev. 0, Battelle – Pacific Northwest Division, Richland, Washington.

Rajaratnam N. 1976. *Turbulent Jets*. Elsevier Science Publishers, New York.

Rassat SD, LM Bagaasen, LA Mahoney, RL Russell, DD Caldwell, and DP Mendoza. 2003. *Physical and Liquid Chemical Simulant Formulations for Transuranic Wastes in Hanford Single-Shell Tanks.* PNNL-14333, Pacific Northwest National Laboratory, Richland Washington.

Speers RA, KR Holme, MA Tung, and WT Williamson. 1987. "Drilling fluid shear stress overshoot behavior." *Rheologica Acta,* Vol. 26, pp. 447-452.

Wilson DA, ML Restivo, HN Guerrero, TJ Steeper, RE Eibling, EK Hansen, TM Jones, and KR Eberl. November 2004. *One-Eighth Scale Pulse Jet Mixer (PJM) - Design Parameters Scale Law Testing.* WSRC-TR-2004-00430 Rev. 0 (SRNL-RPP-2004-00069 Rev. 0), Westinghouse Savannah River Company, Aiken, South Carolina.

Zarruk GA, KA Chang, and EA Cowen. 2002. *Reynolds Number Dependence of the Neutrally Buoyant* Turbulent *Jet*. American Physical Society, 53rd Annual Meeting of the Division of Fluid Dynamics, November 19–21, Washington, DC.

Appendix A

Large-Tank 4PJM Scaling Experiments

Appendix A Contents

Figures

Tables

Appendix A

Large-Tank 4PJM Scaling Experiments

The Pulse Jet Mixer (PJM) Task Team developed an integrated approach for scaled testing to validate PJM mixing in Waste Treatment Plant (WTP) vessels containing non-Newtonian fluids. Large-scale PJM mixing tests of a 4PJM array were conducted at the large-tank 336 Building facility to provide design information about the operating parameters critical for the mixing and mobilization of the tank contents. The large-scale PJM test program used one transparent and one opaque stimulant, which are described in Appendix D.

A.1 Large-Scale PJM Test Stand

This appendix provides additional detail to support the information presented in Section 4 of the main report. The 336 Building contains three large-scale tanks: 1) a 1/4-scale model of a vertically oriented 1-million-gallon double-shell tank, 2) a vertically oriented cone bottom tank, and 3) a vertically oriented supernatant tank with an elliptically shaped bottom. The supernatant tank was used for the large-tank test system discussed in this report. The large-tank test stand included the supernatant tank, 4PJM pulse tubes, and a compressed air controller to pulse the tubes. An observation bridge 3 ft (0.914 m) from the top of the tank was used for visual observations and instrumentation. The bridge contained a 2 × 2.5 ft (0.610 m × 0.762 m) covered port for installing test equipment.

A.1.1 PJM System

The pulse-jet tubes are held in place using cross beams that traverse the diameter of the tank and are welded to the tank sides, as shown in Figure A.1. In addition to the support beams on the top of the tank, two tie beams connect the pulse tubes (in pairs) and provide additional support to prevent their vibration during PJM operation. The tie beams are situated about 6 ft (1.83 m) from the tank floor (as measured from the center of the tank). The pulsed jet tubes are positioned approximately at the center of the four quadrants of the supernatant tank at about 9 inches (0.229 m) from the floor of the tank.

Slight asymmetries that exist between the PJMs are documented in WTP-RPT-081, Section 2.4 (Bontha et al. 2003). These asymmetries, in combination with PJM control system tolerances, have been shown to contribute to the offset of core fluid upwelling from the center of the tank during PJM operations. The pulse tubes are labeled A, B, C, and D, as shown in Figure A.2, which includes some PJM and tank dimensions. Additional as-built dimensions of the large-tank test stand and pulse tubes were reported by Bontha et al. (2003).

Figure A.1. Top of Large-Scale Test Tank Showing PJM Support Structure; the PJM pressure controller is visible in the bottom left behind the chair.

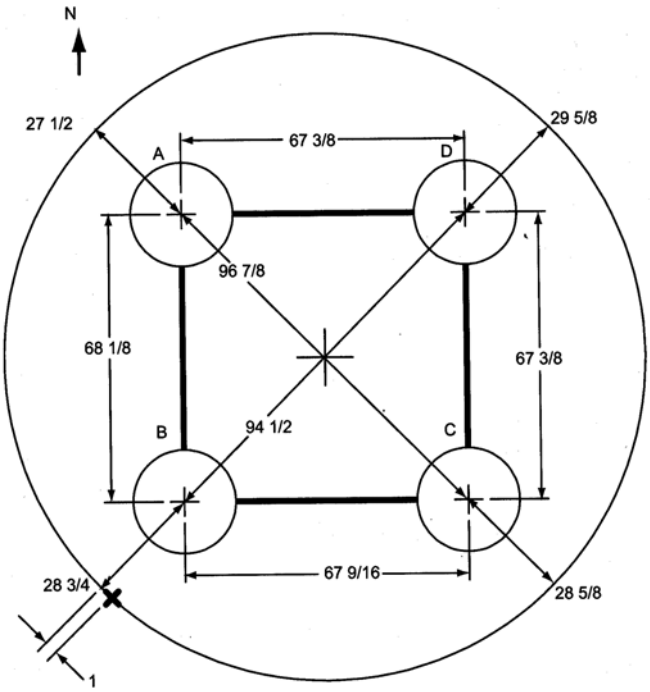

Figure A.2. Orientation and Distance of PJM Center to Center and PJM Center to Tank Wall at Bottom of PJMs just Above Weld to Cone at ~30 in. [~0.762 m] Elevation (dimensions in inches)

A.1.2 PJM Operation

A compressor/accumulator combination was used to regulate the airflow to the jet pump pairs that operate the PJMs. The diesel-powered compressor made by Sullair was capable of delivering 1600 cfm at an operating pressure of 100 psig to the jet pump pairs. A 240 gal (1000 L) accumulator vertical air receiver tank with pressure relief valves and timed electronic drain valve was used to provide air storage. Both the compressor and the accumulator were located outside the 336 Building test facility.

A.1.3 Camera Wells

Simulant motion was detected visually with cameras and velocity probes, as shown in Figures 4.5 and 4.6 of the main report. Video systems inserted into camera wells were used to detect the mixed and unmixed regions in the transparent simulant. A small video camera moved up and down inside the transparent camera well to record the images. The boundary between the mixed and unmixed regions was also recorded manually.

Video camera observation wells were used to monitor the fluid for the establishment of a repeating, periodic condition indicated by near-zero growth in the size of the mobilized (cavern) region. At this periodic condition, the camera wells were used to characterize the extent of the mobilized volume within the tank. The camera displays and tag switches, shown in Figure A.3, were connected to the data acquisition and control system (DACS) so that specific observation events could be time-marked on the continuous data acquisition log. Tag switches were assigned to each individual video well so that observed events (primarily the detection of simulant mobilization) could be marked in time and recorded with the analog data. Video recordings of test observations were made, including any tank surface imaging that might prove interesting. The video camera systems were not used to track rapid cavern growth.

Figure A.3. Camera Well Data Acquisition Hardware Showing Three Video Monitors, Each Displaying Four Camera Well Locations per Screen, and Screen Showing Camera Elevations and Tag Switch Box

Cavern height measurements using camera wells or velocity probes were the critical test measurements made during this activity. These measurements were quantifiable to a performance check. Usable results obtained with qualitative data could be used to compare the relative cavern heights of scaled tests.

A.1.4 Liquid-Level Sensor

The change of the liquid height in each pulse tube was individually measured using 12-ft (3.6576 m) long Teflon coated capacitance liquid level sensors (fabricated by Drexelbrook Inc.), as shown in Figure A.4. These sensors were mounted in the center of each pulse tube through one end of a "T" fitting attached to the 2-inch flange connector at the top of the pulse tube.

During PJM operation, liquid/slurry completely filled the pulse tubes and entered ~15 ft into the air/vacuum lines. The vacuum lines were filled to ensure that all PJMs fired at the same time. Once the liquid/slurry entered the air/vacuum line, the level probe reading became saturated at the maximum value of 140 inches (3.556 m). This additional fluid made a negligible contribution to nozzle velocity because it makes up a relatively small fraction of total pulse tube volume (2.5 versus 250 gal, ~1%).

Figure A.4. Drexelbrook 509-15 Series RF Level Transmitter

A.1.5 Valeport EM Flow Sensors

Velocity probes were used to measure the fluid velocity in several directions within their range. Local velocity values in the large tank during PJM operation were measured using 3.2-cm (1.259-inch) disc-shaped Valeport 802 electromagnetic (EM) flow sensors, as shown in Figure A.5. The Valeport EM flow sensors were chosen for this application primarily because of their ruggedness and their applicability for measuring velocities in the presence of solids in the test system (i.e., for fluid velocity measurements during the simulant tests conducted in the large tank). In addition, Valeport sensors also had the advantage of measuring the flow in two dimensions. In this application, the local velocity changes were measured vertically and azimuthally.

Velocity mapping was done by mounting the velocity probes (at the end of a 12.5-inch [0.3175-m] extension rod) horizontally to a 0.75-inch (0.01905-m) stainless steel pipe approximately 20 ft long. The spacing between each velocity probe was 24 inches (0.6096 m), and the lowest probe was at an elevation of 30 inches (0.762 m) from the tank floor at the centerline. This is shown schematically in Figure A.6. The probes were numbered 1 to 5 starting with 1 at the top (126 inch [3.2004 m] elevation) to 5 at the

Figure A.5. Valeport Direct Reading Electromagnetic Current Meter Model 802

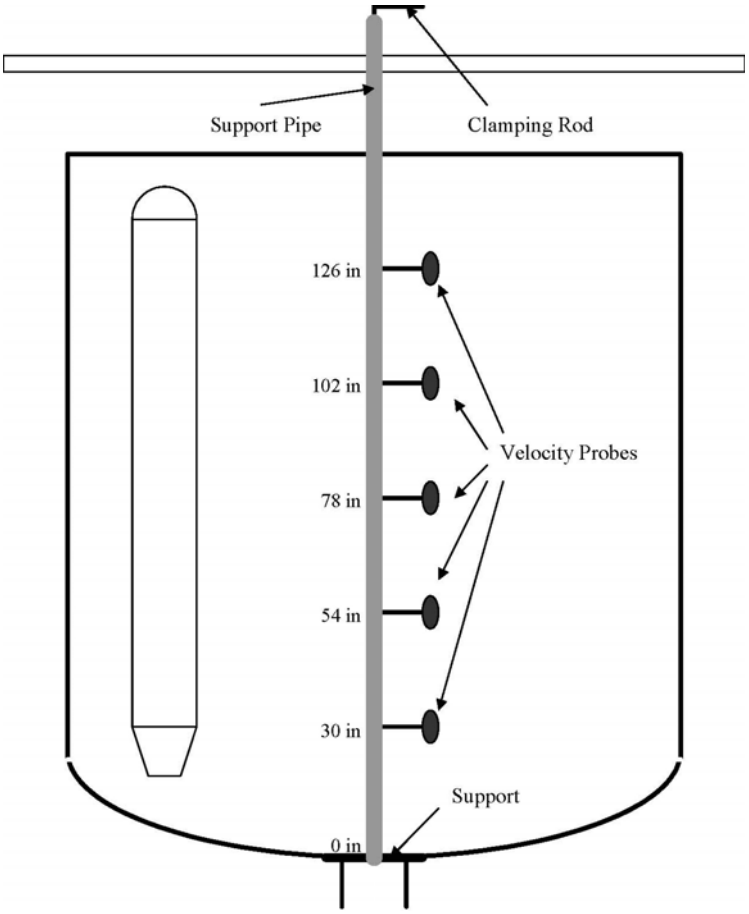

Figure A.6. Schematic of Velocity Probe Support Used in the Large-Tank Test Stand

lowest point (30-inch [0.762-m] elevation). To stabilize the probes, the probe support was anchored at the bottom of the tank and to the tank bridge at the top. The arrangement allowed the velocity probe to slide radially outward (by 12 inches [0.3048 m]) and bring the velocity sensor heads to the tank centerline or rotated to map velocity at different angular positions around a 12.5-inch (0.3175-m) radius circle.

A.1.6 Measurement Uncertainty

The Measurement Computing PCI-DAS6402/16 analog input board used in the DACS has 16 bit resolution (0.001526 percent). Based on this, the resolutions for the inputs from the various sensors are shown in Table 4.1 of the main report. The actual system resolution/accuracy is, however, limited by the sensors and signal conditioning, which are summarized in Table A.1. Additional details for these sensors are listed in Bontha et al. (2003).

Table A.1. Accuracy of Sensors and Corresponding Signal Conditioning Equipment Used in Large-Tank Testing

Variable	Manufacturer	Sensor Model	Transmitter Model	Accuracy
Velocity	Valeport	3.2 cm discus	802	± 5.0E-03 m/s + 1% of each axis
Level Probes	Drexelbrook	700-0002-057	408-8232-001	0.25% of span = 0.35 inches for the 140 inch span
Pulse Tube Pressure	Cecomp Electronics	DPG100	F4DR	± 0.25% of full scale = 0.25 psi for a span of 100 psi
Temperature	Omega	Type K T/C	none	± 2.2ºC

A.1.7 Data Acquisition and Storage

All data from the experiments, including date, time, liquid levels, pressures, velocities, and temperature, were monitored continuously and recorded digitally on a computer using DASYLab Version 5.5 data acquisition software installed on a Micron Millennia XRU PC running Windows 98. The DACS sampled all channels at 32 Hz frequency and averaged the data over one-second intervals. These one-second averages were electronically recorded in the data log files. The electronic data files were saved as ASCII or text files. Each electronic entry in the file included a date/ time stamp, and the file included a header that at a minimum contains information regarding the test objective and the location of the velocity and density probes. All data from the experiments were transferred to the share drive and stored in duplicate.

A.2 Large-Scale Test Summary

A significant number of tests have been conducted in the large-scale test tank using Laponite and clay simulants. A chronological list of the tests and a brief categorization of the types of tests are shown in Table A.2. The test sequence numbers are defined in Table 4.5 of the main report. The test sequences are indicative of the type of test and specific test objectives:

- S1: Initial constant volume tests to determine the minimum and maximum discharge velocities (discharge time) to be used for the test matrix.
- S2: Constant volume tests at V_0 with caverns measured at increasing velocity, U.

Table A.2. List of Tests Conducted in Large-Scale Test Fixture[(a)]

Date	Run Number/ Reference Number	Discharge Parameter				PJM Operation		Test Category or Description
		U (ft/s)	V (ft^3)	P (bar)	t (s)	Time (min)	Total Test Time (min)	
Laponite Simulant in Large Scale Test Tank								
030831	S1-1/L-1	10.4	27.3	0.7	30	251	251	Determine minimum and maximum achievable discharge velocities to be used for the test matrix.
	S1-2&3/L-2	19.9	29.5	1.8	17	82	390	
030920	S2-1/L-3	15.5	28.0	1.2	21.4	241	241	Evaluate cavern development in Laponite using a common discharge volume with increasing discharge velocities.
	S2-2/L-4	16	28.0	1.4	20.5	263	504	
	S2-3	25.3	28.3	2.8	12.8	145	649	
	S2-4	30.5	28.0	4	10.8	39	688	
030905	S2-1	13.8	27	1	23.4	424	424	Evaluate the effect of increasing discharge velocities at a constant discharge volume.
030909	S2-1	13.8	25	1	20.2	667	667	Evaluate cavern development in Laponite using a common discharge volume with increasing discharge velocities.
030911	S2-1/L-5	12.7	25	0.85	22.7	345	345	Evaluate the effect of increasing discharge velocities at a constant discharge volume.
	S2-2/L-6	14.3	25	1.1	20.2	251	596	
	S2-3/L-7	15.9	25.4	1.3	18.1	143	739	
	S2-4/L-8	17	25	1.4	17	161	918	
	S2-5-1	--	--	2	13.5	35	953	
	S2-5-2	--	--	4	9	30	983	
030914	RR-1-1	26.2	25.1	3.05	10.9	298	298	Evaluate gas retention and release (RR). Nominally, the test was conducted to note: • Time of breakthrough • Time of flow observed in tank "annular area" (at or near wall of tank) • Time of turbulent flow observed in annular area • Time of full mobilization of Laponite with no non-sheared fragments present
	RR-1-2	37.5	25.1	5	8	68	366	
030915	S3-1/L-9	16.9	12.6	1.4	8.2	518	518	Evaluate cavern development in Laponite using constant PJM discharge velocity with incremental volumes.
	S3-2/L-10	16.9	15.7	1.4	10.4	107	635	
	S3-shutdown	--	25	4	9	60	NA	--
	S3-shutdown	--	25	5	8	29	NA	--
030917	S3-1/L-11	13.8	12.6	1	10	249	249	Evaluate the effect of increasing discharge volumes at a constant discharge pressure. --
	S3-2/L-12	13.8	15.7	1	12	129	400	
	S3-3/L-13	13.8	18.8	1	14.8	203	629	
	S3-4/L-14	13.8	22	1	17	186	845	
	S3-5/L-15	13.8	25.1	1	20.2	164	1035	
031028	S2-Suppl-1/ L-16	15.5	25.1	1.2	17.6	195	249	Determine cavern size through the injection of dye into the Laponite at the beginning of the test and monitoring dye concentration in the cavern throughout the test.
031030	S2-Supp2-1	15.9	25.1	1.3	18.1	368	--	Determine cavern size by injecting dye into the Laponite after operating the PJMs long enough to establish a fairly stable cavern and monitoring dye concentration in the cavern throughout the remainder of the test.
031106	S5-T2M-1	28.2	25.1	3.05	10.2	182	--	Determine the time to mix the tank using dye after the Laponite had time to set up.
	S5-T2M-2	40.5	25.1	5	7.1	62	389	
	S5-T2M-3	28.2	25.1	3.05	10.2	157	556	

(a) These data are only observations. Reviewed data are presented in the tables shown in Section 4.

Table A.2 (contd)

Date	Number	Discharge Parameter				PJM Operation		Test Category or Description
		U (ft/sec)	**V** (ft^3)	**P** (bar)	**t** (s)	**Time** (min)	**Total Test Time** (min)	
031118	S2-1/L-17	14	25.1	1	20.2	410	410	Evaluate the repeatability of tests using same testing conditions.
	S2-2	15.5	25.1	1.2	18.6	218	628	
031120	S2-1	14.	25.1	1	20.2	70	70	Evaluate the repeatability of test runs using same testing conditions but starting at lower PJM velocities and increasing in steps to the test conditions.
		--	--	1.1	18.6	66	136	
		16.5	25.1	1.4	17	467	603	
031204	RR-1	34.4	25.1	4.48	8.6	276	276	Evaluate performance of PJM operation to remove oxygen bubbles (from hydrogen peroxide decomposition) from Laponite under batch removal test conditions.
Kaolin-Bentonite Clay Simulant in Test Tank								
031212	RR-1	34.4	25.1	4.48	8/6	--	--	Evaluate performance of PJM operation to remove oxygen bubbles produced from hydrogen peroxide decomposition, from the kaolin-bentonite slurry under batch removal test conditions.
031214	S2-1/L-18	--	--	1.2	18.6	361	361	Evaluate cavern height in kaolin bentonite slurry using dye, beads and RF fish tags.
	S2-2	--	--	1.6	15.7	361	374	
031216	RR-1	34.4	25.1	4.48	8.6	266	628	Evaluate performance of PJM operation to remove oxygen bubbles (from hydrogen peroxide decomposition) from a kaolin-bentonite slurry under batch continuous hydrogen peroxide addition test conditions.
040322	--	--	--	--	--	--	--	Surface level measurement
040323	--	--	--	--	--	--	--	Surface level measurement
040324	--	--	--	--	--	--	--	Surface level measurement
040325	--	--	--	--	--	--	--	Surface level measurement
040525	L-19 & L-20	--	--	--	--	--	--	--
040720	--	--	--	--	--	--	--	Gas release
040722	--	--	--	--	--	--	--	Gas holdup
040723	--	--	--	--	--	--	--	Gas release
040730	--	--	--	--	--	--	--	--
040819	--	--	--	--	--	--	--	Weigh system calibration

- S3: Constant velocity tests at U_3 with discharge volume, V, incrementally increased.
- S4: Optional testing depending on previous test results and available schedule. Constant velocity tests at UMax with discharge volume, V, incrementally increased.
- S5: Transient test for U_4V_0 or $U_{Max}V_0$.

During analysis, if the test was deemed applicable for providing more than one type of data, it was exploited.

A.3 Cavern, Breakthrough, and Time-to-Mix Tests Using Laponite

Cavern tests were designed to evaluate the size of the mobilized region of a cylindrical tank with an elliptical tank bottom and symmetrically spaced PJMs discharging vertically downward. Breakthrough occurred when the caverns reach the characteristic height of the mobilized region, H_C, or cavern height.

Time-to-mix tests were added into the test matrix by means of a test exception. The criteria for evaluating time to mix included:

- Time to breakthrough at the simulant surface
- Time to observe simulant movement down the tank wall
- Time for the simulant at the wall to exhibit turbulent motion (fully mixed)
- At times neutral buoyant beads were added near the middle or at the wall and documented when they reappeared.

A significant number of tests were conducted in the large-scale test tank, as shown in Table A.2. Data from the specific tests that have been used to support the scaling analyses are summarized in Tables 4.6 through 4.9 of the main report. Additional details of the tests that were conducted at large scale are described here. All tests in the large tank were conducted at an H/D_T of 0.9. The tests were conducted following the same procedure:

- Prior to the start of the test, set the PJM test conditions for the next test condition.
- If using Laponite, allow the simulant to gel at least 18 hours.
- Start the PJMs.
- Add dye as appropriate.
- Record observations regarding cavern growth or breakthrough.
- Take core samples as appropriate.
- Take samples for rheological measurements pre- and post-test and as appropriate.

Detailed test summaries were compiled to document observations made during the majority of tests conducted in the large tank that are listed in Table A.2. These summaries provide plots tracking cavern growth with time based on observations using the submerged cameras and observations made at the simulant surface. Information obtained from these summaries is included in this appendix to provide additional insight into the tests including descriptions of cavern formation, breakthrough, and flow patterns in the outer portions of the tank. ***These data are only observations. Reviewed data are presented in the tables shown in Section 4.*** *The data presented in this appendix as test observations are preliminary measurements and may differ slightly from the corrected data shown in Section 4. However, the trends presented in the following subsections may provide additional understanding regarding mixing in these complex systems.*

A.3.1 Scoping Test 030831-S1 Runs 1, 2, and 3

The purpose of this test sequence was to determine minimum and maximum achievable discharge velocities to be used during the remainder of the test matrix by incrementally increasing discharge pressure, volume, and velocity. This test included three runs at the conditions summarized in Table A.3.

Steady state was confirmed during Run 1 after 251 minutes of operation. Cavern growth is shown in Figure A.7; only observation from cameras C10 and C11 detected an interface of the cavern. Horizontal interfaces were observed by both cameras. None of the other cameras recorded a cavern interface, indicating that the cavern was small and centered somewhere between cameras C10 and C11, as indicated in Figure A.8. Run 2 was initiated at incrementally increased PJM operating conditions;

Table A.3. Test 030831-S1 Operating Conditions

Parameter	Run 1	Run 2	Run 3
$U_{discharge}$	10.4 ft/s	13.8 ft/s	19.9 ft/s
$V_{discharge}$	27.3 ft^3	28.1 ft^3	29.5 ft^3
$P_{discharge}$	0.7 bar	1 bar	1.8 bar
$t_{discharge}$	30 s	23.4 s	17 s
PJM operating time during test	251 min	40 min	82 min
Total PJM operating time	251 min	291 min	373 min
Run with equivalent $P_{discharge}$ and $t_{discharge}$	--	30902-S2-1	--

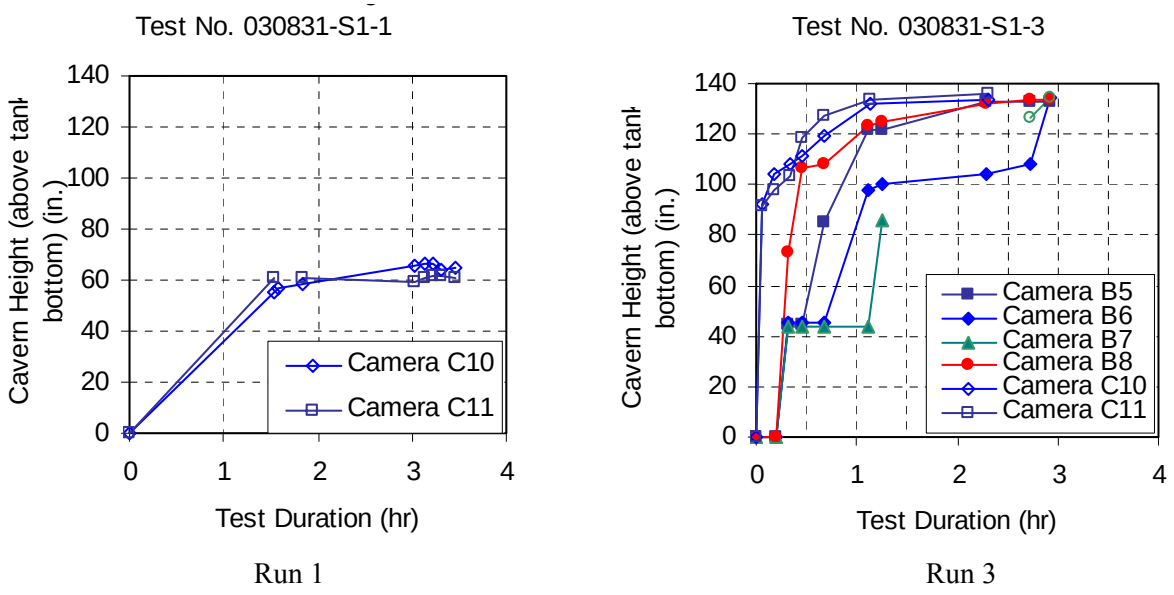

Run 1 Run 3

Figure A.7. Absolute Cavern Interface Heights Observed During Test 030831-S1 Runs 1 and 3

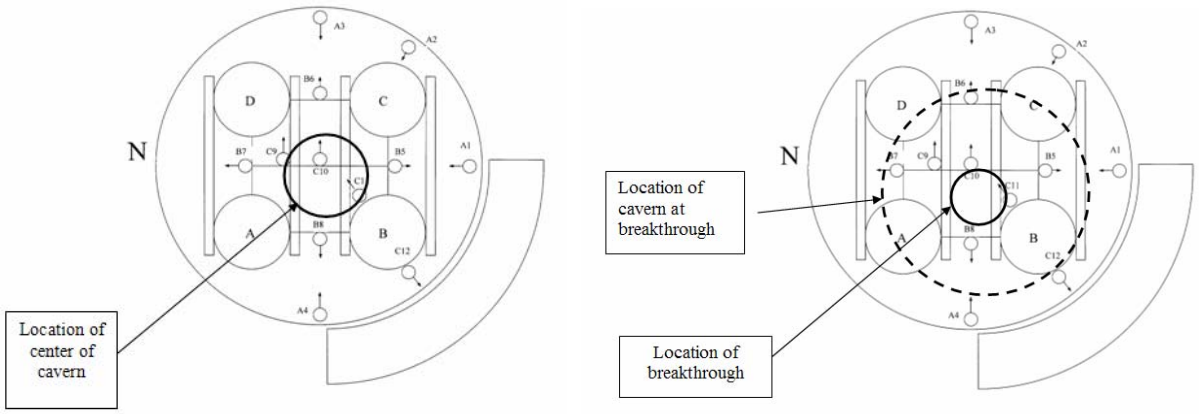

Run 1 Run 3

Figure A.8. Observations at End of Test 030831-S1 Runs 1 and 3

however, after 40 minutes there was minimal observable change in the cavern level, so the PJMs were stopped. The total time under these conditions was insufficient to assume or verify steady state. Run 3 was initiated with significantly increased operating conditions, and breakthrough was declared 82 minutes after the run started. At breakthrough, inspection of the Laponite surface showed evidence of mobilized surface expansion from a point between cameras B8, C10, and C11. The mobilized material expanded over the surface as the level rose and retreated as the level fell. Breakthrough was reported by camera C11 operators nearly one hour later, and cameras B5, B6, B8, and C10 reported horizontal interface levels ranging from 132.87 to 133.3 inch absolute height at that time. Absolute camera height is plotted in Figure A.7, and the extent of the breakthrough is shown in Figure A.8.

A.3.2 Constant Volume Test 030902-S2 Runs 1, 2, 3, 4

The purpose of this test sequence was to evaluate cavern development in Laponite using a common discharge volume with increasing discharge velocities as summarized in Table A.4. Steady state for Run 1 was confirmed after 232 minutes of PJM operation. Cavern interfaces were observed at cameras C10, C11, and B8, as shown in Figure A.9. Camera observations suggest that the top of the cavern was somewhere between the three cameras and probably shifted towards camera C8 and C11. The fact that the other B cameras did not display interface locations suggests that the cavern was relatively narrow. The cavern position based on these observations is shown in Figure A.10.

Table A.4. Operating Conditions for Test 030902-S2

Parameter	Test 030902-S2			
	Run 1	**Run 2**	**Run 3**	**Run 4**
$U_{discharge}$	15 ft/s	16 ft/s	25.3 ft/s	30.5 ft/s
$V_{discharge}$	28.0 ft^3	28.01 ft^3	28.3 ft^3	28.01 ft^3
$P_{discharge}$	1.2 bar	1.4 bar	2.8 bar	4.0 bar
$t_{discharge}$	21.4 s	20.5 s	12.8 s	10.8 s
PJM operating time during test	241 min	263 min	145 min	39 min
Total PJM operating time	241 min	504 min	649 min	688 min

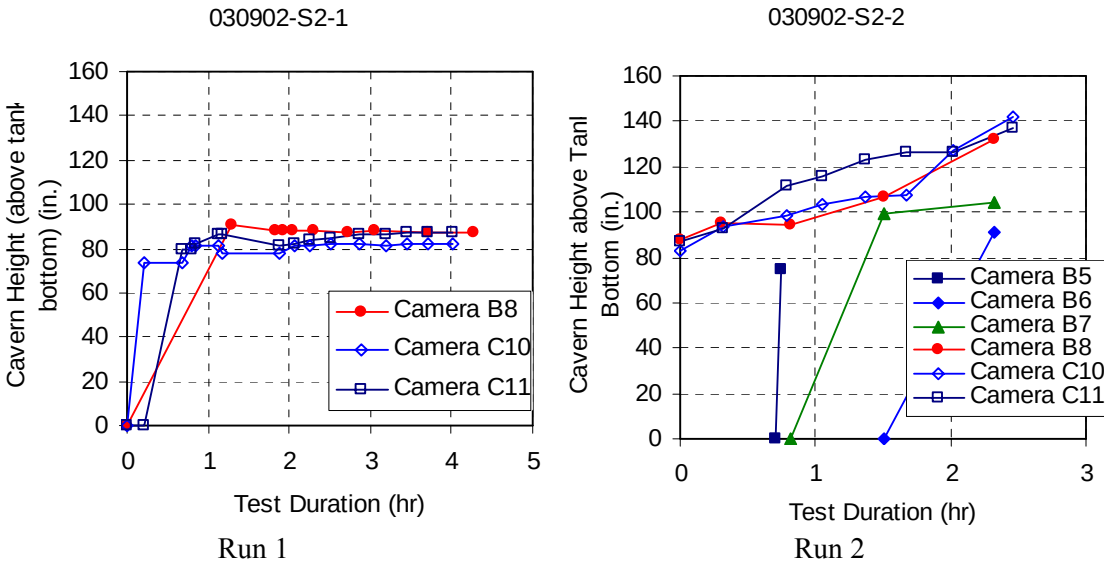

Figure A.9. Absolute Cavern Heights Observed During Test 030902-S2 Runs 1 and 2

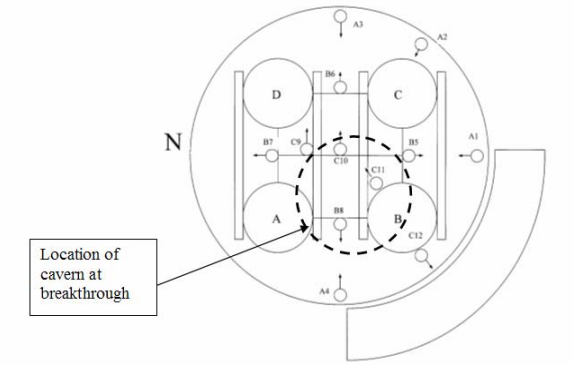

Figure A.10. Approximate Cavern Location for Test 030902-S1 Run 1

During Run 2, breakthrough of sheared Laponite was observed, and the run was terminated. Cavern growth as a function of time is shown in Figure A.9. Breakthrough of sheared Laponite at the surface appears to involve a gradual transition from a rubble-like, rough surface (as observed from the observation deck at the southwest rim of the tank) to a smooth, glassy surface indicative of liquid. During the rough stage, the surface of the Laponite expanded with cracks developing between discrete blocks of material. These cracks appeared to fill with upwelling liquid during the discharge stroke of the PJMs, and the entire mass moved radially outward toward the wall of the tank; then the entire surface appeared to partially settle back nearly to the original position before expansion.

During Runs 3 and 4, observations of the flow patterns in the interior of the tank were documented. At the completion of Run 3, the Laponite appeared fully mobilized as observed by all cameras except A2, A3, A4, and C12, which intermittently showed evidence of net movement. All four B cameras observed reverse flow (material moving down during discharge stroke of PJM) after 13 minutes of operation; this condition persisted throughout the remainder of the test. During Run 4, all B and C cameras (except C12) showed either reverse or turbulent flow.

A.3.3 Constant Volume Test 030905-S2 Run 1

The conditions for this test were similar to Test 030831-S1-Run 2. This test included only one run. Conditions are summarized in Table A.5. The cavern interface growth during the test is shown in Figure A.11 with all interfaces categorized as indeterminate; several unplanned shutdowns of the PJMs, shown on the plot as PRESCON first loss, occurred during this test.

Table A.5. Operating Conditions for Test 030905-S2

Parameter	Run 1
$U_{discharge}$	13.8 ft/s
$V_{discharge}$	27 ft^3
$P_{discharge}$	1 bar
$t_{discharge}$	23.4 s
PJM operating time during test	424 min
Total PJM operating time for day	424 min
Run with equivalent $P_{discharge}$ and $t_{discharge}$	090831-S1-2

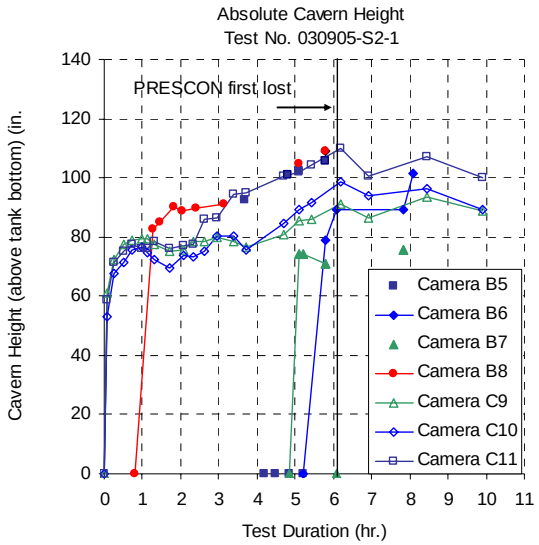

Figure A.11. Absolute Cavern Interface Heights Observed During Test 030905-S2 Run 1

An apparent achievement of steady state was observed by cameras C9, C10, C11, and B8 one hour into the test. However, undetected cavern growth was occurring, and cameras B5, B6 and B7 were beginning to show the edge of the cavern after additional operation. Subsequently, cameras C9, C10, and C11 began to show significant upward growth of their respective interfaces. From then on, typically one or two cameras at a time would display cavern growth while the others remained relatively constant. This was probably due to either an irregular growth pattern or a slow lateral wobbling behavior of the cavern.

A.3.4 Constant Volume Test 030909-S2 Runs 1, 2, 3

During this test sequence discharge velocity was incrementally increased three times, as shown in Table A.6. Five unanticipated shutdowns of the PJMs occurred during Run 1, but operation was quickly restored. Steady state was declared ~9 hours into the test. Camera observations are shown in Figure A.12. No A cameras indicated an interface; B cameras showed indeterminate interfaces, and C cameras observed interfaces right after steady state was assumed, but the values for C9 and C10

Table A.6. Operating Conditions for Test 030909-S2

Parameter	Test 030909-S2		
	Run 1	Run 2	Run 3
$U_{discharge}$	13.8 ft/s	15.3 ft/s	16.8 ft/s
$V_{discharge}$	25.0 ft^3	24.9 ft^3	24.9 ft^3
$P_{discharge}$	1.0 bar	1.2 bar	1.4 bar
$t_{discharge}$	20.2 s	18.6 s	17.0 s
PJM operating time during test	667 min	202 min	171 min
Total PJM operating time for day	667 min	869 min	1,040 min
Run with equivalent $P_{discharge}$ and $t_{discharge}$	030917-S3-5	031118-S2-2	030911-S2-4
Run with equivalent $P_{discharge}$ and $t_{discharge}$	031118-S2-1	--	--
Run with equivalent $P_{discharge}$ and $t_{discharge}$	031120-S2-1	031214-S2-1	031120-S2-1

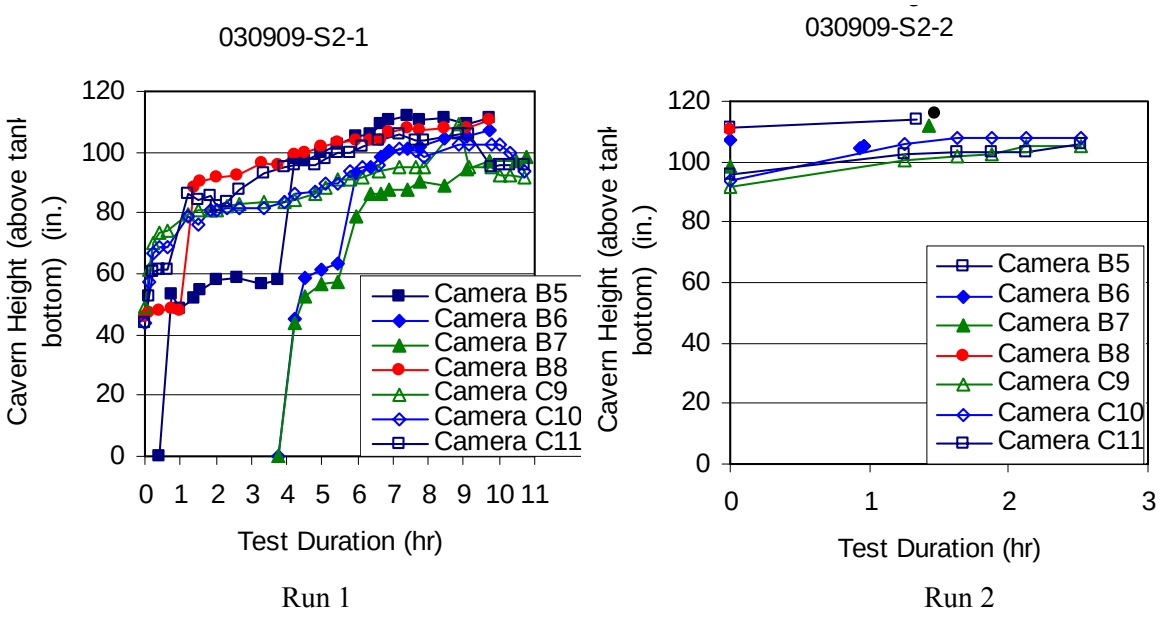

Figure A.12. Absolute Cavern Interface Heights Observed During Test 030909-S2 Runs 1 and 2

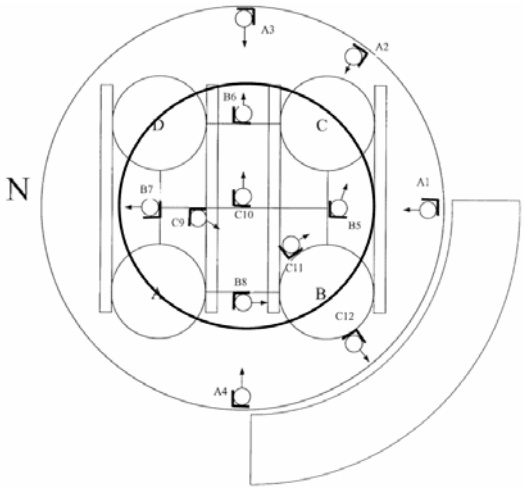

Figure A.13. Approximate Cavern Location for Test 030909-S2 Run 1

decreased more than 2 inches during the steady-state period. The cavern appeared to be centered in the tank based on similar interface levels at all of the B cameras, as depicted in Figure A.13. Examination of the transient cavern levels suggests that true steady state may not have been achieved at any time because two or more interfaces appeared to be growing at a rate of more than 2 inches per hour at any point in time. There may have been a nearly steady-state condition achieved after 6 to 8 hours of testing, but beyond that point the Laponite appeared to be weakening, making it difficult to locate interfaces.

Steady state for Run 2 was identified ~1.5 hours after the start of the run, as shown in Figure A.12. The Laponite appeared "more fluid" and "more turbulent" in cameras C9, C10, and C11 in earlier tests. This observation and the apparent recession of cavern heights during the latter stages of Run 2 suggest change of cavern configuration during relatively steady state conditions. These changes may represent a

partial recongealing of the sheared Laponite, rotation of the cavern without loss of cavern volume, or merely differences in interpretation of camera views.

Run 3 lasted approximately 3 hours; breakthrough was reported ~2 hours into the run. At breakthrough, the Laponite fluid was observed welling up in the center of the tank ("slow and viscous") and moving out between the PJMs.

A.3.5 Constant Volume Test 030911-S2 Runs 1, 2, 3, 4, 5

This test sequence evaluated the effect of incrementally increasing discharge velocity, as shown in Table A.7.

Table A.7. Operating Conditions for Test 030911-S2

Parameter	Test 030911-S2					
	Run 1	**Run 2**	**Run 3**	**Run 4**	**Run 5-1**	**Run 5-2**
$U_{discharge}$	12.7 ft/s	14.3 ft/s	15.9 ft/s	17ft/s	TBD	TBD
$V_{discharge}$	25 ft^3	25 ft^3	25.4 ft^3	25 ft^3	TBD	TBD
$P_{discharge}$	0.85 bar	1.1 bar	1.3 bar	1.4 bar	2 bar	4 bar
$t_{discharge}$	22.7 s	20.2 s	18.1 s	17 s	13.5 s	9 s
PJM operating time during test	345min	251 min	143 min	161 min	35 min	30 min
Total PJM operating time for day	345 min	596 min	739 min	918 min	953 min	983 min

Steady-state conditions for Runs 1 through 4 are shown in Figure A.14. After Run 1, the cavern appeared to encompass most of the region between the PJMs and clearly extended out as far as cameras B5 and B8, as shown in Figure A.15.

During Run 4, cameras B8, C9, C10, and C11 showed an interface of the cavern at steady state. These observations suggested a deviation from the behavior of the cavern in the previous two tests, where increasing discharge velocity initially resulted in an upper extension of the center of the cavern interface that could not be sustained as the cavern slowly broadened along its sides. The center of the cavern appeared to be shifted more toward cameras B8 and B11 than in the previous run because these cameras reported the highest and second highest interfaces, and B6 did not report an interface, as shown in Figure A.15. The center is also probably shifted slightly toward B5 since B7 did not report an interface, but camera B5 also reported the lowest interface for this test.

The purpose of Run 5 was to determine conditions for observing rollover, as indicated by observed downward flow of bubbles during PJM discharge on the A cameras. Cavern interface height data are plotted in Figure A.14. Operation at the first set of conditions was terminated after 35 minutes because cavern heights were not changing very fast and were not near the Laponite surface. The PJMs operated for 30 minutes at the second set of conditions. Cavern breakthrough was reported by the C camera operator. The B cameras were not monitored for observations for this portion of the test. Camera A4 observed downward flow of material at absolute heights of 68.5, 86.52, and 104.52 inches, respectively. Similar flow was noted on camera A1 at 104.11 in. absolute height.

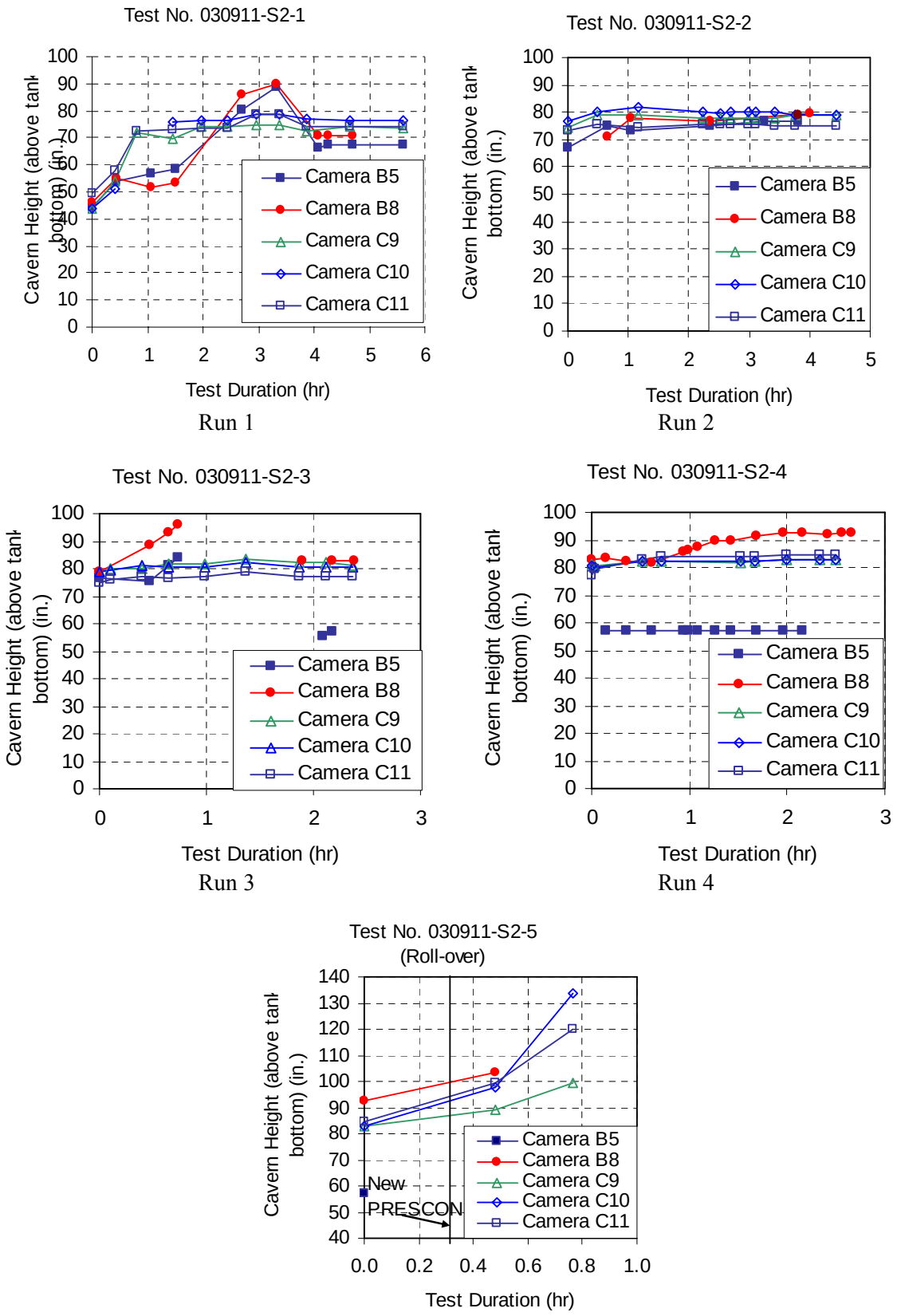

Figure A.14. Absolute Cavern Interface Heights Observed During Test 030911-S2 Runs 1, 2, 3, 4 and 5

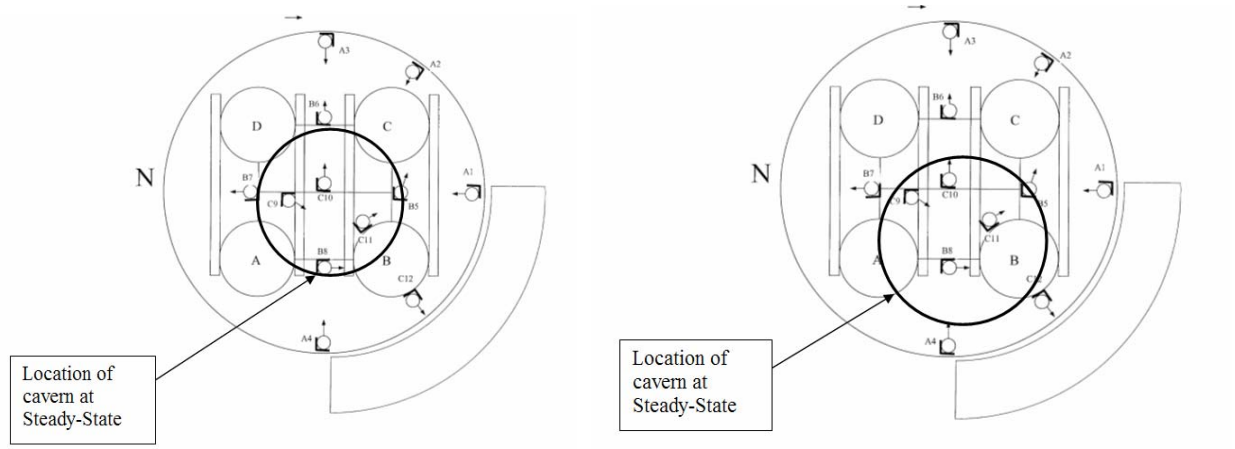

Run 1 Run 4

Figure A.15. Approximate Cavern Location at Steady State for Test 030911-S2 Runs 1 and 4

A.3.6 Time to Mix Test 030914-RR

This was the first of several special tests to evaluate specific needs. The purpose of this test sequence was to support eventual evaluation of gas retention and release; however, the focus was obtaining data to support evaluation of the time to mix. Nominally, the test noted 1) time of breakthrough, 2) time of flow observed in tank annular area (at or near tank wall), 3) time of turbulent flow observed in annular area, and 4) time of full mobilization of Laponite with no non-sheared fragments present. Test conditions are listed in Table A.8.

Data plotted in Figure A.16 show variations in observed interfaces. Breakthrough was initially observed ~30 minutes after the test started. Significant flow reversal (downward flow during PJM discharge stroke) was observed by all A cameras. Flow reversal was most pronounced in cameras A1 and A4, where it was observed throughout the column ~2 hours into the test. About 4½ hours into the test both A2 and A3 indicated reverse flow, very slight in A2. Flow appeared to increase toward tank bottom.

A vertical interface that was first noted in a traverse with camera C11 ~90 minutes into the test that showed "solid" Laponite on the left side of the view (outboard side of tank) throughout a significant vertical distance. The Laponite appeared fully and turbulently mobilized at a height of 121.79 inches and above, but indicated a mixture of plug flow and turbulent flow below this level, with a distinct interface.

Table A.8. Operating Conditions for Test 030914-RR

Parameter	Run 1	Run 2
$U_{discharge}$	26.2 ft/s	37.5 ft/s (est.)
$V_{discharge}$	25.1 ft^3	25.1 ft^3
$P_{discharge}$	3.05 bar	5 bar
$t_{discharge}$	10.9 s	8.0 s
PJM operating time during test	298 min	68 min
Total PJM operating time for day	298 min	366 min

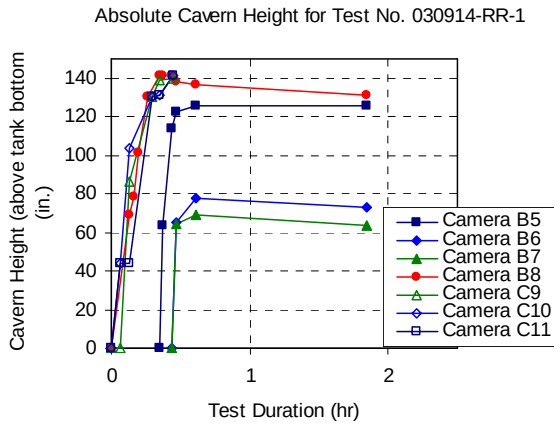

Figure A.16. Absolute Cavern Interface Heights Observed During Test 030914-RR-1

This behavior and observations of the surface as shown in Figure A.17 suggest that a cylindrical or funnel-shaped interface had developed, one edge of which was observed near camera C11. An upwelling plume of sheared Laponite inboard of camera C11 was spreading near and at the surface, moving toward the tank periphery with each pulse. This movement near and below the surface is supported by observations in cameras C12, A1 and A4. The time-to-mix criteria are summarized for this run in Table A.9.

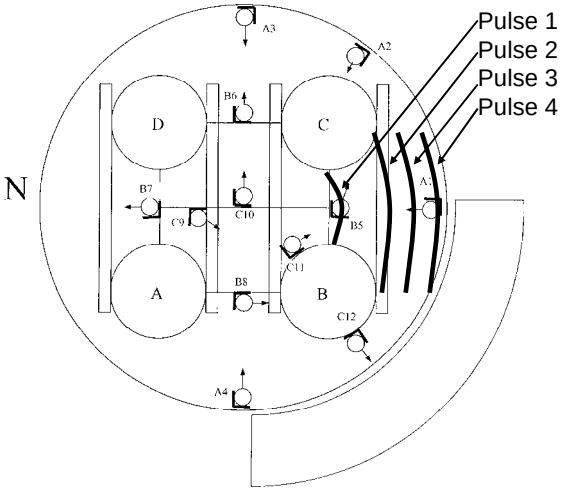

Figure A.17. View of Progression of Laponite Across the Surface with Sequential PJM Pulses Observed ~75 min after the start of Test Run 030914-RR-1

Table A.9. Assessment of Time to Mix Criteria for Test 030914-RR

Criteria for Time to Mix	Observation during Test Run 030914-RR Run 1
Time to breakthrough	~30 min
Time flow observed in annular area	~ 2 hours
Time of turbulent flow observed in annular area	Not attained
Time of full mobilization	Estimated to be 2 hours

A.3.7 Constant Velocity Test 030915-S3 Runs 1, 2

The purpose of this test sequence was to evaluate cavern development in Laponite using a constant PJM discharge velocity with incremental volumes, as shown in Table A.10, Runs 1 and 2. Run 3, the shutdown test, observed Laponite homogenization and mobilization effects, development of an annular area, characterized the rheology of the Laponite at various conditions, and generally observed the spatial extent of the cavern. Run 1 steady state was confirmed at the end of the test. All A cameras showed plug flow of solid Laponite at steady state. Run 2 breakthrough was also confirmed at the end of the test. Cavern growth for Runs 1 and 2 is shown in Figure A.18.

Table A.10. Operating Conditions for Test 030915-S3

Parameter	Test 030915-S3			
	Run 1	**Run 2**	**Run 3-1**	**Run 3-2**
$U_{discharge}$	~16.9 ft/s	~16.9 ft/s	NA	NA
$V_{discharge}$	12.6 ft^3 (est.)	15.7 ft^3 (est.)	25 ft^3	25 ft^3
$P_{discharge}$	1.4 bar	1.4 bar	4 bar	5 bar
$t_{discharge}$	8.2 s	10.4 s	9 s	8 s
PJM operating time during test	518 min	107 min	60 min	29 min
Total PJM operating time	518 min	635 min	NA	NA
Run with equivalent $P_{discharge}$ and $t_{discharge}$	--	--	030911-S2-5-2	--

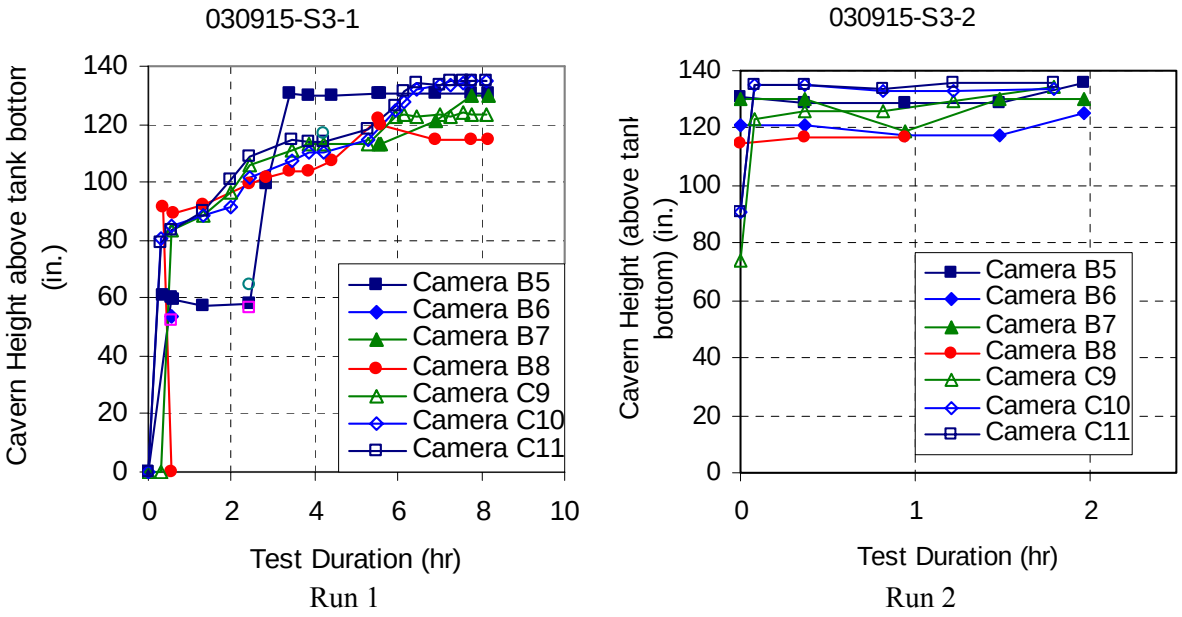

Figure A.18. Absolute Cavern Interface Heights Observed for Test 030915S3 Runs 1 and 2

A.3.8 Constant Pressure Test 030917-S3 Runs 1, 2, 3, 4, 5

During runs 1 through 5, summarized in Table A.11, discharge time was increased incrementally from 10 to 20 seconds. Cavern growth for these runs is plotted in Figure A.19. All runs ended after attaining steady state. As mixing time progressed, the cavern interfaces became less distinct.

Table A.11. Operating Conditions for Test 030917-S3

Parameter	Test 030917-S3				
	Run 1	**Run 2**	**Run 3**	**Run 4**	**Run 5**
$U_{discharge}$	13.8 ft/s	13.8 ft/s	13.8 ft/s	13.8 ft/s	13.8 ft/s
$V_{discharge}$	12.6 ft^3	15.7 ft^3	18.8 ft^3	22 ft^3	25.1 ft^3
$P_{discharge}$	1 bar	1 bar	1 bar	1 bar	1 bar
$t_{discharge}$	10 s	12 s	14.8 s	17 s	20.2 s
PJM operating time during test	249 min	129 min	203min	186 min	164 min
Total PJM operating time for day	249 min	400 min	629 min	845 min	1035 min
Run with equivalent $P_{discharge}$ and $t_{discharge}$	--	--	--	--	030909-S2-1
Run with equivalent $P_{discharge}$ and $t_{discharge}$	--	--	--	--	031118-S2-1
Run with equivalent $P_{discharge}$ and $t_{discharge}$	--	--	--	--	031120-S2-1

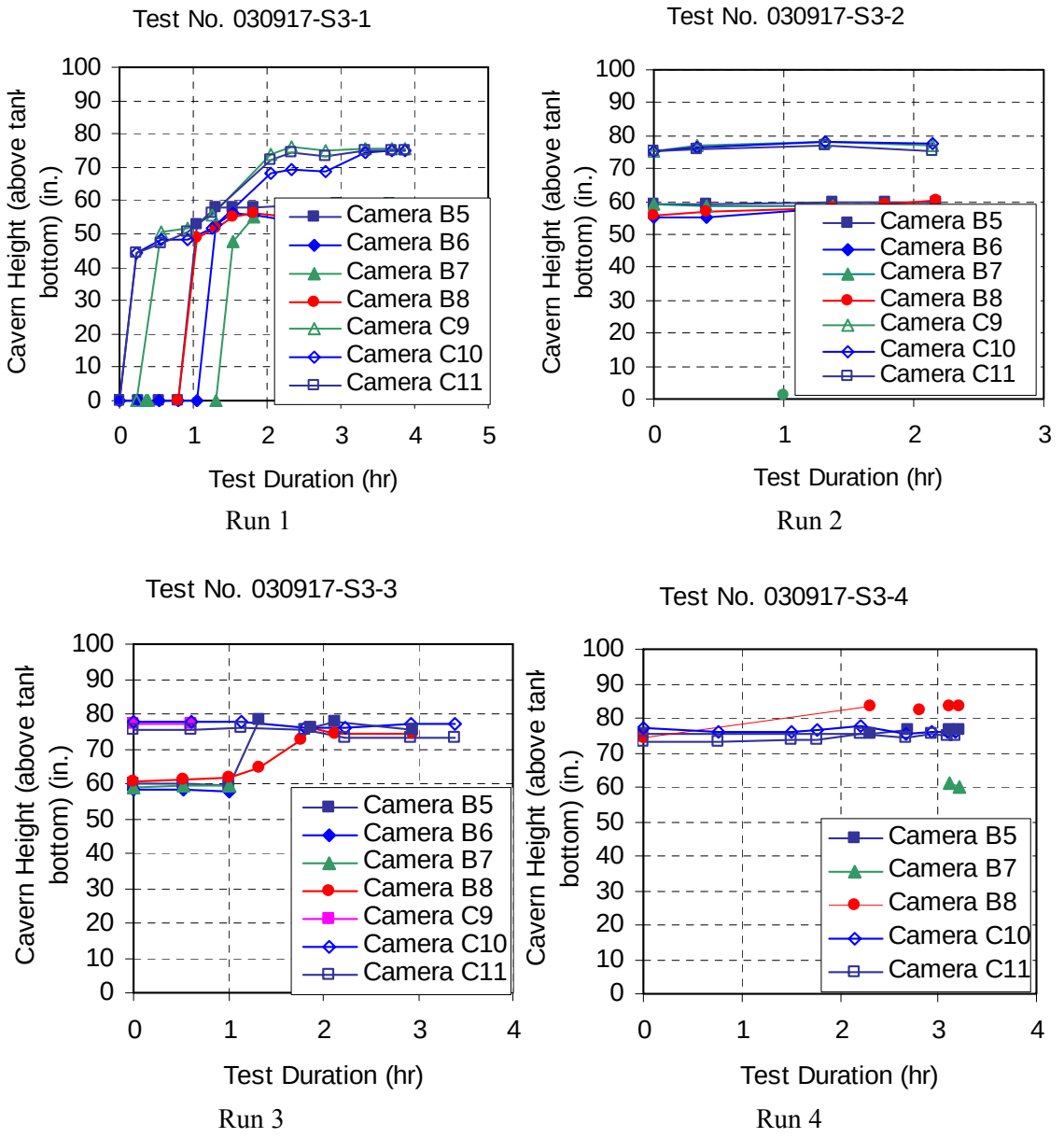

Figure A.19. Absolute Cavern Interface Heights Observed During Test 030917-S3 Runs 1 Through 4

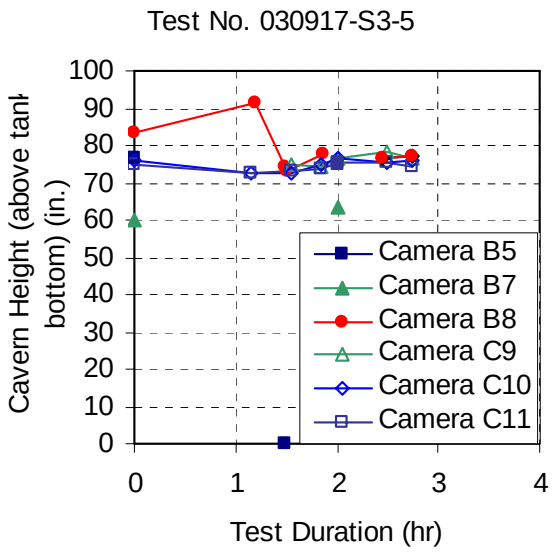

Run 5

Figure A.19 (contd)**.** Absolute Cavern Interface Heights Observed During Test 030917-S3 Run 5

A.3.9 Constant Volume Test with Dye Injection 031028-S2-Supp1 Run 1

This test to determine cavern size, described in Table A.12, included injecting dye into the Laponite at the beginning of the test and monitoring dye concentration in the cavern throughout the test.

Table A.12. Operating Conditions for Test 0301028-S2-Supp1-1

Parameter	Run 1
$U_{discharge}$	15.5 ft/s
$V_{discharge}$	25.1 ft^3
$P_{discharge}$	1.2 bar
$t_{discharge}$	17.6 s
PJM operating time during test (to confirmed steady-state)	195 min
Total PJM operating time	249 min

During Run 1, after four minutes of PJM operation, the PJMs were stopped to add a mixture of 58 g of Brilliant Blue dye in about 2 gallons of Laponite to the test tank through an injection port at the bottom of the tank using a diaphragm pump. About 8 gallons of additional undyed Laponite were added after dye injection to clear the injection tube of dye. Total time to inject the dye and Laponite was 10 minutes. After dye injection was completed, the PJMs were restarted and operated for ~5-1/2 hours. Steady-state conditions were assumed ~2-1/2 hours later and confirmed ~3-1/4 hours later based on observations using the C cameras, as shown in Figure A.20. Dye was observed on the Laponite surface ~15 minutes after completion of dye injection. The steady state cavern configuration and locations of dye observed on the surface are shown in Figure A.21.

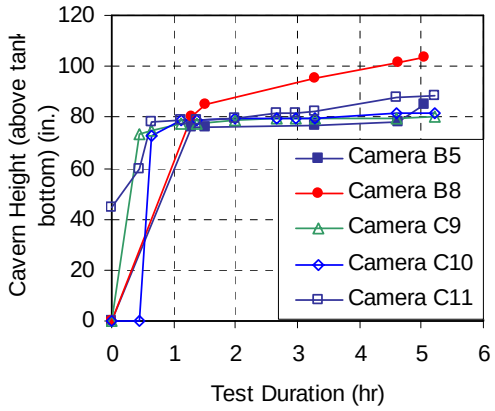

Figure A.20. Absolute Cavern Interface Heights Observed During Test 031028-S2-Supp1Run 1

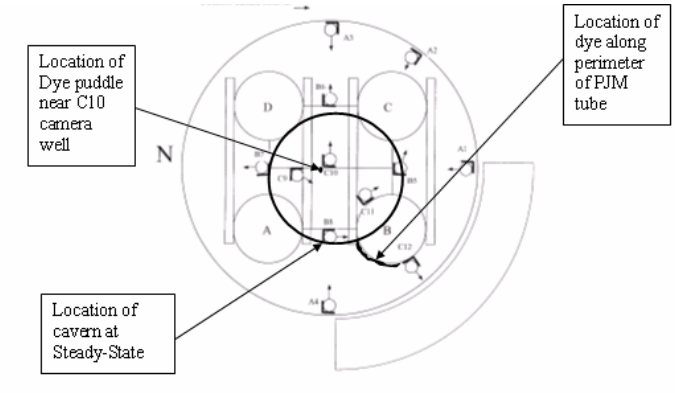

Figure A.21. Approximate Cavern Location at Steady State for Test 031028-S2-Supp1Run 1

Analysis of the absorbance and calculation of the percent that the fluid that was mixed based on measurement of absorbance is plotted in Figure A.22 and described in *Chemical Tracer Techniques for Assessing Mixing Performance in Non-Newtonian Slurries for WTP Pulsed Jet Mixer Systems* by Poloski et al. (2004). At completion of the test, the fluid was less than fully mixed.

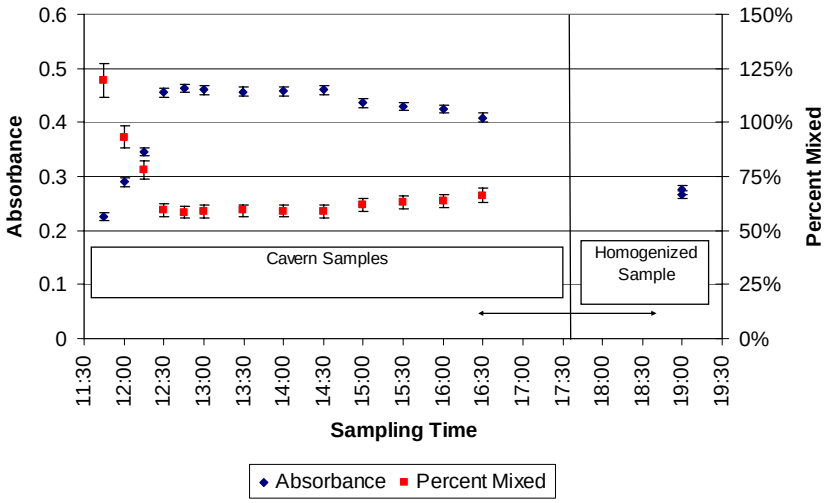

Figure A.22. Absorbance Plots for Test 031028-S2-Supp1 Run 1

A.3.10 Constant Volume Test with Dye Injection 031030-S2-Supp2 Run 1

This test to determine cavern size, described in Table A.13, included injecting dye into the Laponite at the beginning of the test and monitoring dye concentration in the cavern throughout the test.

Table A.13. Operating Conditions for Test 0301028-S2-Supp2

Parameter	Run 1
$U_{discharge}$	15.9 ft/s
$V_{discharge}$	25.1 ft^3
$P_{discharge}$	1.3 bar
$t_{discharge}$	18.1 s
PJM operating time	368 min

After ~1-3/4 hours of PJM operation, a mixture of 58 g of Brilliant Blue dye and about 3 L of Laponite was added through an injection port at the bottom of the tank while the PJMs were still operating. About 3 L of additional undyed Laponite was added after dye injection to clear the injection tube of dye. A peristaltic pump was used to add the dye and additional Laponite over a 44-minute period. The PJMs were operated for 6.1 hours when the last camera observations were made. Steady state was not achieved. Breakthrough, which occurred ~5 hours into the test, was characterized by cavern interfaces observed at the surface by the cameras and an applesauce appearance of the Laponite surface that showed lateral flow components in different locations at the surface. There was no upwelling of glassy material at the surface when breakthrough was declared, and no evidence of added dye on the Laponite surface during the test. However, two cameras did detect dye. At ~2 hours, camera C10 observed a glob of dye nearby at the end of a discharge cycle while observing a cavern interface at 89.92 inch absolute height. Faint traces of added dye were also observed by one of the A cameras ~30 minutes into the test. Cavern growth during the tests is plotted in Figure A.23 and the cavern location is outlined in Figure A.24.

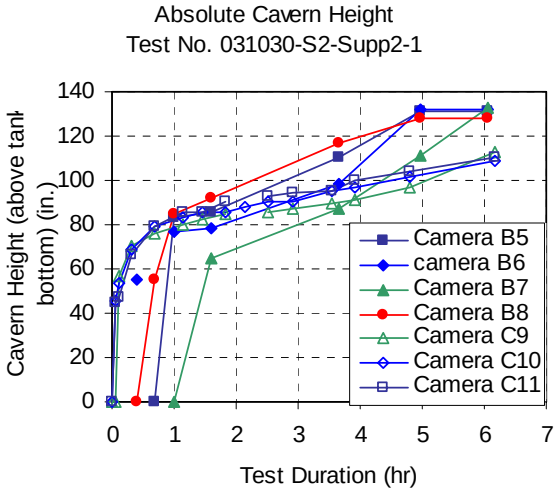

Figure A.23. Absolute Cavern Interface Heights Observed During Test 031030-S2-Supp2 Run 1

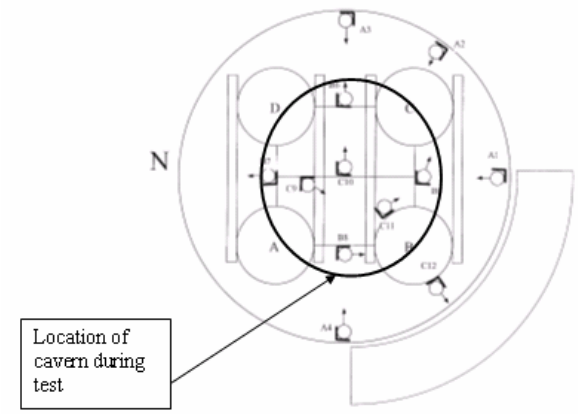

Figure A.24. Approximate Cavern Location During Test 031030-S2-Supp2 Run 1

Analysis of the absorbance and calculation of the percent of fluid that was mixed based on measurement of absorbance is plotted in Figure A.25 (Poloski et al. 2004). These calculations show that the fluid approached the ~90% mixed condition at the end of the test.

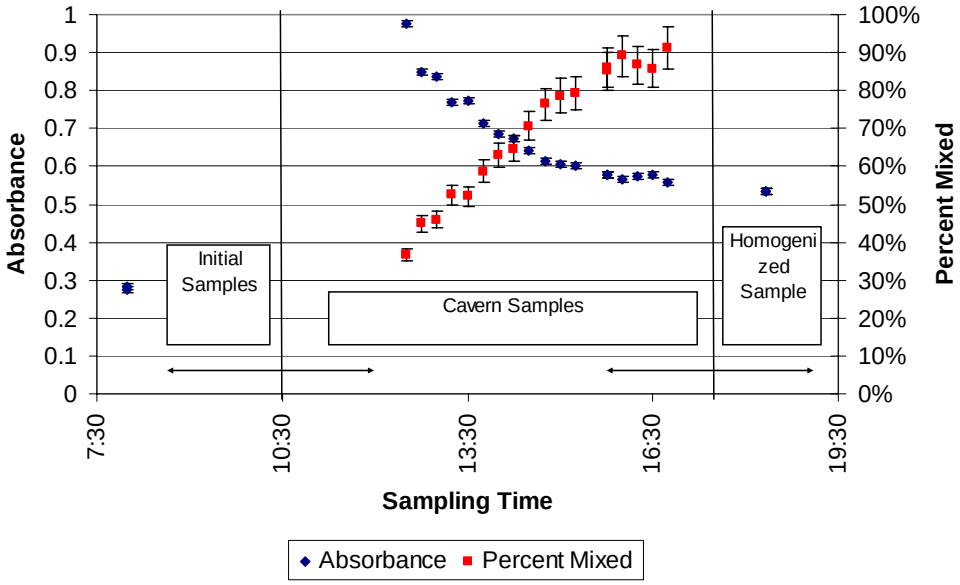

Figure A.25. Absorbance Plots for Test 031030-S2 Supp2 Run 1

A.3.11 Time-to-Mix Test 031106-S5-T2M

The purpose of this test sequence, shown in Table A.14, was to determine the time to mix the tank by observing the concentration of dye in Laponite. Run 1 was conducted starting from a gelled state. During Run 2, the tank was rehomogenized. Run 3 was a repeat of Run 1 starting from the fully mixed condition directly after the completion of Run 2. No cavern growth was tracked. However, the time to mix criteria monitored were 1) time of breakthrough, 2) time of flow observed in tank "annular area" (at or near the wall of the tank), 3) time of turbulent flow observed in the annular area, and 4) time of full mobilization of Laponite with no non-sheared fragments present.

Table A.14. Operating Conditions for Test 031106-S5-T2M

Test 031106-S5-T2M			
Parameter	**T2M-1**	**T2M-2**	**T2M-3**
$U_{discharge}$	28.2 ft/s	40.5 ft/s	28.2 ft /s
$V_{discharge}$	25.1 ft^3	25.1 ft^3	25.1 ft^3
$P_{discharge}$	3.05 bar	5 bar	3.05 bar
$t_{discharge}$	10.2 s	7.1 s	10.2 s
PJM operating time	182 min	62 min	157 min

Dye injection started 7 minutes into the run and was completed after ~9 minutes. Dye injection consisted of mixing 58.04 g of Brilliant Blue with about 3 L of Laponite and injecting the mixture into the bottom of the tank using a peristaltic pump. Additional Laponite (about 3 L) was added to clean out the dye container and clear the injection port of dye. It was estimated that about 54 g of the dye was actually injected (estimated by the amount remaining in the container after cleaning with additional Laponite).

Observations of the Laponite surface during this test indicated that the Laponite surface sheared before dye injection on the first discharge pulse of the PJMs and breakthrough occurred on the second pulse. Camera D on the catwalk recorded this event. Data plotted in Figure A.26 show the approximate location and dimensions of the fresh material spread on the Laponite surface at the beginning of the test. Later inspection of the Laponite surface after ~1 hour of operation showed that fresh, low-viscosity material reached the surface during the last second of the discharge pulse and spread outward like a wave to a distance about 1–2 ft from the perimeter of the tank.

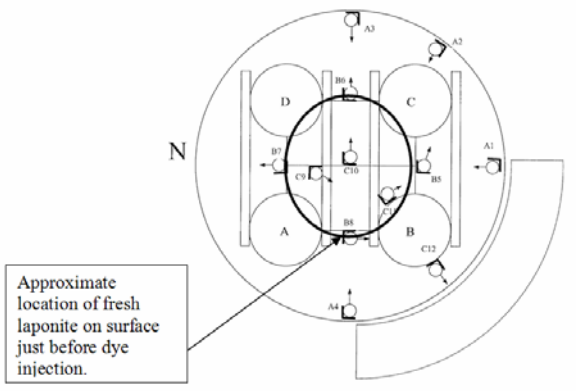

Figure A.26. Plan View Showing Approximate Location of Fresh Laponite on the Surface Just Before Dye Injection

Observations ~5 minutes into the test for cameras C9, C10, and C11 at ~ 124 inches absolute height confirmed that the central portion of the tank was turbulent near the surface at the beginning of the test. Flow at Camera C12 was described as stagnant at all but the highest level, where the flow was described as slightly upward and lateral.

Observations by all of the B cameras ~15 minutes after the test started showed highly sheared flow at elevations of ~ 69, 84, 109, and 124 inches absolute height. Flow observed by cameras B5 and B8 was described as turbulent at the lower three elevations. Flow observed by cameras B6 and B7 was described

as between stagnant and turbulent at the lowest level (69 inch absolute height). At the second lowest level, cameras B6 and B7 described flow as stagnant through most of the discharge and slightly turbulent at the end. About 45 minutes after initiating the test, all cameras were near their lowest positions—about 44 inch absolute height—and showed pronounced downward flow during discharge. Camera C12 monitored bubble movement at different levels; Table A.15 shows bubble movement during discharge and suction portion of the cycles and the net bubble movement per cycle.

Table A.15. Observed Bubble Movement by Camera C12

Time from Test Start (min)	**Absolute height** (in.)	**Bubble Displacement During Discharge** (in.)	**Bubble Displacement During Suction** (in.)	**Net Bubble Displacement** (in./cycle)
29	124	3.4	- 4.9	- 1.5
39	104	0.2	- 1.2	- 1.0
45	84	- 0.2	- 0.6	- 0.8
64	64	- 0.2	- 0.4	- 0.6
68	45	0.0	- 0.7	- 0.7
95	45	--	--	~0.5
~95	51	--	--	~0.8

Quantitative measurements were also made by observing bubbles with the A cameras near the bottom of the camera wells ~90 minutes after the start of the test as tabulated in Table A.16 which shows the motion observed. These observations indicate that there was significant, albeit slow, circulation of Laponite near the walls.

Table A.16. Observed Bubble Movement by A Cameras

Camera	**Absolute camera height** (in.)	**Bubble Displacement During Discharge** (in.)	**Bubble Displacement During Suction** (in.)	**Net Bubble Displacement** (in./cycle)
A1	10	- 2.8	- 2.4	- 5.2
A2	15	- 1.3	- 4.4	- 5.7
A3	16	- 4.8	- 4.6	- 9.4
A4	~14	> -10	NA	>10

Run 2 was conducted to rehomogenize the tank after completion of Run 1. Dye samples and homogenized samples taken during Run 2 were analyzed to determine the absorbance and percent of mixing (Poloski et al. 2004). These data are plotted in Figure A.27 and show that the tank was fully mixed about 1 hour after the test started. The time-to-mix criteria are summarized for this run in Table A.17.

Run 3 was conducted to measure the time to mix using dye as an indicator and to make observations on flow characteristics to determine whether stagnant areas from the first test run (031106-5-T2M-1) reappeared following rehomogenizing the tank during the second test run (031106-5-T2M-2) at PJM conditions of 5 bar discharge pressure and 7.1 seconds discharge time.

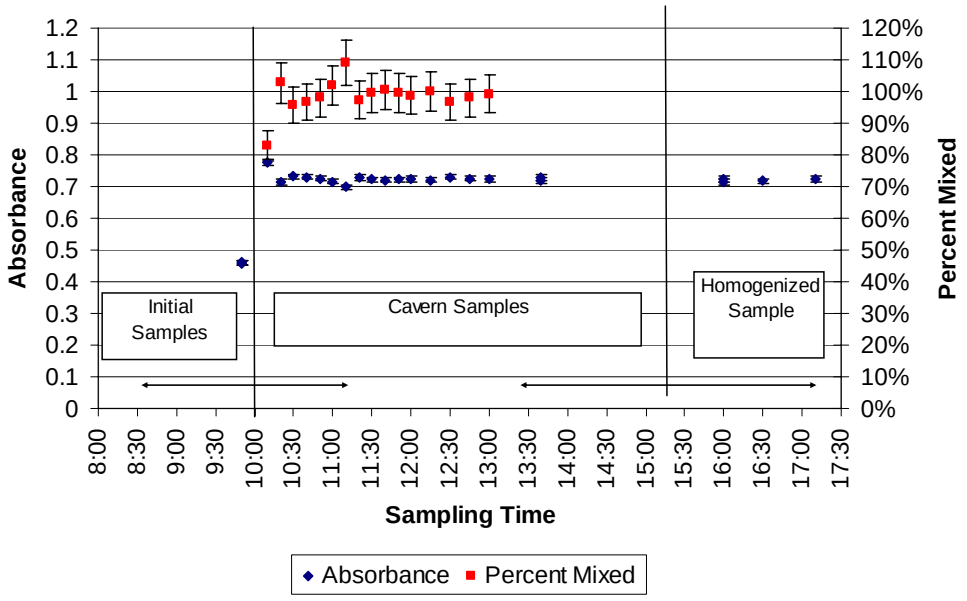

Figure A.27. Absorbance Plots for Test 031106-S5-T2M Runs 1 and 2

Table A.17. Assessment of Time-to-Mix Criteria for Test 031106-S2-T2M Run 1

Criteria for Time to Mix	Observation during Test 031106-S5-T2M Run 1
Time to breakthrough	~2 min
Time flow observed in annular area	~ 15 min
Time of turbulent flow observed in annular area	Not attained
Time of full mobilization	Estimated to be ~ 60 min

After 2 minutes of operation, initial baseline calorimetry samples were obtained. The PJMs were stopped during dye injection. No video was taken during the test to document flow conditions at different camera positions. However, observations made with the cameras are summarized in Table A.18. Turbulent flow represents rapid flow with rapid changes in flow directions of large magnitude so that a general flow direction can not be made. Upward horizontal and downward flow may represent plug or laminar flow but with flow lines parallel and predominantly in one direction.

Dye samples taken during Run 3 were analyzed to determine the absorbance and percent of mixing (Poloski et al. 2004). The data are plotted in Figure A.28 and show that the tank was fully mixed about 30 to 45 minutes after the start of Run 3. The time-to-mix criteria are summarized for this run in Table A.19.

Table A.18. Qualitative Flow Observations During PJM Discharge

Camera	Nominal Absolute Camera Height (in.)					
	46- 47	**64**	**84**	**104**	**124**	**131**
A1	Downward flow	Downward flow	Downward flow	Downward flow	Initial upward flow followed by stagnation then downward flow	Upward flow followed by downward flow
A2	Stagnant	Downward flow ~1.5 in.	Downward flow	Stagnant with slight downward flow	Initial upward flow followed by stagnation then downward flow	Upward flow followed by stagnant flow
A3	Downward flow	Downward flow	Downward flow but least magnitude of the A cameras	Downward flow	Initial upward flow followed by stagnation then downward flow	Upward flow followed by downward flow
A4	Slight downward flow	Downward flow	Downward flow but greatest magnitude of A cameras	Downward flow but greatest magnitude of the A cameras	Initial upward flow followed by stagnation then downward flow	Initial upward flow followed by period of stagnation then downward flow
B5	Turbulent flow	Rapid downward flow	Turbulent flow with initial upward, then horizontal, then downward trend	Horizontal flow followed by slight downward flow	Rapid initial upward flow followed by horizontal flow	Rapid initial upward flow followed by horizontal flow
B6	Turbulent flow	Rapid downward flow	Turbulent flow initially upward, then horizontal, then downward	Initially upward followed by horizontal then downward flow	Rapid initial upward flow followed by horizontal flow	Rapid initial upward flow followed by horizontal flow
B7	Turbulent flow	Rapid downward flow but lowest flow rate of the B camera	Turbulent flow, initially upward, then horizontal, then downward trend	Initially upward then horizontal, then downward flow; stagnant near end	Rapid initial upward flow followed by horizontal flow	Rapid initial upward flow followed by horizontal flow
B8	Turbulent Flow	Rapid downward flow	Turbulent flow initially upward, then horizontal, then downward	Initial downward flow followed by diagonally downward flow	Rapid initial upward flow followed by horizontal flow	Rapid initial upward flow followed by horizontal flow
C9	Turbulent flow	Turbulent flow	Turbulent flow	Turbulent flow	Turbulent flow	Turbulent flow
C10	Initially up-ward then turbulent flow	Turbulent flow	Turbulent flow with strong up-ward component	Turbulent flow with strong up-ward component	Turbulent flow with strong up-ward component	Turbulent flow
C11	Turbulent flow	Initially stagnant, slight horizontal component followed by turbulent flow	Initial turbulent flow with strong upward com-ponent followed by stagnation	Turbulent flow	Turbulent flow	Turbulent flow
C12	Initially stagnant, turbulent near end of discharge	Stagnant flow	Stagnant flow	Stagnant flow	Nearly stagnant with movement ~1 in. upward and 1 in. horizontal during discharge	Nearly stagnant with movement about 1 in. upward and 1 in. horizontal during discharge

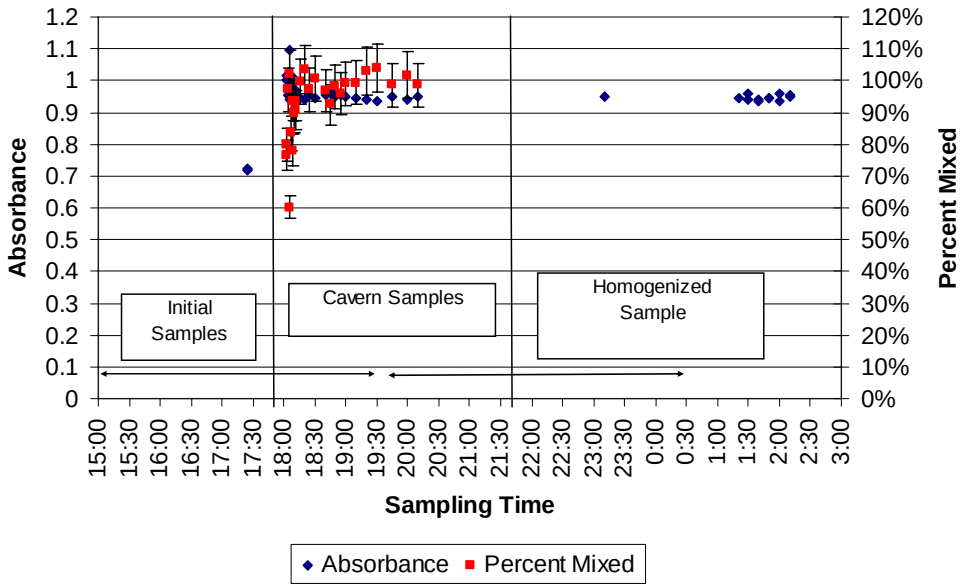

Figure A.28. Absorbance Plots for Test 031106-S5-T2M Run 3

Table A.19. Assessment of Time to Mix Criteria for Test 031106-S5-T2M Run 3

Criteria for Time to Mix	Observation During Test 031106-S5-T2M Run 3
Time to breakthrough	Not recorded assumed to be similar to Run 1
Time flow observed in annular area	~60 min or less
Time of turbulent flow observed in annular area	Not attained
Time of full mobilization	~60 min or less

A.3.12 Constant Volume Test with Dye Injection 031118 Runs 1, 2

The purpose of this test was to evaluate the reproducibility of the test results. This test duplicated PJM operating conditions for test 030909-S2 Run 1 and Run 2 and matched other test conditions. The test conditions are listed in Table A.20.

During Run 1, dye injection commenced after ~1 hour of PJM operation and lasted for ~40 minutes. Dye injection consisted of mixing 55.4 g of Brilliant Blue dye with approximately 3 L of Laponite and injecting it into the bottom of the tank while the PJMs were operating. An additional 3L of clean Laponite was used to clean out the dye container and to clear the injection line of dye. Cavern growth is plotted in Figure A.29 with steady state observed after ~5 hours of mixing. Steady state during Run 2 occurred ~1 hour after the start of mixing.

Table A.20. Operating Conditions for Test 031118-S2

Parameter	Test 031118-S2	
	Run 1	Run 2
$U_{discharge}$	14 ft/s	15.5 ft/s
$V_{discharge}$	25.1 ft^3	25.1 ft^3
$P_{discharge}$	1 bar	1.2 bar
$t_{discharge}$	20.2 s	18.6 s
PJM operating time during test	410 min	218 min
Total PJM operating time for day	410 min	628 min
Run with equivalent $P_{discharge}$ and $t_{discharge}$	030909-S2-1	030909-S2-2
Run with equivalent $P_{discharge}$ and $t_{discharge}$	030917-S3-5	031214-S2-1
Run with equivalent $P_{discharge}$ and $t_{discharge}$	031120-S2-1	031118-S2-2

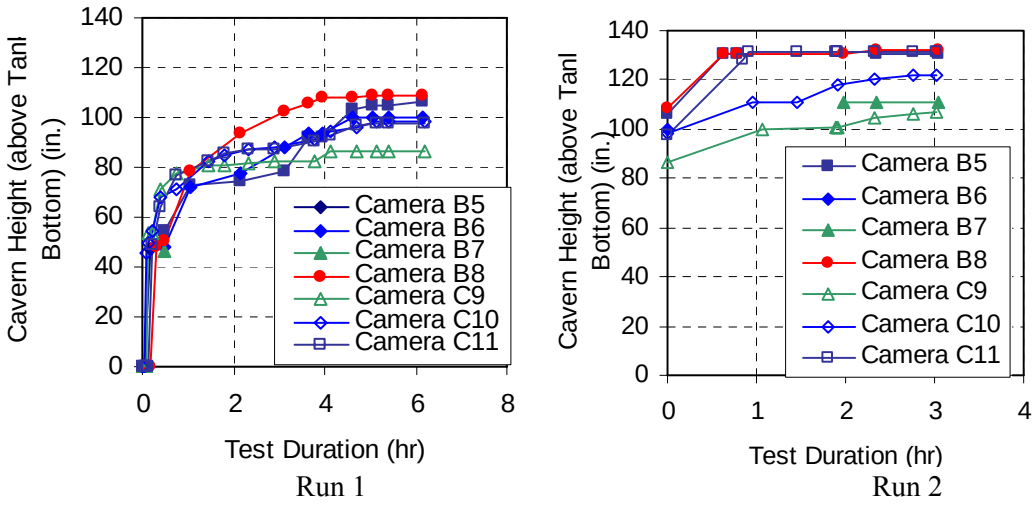

Figure A.29. Absolute Cavern Interface Heights Observed During Test 031118-S2 Runs 1 and 2

The approximate cavern location observed during Run 1 is shown in Figure A.30. Analysis of the absorbance and calculation of the fluid that was mixed from the absorbance is plotted in Figure A.31 (Poloski et al. 2004). These calculations show that the fluid was fully mixed after completion of Run 2.

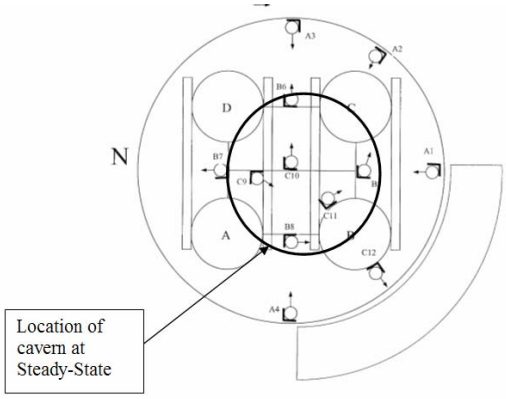

Figure A.30. Approximate Cavern Location at Steady State for Test 031118-S2 Run 1

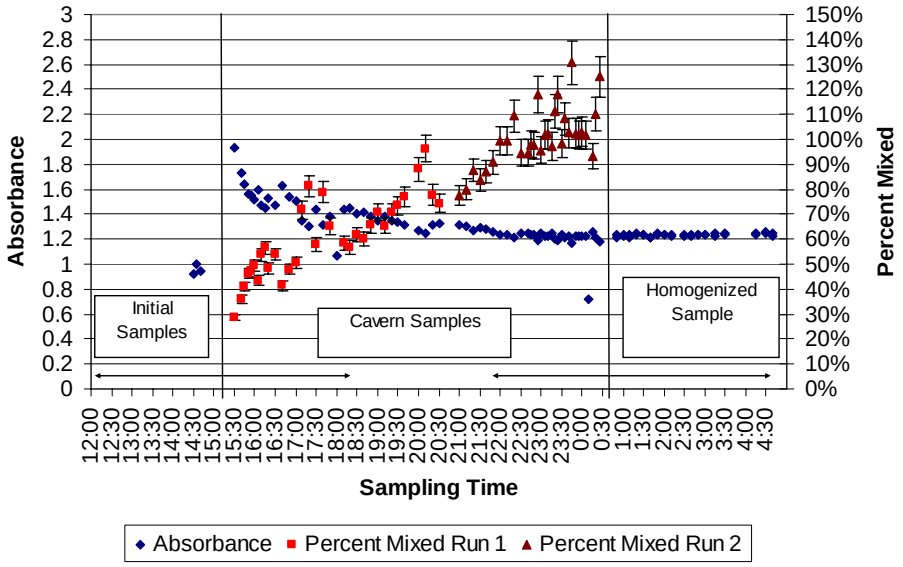

Figure A.31. Absorbance Plots for Test Run 031118-S2 Runs 1 and 2

A.3.13 Constant Volume Test with Dye Injection 031120 S2 Run 1

The purpose of this test sequence was to evaluate the reproducibility of the results using the same conditions but starting at lower PJM velocities and increasing in steps to the conditions listed in Table A.21.

Table A.21. Operating Conditions for Test 031120-S2 Runs 1, 2, and 3

Parameter	Run 1	Run 2	Run 3
$U_{discharge}$	14 ft/s	NA	16.5 ft/s
$V_{discharge}$	25.1 ft^3	NA	25.1 ft^3
$P_{discharge}$	1 bar	1.1	1.4 bar
$t_{discharge}$	20.2 s	18.6 s	17 s
PJM operating time during test	70 min	66 min	467 min
Total PJM operating time for day	70 min	136 min	603 min
Run with equivalent $P_{discharge}$ and $t_{discharge}$	030909-S2-1	--	030909-S2-3
Run with equivalent $P_{discharge}$ and $t_{discharge}$	031118-S2-1	--	030911-S2-4
Run with equivalent $P_{discharge}$ and $t_{discharge}$	030917-S3-5	--	--

Prior to dye injection the PJMs were operated during Runs 1 and 2. Dye injection occurred over a 30-minute period that began after 1 hour of PJM operation during Run 3. Dye injection consisted of mixing 55.4 g of Brilliant Blue dye with approximately 3 L of Laponite and injecting it into the bottom of the tank while the PJMs were operating. An additional 3 L of clean Laponite was used to clean out the dye container and to clear the injection line of dye.

Data plotted in Figure A.32 show how the observed cavern interface heights varied during the test. Cameras B5, C9, C10, and C11 were approaching steady-state conditions when the PJM discharge pressure was increased to the second setting. After ~66 minutes of operation the PJM discharge pressure was increased to the third setting. After ~ 30 minutes at this condition, breakthrough was observed.

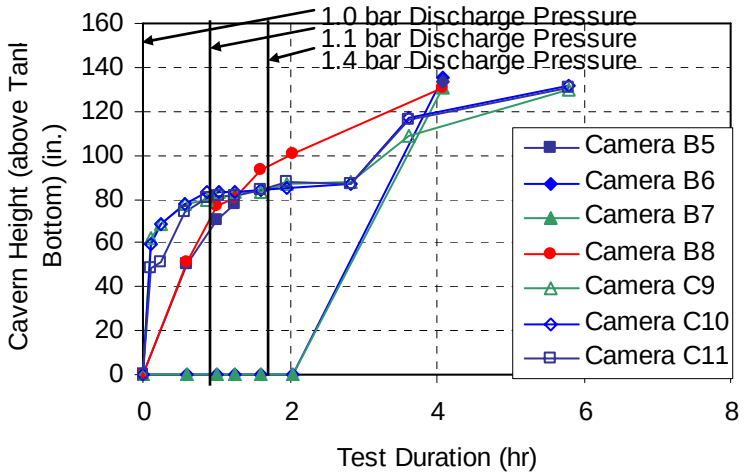

Figure A.32. Absolute Cavern Interface Heights Observed During Test 031120-S2 Runs 1, 2, and 3

After all of the B cameras and cameras C10 and C11 observed breakthrough conditions at the Laponite surface, various cameras were moved to different heights to document flow conditions. These observations are documented in Tables A.22 through A.25.

Table A.22. Flow Characteristics Observed by Camera C10 at Different Positions During Run 3

Absolute Height of Camera Position During PJM Discharge (in.)	**Flow Characteristics**
74–80	Very high vertical velocity (much greater than camera vertical movement rate)
80–87	Very high vertical velocity
87–94	Moderate to high vertical velocity with occasional high lateral flow components
94–101	Moderate vertical velocity with high lateral flow velocity component most of the time
101–112	Vertical velocity was slightly higher than plug flow, with significant lateral flow velocity component
112–125	Vertical flow velocity slightly higher than plug flow with modest lateral flow velocity component
125– ~132	Vertical flow varied from slightly above to slightly below plug flow with a slight lateral flow component.
NA	Very slight lateral flow velocity component.

Table A.23. Flow Characteristics Observed by B Cameras at Different Positions During Run 3 Discharge

Absolute Height of Camera Position (in.)	Flow Characteristics			
	Camera B5	**CameraB6**	**Camera B7**	**Camera B8**
47	Initially slightly turbulent, then stagnant	Stagnant	Stagnant	Initial lateral flow followed by downward flow and finally stagnant
54	Mostly stagnant	Mostly stagnant	Mostly stagnant	Mostly stagnant
64	Mostly stagnant	Mostly stagnant	Mostly stagnant	No vertical flow but slight lateral flow
74	Very little vertical but significant lateral flow	Very little vertical but significant lateral flow	Very little vertical but significant lateral flow	Very little vertical but significant lateral flow
84	slight vertical but significant lateral flow	Slight vertical flow but significant lateral flow	Slight vertical flow but significant lateral flow	Slight vertical flow but significant lateral flow
94	Vertical plug flow with significant lateral flow	Vertical plug flow with significant lateral flow	Vertical plug flow with significant lateral flow	Vertical plug flow with significant lateral flow
104	Vertical plug flow with significant lateral flow	Vertical plug flow with significant lateral flow	Vertical plug flow with significant lateral flow	Vertical plug flow with significant lateral flow
114	Vertical plug flow with significant lateral flow	Vertical plug flow with significant lateral flow	Vertical plug flow with significant lateral flow	Vertical plug flow with significant lateral flow

Table A.24. Bubble Motions Observed by B Cameras at Different Positions and Times During Run 3

Set	64 in. absolute height		66.5 in. absolute height		69 in. absolute height	
	Vertical Movement (in.)	**Horizontal Movement** (in.)	**Vertical Movement** (in.)	**Horizontal Movement** (in.)	**Vertical Movement** (in.)	**Horizontal Movement** (in.)
Camera B5						
1st	Up ¾	Left ⅛	Up ¾	Left ½	Up 1¼	Left 2
2nd	Up ⅞	Left ⅛	Up 1	Left 1½	Up 1¾	Left 3½
3rd	Up 1¾	None	Up 1½	Left 1½	Up 2½	Left 3¼
Camera B6						
1st	Up 1	Left 1/16	Up 1¾	Left ¾	Up 1¾	Left ¾
2nd	Up 1⅝	Left ⅛	Up 1½	Left ⅝	Up 1½	Left 1
3rd	Up 1¾	Left ¼	Up 1½	Left ⅜	Up 2	Left 1½
Camera B7						
1st	Up 1⅝	None	Up 1½	Left ¼	Up 2	Left 1 5/16
2nd	Up 1¾	None	Up 1¼	Left ¼	Up 2½	Left ¾
3rd	Up 2	Left⅛	Up 1¾	Left ½	Up 2	Left 1¾
Camera B8						
1st	Up 1, down ¾	Left ½	Up 1	Left 1½	Up 1¾	Left 5½
2nd	Up 1, down 1½	Left 1	Up 1, down 2	(no data)	Up 1½, down ¼	Left 2½
3rd	Up 1, down 1¾	Left ½	Up 1½, down ½	Left 1¾	Up 1¾, down ½	Left 2⅞

Table A.25. Bubble Movement During PJM Operation at Various Locations During Run 3

Camera	Initial Position (absolute height) (in.)	Initial Position (absolute height) (in.)	Net Bubble Movement (in./cycle)
A1	5.10	0.06	5.04
A1	6.13	1.12	5.01
A2	6.26	3.05	3.21
A2	5.83	2.86	2.97
A3	6.16	2.64	3.52
A3	5.39	1.79	3.60
A4	6.91	2.40	4.51
A4	5.38	0.72	4.66
B5	12.59	3.32	9.27
B6	12.25	4.58	7.67
A1	59.71	57.18	2.53
A1	57.97	54.58	3.39
A1	48.42	44.03	4.39
A2	59.35	56.11	3.24
A2	57.28	54.34	2.94

Analysis of the absorbance and calculation of the fluid that was mixed from the absorbance is plotted in Figure A.33 (Poloski et al. 2004). These calculations show that the fluid was fully mixed after the completion of the run. The time-to-mix criteria are summarized for Run 3 in Table A.26.

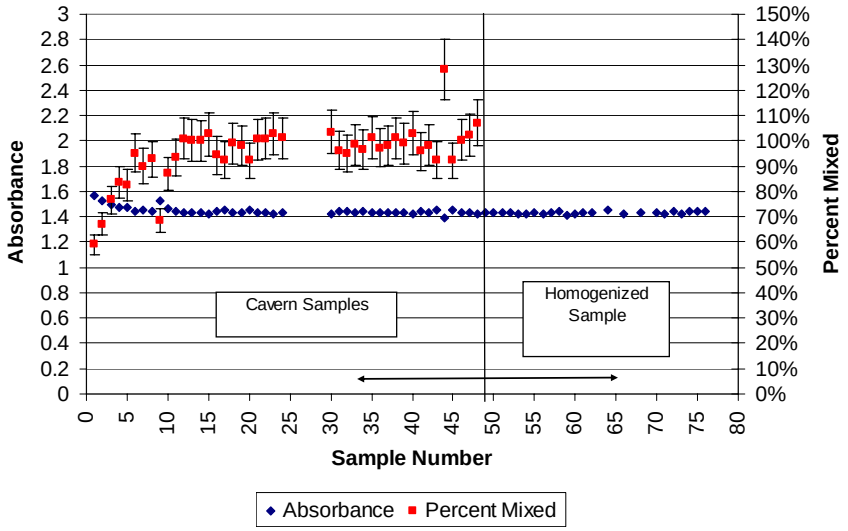

Figure A.33. Absorbance Plot for Test 031120-S2 Run 3

Table A.26 Assessment of Time to Mix Criteria for Test 031120-S2 Run3

Criteria for Time to Mix	Observation During Test Run 0311120-S2 Run 3
Time to breakthrough	~30 min at breakthrough PJM settings; ~166 min of PJM operation during the three PJM operating conditions
Time flow observed in annular area	~ 2 hours at condition S2 Run 3
Time of turbulent flow observed in annular area	Not attained
Time of full mobilization	Estimated to be 2 hours

A.4 Tests with Clay Simulant

Only two tests were conducted with clay simulant to support the scaling analysis. The remainder of the clay simulant tests involved gas generation and release. To track fluid motion in opaque simulants, two unique characterization methods, radiofrequency (RF) passive integrated transponder (PIT) tags and beads, were inserted into the simulant.

A.4.1 Using Passive Integrated Transponder Tags to Track Cavern Growth

A PIT tag (Biomark, Inc., Boise, ID model 1411ST) is an integrated circuit and antenna encapsulated in glass, as shown in Figure A.34. The tags are cylindrical, 12 mm long, 2.1 mm in circumference, and 90 mg in mass. Tags are activated by a transceiver/reader (Destron-Fearing FS2001F) and programmed to transmit a unique digital code (at 134.2 kHz) back to the reader, where the code is displayed and/or stored.

Figure A.34. PIT Tag with a Dime for Size Comparison

Eight PIT tag readers and antennas were used to determine the location of the cavern by identifying the presence of tags. Four were the racket type shown in Figure A.35, which were fixed in place in the simulant near the top of the tank and recorded the locations of the tags moving past the reception area. The other antennas were cylindrical and custom-made (Biomark, Inc.). They were moved up and down inside wells manually to record the locations of RF tags moving through the reception area over the entire depth of simulant. The position of an antenna inside the well was determined with a measuring device fastened to the antenna at a known point; depth was referenced from the top of the antenna well.

The custom antennas were installed in PVC pipe 5.08 cm in diameter that was capped at the bottom and served as an antenna well. The cylindrical antennas were 4 cm in diameter, 25.5 cm long, and had a range of about 8 to 10 cm, as shown in Figure A.36. Each antenna well was placed in the simulant perpendicular to the fluid surface and firmly attached to a walkway above the center of the tank or to other solid structures. The horizontal position of each antenna was measured as the distance along the walkway railing from the west side of the tank and is summarized in Table A.27.

Figure A.35. Racket-type Antenna Connected to a PIT Tag Reader

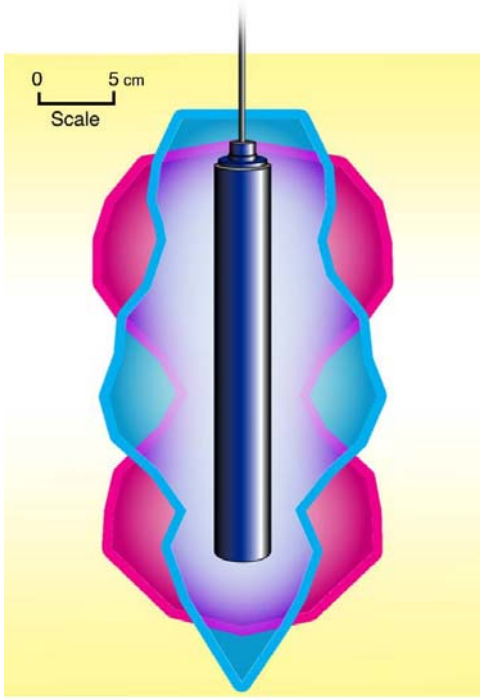

Figure A.36. Antenna Range Patterns Used to Identify PIT Tags. Red area is detection zone when PIT tag long axis is perpendicular to vertical axis of antenna. Blue area is detection zone when tag long axis is parallel to vertical axis of antenna.

Table A.27. Locations of PIT Tag Reader Antennas. Radial coordinate was measured as horizontal distance along tank walkway railing from the west side of the tank. Azimuthal coordinate was measured from tank center for racket antennas; orientation applies only to the racket antennas.

Antenna Code	Radial Coordinate (cm)	Azimuthal Coordinate (cm)	Elevation Coordinat (cm)	Antenna Orientation
W1	206	--	64	--
W2	142	--	51	--
W3	142	--	0	--
W4	157	--	-56	--
A1	318	137	--	Parallel to bridge
A2	257	56	--	Perpendicular to bridge
A3	145	119	--	Parallel to bridge
A4	25	178	--	45° angle to walkway

A.4.2 Constant Volume Test Using Dye, Beads, and Tags 031214-S2 Runs 1, 2

The purpose of this test sequence was to evaluate cavern height in kaolin-bentonite slurry using dye to determine concentration distribution, PIT tags to track fluid motion, and beads to obtain bead distribution in core samples. Test conditions for the two runs are listed in Table A.28.

Table A.28. Test Conditions During Test 031214-S2

Parameter	Run 1	Run 2
$P_{discharge}$	1.2 bar	1.6 bar
$t_{discharge}$	18.6 s	15.7 s
PJM operating time during test	361 min	374 min
Total PJM operating time	361 min	735min
Run with equivalent $P_{discharge}$ and $t_{discharge}$	030909-S2-2	--

A.4.2.1 Test 031214-S2 Run 1

Before the start of Run 1, 250 RF tags and plastic neutral density beads were inserted into each pulse tube. They were dispersed throughout the tank when the PJMs were started. Run 1 started at 23:42 on December 14 and lasted until 5:43 on December 15, 2003. After 3 hours and 42 minutes it was assumed that the tank had reached a steady state. At this time slurry samples were obtained for baseline calorimetry analysis before injecting dye. Dye injection started after ~3-3/4 hours of PJM operation and was completed in ~18 minutes. Dye injection consisted of mixing 500 g of Brilliant Blue dye with water and adding it incrementally during the suction portion of several PJM cycles. The injection line was flushed after dye injection was complete. About 38 minutes after that, intense blue dye was observed on the slurry surface.

After 4 hours of operation, cavern interfaces were tentatively determined by cameras A1, A4, B5, B8, C9, and C10 locating a population of what appeared to be beads touching the camera well wall and tracking them until they disappeared. Table A.29 lists elevations where interfaces were believed to exist based on these observations.

Table A.29. Location of Possible Interface Based on Observations of Beads at Camera Well Walls

Camera	Absolute Elevation (in.)
A1	56.4
A2	NA
A3	NA
A4	63.6
B5	76.3
B6	NA
B7	NA
B8	63.0
C9	84.4
C10	63.5
C11	NA
C12	NA

Run 1 was terminated after ~6 hours of PJM operation; core samples were taken to analyze bead and color content. The PIT tag observations from this test are summarized in Table A.30. During this run no tags were observed by any of the fixed-position racket-type antennas, indicating that the simulant was not moving in the areas where these antennas were located.

Table A.30. Data from Test Beginning on December 14, 2003 on Steady-State Elevations of PIT Tag Reader Antennas

Time (hr:min)	**PJMs**		**Steady State Elevation for PIT tag antennas** (cm)							
	Drive Pressure (bar)	**Drive Time** (sec)	**W1**	**W2**	**W3**	**W4**	**A1**	**A2**	**A3**	**A4**
2:42	1.2	18.6	71	152	142	132	None	None	None	None
4:04	1.2	18.6	71	152	142	122	None	None	None	None
5:00	1.2	18.6	71	152-182	163-182	71-81	None	None	None	None
5:46	1.2	18.6	--	--	163	122	None	None	None	None

A.4.2.2 Test 031214-S2 Run 2

Run 2 began at 15:18 and ran until 21:34 on December 15, 2003. Before this test started, PIT tags were placed on the top of the simulant in a grid pattern, as shown in Figure A.37. The antennas and wells were in the same positions as the first test. The first recording of a PIT tag by a stationary antenna occurred at 18:20, indicating that the increase in drive pressure from Run 1 to Run 2 was enough to expand the area of mixing into the reception range of stationary antenna A2. After ~2-1/4 hours of

Figure A.37. Cluster of PIT Tags on the Surface of Clay Simulant in Large-Scale Tank. On the right is PVC pipe with a funnel attached at the top that was used to position the tags and beads in a grid on the surface of the simulant.

operation during Run 2, the RF tags were determined to be at steady state. The PJMs were stopped after 6-1/4 hours of operation. The results of the second test are summarized in Table A.31.

Table A.31. Data from the Test that Began on December 15, 2003 on the Steady-State Elevations of the PIT Tag Reader Antennas

Time (hr:min)	**PJMs**		**Steady-State Elevation for PIT Tag Antennas** (cm)							
	Drive Pressure (bar)	**Drive Time** (sec)	**W1**	**W2**	**W3**	**W4**	**A1**	**A2**	**A3**	**A4**
17:20	1.6	15.7	183	183	163	223	--	--	--	--
18:20	1.6	15.7	--	--	173	233	None	--	None	None
18:51	1.6	15.7	163	223	163	213	--	--	--	--
20:20	1.6	15.7	163	223	163	213	--	--	--	--

A.4.2.3 Use of Coring to Determine PJM Mixing

Core samples were used to identify the distribution of lexan beads and dye to determine the size and extent of caverns and the homogeneity of bead and dye mixing to indicate the degree of mixing of the slurry. On December 15, 2003 cores were sampled from the 336 large-scale tank after each of two cavern tests and one mobilization test. Cores were taken with 2.54-cm-diameter schedule 200 PVC pipe and inserted vertically into the clay, as shown in Figure A.38. A cement vibrator was used to help place the core within the simulant. The cores were capped with 2.54 cm test plugs and removed, then frozen in a walk-in freezer. The frozen cores were cut into 10.1-cm sections, and the number of beads within each section was recorded. The amount and distribution of dye was also determined from each core section.

Figure A.38. Section of the Tank with a Core Placed in the Simulant Before Capping and Removal

Core Samples from Test 031214-S2 Run 1. Core samples from cavern test 1 were taken at 6:00 AM on December 15, 2003. Three cores were taken in total. Two were centrally located below the access bridge, and the third was taken farther from the center of the tank, as shown in Figure A.39.

The beads appear to disperse at higher levels toward the center of the tank. The beads were all at least 31 inches from the surface and distributed only through the bottom few feet of each core. The density of beads in the individual core layers was found to be slightly higher in cores farther from the center of the tank (cores 1 and 2).

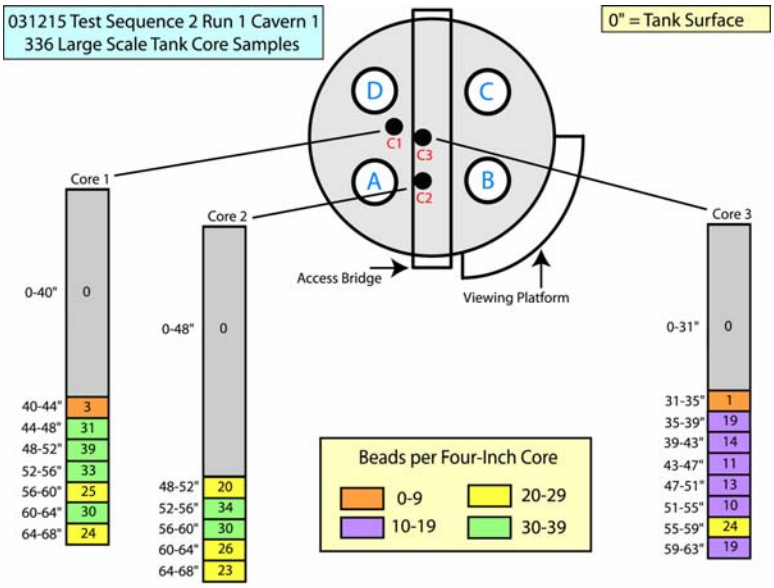

Figure A.39. Top View of Tank Showing Placement of Core Samples from Run 1 and Distribution of Beads Observed in Layers of Each Core

Core Samples from Test 031214-S2 Run 2. A second cavern test was conducted on December 15, 2003. Three core samples were taken from different locations than on the previous run, as shown in Figure A.40.

With the exception of Core 1, the beads were distributed throughout the entire depth of the other two cores. Beads broke through the surface near the center of the tank, and bead densities were highest in the center of the tank (cores 2 and 3). As in the previous trial, the beads were concentrated in the bottom portion of the core farthest from the center of the tank (core 1), and the bead densities in individual layers tended to be higher in the lower portion of the outermost core.

Core Samples after Mobilization. Cores were used to sample the distribution of beads and dye in the simulant after a mobilization test. The test was conducted on December 16 at 3:45 AM. The same procedure, inserting, capping, and freezing the cores, described for the cavern tests was used. However, for this test, five cores were sampled, as shown in Figure A.41. The distributions of beads by layer was then compared with a theoretically ideal uniform distribution of beads with equal numbers in each core layer to assess the degree of homogeneity of the mixing listed in Table A.32.

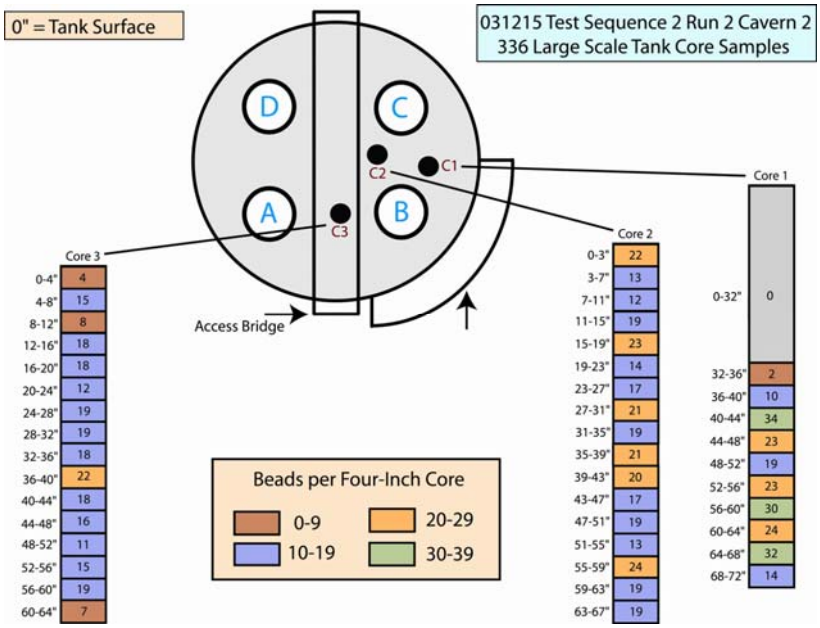

Figure A.40. Top View of Tank Showing Positions of Core Samples from Run 2 and Distribution of Beads in Layers of Each Core

The goodness-of-fit tests showed that cores 2 and 4 were not significantly (P>0.05) different from a perfectly homogeneous mixture. Core 4 was very near the center of the tank, and core 2 was taken from the outer area of the tank. Core 5 was close to core 4 but was considered significantly (P<0.05) different from homogeneous. Core 3 was the most heterogeneous of the five samples.

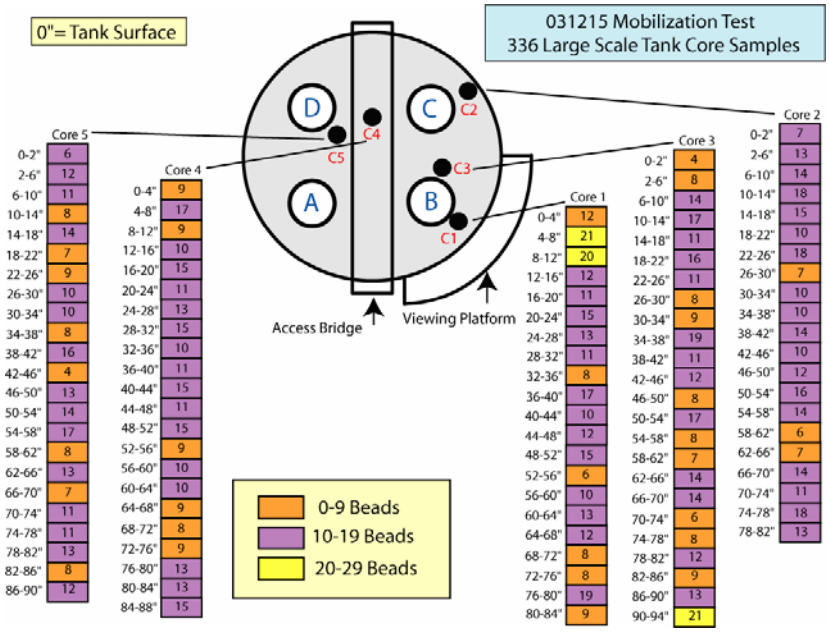

Figure A.41. Top View of Tank Showing Placement of Five Cores and Distribution of Beads Counted in Core Layers from Each Core

Table A.32. Mean Number of Beads per 10.1-cm Layer in Each Core and *P* Values of a Chi-Square Test to Determine the Level of Conformity to a Perfectly Homogeneous Distribution of Beads.

	Core 1	Core 2	Core 3	Core 4	Core 5
Mean number of beads per layer	3.12	3.14	2.93	2.92	2.70
Standard deviation	1.03	0.89	1.02	0.67	0.78
Minimum	1.50	1.50	1.50	2.00	1.00
Maximum	5.25	4.50	5.25	4.25	4.25
Chi-Square P	0.03*	0.21	0.01*	0.54	0.05*
* A significant result is rejection of homogeneity.					

A.4.3 Constant Volume Test 040525-S2 Runs 1 through 9 with Clay Simulant

The purpose of this test was to evaluate the combinations of PJM drive times and drive pressures required to cause a surface breakthrough of the mixing cavern in the kaolin-bentonite waste simulant. Test conditions for the nine runs are summarized in Table A.33.

Two cameras were mounted on the viewing platform with views of the tank surface and operated for the entire length of the run, which lasted up to 17 minutes. Test runs consisted of nine PJM drive time/ drive pressure settings and corresponding visual observations of the simulant surface for each setting. PJM nozzle velocities and discharge volumes were not calculated for this test. PJM cycle time for all runs was 60 seconds, and the ΔH varied from 93 to 100 inches, depending on the run.

The simulant was well mixed immediately before testing began. Each run of the test lasted approximately 15 to 17 minutes, and the total time elapsed for the test was 2 hours, 22 minutes. The simulant (kaolin-bentonite) level measured from the tank rim was 42 inches, for a fill height of 137 inches.

Table A.33. Test Conditions During Test 040525-S2 Runs 1 through 9

Run No.	PJM Drive Time/Avg. ΔH (sec/in.)	Drive Pressure (bar)	PJM Run Time/ Cumulative Time (min)	Surface Observations/Comments
1	25/100	1.0	16/16	6 PJM strokes then restarted
2	17.5/100	1.8	17/33	Wrinkled, cracked surface-no upwelling
3	14.4/93	2.0	15/48	Same as Run 2
4	16/100	2.0	15/63	Same as Run 2
5	13/95	2.4	15/78	Wrinkles smoothed out-small bubbles rising to surface at center.
6	14.5/100	2.4	17/95	Same as Run 5, but more bubbles rising to surface.
7	12.9/95	2.5	16/111	Same as Run 5—No lateral movement of surface
8	14/100	2.5	16/127	Bubbles with upwelling simulant—tracers placed at tank center—breakthrough beginning
9	12.2/95	2.7	15/142	Definite lateral movement on surface—breakthrough declared definite by observer

Drive pressure was gradually increased in successive test runs, with some settings combined with more than one PJM stroke length/drive time. In general, as drive pressures increased, activity on the simulant surface at tank center became more vigorous. This activity was enhanced when a longer PJM discharge stroke was applied for a given pressure setting. For the first seven runs of the test, no breakthrough or upwelling of simulant was observed at the surface, only varied degrees of surface wrinkling or deformation. Bubbles began to appear on the simulant surface following the discharge stroke in Run 5 and increased in Runs 6 and 7. At the beginning of Run 8, the stroke length was increased by ~5 inches over the previous run while using the same drive pressure (2.5 bar). This slight adjustment was apparently sufficient to initiate breakthrough. Buoyant surface tracers (ping-pong balls) were placed on the surface at tank center after Run 7. Breakthrough was declared as "definite" by the observer, and the surface tracers were moving demonstrably toward the tank walls from the center during discharge strokes.

A.5 Velocity Field Mapping

The velocity profile developed by the jet emitted from the PJM as it flowed upward in the tank was measured in situ in real time using an ultrasonic velocity probe that was described in Section 4.7.1 of the main report. Understanding the magnitude and extent of this velocity field provides insight into the mixing process developed by cycling the PJMs.

A.5.1 Approach

The velocity mapping of PJMs was conducted to produce two target nozzle velocities of 8 and 12 m/s with a 60-second cycle. In the mode operated, the velocity profiles for each pulse were triangular spikes peaking at around the target value.

A.5.2 Kaolin-Bentonite Simulant Properties

The kaolin-bentonite simulant rheological properties were measured before and after the velocity characterization. The simulant properties are summarized in Table A.34.

Table A.34. Measured Rheological Properties of the Kaolin-Bentonite Simulant (Bingham Model) Before and After Upwelling Tests

Facility	**Yield Stress** (Pa)	**Consistency (viscosity)** (Pa·s)
336 4PJM (before)	29.28	0.02042
336 4PJM (after)	28.39	0.02019

A.5.3 Kaolin-Bentonite Simulant Tests and Results

The plan for 336 was to measure at 8 and 12 m/s at H_{VP}/D_T levels of 0.3, 0.6 and 0.85. The measurement probe was attached to a pole with a 10.5 inch extension. The pole was inserted vertically into the tank at a position ~15.6 inches west of tank center. At each elevation the pole was turned east, west, south and north, and a measurement was taken.

For the 336 PJM measurements, only data from channels 25 through 40, corresponding to >25 and <40 mm, from the probe face were kept for evaluation. Measurements were made every 0.2 second (1500 in 5 minutes). Table A.35 summarizes locations and conditions of the 336 4PJM measurements. The upwell velocity results are included in Section 4 of the main report (Tables 4.20, 4.22, and 4.23).

Table A.35. 336 4PJM Test Conditions

Test	Nominal H/D	Direction
040526-vel3	0.85	W
040526-vel4	0.85	S
040526-vel6	0.85	E
040526-vel7	0.85	N
040526-vel8	0.85	W
040526-vel9	0.85	S
040526-vel10	0.85	S
040526-vel11	0.85	W
040526-vel12	0.85	N
040526-vel13	0.85	E
040526-vel14	0.85	E
040526-vel15	0.85	N
040526-vel16	0.85	W
040526-vel17	0.85	S
040526-vel18	0.6	S
040526-vel19	0.6	S
040526-vel20	0.6	W
040526-vel21	0.6	N
040526-vel22	0.6	E
040526-vel24	0.6	E
040526-vel25	0.6	N
040526-vel26	0.6	W
040526-vel27	0.6	S
040526-vel28	0.6	S
040526-vel29	0.6	W
040526-vel30	0.6	N
040526-vel31	0.6	E
040526-vel32	0.6	E
040526-vel33	0.6	N
040526-vel34	0.6	W
040526-vel35	0.6	S
040527-vel1	0.6	E
040527-vel2	0.6	S
040527-vel5	0.6	N
040527-vel6	0.6	N
040527-vel7	0.3	W
040527-vel9	0.3	S
040527-vel10	0.3	E
040527-vel11	0.3	E
040527-vel12	0.3	S
040527-vel14	0.3	W
040527-vel16	0.3	N
040527-vel17	0.3	N
040527-vel18	0.3	W
040527-vel19	0.3	S
040527-vel20	0.3	E

A.6 References

Bontha JR, JM Bates, CW Enderlin, and MG Dodson. 2003. *Large Tank Experimental Data for Validation of the FLUENT CFD Model of Pulsed Jet Mixers.* PNWD-3303, Battelle – Pacific Northwest Division, Richland, Washington.

Poloski et al. 2004. *Chemical Tracer Techniques for Assessing Mixing Performance in Non-Newtonian Slurries for WTP Pulsed Jet Mixer Systems.* PNWD-3494, Battelle – Pacific Northwest Division, Richland, Washington.

Appendix B

Small-Tank Scaling Experiments Conducted at APEL at 1/4 Scale with One and Four PJMs

Appendix B Contents

Figures

Tables

Appendix B

Small-Tank Scaling Experiments Conducted at 1/4 Scale with One and Four Pulse Jet Mixers

The small-tank test stand, also referred to as the Applied Process Engineering Laboratory (APEL) Single-PJM test stand, was designed by AEA Technology to be nearly prototypic of the actual PJMs in terms of the pulse tube inner-diameter (ID) to nozzle-diameter ratio. This system was used to evaluate the mixers in a well-controlled environment to provide data for validation of the TEMPEST hydrodynamic predictive capability near tank surfaces (Bontha et al. 2003). For this series of tests, the system was configured as a 1/4-scale model of the large-scale test tank located in the Battelle – Pacific Northwest Division (PNWD) 336 Building with a scaling factor of 4.53.

B.1 APEL Single-PJM Test Stand Description

The small-scale test stand is shown in Figure B.1. It consists of a ~0.864 m ID x 2.36 m high (~34 inch ID x 7.75 ft high) tank made of clear Plexiglas with an elliptical bottom. The tank has a false (flat) insert to enable testing in a flat-bottom configuration.

A single pulse tube made out of clear plastic was positioned centrally within the tank on a mounting assembly that enables adjustment of the pulse tube nozzle position from the bottom of the tank. The pulse tube has dimensions of 0.254 m ID, 0.279 m OD, and 1.22 m high (10 in. × 11 in. × 4 ft) with the lower end tapered to a 60-degree nozzle of 5.08E-02-m (2-inch) diameter. The upper end of the pulse tube is flat, with a 5.08E-02-m (2-inch) threaded opening in the center.

The small-scale test stand pilot-scale configuration allowed experiments to be conducted on an energy-per-unit-volume basis similar to the large tanks in the Hanford Waste Treatment Plant (WTP). Additional features included:

- Clear and transparent construction materials for both tank and PJMs to enable visualization of the flow behavior of the fluid in the tank and inside the pulse tube during operation.
- Flat and round (or elliptical) bottom configurations to evaluate the effect of tank geometry on mixer performance.
- Adjustable tank height. The ~2.06 m (6.75 ft) height of the tank was intentionally significantly larger than the ~0.864 m (~34 inch) diameter to permit evaluation of the influence of H/D_T on mixer performance over a broad range of conditions (<1 to ~2.5).
- An adjustable pulse-tube mounting system provided the ability to adjust the pulse-tube nozzle standoff from the bottom of the tank to evaluate its impact on mixer performance.
- The test stand was configured to test single and multiple pulse tube configurations. The single pulse tube had a 0.254 m (10 inch) ID and was ~1.52 m (5 ft) high.

The measurement and test equipment used to support tests in the small-tank test stand are listed in Table B.1.

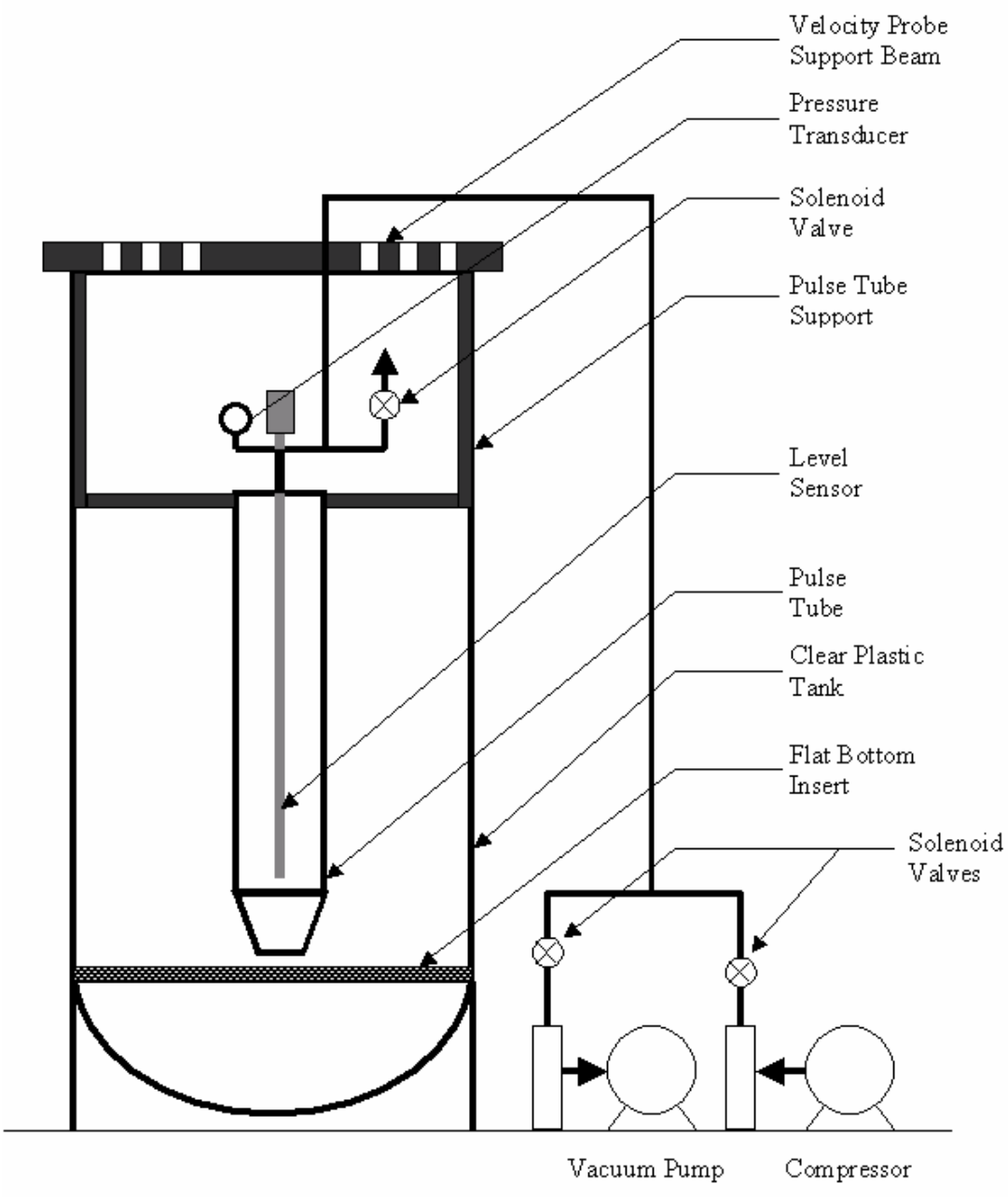

Figure B.1. Schematic Vertical Cross Section of the APEL Single-PJM Test Stand

Table B.1. Measurement and Test Equipment List

Measured Variable	Sensor	Vendor	System	Accuracy
Level	Capacitance level probe	Drexelbrook	APEL single and 4PJM systems	±0.1 in.
Pulse tube pressure	Pressure transducer with capacitive ceramic sensor	Endress+Hauser	APEL single and 4PJM systems	±0.1 psi
Liquid mass flow	Coriolis mass flow meter	MicroMotion	APEL single and 4PJM systems	±0.10% of full range for liquids; ±0.5 kg/m^3 density

B.2 APEL Single PJM Scaling Experiments

B.2.1 Cavern Tests

A cavern is a mixing volume generated within a non-Newtonian fluid by a jet of fluid ejected from a pulse tube. The shear strength of the fluid limits the size of the cavern to a volume in which the kinetic energy imparted to the fluid by the jet overcomes the shear strength of the fluid, so the higher the shear strength the smaller the cavern. Several materials were tested (Laponite, Carbopol, Rhodicare, and a simulated AZ-102 waste) to identify those that would respond like actual waste. Both Carbopol and Rhodicare have a syrup-like consistency, while Laponite and the simulated AZ-102 waste are both thixotropic and exhibit shear-thinning behavior. Based on these tests, Laponite was chosen as the most representative of real waste. The results of all of the tests are summarized in Table B.2.

The principal purpose for the single pulse tube tests was to compare the behavior of various non-Newtonian candidate fluids and choose one that closely simulates real waste. For these tests (e.g., cavern interface with the non-mixing areas), cavern heights were measured as a function of PJM nozzle velocity for three environmentally friendly waste simulant candidates, Laponite, Carbopol, and Rhodicare, and compared with the behavior of actual AZ-102 waste simulant.

B.2.2 Simulant Tests and Results

A series of pulse jet velocities and pulse lengths was applied to each material to provide the data to calculate a characteristic number that changed with reduced velocity. These numbers indicated that Carbopol and Rhodicare exhibit similar behavior, falling on the same curve. Laponite falls on a distinctly different curve, and the simulated AZ-102 fell on a curve close to that defined by Laponite (Poloski et al. 2004).

In this section, Figures B.2 through B.9 each include two graphs. Set “a” plots pulse tube pressure, level probe readings, and the supply pressure as a function of time for data recorded every 0.1 second; and set “b” plots calculated velocity based on the rate of change of the level probe data shown in the “a” set. The velocity calculation for the “b” plots is as follows: the ratio of the cross-sectional area of the pulse tube to the nozzle area is 100, and the rate of change in level probe reading for sequential data points is cm (ΔH) per 0.1 second; thus, the nozzle velocity (NV) is 1000 ΔH cm/s. These figures document the basic behavior of each simulant system in the single PJM as indicated by level probe and pressure measurement data.

Table B.2. Single-PJM Test Data

Simulant	Date	Test No.	Run No.	Log File	Velocity (ft/sec)	Average Cavern Height (in.)				Tank Fill Height (in.)
						at Wall		at Max		
					target	Max	Min	Max	Min	
Laponite	6/26/2003	1	1	030626R1	15.0	19.7	18.5	22.6	21.1	53.0
Laponite	6/26/2003	2	3	030626R4	23.0	27.7	26.8	31.4	29.9	53.0
Laponite	6/26/2003	3	4	030626R6	33.0	37.8	36.5	39.4	38.1	53.0
Laponite	6/26/2003	4	5	030626R8	46.0	41.2	39.9	42.4	40.8	53.0
Laponite	6/26/2003	5	6	030626R10	55.0	41.2	39.9	42.7	41.2	53.0
Laponite	6/28/2003	6	1	030628R1	34.0	24.2	23.8	24.8	24.3	52.4
Laponite	6/28/2003	7	2	030628R2	33.0	26.3	25.7	28.2	27.4	52.4
Laponite	6/28/2003	8	3	030628R4	36.0	33.0	32.0	35.4	34.3	52.0
Laponite	6/28/2003	9	4	030628R6	33.0	33.3	32.0	35.6	34.0	51.9
Laponite	6/28/2003	10	5	030628R8	34.0	33.6	32.0	36.6	34.8	51.8
Laponite	6/28/2003	11	6	030628R9	35.5	34.3	32.6	38.1	35.9	51.7
Carbopol	7/2/2003		3	030702R3	22.0	14.9	13.8	11.4	no data	53.3
Carbopol	7/2/2003		4	030702R5	33.5	18.9	17.7	14.6	no data	52.8
Carbopol	7/2/2003		5	030702R6	46.0	34.4	33.2	17.4	no data	52.7
Carbopol	7/2/2003		6	030702R8	56.0	not visible		19.0	no data	52.7
Carbopol	7/2/2003		7	030702R10	33.5	no data taken		11.9	no data	52.5
Carbopol	7/2/2003		8	030702R12	34.0	no data taken		14.5	no data	52.6
Carbopol	7/2/2003		9	30702R14	35.5	18.6	16.2	17.0	no data	52.4
Rhodicare 2%	7/11/2003		4	30711R5	40.5	8.4	no data	no data	no data	54.5
Rhodicare 2%	7/11/2003		5	30711R6	45.0	10.9	no data	no data	no data	55.6
Rhodicare 2%	7/11/2003		6	30711R7	47.0	10.0	no data	no data	no data	56.2
Rhodicare 2%	7/11/2003		7	30711R8	58.0	14.7	no data	no data	no data	57.6
Rhodicare 2%	7/11/2003		8	30711R9	57.0	15.1	no data	no data	no data	55.9
Rhodicare 0.75%	7/24/2003		1	30724R2	23	10.9	no data	no data	no data	54.2
Rhodicare 0.75%	7/24/2003		2	30724R4	28	15.2	no data	no data	no data	54.2
Rhodicare 0.75%	7/24/2003		3	30724R5	32.5	12.7	no data	no data	no data	54.1
Rhodicare 0.75%	7/24/2003		4	30724R7	33.5	16.4	no data	no data	no data	54.1
Rhodicare 0.75%	7/24/2003		5	30724R8	33.0	16.9	no data	no data	no data	54.2
Rhodicare 0.75%	7/24/2003		6	30724R9	43.0	17.9	no data	no data	no data	54.2
Rhodicare 0.75%	7/24/2003		7	30724R10	53.0	18.3	no data	no data	no data	54.4
AZ-102	7/31/2003			30731R1	No data taken other than PJM operation information					
AZ-102	7/31/2003		6	30731R6	54.2	13.6	12.2	no data	no data	49.6
AZ-102[(a)]	7/31/2003		6	30731R6	54.2	21.2	19.5	no data	no data	49.6
AZ-102-Dil	8/3/2003		3	30803R5	14.8	18.9	no data	no data	no data	39.1
AZ-102-Dil	8/3/2003				No data taken other than PJM operation information					
(a) = Measurements made at the top of the transition layer.										

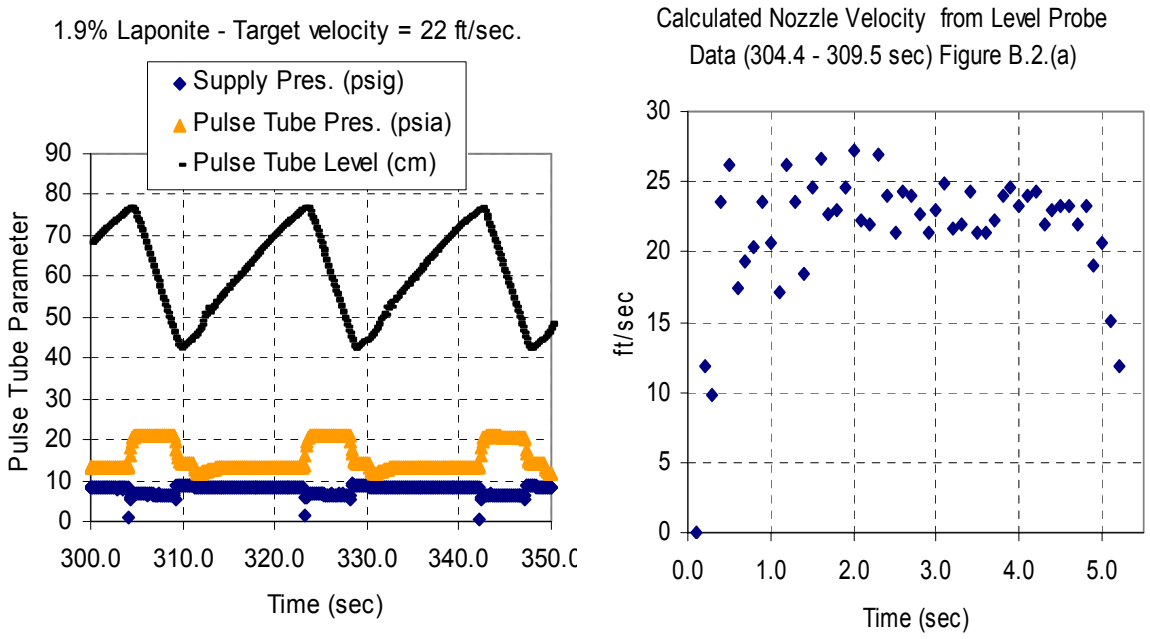

(a) (b)

Figure B.2. (a) Pulse Tube Level and Pressure Profiles for a Run with Laponite. PJM Test, 6/26/2003 testing with 1.9% Laponite, stroke = 12 in. (30 cm), target velocity = 22 ft/sec; (b) calculated NV as a function of time during typical pulse as indicated by changes in level probe reading, level probe data (304.4–309.5 sec).

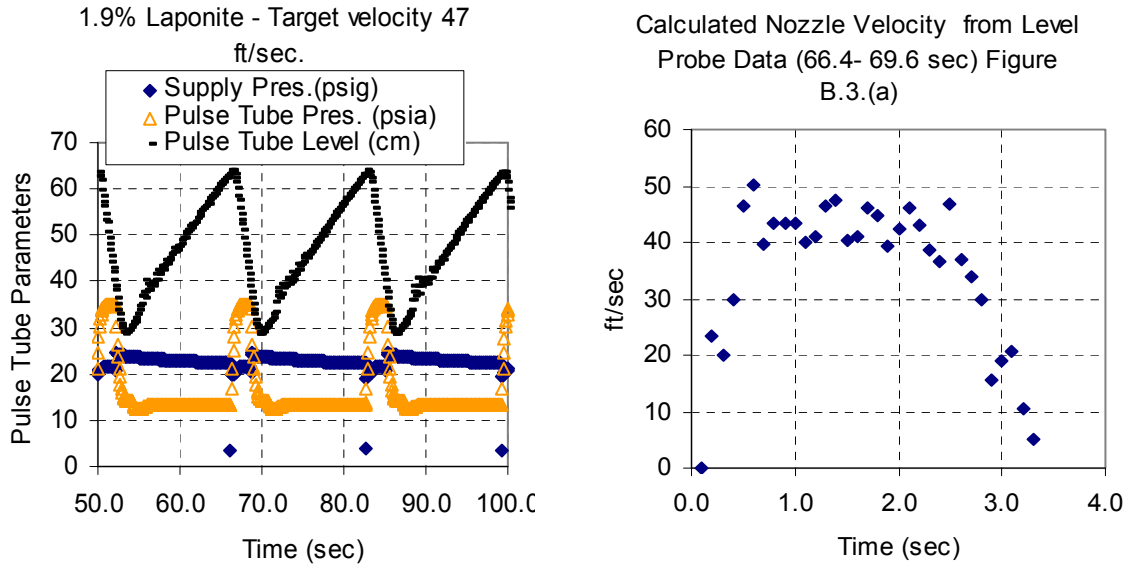

(a) (b)

Figure B.3. (a) Pulse Tube Level and Pressure Profiles for Laponite Run. PJM test 6/26/2003-4-5, with 1.9% Laponite, stroke = 13.9 in. (35 cm), target velocity = 47 ft/sec; (b) calculated NV as a function of time during a typical pulse as indicated by changes in level probe reading, level probe data (66.4–69.6 sec).

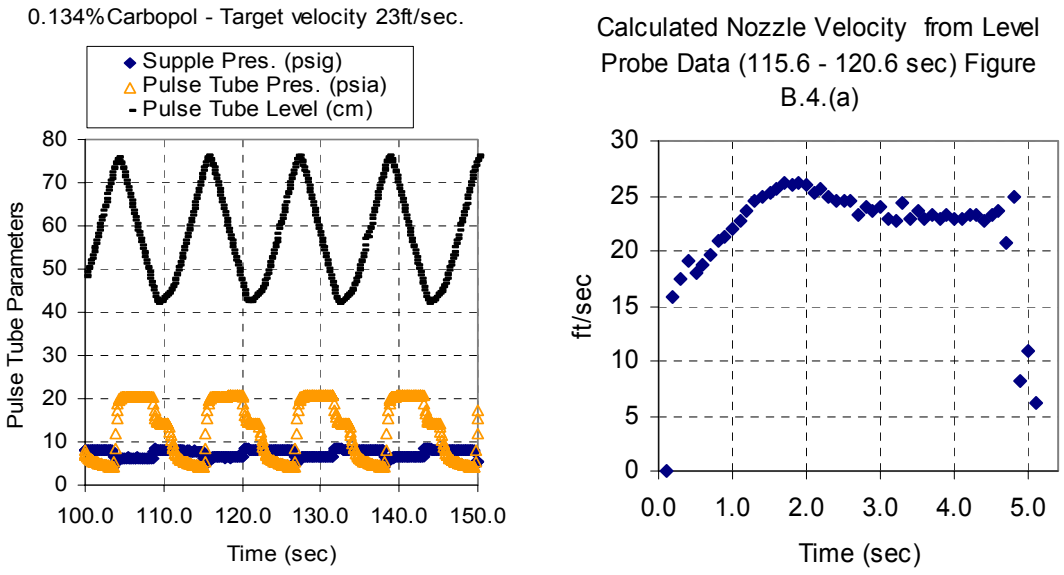

(a) (b)

Figure B.4. (a) Pulse Tube Level and Pressure Profiles for a Run with Carbopol. PJM test 7/02/2003-3, with 0.134% Carbopol, stroke = 13.9 in. (35 cm), target velocity = 23 ft/sec; (b) calculated NV as a function of time during a typical pulse as indicated by changes in level probe reading; level probe data (115.6–120.6 sec).

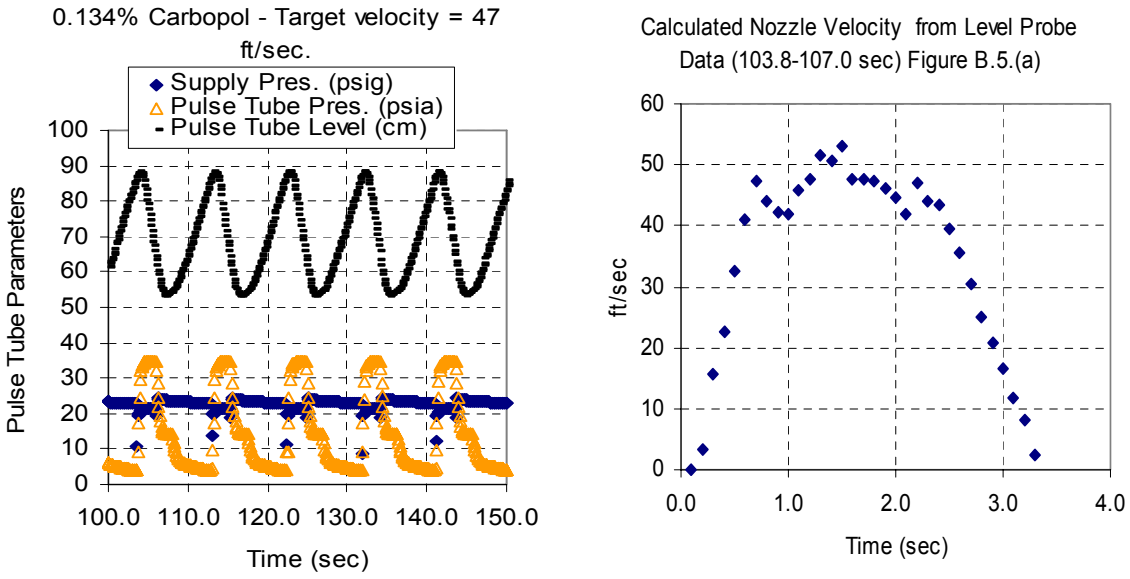

(a) (b)

Figure B.5. (a) Pulse Tube Level and Pressure Profiles for a Run with Carbopol. PJM test 7/2/2003–6, with 0.134% Carbopol, stroke = 13.9 in. (35 cm), target velocity = 47 ft/sec; (b) calculated NV as a function of time during a typical pulse as indicated by changes in level probe reading; level probe data (103.8–107.0 sec).

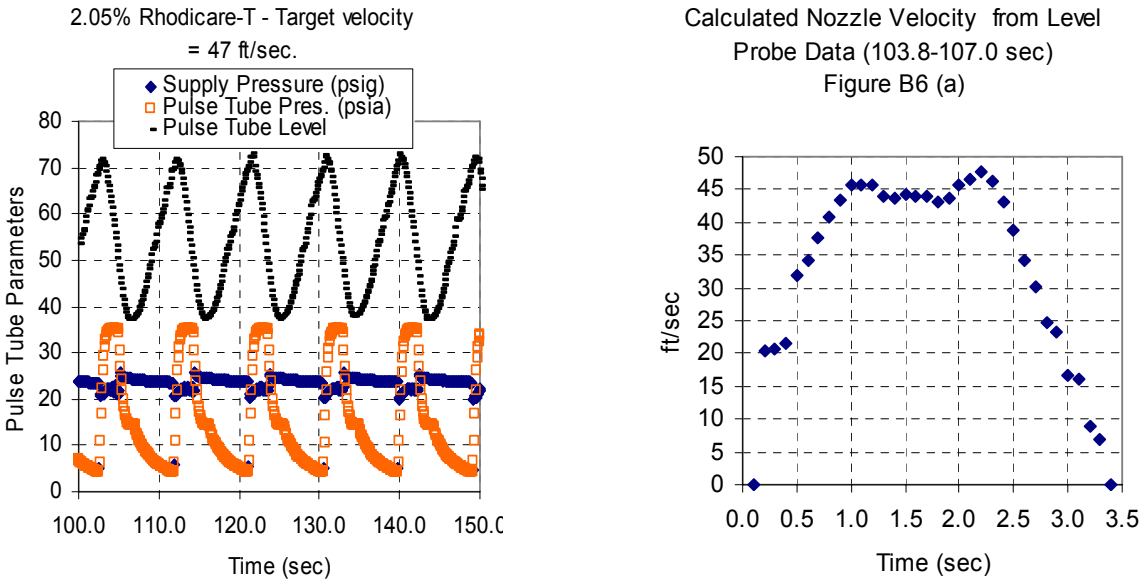

(a) (b)

Figure B.6. (a) Pulse Tube Level and Pressure Profiles for a Run with Rhodicare; PJM test 7/11/2003–6, with 2.05% Rhodicare, stroke = 13.9 in. (35 cm), target velocity = 47 ft/sec; (b) calculated NV as a function of time during typical pulse as indicated by changes in level probe reading; level probe data (103.8–107.0 sec).

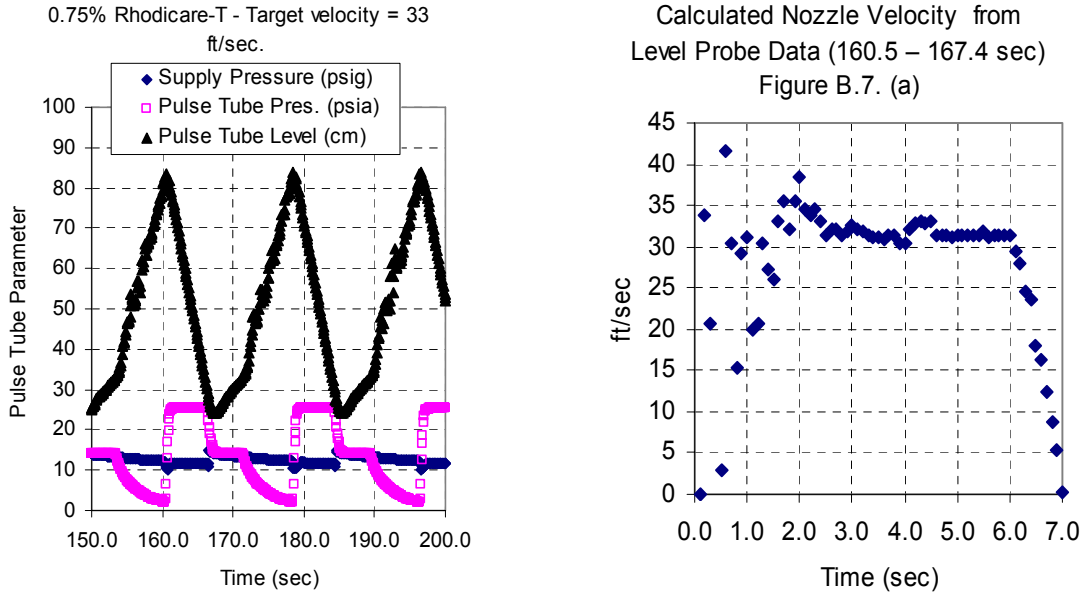

(a) (b)

Figure B.7. (a) Pulse Tube Level and Pressure Profiles for a Run with Rhodicare. PJM test 7/24/2003–8, with 0.75% Rhodicare, stroke = 23.8 in. (60.4 cm), target velocity = 33 ft/sec; (b) calculated NV as a function of time during a typical pulse as indicated by changes in level probe reading; level probe data (160.5–167.4 sec).

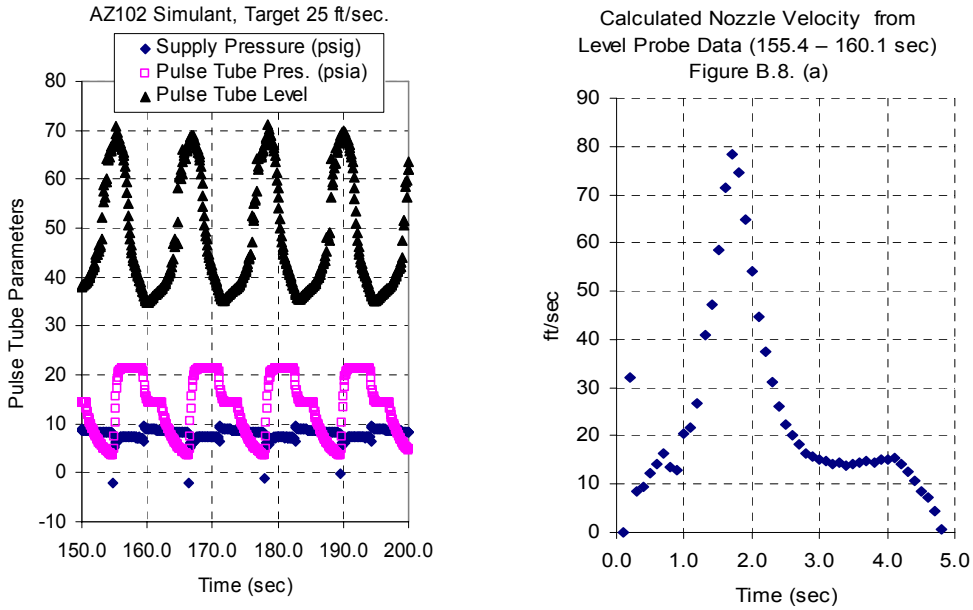

(a) (b)

Figure B.8. (a) Pulse Tube Level and Pressure Profiles for a Run with AZ-102. PJM test 7/31/2003–5, testing at stroke = 13.9 in. (35 cm), target velocity = 25 ft/sec;
(b) calculated NV as a function of time during a typical pulse as indicated by changes in level probe reading; level probe data (155.4–160.1 sec).

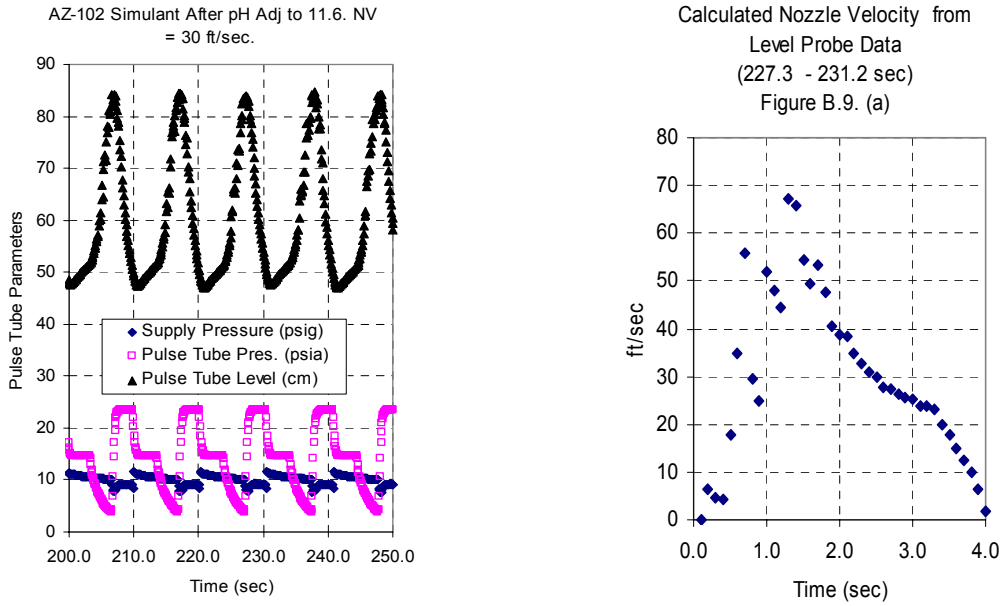

(a) (b)

Figure B.9. (a) Pulse Tube Level and Pressure Profiles for AZ-102 Run After pH Adjusted to 11.6. PJM test 030803R1, testing at stroke = 13.9 in. (35 cm), target velocity = 30 ft/sec;
(b) calculated NV as a function of time during a typical pulse as indicated by changes in level probe reading; level probe data (227.3–231.2 sec).

B.3 APEL 4PJM Scaling Experiments

B.3.1 Description

The APEL 4PJM test stand is a linearly scaled version of the 4PJM test setup in the 336 test facility. The scaling factor is 4.53. It consists of four PJMs constructed of a 5-inch (5.29-inch ID) schedule 10 stainless steel pipe tapered to a custom-built nozzle of 0.88 inch ID. The length of the cylindrical section of the PJMs is 48 inches. The height was intentionally set longer than the PJMs in the 336 test facility to enable testing at higher H/D_T ratios than were possible at the larger scale. The PJMs are situated around the center of the tank in a square along a pitch diameter of 21.24 inches. The height of the nozzles from the tank floor is 2.1 inches. Figure B.10 shows an example of a single pulse cycle.

Unlike conventional PJMs, whose operation is regulated by jet pump pairs driven by compressed air, the APEL 4PJM test system used a series of solenoid valves and a combination of an air compressor and vacuum pump to simulate the drive and suction phases of PJM operation. These operations were controlled through a control logic program using DASYLab data acquisition and control software (DACS), which turns the appropriate solenoid valves on and off at specified time intervals. The duration of each phase, the applied pressure, and vacuum are all variables that can be varied independently to simulate the operation of the actual PJMs.

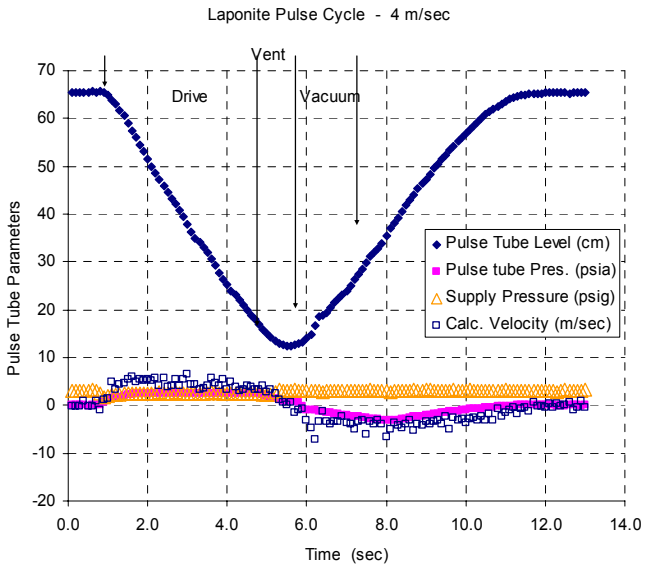

Figure B.10. Example Laponite Pulse Cycle at Target NV of 4 m/s. Each curve represents the average of three or more cycles.

B.3.2 Instrumentation and Calibration

Each PJM was outfitted with a Drexelbrook liquid-level capacitance sensor/transmitter and an Endress+Hauser ceramic pressure transducer, which enabled continuous measurement of the slurry level and pressure inside the PJM during operation. Additional sensors included in the test system are Type K thermocouples that measure the temperature of the tank contents and ambient temperature.

The pressure transducer (Cerabar T PMC 131 from Endress+Hauser) shown in Figure B.11 has a capacitive ceramic sensor for absolute and gauge pressure. It is designed to measure absolute pressure for gases, vapors, and liquids. It is extremely stable and resistant to overload. The pressure to be measured causes a small deflection of the ceramic diaphragm of the sensor; a change in capacitance proportional to the pressure is measured by electrodes on the ceramic sensor. This pressure transducer can measure a maximum of 40 bars. The output signal is 4-20 mA.

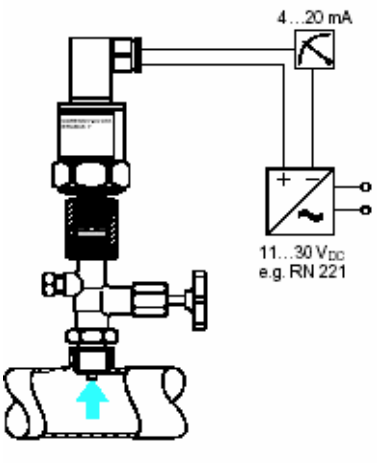

Figure B.11. Pressure Transducer Configuration

B.3.3 Correlation of PJM Nozzle Velocities as Indicated by Tank Level Rise, Drive Time, and Capacitance Level Probe Data

The most important independent variable in the PJM experimental testing program is the drive velocity at each pulse tube nozzle. Drive velocity was estimated using Drexelbrook liquid level probes to measure the liquid level in each pulse tube as a function of time. The liquid levels and pulse tube geometry are used to determine the simulant velocity exiting each nozzle as a function of time. The level probes use radiofrequency (RF) signals and the fluid dielectric properties to change the measured capacitance. The liquid level probes were performance checked to ensure accurate results. The performance check procedure involves changing the liquid level in the tank over the range of measurements and checking the probe response. These are static measurements; the liquid level is held constant at each level during the performance check.

APEL 4PJM mixing experiments have been conducted with several simulants, listed in Table B.3, that include Laponite and clay (kaolin-bentonite). Drive velocities during these tests varied from roughly 4 m/s to as high as 18 m/s,. Using these measurements and the test stand geometry, the drive velocity

Table B.3. PJM Test Stands and Range of Test Conditions

	APEL 4 PJM	336 4 PJM
Laponite	Shear strength to 100 Pa. Drive velocities from 4 to 18 m/s	Shear strength to 140 Pa. Drive velocities from 6 to 11.5 m/s
Clay	≥30 Pa shear stress	≥30 Pa shear stress
Test stand purpose	PJM mixing and gas retention and release scale-up data	PJM mixing and gas retention and release scale-up data

functions were determined independently from the Drexelbrook liquid level probes in the pulse tubes. External liquid level measurements were obtained by several methods: 1) videotape of the liquid level and a tape measure and 2) ultrasonic liquid level probes. The suitability of the level probes was assessed by comparing the drive function derived from the PJM liquid level probes to the drive function obtained from the external liquid level measurements. The shape of the curve, the peak velocity, and the velocity averages were compared. Based on the results, the following calculations were performed:

- For conditions in which the level probes provided acceptable results, the average drive velocities were calculated and reported.
- The average drive delta P (pressure) was calculated from the pressure time data and reported.
- Based on a suitable mathematical model, the velocity averages were calculated and reported.

In Figure B.12, average discharge velocities of the fluid (from tank level data) in the PJM orifice are plotted for eight runs as functions of the drive time. Four runs were completed with a Laponite slurry and four with kaolin-bentonite slurry at target velocities of 4, 8, 12, and 16 m/s.

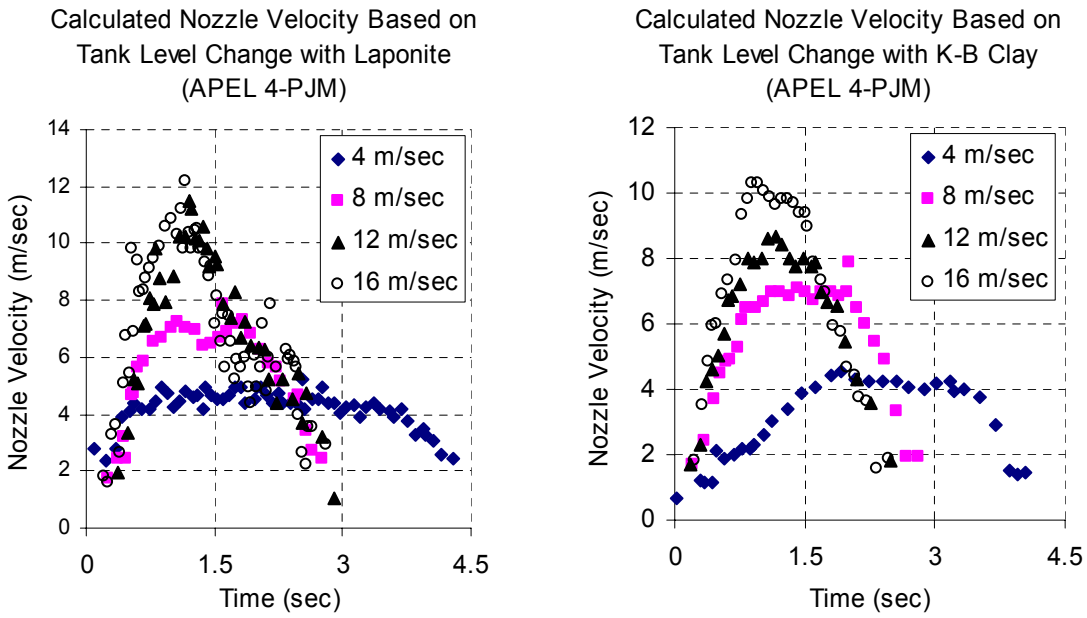

Figure B.12. Discharge Velocities from Tank Level Data as Functions of Drive Time These data were derived from videotapes made of the tank level moving against a stationary scale appropriately placed in the field of view.

The data shown in Figure B.12 were produced from a videotape frame-by-frame determination of the liquid surface level in the tank as it moves up and down against a fixed scale also in each frame. These velocity profiles compare favorably with those computed from the Drexelbrook capacitance probes.

For the tank level-Drexelbrook liquid level sensor cross-check, the 4PJM was operated in a standard mode (i.e., DASYLab was programmed to produce a continuous sequence of identical pulses). Cross-checks were made for two simulants (Laponite and kaolin-bentonite) at four target nozzle velocities (4, 8, 12, and 16 m/s). For these tests the static level was about 80 cm, the drive length was 53.9 cm, and the total cycle time was 13.3 seconds. Table B.4 summarizes the parameter settings for each run condition.

Table B.4. Operating Conditions for 4PJM Target Nozzle Velocity

Material/Target Nozzle Velocity (m/s)		Drive Phase (s)	Vent Phase (s)	Vacuum Phase (s)	Supply Pressure (psig)
Laponite	4	4.0	1.0	2.0	3.1
Laponite	8	2.0	1.0	2.1	7.8
Laponite	12	1.3	1.5	2.4	15.8
Laponite	16	1.0	1.5	2.6	23.3
Kaolin-Bentonite	4	4.0	1.0	2.4	3.4
Kaolin-Bentonite	8	2.0	1.0	2.4	8.6
Kaolin-Bentonite	12	1.3	1.5	2.4	17.5
Kaolin-Bentonite	16	1.0	1.5	2.5	24.5

A test run was initiated by setting the parameters in the DASYLab program, renaming the data acquisition files, manually resetting the supply pressure, powering up the solenoid controlled valves, and turning on the DASYLab auto pulse routine. If it was clear that a stable pulse cycle was not going to be established in the first few cycles, the auto pulse routine was turned off and adjustments made to the operating parameters (typically raising or lowering the vent or vacuum phase duration). If the stroke length (the distance between the highest and lowest simulant levels in the pulse tube as indicated by the Drexelbrook liquid level sensor) was more than a few centimeters off the target of ~ 54 cm, the supply pressure was adjusted up or down as appropriate.

Once a stable pulse cycle was established, it was allowed to run at least 5 to 10 minutes before an observer with a video camera and time indicator began to record the tank level as a function of time with a millimeter tape scale included in the picture. At the same time, the DasyLab data acquisition function was turned on to record level sensor data, pulse tube pressure, supply pressure, simulant temperature, ambient temperature, and a calculated nozzle velocity ten times per second. After the observer had recorded about 10 acceptable tank level cycles, data acquisition was turned off and the test concluded at that target velocity.

Figure B.13a, b, c provides additional examples of the pulse cycles generated during these tests. Each plot consists of data averaged from three consecutive cycles and the individual level sensors. The data are plotted in units of 0.1 second. The drive, vent, and vacuum stages that shape the pulse are indicated between the vertical arrows. For the 4-m/s target nozzle velocity, the pulse cycle discharge phase coincides with the drive stage of the cycle, and a nozzle velocity of about 4 m/s is achieved. On the other hand, for a target nozzle velocity of 16 m/s, the pulse cycle discharge phase is made up of both the drive and vent stages. This almost doubles the actual pulse tube discharge time and thus reduces the actual nozzle discharge velocity correspondingly because the discharge volume does not change. Instead of a 1-sec pulse at 16 m/s, a 2.5-sec variable speed pulse peaking at about 12 m/s is generated. However, this kind of pulse tube cycle meets the purpose of the sensor, tank level comparison, very well.

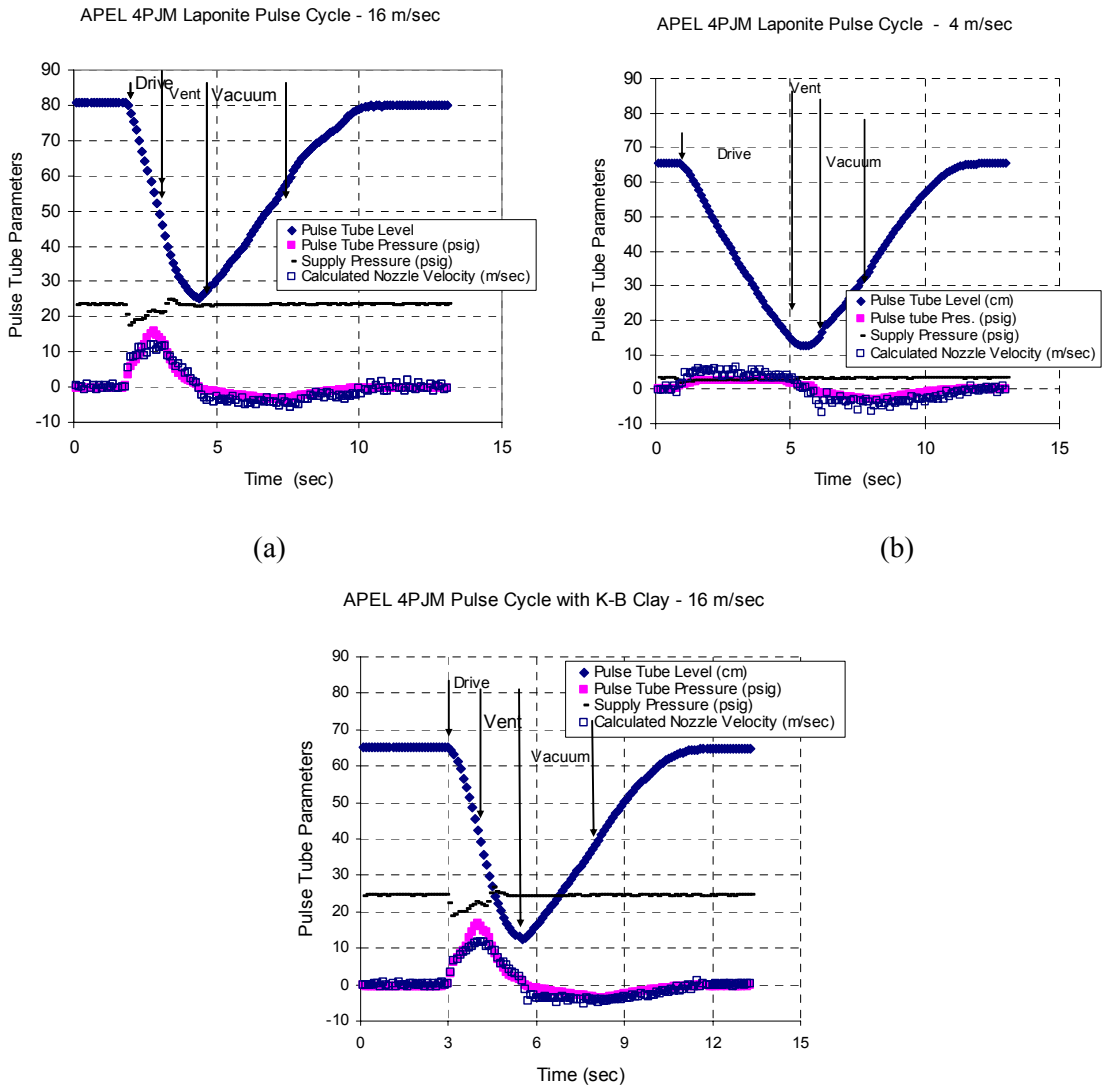

Figure B.13. (a) Example Laponite Pulse Cycle at Target NV of 16 m/s.
(b) Example Kaolin-Bentonite Pulse Cycle at Target NV of 4 m/s.
(c) Example Kaolin-Bentonite Pulse Cycle at Target NV of 16 m/s.

B.3.4 Cavern Tests with Laponite

For this study, a cavern was defined as a mixing volume generated within a non-Newtonian fluid by the jet of fluid being ejected from the pulse tube. The shear strength of the fluid limited the size of the cavern to a volume in which the kinetic energy imparted to the fluid by the jet overcame the shear strength of the fluid, so the greater the shear strength the smaller the cavern. Table B.5 summarizes all of the cavern development tests using Laponite.

Table B.5. Cavern Development Results Using Laponite as the Waste Simulant[(a)]

Reference Number	Date	Run No.	Drive		Nozzle Velocity (ft/sec)	Average Cavern Height (in.)		Tank Fill Height
			ΔH(in.)	Δt(s)		Maximum at Wall	Maximum	
M-1	8/29/2003	1	23.9	7.3	9.8	10.5	14.8	29.9
M-2	8/29/2003	2	23.8	4.8	14.3	11.9	15.6	29.8
	8/29/2003	3	23.9	3.6	20	30.3	31.9	29.8
M-3	9/3/2003	1	23.9	6	12	nm(a)	18.3	29.3
M-4	9/3/2003	2	23.9	5.1	14	8.2	18.5	29.3
	9/3/2003	3	23.9	4.8	15	Run abandoned		29.3
	9/3/2003	4	23.9	3	24	nm	nm	29.3
M-5	9/5/2003	1	23.9	5.1	14	nm	17.6	29.7
	9/5/2003	2	23.9	4	18	Run abandoned		29.7
	9/5/2003	3	23.9	3.3	22	Run terminated - breakthrough		29.7
M-6	9/8/2003	1	23.9	4.5	16	8.5	16.2	29.4
M-7	9/10/2003	1	23.9	4	18	Run terminated - breakthrough		29.8
	9/11/2003	1	21.2	4.6	14	Run terminated - DAC failure		29.5
M-8	9/13/2003	1	21.2	4.6	14	15.2	16.1	29.7
	9/13/2003	2	21.2	3.5	18	Run terminated - no cavern change		29.6
M-9	9/15/2003	1	21.2	4.3	15	nm	10.9	29.6
M-10	9/15/2003	2	21.2	3.2	20	nm	15.8	29.6
M-11	9/16/2003	1	21.2	3.7	17	nm	17.7	29.5
M-12	9/18/2003	1	21.2	4.3	15	nm	15.8	29.7
	9/18/2003	2	21.2	3.2	20	nm	nm	29.7
12 Station Measurements								
	9/19/2003	1	21.2	3.2	20	Cavern fissured and test discontinued		29.7
M-13	9/21/2003	1	21.2	3.2	20	nm	19.4	29.7
M-14	9/22/2003	1	21.2	2.9	22	Breakthrough observed		29.7
	9/26/2003	1	21.2	2.4	26	Timed to breakthrough		30
M-15	9/30/2003	1	21.2	4.3	15	nm	17.8	51.8
M-16	9/30/2003	2	21.2	2.6	25	29.5	30.1	51.4
M-17	9/30/2003	3	21.2	1.8	35	Breakthrough observed		51.7
	10/2/2003	1	21.2	6.4	10	Run terminated - cavern too small		51.3
	10/2/2003	2	Nm	nm	nm	Run terminated - cavern too small		51.3
M-18	10/3/2003	1	21.2	3.2	20	nm	nm	51.4
M-19	10/3/2003	2	21.2	2.1	30	31.9	36.1	51.4
	10/3/2003	2	21.2	2.1	30	Shear plane formed at top of cavern		51.4

(a) nm – not measured

The cavern development tests were carried out by allowing the Laponite to set up and then running the 4PJM setup at a predetermined condition. While the PJMs were operating, the dimensions of the mixing cavern were carefully measured by observers every 5 to 10 minutes using preset measuring tapes affixed to the surface of the 4PJM tank at azimuthally prescribed positions around the circumference of the tank. When the cavern height measured at the wall of the mixing vessel ceased to significantly increase over a 20-minute period, it was concluded that the cavern had reached it maximum dimensions. The dimensions recorded are given in Table B.5.

The values in Table B.5 represent the average of several readings taken by more than one observer over several pulse tube cycles. Each observer made visual measurements until satisfied that the value observed was reproducible. Because Laponite solutions are transparent, the observer was able to see the top of the mixing cavern both at the wall of the PJM vessel and at its maximum height toward the center of the vessel. It was noted that this high point was not necessarily at the geometric center of the vessel.

Brilliant Blue dye was added to the mixing cavern of some of the Laponite tests to delineate the cavern more clearly. This was done by adding a concentrated dye solution though the top of one of the pulse tubes, improving the contrast between the mixing and non-mixing portions of the tank fill. After each individual test, the tank contents were homogenized by vigorously pulsing the jets. Additional dye or different colors could be used to again produce good contrast between mixing and non-mixing regions.

Occasionally, when generating a mixing cavern using a higher pulse tube nozzle velocity, a larger cavern formed, but the weak Laponite gel would fracture rather than just erode away. When the fracture developed, the mixed simulant was injected along the plane of the fracture, causing it to spread apart and drastically change the geometry of the cavern. When this occurred, the test was terminated.

B.3.5 Time-to-Mix Tests

The objective of these tests was to determine the time it took for dye injected into the clay simulant to become completely dispersed throughout the simulant. Run parameters are given in Table B.6.

Table B.6. Time-to-Mix Tests in the APEL 4PJM

Simulant	Date	Run No.	Test Description	Tank Fill Height
Laponite	9/26/2003	1	Time to mix studies; mixing followed by observing disappearance of undyed material; PJM vessel nozzle velocity ~26 ft/sec, ΔH = 21.3 in.	29.7 in.
Kaolin-Bentonite	11/15/2004 11/17/2006	1	Time to mix studies; samples removed via six sampling ports; PJM vessel nozzle velocity ~26 ft/sec, ΔH = 21.3 in.	29.7 in.

B.3.5.1 Approach Time to Mix Tests and Results

For the Laponite test, the simulant tank was filled with Laponite and allowed to gel for 18 hours. A known quantity of Brilliant Blue dye was placed in the pulse tubes. Pulsing began at a known break-through nozzle velocity. With breakthrough, mixed Laponite (containing the dye) was pumped onto the surface of the gelled undyed Laponite, causing the undyed material to sink with each pulse. Gelled Laponite was progressively mobilized from the bottom of the sinking gelled mass and incorporated into the mixing portion.

For the kaolin-bentonite simulant, a known quantity of Brilliant Blue dye was placed in the mixer tank. Samples (20 mL vials) of the clay simulant were collected continuously from six locations in the tank while the PJMs were operating. The samples were pumped out of the tank using peristaltic pumps operating at a few milliliters per minute. Each vial had a unique identification number. The time of filling was recorded. Knowing the effective volume of the sampling line and the pumping rate, the actual time interval represented by each sample could be calculated. The time it took for all six samples to come to the same concentration was a measure of the mixing time.

B.3.5.2 Laponite Time to Mix Test and Results

For Laponite tests, the simulant tank was filled with Laponite and allowed to gel for 18 hours. A known quantity of Brilliant Blue dye was placed in the pulse tubes. Pulsing began and time was measured from the beginning of the first pulse. Observers with synchronized stop watches were in position east, north, west, and south of the tank to time the breakthrough event and the progressive disappearance of unmixed Laponite. Figure B.14 gives a summary of the observed results. The breakthrough occurred about 1 minute after the test started. The first pulse caused Laponite to bulge at the center, the second pulse caused the injection of dyed Laponite three-fourths of the way to the top of the Laponite, the third pulse caused an approximately 9-inch crack to form in the center of the Laponite at the point where maximum bulging occurred, and the fourth pulse caused dyed liquified Laponite to erupt though the crack produced on the previous pulse. Each succeeding pulse caused more mobilized Laponite to pour onto the surface, and the original gelled surface sank with each succeeding pulse. Table B.7 summarizes other key measurements made during the test.

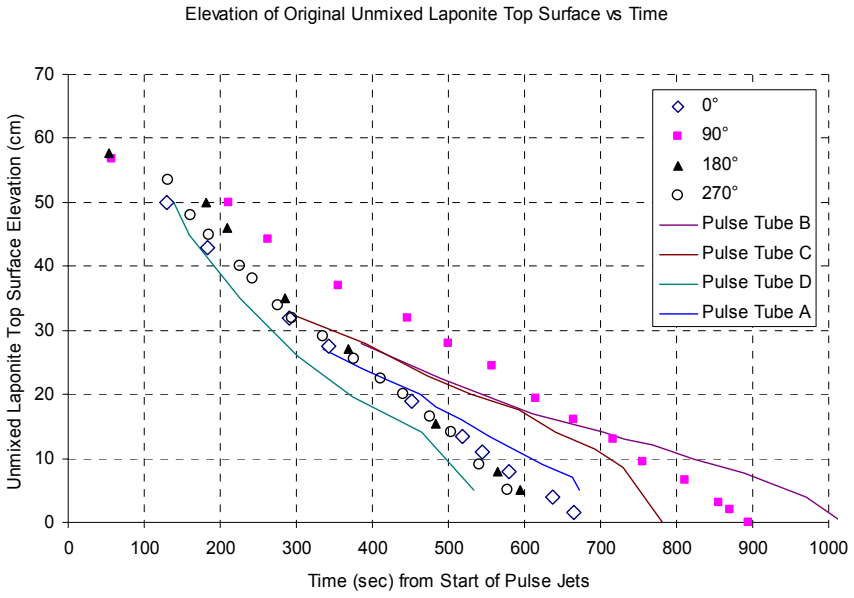

Figure B.14. Incorporation of Unmixed into Mixed Laponite Measured as a Function of Time by Plotting Elevation of Top of Original Unmixed Laponite as it Sank Beneath the Surface. Connected data points are from the azimuthal positions between the pulse tubes; unconnected data points taken behind pulse tube between it and vessel wall.

Table B.7. Assessment of Time-to-Mix Criteria for APEL 4PJM Test 030926R1

Criteria for Time to Mix	Observation during Test Run 030926R1
Time to breakthrough	~1 min
Time flow observed in annular area	~17 min or less
Time of turbulent flow observed in annular area	Not attained
Time of full mobilization	~17 min

B.3.5.3 Kaolin-Bentonite Time-to-Mix Tests and Results

The two dye tests listed in Table B.6 were performed on November 15 and 17, 2003. In the November 15 test, Brilliant Blue dye was added to the top of the tank before agitation began. Within a few pulses the dye had moved from the center of the tank to the walls. As the dye was incorporated into the mixing cavern, it coated the wall and slowly moved down the wall into the boundary layer (Figure B.15 a, b). Due to the heterogeneous appearance of this test, on November 17 dye was added slowly to the bottom of the tank to encourage adequate mixing before a large amount of dye reached the top of the tank. This technique reduced the heterogeneous appearance at the tank wall and appeared to be a superior method of dye addition (Figure B.16). Table B.8 gives some key observations about these kaolin-bentonite tests.

Table B.8. Assessment of Time to Mix Criteria for APEL 4-PJM Tests 031115R1 and 031117R1

Criteria for Time to Mix	Observation During Tests 031115R1 and 031117R1
Time to breakthrough	With first pulse
Time flow observed in annular area	Believed to have been initiated with breakthrough
Time of turbulent flow observed in annular area	Not attained
Time of full mobilization	Believed to have been initiated with breakthrough

Figure B.15. (a) Dye Ring from Top Addition of Dye on11/15/03; (b) Dye Ring from Top Addition of Dye on 11/15/03 after Several Hours of Mixing

Figure B.16. Dye Pattern after Injection on November 17, 2003

Preliminary results from the November 17, 2003 test, shown in Figure B.17, depict a transient response that reaches a steady-state condition in approximately 35 minutes. The lag time from the tank to the sample container must be subtracted from these data before the transient nature of the tank can be estimated. Lag time is the amount of time it takes a quantity of simulant to travel the length of the sampling line. An approximation made at the time of the test suggested that lag time was on the order of five minutes.

Figure B.18 shows the steady-state behavior of samples taken from six sampling stations corresponding to six different locations from the mixing vessel. These data indicate that the material was homogeneous in the six areas where the samples were drawn. Using mass balance calculations, the data also indicate that the tank is approximately 93.9 ≤3.3% mixed. Both of these tests produced results that are for information only and are presented here to illustrate the tracer approach for characterizing the extent of mixing.

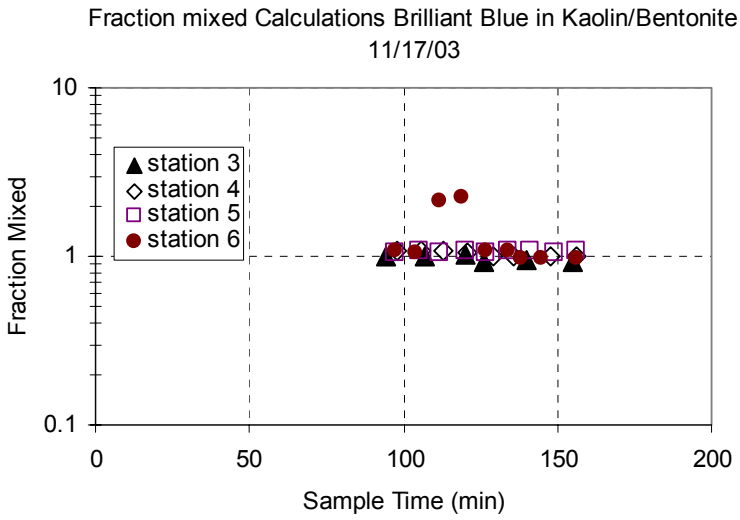

Figure B.17. Transient Response of November 17, 2003 Dye Test

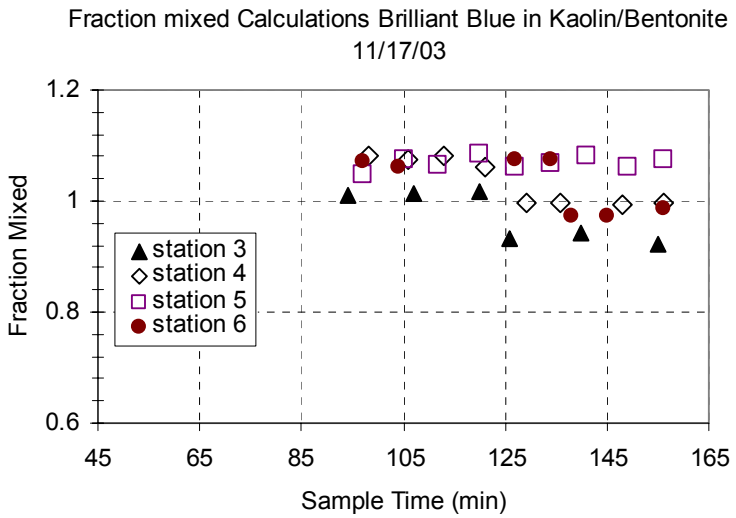

Figure B.18. Response of November 17, 2003 Dye Test from Four Locations; 101.2 ± 5.5% Mixed

B.3.6 Measured Upwell Velocities in the APEL 4PJM

The data obtained from the APEL 4PJM have a well-defined scaling relationship to the 336 4PJM, which is 4.53 times larger. One can compare the upwell velocities measured for the two systems on a nondimensional basis. These nondimensional numbers should be nearly the same for both systems for a good scaling relationship to exist. (Upwelling in these mixing tanks is the result of the working fluid being jetted into the tank from the pulse jets. This upwelling causes the mixing caverns to develop.)

B.3.6.1 Approach

The APEL 4PJM was operated to produce target nozzle velocities of 8 and 12 m/s during a cycle period of 13.3 seconds, while the 336 4PJM has a 60-second cycle period. In the mode operated, the velocity profiles for each pulse were triangular spikes peaking at around the target value. For tests at APEL, peak values were 11 to 12 m/s for the 12 m/s target, depending on how they were calculated; the pressure pulse indicated a maximum velocity of about 11.3 m/s, while level probe data gave about 12.3 m/s. Actual peak nozzle velocities for the 8 m/s target velocity were about 9.8 m/s, again based on the pressure pulse profile, while level probe data indicated a peak velocity of about 9.4 m/s. For tests at 336, peak velocity values were 5.5 m/s and from 8.2 to 8.7 m/s if calculated from level probe data. Actual average velocity data calculated from level probe data were 4.9 m/s and 6.8 to 7.0 m/s.

The waste simulant was a kaolin-bentonite mixture with a yield stress of 34.3 Pa and a consistency of 0.0223 Pa-s measured at the beginning of the upwelling tests. The values measured for the kaolin-bentonite mixture used for the 336 tests were a yield stress of 29.3 Pa and consistency of 0.0204 Pa-s before the start of the tests and a yield stress of 28.4 Pa and a consistency of 0.0202 Pa-s afterward.

The ultrasonic velocity probe system used to measure the upwelling velocities was a UVP Monitor Model UVP-DUO with Software Version 3, which is described in Section 4 of the main report. For the upwell velocities measured at APEL and 336, all channels between 25 and 40 mm were averaged to give a velocity number. These sets of data were produced every 0.2 second for 5-minute runs resulting in 1500

data sets for each test condition. For the APEL 4PJM this would include about 23 pulse jet cycles (at 13.3 sec/cycle) for each test condition.

B.3.6.2 Kaolin-Bentonite Upwell Velocity Tests

Table B.9 lists the APEL 4PJM tests that were successful. The original plan called for measurements to be made for target nozzle velocities of 4, 8, and 12 m/s; for $H_{VP}D_T$ levels of 0.4, 0.63, and 0.8; and for four quadrants centered at 0°, 90°, 180°, and 270° where H_{VP} is the elevation of the velocity probe. In the APEL 4PJM, the UVP was supported on a pole that was coaxial with the vertical center line of the tank. The probe holder that was attached to the pole held the probe straight down and about 2.5 inches away from the pole in the horizontal direction, so the horizontal linear distance between the 0° to 180° or the 90° to 270° positions was about 5 inches. A typical measurement sequence for a given PJM target nozzle velocity was to start at either the highest or lowest H_{VP}/D_T, take velocity data in each quadrant for 5 minutes, then move to the next H_{VP}/D_T. After all the data were collected for one PJM nozzle velocity, the PJM was set for another nozzle velocity, and the measurement sequence was repeated, starting at the last H_{VP}/D_T measurement level for the previous PJM target velocity. As is clear from Table B.9, data were gathered at only two nozzle velocities (8 and 12 m/s) and at all three H_{VP}/D_T levels at only 12 m/s.

Table B.9. APEL 4PJM Upwell Velocity Test Conditions

Test	Nozzle Velocity	H_{VP}/D_T	Azimuth
7-13-CLY Run 009	12 m/s	0.63	0°
7-13-CLY Run 010	12 m/s	0.63	90°
7-13-CLY Run 011	12 m/s	0.63	180°
7-13-CLY Run 012	12 m/s	0.63	270°
7-13-CLY Run 013	12 m/s	0.4	0°
7-13-CLY Run 014	12 m/s	0.4	90°
7-13-CLY Run 015	12 m/s	0.4	180°
7-13-CLY Run 016	12 m/s	0.4	270°
7-13-CLY Run 019	12 m/s	0.4	270°
7-13-CLY Run 020	12 m/s	0.4	0°
7-13-2004-4PJM Vel 0000	12 m/s	0.4	180°
7-13-2004-4PJM Vel 0001	12 m/s	0.63	0°
7-13-2004-4PJM Vel 0002	12 m/s	0.63	90°
7-13-2004-4PJM Vel 0003	12 m/s	0.63	180°
7-13-2004-4PJM Vel 0004	12 m/s	0.63	270°
7-13-2004-4PJM Vel 0005	8 m/s	0.63	270°
7-13-2004-4PJM Vel 0006	8 m/s	0.63	180°
7-13-2004-4PJM Vel 0007	8 m/s	0.63	90°
7-13-2004-4PJM Vel 0008	8 m/s	0.63	0°
7-13-2004-4PJM Vel 0009	8 m/s	0.8	0°
7-13-2004-4PJM Vel 0010	8 m/s	0.8	90°
7-13-2004-4PJM Vel 0011	8 m/s	0.8	180°
7-13-2004-4PJM Vel 0012	8 m/s	0.8	270°
7-13-2004-4PJM Vel 0013	12 m/s	0.8	270°
7-13-2004-4PJM Vel 0014	12 m/s	0.8	180°
7-13-2004-4PJM Vel 0015	12 m/s	0.8	90°
7-13-2004-4PJM Vel 0016	12 m/s	0.8	0°

The velocity probe data were collected by the UVP-DUO software during the test. The velocity data file was then exported into a text file, which was opened in Excel® and resaved as an Excel file. This file contains the operating parameters of the UVP system and the velocity data for channels 0 through 99. For the APEL 4PJM measurement setup, only channels corresponding to >25 and <40 mm (channels 44 through 76) from the probe face were kept for evaluation. As stated previously, measurements were made every 0.2 seconds, or 1500 in five minutes. Each time channels 44 through 76 were averaged, and the standard deviation for the channels was also computed in Excel. In the final step, if the average standard deviation of channel velocity values was greater than 0.5, the value was rejected as a valid velocity measurement. Also, average values greater than 75% of the velocity range were rejected. This last requirement was found to truncate velocity data that otherwise appeared to be valid, and it was decided to keep these averages as part of the valid data set because they displayed low standard deviations and occurred in the middle of upwelling peaks where high values would be expected. Once the basic velocity data were generated, they were corrected by the system calibration factor generated by NorthWest Research Associates of Bellevue, Washington. Based on their evaluation of the system, each velocity value needed to be multiplied by 1.0737 and have 5.8 mm/s added. All data reported in Table B.9 have been so corrected. The upwell velocity results are presented in Section 4 of the main report.

B.4 References

Bontha JR, JM Bates, CW Enderlin, and MG Dodson. 2003. *Large Tank Experimental Data for Validation of the FLUENT CFD Model of Pulsed Jet Mixers.* PNWD-3303, Battelle – Pacific Northwest Division, Richland, Washington.

Poloski AP, PA Meyer, LK Jagoda, and PR Hrma. 2004. *Non-Newtonian Slurry Simulant Development and Selection for Pulse Jet Mixer Testing*. PNWD-3495, Battelle – Pacific Northwest Division, Richland, Washington.

Appendix C

Small-Tank Scaling Experiments Conducted at SRNL at 1/9 Scale with One and Four PJMs

Appendix C Contents

Figures

Tables

Appendix C

Small-Tank Scaling Experiments at SRNL

The Pulse Jet Mixer (PJM) Task Team developed an integrated approach for scaled testing to validate PJM mixing in Waste Treatment Plant (WTP) vessels containing non-Newtonian fluids. As part of this effort, Savannah River National Laboratory (SRNL) was directed to conduct a series of experiments using a scaled test apparatus located at the SRNL Building 786-A. It was an approximately 1/9-scale model of the 336 test facility at Battelle – Pacific Northwest Division (PNWD).

Scaled PJM mixing tests of a single PJM and a 4PJM array were initiated to provide design information on the operating parameters critical for the uniform movement (total mobilization) of the tank contents. The SRNL PJM program used a transparent and an opaque simulant. The transparent simulant was Laponite RD® (Southwestern Clay Products), a thixotropic colloidal synthetic clay that forms stable gel networks when unsheared. The simulant was a mixture of Laponite RD powder (approximately 2 wt%) and water. Due to the thixotropic nature of Laponite, its flow behavior is dynamic, and it was allowed to gel until reaching a target shear strength. After the gelling period, the PJM system was started and a mixing cavern was formed. At this point the system was operated to provide constant shearing in the mixing cavern until steady-state flow behavior was approached. The opaque simulant was provided by PNWD and was a composite of 80% kaolin and 20% bentonite mixed with water up to a loading of approximately 27 wt%. Water was then added to the simulant as required by the test program to adjust the rheological characteristics to other target values.

C.1 SRNL Single PJM Test Stand

This section describes the SRNL single PJM test stand, experimental approach, and instrument calibrations. The SRNL single-PJM test stand was used to demonstrate the scaling laws for mixing.

C.1.1 Description

The SRNL single-PJM test stand is a linearly scaled version of the single-PJM test setup in the PNWD Applied Process Engineering Laboratory (APEL) test facility. The SRNL single-PJM test stand, which is shown in Figure C.1, consisted of a clear cylindrical shell with a stainless steel 2:1 elliptical head. The photograph shows the test stand filled with Laponite simulant with an intermediate-height cavern developed during system shakedown runs. The clear acrylic test tank internal diameter was 17.25 inches and the internal height 43 inches. One PJM fabricated from 5-inch NPS, schedule 40S stainless-steel pipe was located along the tank centerline. Average internal diameter of the pulse tube was 5.241 inches. The 60-degree nose cone on the outlet of the PJM had a nozzle diameter of 0.514 inches, and the nozzle centerline elevation was 4.5 inches above the tank head. A drain/sample valve was at the center of the tank head, providing a flush interior profile. Plan and elevation views of the test stand configuration are shown in Figure C.2. A process and instrumentation diagram of the test stand configuration is shown in Figure C.3.

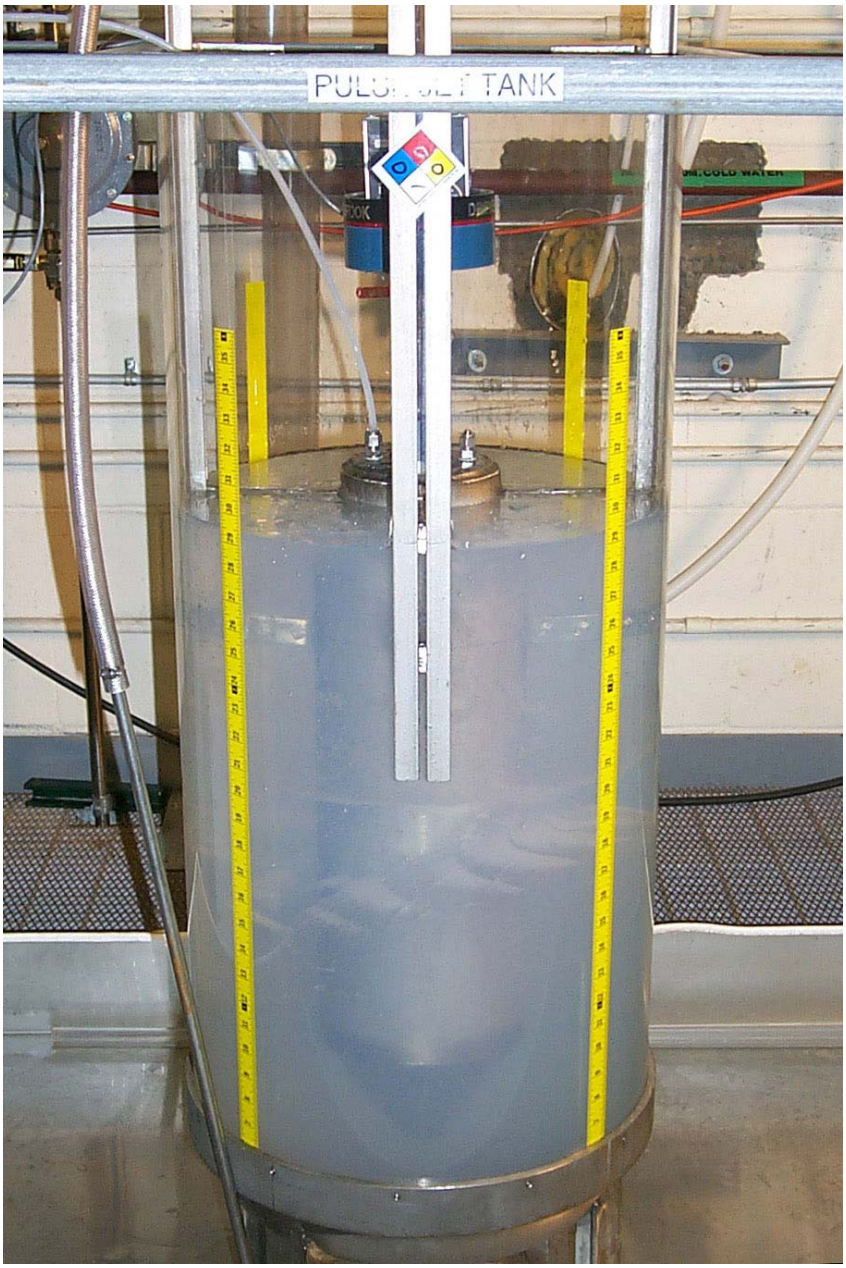

Figure C.1. Photograph of the SRNL Single PJM Test Stand

The APEL test facility tank internal diameter is 33.8 inches; thus, for the SRNL testing the geometric scale factor is 33.8/17.25 = 1.96. The time scale factor is the inverse of the geometric scale factor, so for SRNL testing, temporal events must occur in 1/1.96, the duration of the APEL test.

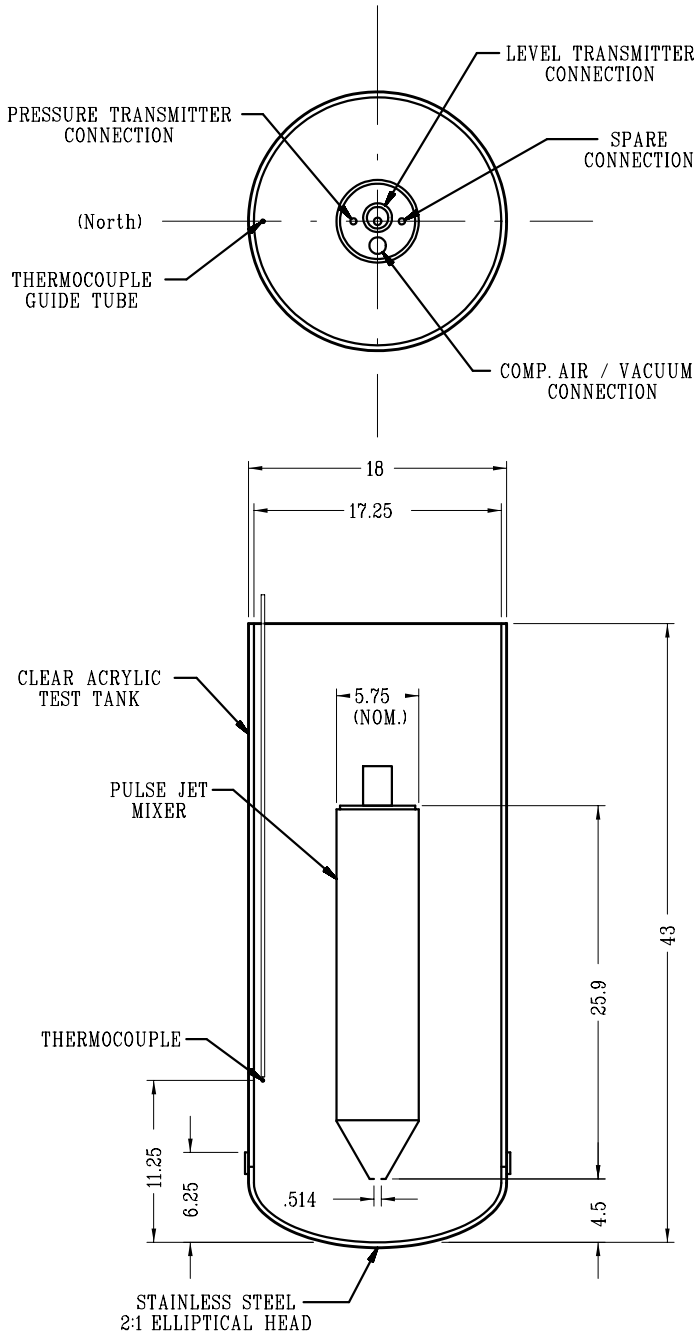

Figure C.2. SRNL Single-PJM Test Stand Plan and Elevation View

C.1.2 Experimental Approach

The test matrix performed was representative of testing conducted at the APEL test facility (half-scale test stand). This design parameter scale-law testing was directed specifically at: 1) obtaining cavern heights at periodic conditions as a function of the discharge velocity and discharge time and 2) observing and evaluating cavern formation and time transients for cavern formation.

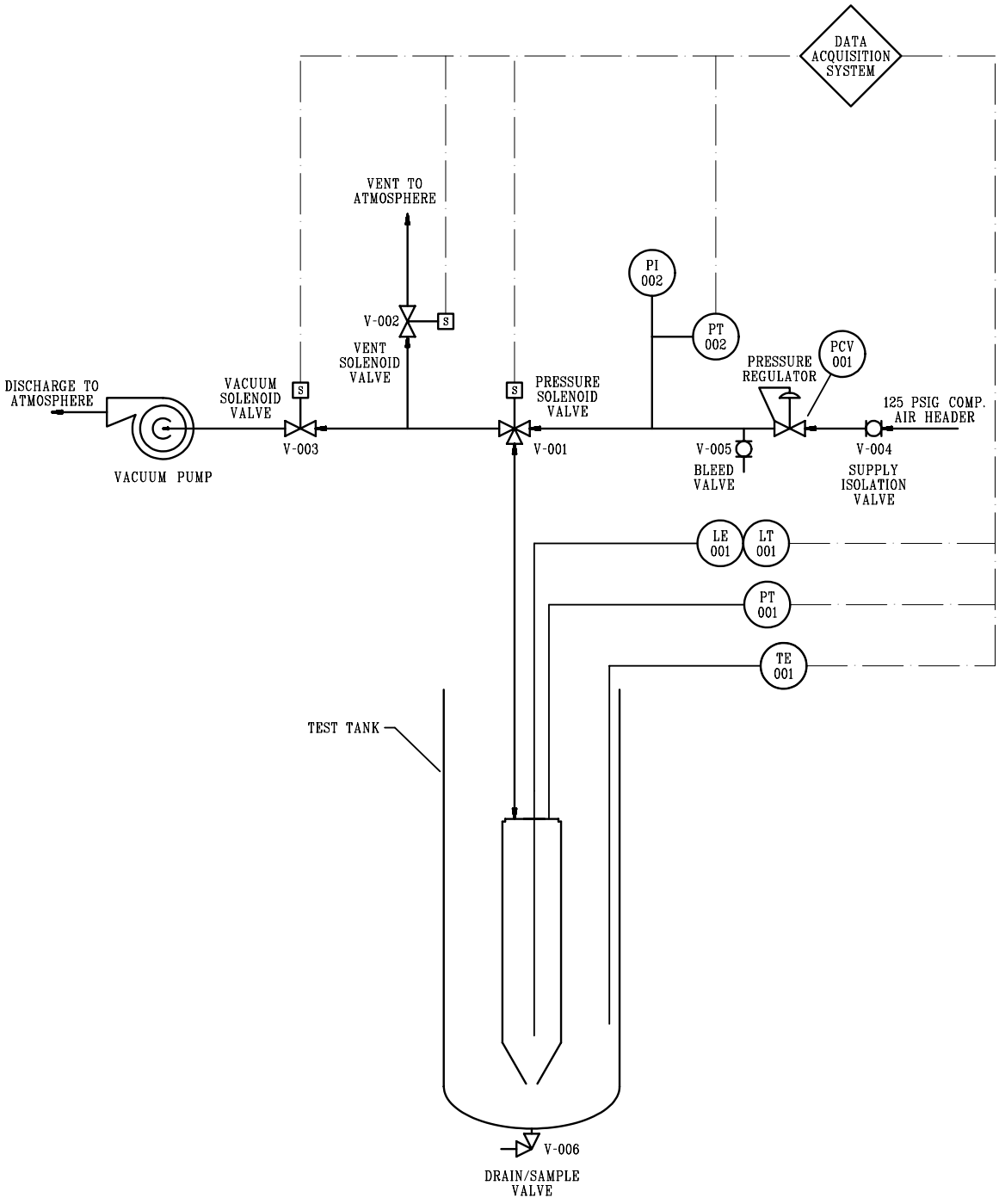

Figure C.3. SRNL Single-PJM Test Stand Process and Instrumentation Diagram

This section contains the experimental approaches used to measure the PJM internal level and pressure, the bulk simulant temperature, compressed air supply header pressure, and the developed cavern height during operation. In addition, the rheology of the non-Newtonian simulants was analyzed to characterize the shear strength of the undisturbed material and provide a rheogram of the yielded material.

The pulse tube and the compressed air supply pressure were measured using Rosemount pressure transmitters connected to their respective pressure sources using 1/4-inch OD poly tubing. The 4-20 mA transmitter output signal was input to the data acquisition and control system (DACS) for data logging during PJM operation.

C.1.2.1 PJM Liquid Level Measurement

The change in liquid height in the pulse tube was measured using a 24-inch-long Drexelbrook capacitance level sensor/transmitter with no time delay (20 ms response time) under manufacturer's modification 91-133. Due to spatial constraints in accommodating the pressure/vacuum line, pressure port, and level probe connection, this capacitance probe was mounted 1/4 inch off the pulse tube centerline. This should, however, have had a negligible impact on level readings. The 0.84-inch-OD capacitance probe was threaded into the 1-inch NPT coupling on top of the PJM.

C.1.2.2 Temperature Measurement

The bulk simulant temperature was measured with a calibrated Omega Type E thermocouple that was on the north side of the test tank, 11-1/4 inches from the bottom and 1/2 inch from the inside wall. The output from the thermocouple was transmitted to the DACS for logging during PJM operation.

C.1.2.3 Cavern Height Measurements

The height of the fluidized simulant in the test tank (i.e., cavern height) was determined by visual observation. For clear simulants like Laponite, the interface between the fluidized and unyielded material was evident because small bubbles entrained in the fluidized region were clearly visible. The cavern height was read directly from adhesive-backed scales attached to the clear acrylic tank wall at 90 degree intervals. The 1/16-inch graduated scales were in the northeast, southeast, southwest, and northwest tank quadrants. They enabled level measurements from the rim of the stainless-steel head at 6.25 to 36 inches.

C.1.2.4 Rheological Measurements

Rheological characterization was conducted in accordance with BNI Guidance 2450-WTP-GPG-RTD-001 Rev. 0 to characterize the shear strength of the undisturbed material and to provide a rheogram of the yielded material (material flowing in the mixing cavern and the PJM). Samples obtained for analysis were identified by date, run number, and type of simulant. Baseline samples were collected of the sheared simulant when it was transferred into the test tank. Shear strength measurements using a shear vane were taken at the start and end of each test run. When a test run cavern had reached steady state, a sample of the fluidized material was collected from the test tank drain valve connection.

C.1.2.5 Single-PJM Operation

The PJM test stand used a series of solenoid valves and a combination of a 125 psig compressed air supply and vacuum pump to simulate the drive and suction phases of PJM operation. There were three solenoid valves, one each for compressed air, vacuum, and vent. The system solenoid valves were controlled to operate the PJM in a time-scaled fashion. A system cycle time consisted of drive time (t_D), vent time (t_V), and vacuum time (t_S). The drive time was entered for a given supply pressure to achieve the desired target nozzle velocity and discharge volume. For a given discharge volume, the vent time was adjusted to obtain the targeted system cycle time. The vacuum cycle ended when the measured PJM level reached the input starting level for the next drive cycle. The duration of each phase and the applied

pressure were varied to simulate the operation of the jet pump pairs. Testing was conducted using a single PJM centered in the test tank and discharging vertically downward.

C.1.2.6 Data Acquisition System and Storage

Data including date, time, pulse tube level and pressure, bulk tank simulant temperature, compressed air supply pressure, and solenoid valve states and times were monitored continuously and recorded digitally with LabView software on a Dell OptiPlex GX1p PC running Windows NT Version 4.0. This workstation had a Pentium III 500-MHz processor, Level 2 Cache, 512 KB integrated system memory, 128-MB ECC SDRAM, and 8 MB video memory. A National Instruments NI 6011E (PCI-MIO-16XE-50) DAQ device was connected to the computer PCI bus. Two input/output modules were installed in a National Instruments NI SCXI-1000 chassis powered by a Rosemount Model 515 power supply. A National Instruments NI SCXI-1303 terminal block and NI SCXI 1102 module were used for instrumentation input signals; a NI SCXI-1161 relay switching module was used for solenoid valve control.

The DACS was set to achieve 10 samples per second (minimum). It was noted during shakedown testing of the system that the DACS sampling frequency would be set to 0.08 seconds to ensure 10 samples/second. This was attributed to the incremental read/write lag in polling the respective signal inputs and recording the data to the data file. Test data from each experiment were logged to an ASCII data file. No changes were made to the control logic program during the testing.

The data on the test computer hard drive was backed up by recording the data onto workgroup server WG03 on the SRNL network. For data analysis, the data files were copied to Excel spreadsheets. A description of the various column labels used in the Excel spreadsheets is listed in Table C.1.

Table C.1. SRNL Single PJM Description of the Excel Spreadsheet Columns

Excel Column	Variable Label	Description	Measured Unit
A	Date	Date the experiment was conducted	month/day/year
B	Time	Time when the data were logged	hr:min:sec
C	PJLVL	Level of the liquid in the pulse tube	inches
D	PJ Pressure	Pressure in the pulse tube	psig
E	T1	Temperature of the bulk tank simulant	°C
F	Supply Pressure	Compressed air supply pressure	psig
G	Pressure Sol	Pressure solenoid valve state	On =1 Off =0
H	Vent Sol	Vent solenoid valve state	On =1 Off =0
I	Vacuum Sol	Vacuum solenoid valve state	On =1 Off =0
J	Pressure Time	Elapsed time the pressure solenoid was energized	s
K	Vent Time	Elapsed time the vent solenoid was energized	s
L	Vacuum Time	Elapsed time the vacuum solenoid was energized	s

C.1.3 Instrumentation and Calibration

The sensors/instruments connected to the DACS were calibrated or performance checked in accordance with the SRNL Conduct of R&D manual. Component identification (see Figure C.3), manufacturer, function/measured variable, calibrated or performance check, range, and accuracy are listed in Table C.2.

Table C.2. SRNL Single PJM DACS Instrument Calibration, Range and Accuracy

P&ID Component Identification	Manufacturer (model/part no.)	Function/ Measured Variable	Calibrated or Performance Checked by	Range (accuracy)
LE-001	Drexelbrook (700-002-057-I024.0)	PJM level	Performance Check/User	9.5 to 35.5 inches (±0.25% of span = ±0.07 in.)
LT-001	Drexelbrook (408-8232-001)			
PT-001	Rosemount (1151DP5E22)	PJM pressure	Calibrated/SRNL EDL Calibration Services	-5 to 35 psig (±0.25% of span = ±0.1 psig)
TE-001	Omega (Type E T/C)	Slurry/liquid temperature	Calibrated/SRNL EDL Calibration Services	0 to 100°C (±1.7°C)
PT-002	Rosemount (1144A0200A22)	Compressed air supply pressure	Calibrated/SRNL EDL Calibration Services	0 to 50 psig (±0.25% of span = ±0.13 psig)
DACS	National Instruments (NI 6011E)	DACS analog input board	Calibrated/SRNL EDL Calibration Services	All channels (±1.51 mV)

The Drexelbrook capacitance level probe was performance checked in situ with the test tank filled with simulant. The level probe transmitter zero and span adjustments were set so that the probe output readings matched the tank level measured by the adhesive-backed tape measure affixed to the clear acrylic tank (±1/8 inch). The level transmitter output signal was input to the DACS for data logging and control during PJM operation. The thermocouple and pressure transmitters were calibrated by SRNL EDL Calibration Services.

The LabView DACS software allows for input scaling to be entered directly, individually, and uniquely for each channel. Each analog input channel to the DACS used the National Instruments NI SCXI-1102 module to convert the input signal to an analog voltage in the range of 2 to 10 volts. DACS channel calibration was performed by SRNL EDL Calibration Services. Instrument and channel calibration data were processed to determine the scaling constants to translate the input signals to appropriate engineering units.

C.2 SRNL Single-PJM Experiments

This section describes the 1/9-scale single-PJM test stand experiments and data summary and results. The SRNL single-PJM test stand and associated operation was intended to duplicate the nondimensional conditions tested in the APEL test facility to demonstrate the scaling laws for mixing. Test instructions were developed and implemented to gather data during cavern development tests.

Dimensional analysis was used to develop parameters to define the test matrix for characterizing the region of mobilization created by the single PJM for specified operating conditions. The test matrix was representative of testing conducted at the APEL.

Testing was conducted using non-Newtonian simulants that exhibit rheological characteristics similar to those predicted for the WTP non-Newtonian waste streams. When possible, the same simulant was used in both the APEL and SRNL test stands. While every effort was made to match simulant rheological properties, any variations between the PNWD and SRNL test stand simulant batches were not detrimental to the test objectives because a nondimensional comparison was performed.

C.2.1 Cavern Tests

These tests involved obtaining cross-sectional measurements of the mixing zone (sheared fluid cavern) resulting from a single PJM centered in the test tank and discharging vertically downward. The cavern test matrix was developed to characterize the cavern height and formation over a range of PJM operations. Cavern testing exercised PJM operating parameters under constant volume and constant velocity test sequences. Constant velocity tests were developed where the nozzle discharge velocity was held constant while the volume discharged was varied. Constant volume testing held the discharge volume constant while varying the nozzle velocity.

In the minimum cavern size evaluated, the cavern interface did not fall below the top rim of the test tank stainless steel head at any time during the pulse cycle. PJM operating parameters were typically increased incrementally for each test condition such that the region of mobilization increased during a test sequence (i.e., constant volume tests typically started by creating a cavern in the simulant at a minimum nozzle velocity and increasing the nozzle velocity in a step-wise fashion). Cavern height at each intermediate operating condition was monitored until a steady-state cavern was achieved.

Laponite RD was used during the cavern testing because it is a transparent non-Newtonian simulant in which the mixing zone (cavern) can easily be detected through the clear acrylic tank wall. Test sequences were initiated on a static unyielded (gelled) Laponite solution. In a transparent simulant the interface between the fluidized and unyielded material is evident because small air bubbles entrained in the fluidized region are visible through the clear tank wall. Experimental data consisted of data defining the PJM operations, cavern size, and simulant rheology.

C.2.1.1 Test Description

Laponite simulant was transferred to the mixing tank, agitated with a mixer, and recirculated with the transfer pump until the tank contents were fully fluidized. To wet the level probe, simulant was pumped into the test tank until the desired level was reached, and then the test tank was drained. With the level probe wetted, simulant was transferred back into the test tank, and the level probe zero and span adjustments were set. Baseline samples of the fully sheared simulant were collected for rheological analysis. Then the Laponite simulant was allowed to build structure (gel) for an appropriate period of time (typically 18 to 24 hours).

After the gel period, the DACS operating parameters were input to the control computer, and the compressed air supply regulator was adjusted to achieve the target velocity and discharge volume. At the start of a test, an initial shear vane measurement of the baseline sample was taken. System operations

were logged to a data file for approximately 10 to 15 pulse cycles and then analyzed to determine whether the target velocity and discharge volume were achieved. Operating parameters were adjusted as required, and when the target conditions were achieved, system operations were logged to a data file for approximately 25 pulse cycles. During the testing, system performance and cavern height progression were monitored. When the cavern height reached steady state, the maximum cavern elevation and cavern elevation at the tank wall were recorded. Cavern measurements were made in the north, northeast, east, southeast, south, southwest, west, and northwest quadrants of the test tank. At the steady-state cavern height, system operations were logged to a data file for approximately 25 more pulse cycles. A sample of the sheared simulant solution was collected from the test tank drain valve for rheological characterization, and a final shear vane measurement of the baseline sample was performed. After a test sequence was completed the test tank was drained, flushed, and cleaned.

C.2.1.2 Data Summary and Results

Several PJM cavern tests were performed with Laponite simulant at different PJM operating conditions. In all tests, the tank was initially filled to 29.4 inches (from the bottom of the tank). The overall data summary is presented in Table C.3 and the rheological characterization of the simulant from each test condition in Table C.4. Cavern elevation data are summarized in Tables C.5, C.6, and C.7.

Table C.3. SRNL Single PJM Cavern Test—Data Summary

Data File Number	Average Velocity (ft/sec)	Average Stroke (in.)	Drive Time Tp (s)	Nominal Velocity (ft/sec)	Yield Stress (Pa)	Cavern Height				Overall Average (in.)	Overall Average Aspect Ratio
						Average Wall		Average Max. Elev.			
						Max (in.)	Min (in.)	Max (in.)	Min (in.)		
Laponite Constant Volume Tests - Tank Level 29.4 in. (1.7 Aspect Ratio)											
030813R2B	22.9	7.1	2.40	25.0	37.2	9.3	8.8	10.2	9.7	9.5	0.55
030813R3B	31.6	6.9	1.50	40.0	38.2	13.3	12.8	13.9	13.3	13.3	0.77
030813R4J	42.9	7.1	0.83	72.2	38.1	18.5	18.0	19.4	18.8	18.7	1.08
030815R1D	33.0	4.8	0.90	43.1	40.0	11.3	10.9	11.9	11.5	11.4	0.66
030815R2C	33.0	6.3	1.30	40.3	42.7	12.6	12.1	13.3	12.9	12.7	0.74
030815R3D	34.9	7.8	1.55	41.9	43.0	13.5	13.0	14.2	13.7	13.6	0.79
030815R4C	35.0	9.4	1.95	40.3	44.4	13.7	13.0	15.3	14.6	14.2	0.82
030815R5C	35.2	12.4	2.60	40.3	45.6	13.8	12.9	15.5	14.6	14.2	0.82
030821R1C	23.7	7.5	2.40	25.0	49.5	7.0	6.4	7.8	7.3	7.1	0.41
030821R2K	35.2	7.1	1.40	42.8	52.4	10.0	9.6	10.7	10.2	10.1	0.59
030821R3E	45.6	7.1	0.85	70.5	54.5	13.9	13.5	14.8	14.4	14.1	0.82

C.3 SRNL 4PJM Test Stand

This section describes the 1/9-scale 4PJM test stand, experimental approach, and instrument calibrations. The 4PJM test stand was used to demonstrate the scaling laws for mixing.

Table C.4. SRNL Single-PJM Cavern Test with Laponite—Rheology Data Summary

Data File Number	Initial Shear Strength (Pa)	Final Shear Strength (Pa)	Average Yield Stress (Pa)	Bingham Plastic Data[(a)]			Power Law Data[(a)]			Herschel-Bulkley Data[(a)]			
				Yield Stress τ_{BP} (Pa)	Consistency η_{BP} (cP)	Fit Factor R^2	PL Consistency K_{PL} (Pa-s^n)	n -	Fit Factor R^2	HB Yield Stress τ_{HB} (Pa)	HB Consistency κ_{HB} (Pa-s^b)	HB Exponent	Fit Factor R^2
Laponite Constant Volume Tests - Tank Level 29.4 in. (1.7 Aspect Ratio)													
030813R2B	35.8	38.5	37.2	5.4	14.0	0.954	0.755	0.461	0.999	0.158	0.699	0.470	0.999
030813R3B	38.5	37.8	38.2	4.7	13.2	0.953	0.568	0.486	0.999	-0.260[(b)]	0.658	0.470	0.999
030813R4J	37.8	38.3	38.1	4.3	12.8	0.955	0.442	0.513	0.999	-0.350[(b)]	0.597	0.479	0.999
030815R1D	37.2	42.8	40.0	5.6	13.5	0.949	0.869	0.441	0.999	0.095	0.841	0.445	0.999
030815R2C	42.8	42.6	42.7	5.3	13.4	0.951	0.768	0.454	0.999	0.072	0.748	0.458	0.999
030815R3D	42.6	43.3	43.0	5.3	13.5	0.972	0.752	0.457	0.999	0.053	0.736	0.460	0.999
030815R4C	43.3	45.5	44.4	5.4	13.5	0.951	0.754	0.456	0.999	0.113	0.779	0.454	0.999
030815R5C	45.5	45.6	45.6	5.2	13.4	0.950	0.726	0.46	0.999	0.056	0.752	0.457	0.999
030821R1C	47.4	51.6	49.5	7.2	14.1	0.946	1.29	0.396	0.999	0.884	0.994	0.427	0.999
030821R2K	51.6	53.1	52.4	7.3	14.0	0.942	1.35	0.389	0.998	0.770	1.084	0.415	0.999
030821R3E	53.1	55.8	54.5	6.5	13.4	0.941	1.12	0.406	0.999	0.229	1.046	0.414	0.999

(a) All flow curves were fitted on the down curve, and parameters are the average of two flow curves.
(b) A negative Herschel-Bulkley intercept is obviously unreal and cannot be physically interpreted as being anything except a value of zero, which would make it basically a Power Law fit. Recommend using the Bingham Plastic or Power Law coefficients.

Table C.5. SRNL Single-PJM Cavern Data—Laponite Constant Volume Test (August 13, 2003)

Location	Cavern Height (in.)									Max/Min Average	Overall Average
	N	NE	E	SE	S	SW	W	NW	Average		
Data File Number: 030813R2B											
Wall (max)	9.00	8.25	9.88	10.00	9.00	9.87	9.00	9.62	9.33	9.08	9.51
Wall (min)	8.50	7.75	9.25	9.62	8.38	9.38	8.50	9.25	8.83		
Max. Elev. (max)	10.00	9.12	11.00	11.62	9.62	10.75	9.75	9.75	10.20	9.94	
Max. Elev. (min)	9.62	8.63	10.38	11.12	9.00	10.25	9.12	9.25	9.67		
Data File Number: 030813R3B											
Wall (max)	13.38	14.50	13.00	13.12	13.00	12.50	12.50	14.38	13.30	13.05	13.33
Wall (min)	12.87	14.00	12.50	12.50	12.50	12.12	12.00	13.88	12.80		
Max. Elev. (max)	13.87	15.62	13.75	13.25	13.25	13.13	13.25	14.87	13.87	13.61	
Max. Elev. (min)	13.25	15.12	13.25	12.87	12.62	12.62	12.75	14.25	13.34		
Data File Number: 030813R4J											
Wall (max)	18.50	18.25	18.87	18.38	19.00	17.25	18.25	19.50	18.50	18.27	18.69
Wall (min)	18.00	17.87	18.38	17.87	18.50	16.87	17.75	19.00	18.03		
Max. Elev. (max)	20.25	19.62	19.75	18.87	19.62	18.12	18.87	20.00	19.39	19.12	
Max. Elev. (min)	19.75	19.12	19.25	18.38	19.00	17.50	18.38	19.38	18.85		

Table C.6. SRNL Single-PJM Cavern Data—Laponite Constant Velocity Test (August 15, 2003)

Location	Cavern Height (in.)									Max/Min Average	Overall Average
	N	NE	E	SE	S	SW	W	NW	Average		
Data File Number: 030815R2C											
Wall (max)	12.88	13.88	14.75	12.25	11.38	11.00	12.88	11.50	12.56	12.34	12.74
Wall (min)	12.50	13.31	14.31	11.69	11.00	10.69	12.44	11.06	12.13		
Max. Elev. (max)	13.38	14.38	14.75	14.00	12.50	11.50	13.38	12.88	13.34	13.13	
Max. Elev. (min)	13.00	14.00	14.31	13.50	12.06	11.00	13.00	12.50	12.92		
Data File Number: 030815R3D											
Wall (max)	13.50	13.50	14.88	12.50	13.63	13.56	13.50	12.75	13.48	13.21	13.58
Wall (min)	13.00	13.00	14.25	12.00	13.13	13.00	13.00	12.25	12.95		
Max. Elev. (max)	13.88	14.75	14.88	14.00	14.50	14.13	14.38	13.25	14.22	13.94	
Max. Elev. (min)	13.25	14.25	14.25	13.38	14.00	13.63	13.75	12.75	13.66		
Data File Number: 030815R4C											
Wall (max)	13.50	13.63	15.00	13.50	13.75	13.75	13.75	12.75	13.70	13.34	14.16
Wall (min)	12.75	13.00	14.25	12.75	13.00	13.00	13.00	12.13	12.98		
Max. Elev. (max)	15.75	14.75	15.00	14.88	15.00	15.00	15.50	16.75	15.33	14.98	
Max. Elev. (min)	15.00	14.13	14.25	14.25	14.25	14.38	14.75	16.13	14.64		
Data File Number: 030815R5C											
Wall (max)	13.63	13.75	15.00	13.56	13.88	14.06	13.75	12.94	13.82	13.35	14.20
Wall (min)	12.63	12.81	14.00	12.50	13.00	13.13	12.94	12.00	12.88		
Max. Elev. (max)	15.88	14.88	15.13	15.13	15.13	15.50	15.75	16.88	15.53	15.05	
Max. Elev. (min)	14.94	13.94	14.13	14.19	14.13	14.63	14.75	15.88	14.57		

Table C.7. SRNL Single-PJM Cavern Data—Laponite Constant Volume Test (August 21, 2003)

Location	Cavern Height (in.)									Max/Min Average	Overall Average
	N	NE	E	SE	S	SW	W	NW	Average		
Data File Number: 030821R1C											
Wall (max)	7.13	6.75	6.88	7.00	7.00	7.25	6.75	7.00	6.97	6.68	7.11
Wall (min)	6.50	6.25	6.25	6.50	6.50	6.63	6.13	6.38	6.39		
Max. Elev. (max)	8.00	7.38	7.63	8.13	8.25	7.63	7.88	7.88	7.84	7.55	
Max. Elev. (min)	7.50	6.75	7.00	7.63	7.63	7.00	7.25	7.25	7.25		
Data File Number: 030821R2K											
Wall (max)	9.88	9.63	9.75	10.00	9.50	10.63	10.50	10.50	10.05	9.81	10.15
Wall (min)	9.38	9.13	9.25	9.50	9.00	10.25	10.13	10.00	9.58		
Max. Elev. (max)	10.75	10.25	10.25	10.13	10.63	11.00	11.88	11.00	10.73	10.48	
Max. Elev. (min)	10.25	9.75	9.75	9.63	10.13	10.50	11.38	10.50	10.23		
Data File Number: 030821R3E											
Wall (max)	14.13	14.38	13.75	13.63	13.00	14.13	15.25	12.88	13.89	13.67	14.14
Wall (min)	13.75	14.00	13.25	13.25	12.50	13.63	14.75	12.50	13.45		
Max. Elev. (max)	15.25	14.63	14.63	14.50	14.50	15.00	15.50	14.75	14.84	14.61	
Max. Elev. (min)	14.75	14.13	14.13	14.00	14.00	14.63	15.00	14.38	14.38		

C.3.1 Description

The SRNL 4PJM test stand is a linearly scaled version of the 4PJM setup in the 336 test facility. The SRNL 4PJM test stand consisted of a clear cylindrical shell with a stainless steel 2:1 elliptical head. The clear acrylic test tank internal diameter is 17.25 inches (average ID = 17.25 inches), and the internal height is 43 inches. Four PJMs fabricated from 2½ NPS, schedule 10S stainless steel pipe spaced at 90-degree intervals on a 10.64-inch pitch diameter discharged vertically downward. The average internal diameter of the pulse tube was 2.625 inches. The 60-degree nose cone on the outlet of the PJM has a nominal nozzle diameter of 0.445 inches, and the nozzle centerline elevation is 1 inch above the tank head. As-built inspection of the PJM nozzle bores determined that the internal diameter of two PJM nozzles was 0.444 inch, and the internal diameter of the other two was 0.445 inch. A drain/sample valve is at the center of the tank head, providing a flush interior profile. Plan and elevation views of the test stand configuration are shown in Figure C.4. The process and instrumentation diagram of the test stand configuration is shown in Figure C.5.

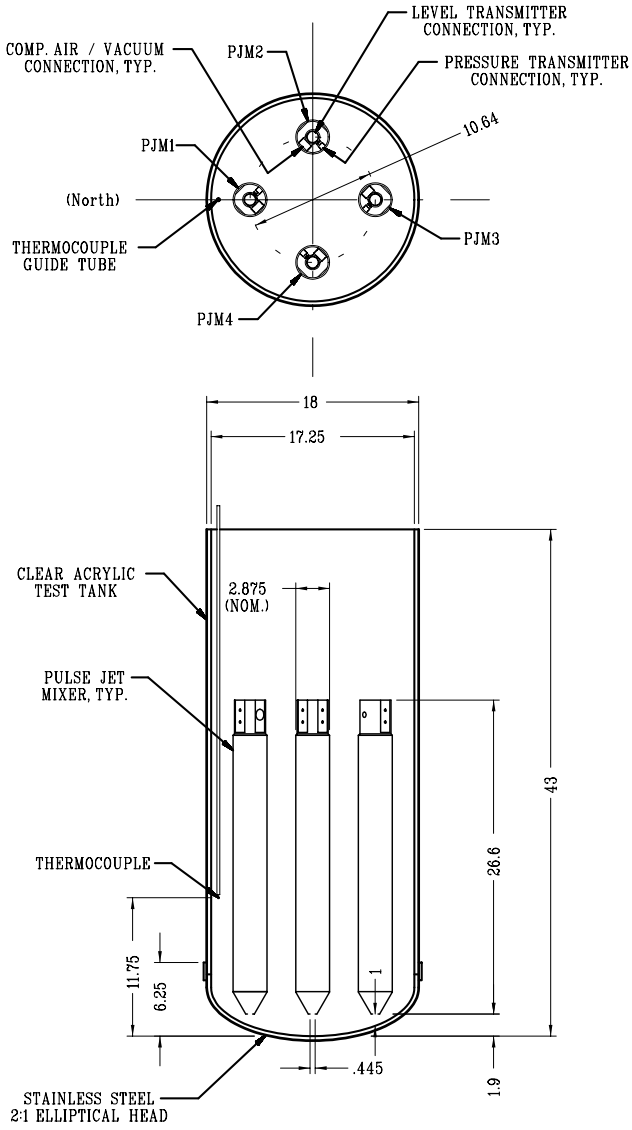

Figure C.4. SRNL 4PJM Test Stand Plan and Elevation View

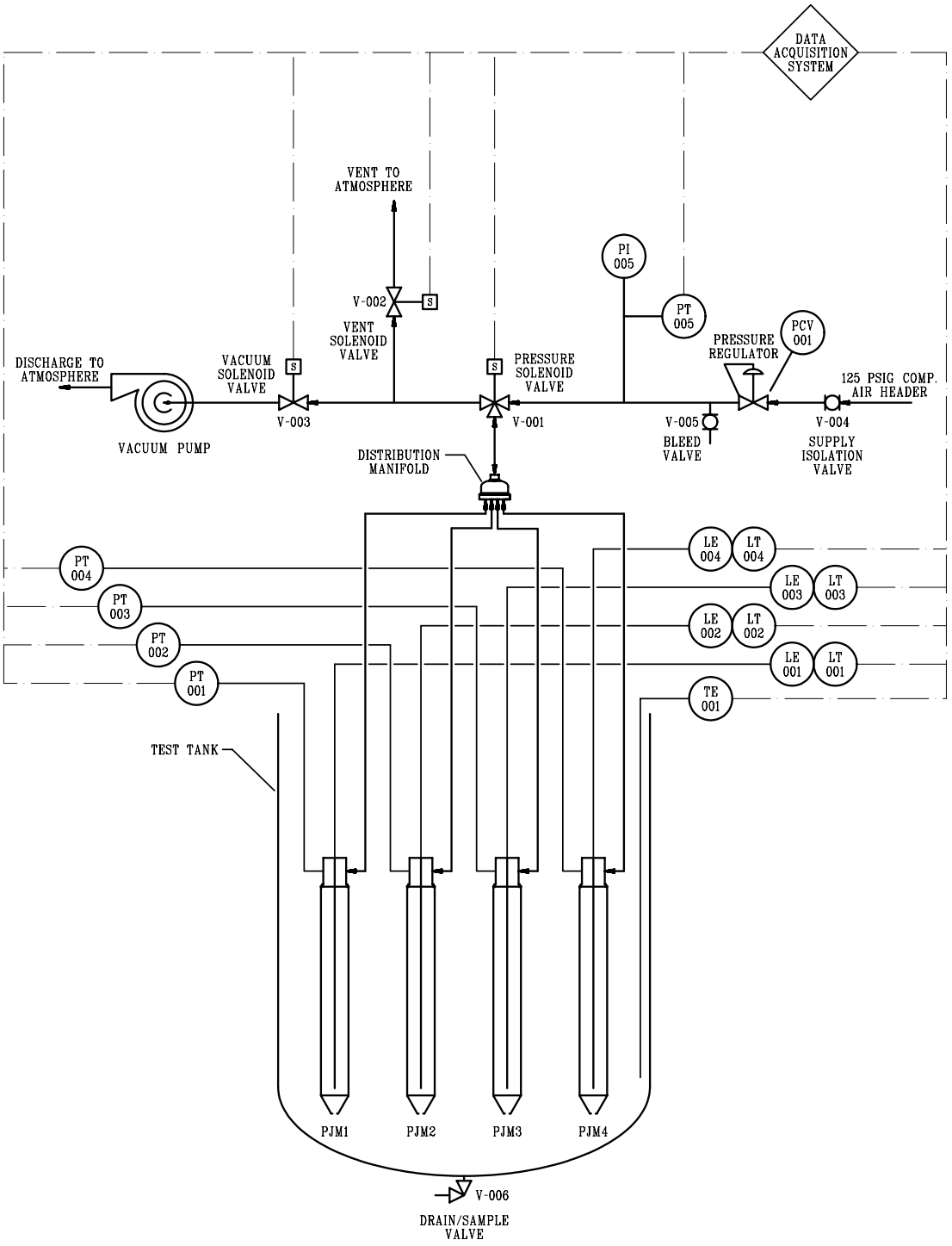

Figure C.5. SRNL 4PJM Test Stand Process and Instrumentation Diagram

The PNWD 336 test tank's internal diameter is 153 inches; thus, for the SRNL testing, the geometric scaling factor was 153/17.25 = 8.87. The time scale factor is the inverse of the geometric scale factor; thus, for SRNL testing, temporal events must occur in 1/8.87 the duration of the APEL test.

C.3.2 Experimental Approach

The test matrix was representative of testing conducted at the 336 test facility large-scale test stand and the APEL 1/4-scale test stand. Like the 1-PJM system, this 4-PJM design addresses the following: 1) obtaining cavern heights at periodic conditions as a function of the discharge velocity and discharge time and 2) observing and evaluating cavern formation and time transients for cavern formation.

This section provides the experimental approaches used to measure the PJM internal level and pressure, bulk simulant temperature, compressed air supply header pressure, and cavern height during operation. In addition, rheological analysis of the non-Newtonian simulants was performed to characterize the shear strength of the undisturbed material and provide a rheogram of the yielded material. However, the experimental approach for the 4PJM test stand was the same as that described in Section C.1 for the single-PJM test stand except for three things. First, for the PJM liquid level measurement, a 0.56-inch OD capacitance probe was threaded into the 3/4-inch NPT connection on top of the PJM along the pulse tube centerline. The output signal from PJM1 level probe was used by the DACS to control the system pulse cycle. The remaining 4-20 mA transmitter output signals were input to the DACS for data logging during PJM operation. And the capacitance probe was not offset from the pulse tube centerline. Second, for temperature measurement, the thermocouple was on the north side of the test tank, 11-3/4 inches from the bottom and ½ inch from the inside wall. Third, the 4PJM operation had compressed air and vacuum applied through a distribution manifold. PJM operations were controlled through a control logic program using LabView software on a Dell OptiPlex GX1p PC running Windows NT Workstation Version 4.0. To establish equivalent hydraulic performance in the PJMs, matched lengths of tubing connected each pulse tube to the distribution manifold. In addition, each PJM pressure transmitter was connected to the pulse tube with matched lengths of impulse line tubing. Testing was conducted using four PJMs on a PCD of 10.64 inches discharging vertically downward. The DACS copied the data files to Excel spreadsheets. The various column labels used in the Excel spreadsheets are listed and described in Table C.8.

Table C.8. SRNL 4PJM Description of the Excel Spreadsheet Columns

Excel Column	Variable Label	Description	Measured Unit
A	Date	Date the experiment was conducted	month/day/year
B	Time	Time when the data were logged	hr:min:sec
C	PJLVL 1	Level of the liquid in pulse tube 1 (north)	inches
D	PJLVL 2	Level of the liquid in pulse tube 2 (east)	inches
E	PJLVL 3	Level of the liquid in pulse tube 3 (south)	inches
F	PJLVL 4	Level of the liquid in pulse tube 4 (west)	inches
G	PJ Pressure 1	Pressure in pulse tube 1 (north)	psig
H	PJ Pressure 2	Pressure in pulse tube 2 (east)	psig
I	PJ Pressure 3	Pressure in pulse tube 3 (south)	psig
J	PJ Pressure 4	Pressure in pulse tube 4 (west)	psig
K	Supply Pressure	Compressed air supply pressure	psig
L	T1	Temperature of the bulk tank simulant	°C
M	Pressure Sol	Pressure solenoid valve state	On =1 Off =0
N	Vent Sol	Vent solenoid valve state	On =1 Off =0
O	Vacuum Sol	Vacuum solenoid valve state	On =1 Off =0
P	Pressure Time	Elapsed time the pressure solenoid was energized	s
Q	Vent Time	Elapsed time the vent solenoid was energized	s
R	Vacuum Time	Elapsed time the vacuum solenoid was energized	s

Sensors and instruments were calibrated as previously discussed in section C.1.3. Component identification (see Figure C.5), manufacturer, function/measured variable, calibrated or performance check, range, and accuracy are listed in Table C.9.

Table C.9. SRNL 4PJM DACS Instrument Calibration, Range and Accuracy

P&ID Component Identification	Manufacturer (model/part no.)	Function/Measured Variable	Calibrated or Performance Checked by	Range (accuracy)
LE-001	Drexelbrook (700-002-027-I024.0)	PJM level	Performance check/User	6.5 to 25.5 inches (±0.25% of span = ±0.05 in.)
LT-001	Drexelbrook (408-8230-004)			
LE-002	Drexelbrook (700-002-027-I024.0)	PJM level	Performance check/User	6.5 to 25.5 inches (±0.25% of span = ±0.05 in.)
LT-002	Drexelbrook (408-8230-004)			
LE-003	Drexelbrook (700-002-027-I024.0)	PJM level	Performance check/User	6.5 to 25.5 inches (±0.25% of span = ±0.05 in.)
LT-003	Drexelbrook (408-8230-004)			
LE-004	Drexelbrook (700-002-027-I024.0)	PJM level	Performance check/User	6.5 to 25.5 inches (±0.25% of span = ±0.05 in.)
LT-004	Drexelbrook (408-8230-004)			
PT-001	Rosemount (3051CD3A22)	PJM pressure	Calibrated/SRNL EDL Calibration Services	-5 to 35 psig (±0.25% of span = ±0.1 psig)
PT-002	Rosemount (3051CD3A22)	PJM pressure	Calibrated/SRNL EDL Calibration Services	-5 to 35 psig (±0.25% of span = ±0.1 psig)
PT-003	Rosemount (3051CD3A22)	PJM pressure	Calibrated/SRNL EDL Calibration Services	-5 to 35 psig (±0.25% of span = ±0.1 psig)
PT-004	Rosemount (3051CD3A22)	PJM pressure	Calibrated/SRNL EDL Calibration Services	-5 to 35 psig (±0.25% of span = ±0.1 psig)
PT-005	Rosemount (1144A0200A22)	Compressed air supply pressure	Calibrated/SRNL EDL Calibration Services	0 to 50 psig (±0.25% of span = ±0.13 psig)
TE-001	Omega (Type E T/C)	Slurry/liquid temperature	Calibrated/SRNL EDL Calibration Services	0 to 100°C (±1.7°C)
DACS	National Instruments (NI 6011E)	DACS analog input board	Calibrated/SRNL EDL Calibration Services	All channels (±1.51 mV)

C.4 SRNL 4PJM Experiments

This section describes the 1/9-scale 4PJM test stand experiments and data summary and results. The SRNL 4PJM test stand and associated operation was intended to duplicate the nondimensional conditions tested in the PNWD 336 and APEL test facilities to demonstrate the scaling laws for mixing. As in the 1PJM experiments, test instructions were developed and implemented to gather data during cavern tests, breakthrough tests, and velocity tests for the 4PJM experiments.

Dimensional analysis was used to develop parameters to define the test matrix for characterizing the region of mobilization created by the 4PJM array for specified operating conditions. The test matrix was

representative of testing at the 336 and APEL facilities. Test instructions were provided in the EES Field Procedure (Wilson et al. 2004).

The cavern tests and test description for 4PJM tests were the same as in the 1PJM experiments, so only the differences are discussed. The only change in the 4PJM test was that PJM operating parameters were then typically increased incrementally for the next test condition such that the region of mobilization increased during the test sequence.

C.4.1.2 Data Summary and Results

Several PJM cavern tests were performed with Laponite simulant at different PJM operating conditions. Testing was conducted with the initial tank level either 15.5 or 25 inches from the bottom of the tank. The overall data summary is presented in Table C.10. Rheological characterization of the simulant from each test condition is presented in Table C.11.

Although a test exception requested testing at an aspect ratio of 1.6, to ensure satisfactory performance of the capacitance level probes and PJM pressure transmitters the maximum tank level for the 4PJM test stand was limited to 25 inches. At tank levels above 25 inches the annular clearance between the capacitance probe and PJM top head could be filled with simulant, potentially affecting the level probe calibration and pressure transmitter penetrations. Gelled simulant in these locations could lead to erroneous instrumentation response. Therefore, the PJM Task Team decided that performing the additional testing at an aspect ratio of 1.45 was sufficient for the program needs.

Aside from the cavern height versus velocity data at a 1.45 aspect ratio, the time sequence to fully mix the tank contents with PJMs operating at a nominal 8 m/s (26.3 ft/sec) nozzle velocity was observed. Specific interests in the time to breakthrough at the tank surface, time to achieve movement down the tank wall, and time for simulant to exhibit turbulent motion at the tank wall were identified. At a nominal velocity of 26.1 ft/sec, cavern breakthrough did not occur.

The nozzle velocity was increased in subsequent testing, and breakthrough was achieved at a nominal 43.6 ft/sec. During this test, fractures of the simulant surface occurred within the first minute of PJM operation. Sheared simulant extruded from a fracture 5 minutes after the test began. Thirteen minutes into the test, sheared simulant was moving across the top surface with each PJM pulse. This sheared material emerged from the center of the tank and migrated toward the wall. At this point, approximately 75% of the top surface was covered with sheared material. This material was sheared but not completely fluidized. At 48 minutes, tank contents were fully sheared but still not completely fluidized, and a neutrally buoyant particle placed in the center of the tank took 38 pulses to migrate to the tank wall. At 134 minutes the tank was fully fluidized, and a neutrally buoyant particle placed in the center of the tank took 26 pulses to migrate to the wall. Flow at the tank wall was not turbulent but was translating downward in a ratcheting motion. In the PJM shadow zones, air bubbles at the tank wall ratcheted downward at approximately 0.1875 to 0.75 inch per pulse. In the regions between the pulse tubes, air bubbles at the tank wall ratcheted downward at approximately 0.375 to 0.5 inch per pulse. At 194 minutes flow conditions at the wall were unchanged, and a neutrally buoyant particle placed in the center of the tank took 25 pulses to migrate to the tank wall. At 209 minutes, the test was terminated.

Table C.10. SRNL 4PJM Cavern Test - Data Summary

Reference Number	Data File Number	Average Velocity (ft/sec)	Drive Time T_P (s)	Nominal Velocity (ft/sec)	Avg Vane Shear Strength (Pa)	Cavern Height			Aspect Ratio	Breakthrough
						Max (in.)	Min (in.)	Avg (in.)		
	Laponite Constant Volume Tests - Tank Level 15.5 in. (0.9 Aspect Ratio)									
S-1	031029R3A	12	2.5	12.2	68.2	7.6	6.8	7.2	0.42	--
S-2	031029R4A	18	1.5	20.4	71	15.5	15.5	15.5	0.9	yes
S-3	031104R1A	14.6	2.05	14.9	99.3	7.3	6.3	6.8	0.39	--
S-4	031104R2A	17.9	1.55	19.7	99.5	12.9	11.9	12.4	0.72	--
S-5	031104R3A	19.6	1.4	21.8	99.1	15.5	15.5	15.5	0.9	yes
S-6	031105R2A	14.3	2.1	14.5	79.3	8.8	7.9	8.3	0.48	--
S-7	031107R1A	16	1.8	17	79.6	10.3	9.3	9.8	0.57	--
S-8	031112R1A	17.4	1.6	19.1	81.6	12.6	11.6	12.1	0.7	--
S-9	031125R1A	19	1.6	19.1	96	10.8	9.8	10.3	0.6	--
S-10	031105R3A	--	0.7	43.6 (SysMax)	83.6	15.5	15.5	15.5	0.9	yes
	Laponite Constant Volume Tests - Tank Level 25.0 in. (1.45 Aspect Ratio)									
S-11	031118R1D	20.5	1.4	21.8	99.4	14.8	13.8	14.3	0.83	--
S-12	031119R1B	24.4	1.17	26.1	89	18.7	17.7	18.2	1.06	--
S-13	031120R1C	17.3	1.8	17	87	9.8	8.8	9.3	0.54	--
S-14	031120R2A	26.1	0.95	32.1	88	19.6	18.7	19.1	1.11	--
S-15	031121R1A	34.8	0.7	43.6	84.2	25	25	25	1.45	yes

Table C.11. SRNL 4PJM Cavern Test with Laponite RD Simulant—Rheology Data Summary

Reference Number	Data File Number	Initial Vane Shear Strength (Pa)	Final Vane Shear Strength (Pa)	Avg Vane Shear Strength (Pa)	Bingham Plastic Data[a]			Power Law Data[a]			Herschel-Bulkley Data[a]			
					Yield Stress τ_{BP} (Pa)	Consistency η_{BP} (cP)	Fit Factor R^2	PL Consistency K_{PL} (Pa-s^n)	n	Fit Factor R^2	HB Yield Stress τ_{HB} (Pa)	HB Consistency κ_{HB} (Pa-s)[c]	HB Exponent b	Fit Factor R^2
	Laponite Constant Volume Tests - Tank Level 15.5 in. (0.9 Aspect Ratio)													
S-1	031029R3A	68.2	N/M[d]	68.2	N/M	N/M	N/M	N/M	N/M	N/M	N/M	N/M	N/M	N/M
S-2	031029R4A	N/M	71	71	6.9	9.66	0.95	1.77	0.31	0.992	2.99	0.574	0.448	0.998
S-3	031104R1A	N/M	99.3	99.3	7.2	9.59	0.953	1.94	0.3	0.989	3.54	0.51	0.462	0.998
S-4	031104R2A	99.3	99.5	99.4	5.7	9.69	0.863	1.26	0.35	0.874	3.26	0.241	0.561	0.885
S-5	031104R3A	99.5	99.1	99.3	N/M	N/M	N/M	N/M	N/M	N/M	N/M	N/M	N/M	N/M
S-6	031105R2A	79.3	83.6	81.5	8.1	9.58	0.956	2.41	0.28	0.988	4.54	0.482	0.471	0.999
S-7	031107R1A	75.9	79.6	77.8	8.3	9.23	0.957	2.61	0.27	0.986	4.92	0.448	0.474	0.999
S-8	031112R1A	79.9	81.6	80.8	9	9.94	0.961	2.88	0.26	0.978	5.81	0.372	0.507	0.998
S-9	031125R1A	96.3	95.8	96.1	11.5	9.5	0.981	4.82	0.2	0.939	9.85	0.117	0.653	0.998
S-10	031105R3A	83.6	N/M	83.6	N/M	N/M	N/M	N/M	N/M	N/M	N/M	N/M	N/M	N/M
	Laponite Constant Volume Tests - Tank Level 25.0 in. (1.45 Aspect Ratio)													
S-11	031118R1D	96.1	100.2	98.2	9.7	10.03	0.967	3.35	0.25	0.969	7.01	0.282	0.546	0.998
S-12	031119R1B	89.1	89.4	89.3	10.3	10.22	0.973	3.69	0.24	0.96	7.89	0.215	0.583	0.998
S-13	031120R1C	86.8	88.4	87.6	10.6	10.02	0.975	4	0.23	0.954	8.46	0.18	0.603	0.997
S-14	031120R2A	88.4	88.5	88.5	10.5	9.9	0.977	3.92	0.23	0.956	8.42	0.169	0.609	0.998
S-15	031121R1A	76.3	83.4	79.9	10.8	9.79	0.973	4.17	0.22	0.954	8.54	0.193	0.59	0.998

(a) All flow curves were fitted on the down curve, and parameters are the average of two flow curves.

C.4.2 Mixing Tests

These tests involved operating the PJM system at a discrete nozzle discharge velocity under scaled constant volume conditions to assess mixing characteristics. Specifically, the time to break through the simulant surface, the time to achieve movement down the tank wall, and the time for the simulant to exhibit turbulent motion at the tank wall were identified to be of interest. When possible, neutrally buoyant beads were added near the middle of the tank or at the wall, and the time for their reemergence was observed and documented.

Mixing tests presented in this section used a non-Newtonian Laponite RD or kaolin-bentonite simulant. The testing was performed with the 4PJM array centered in the test tank and discharging vertically downward. Simulant movement and breakthrough assessments were performed by visual observation. Experimental data were those defining the PJM operations, visual observation of surface motion/ overall mixing, and simulant rheology. The mixing tests description was the same for cavern tests as discussed in subsection C.2.1.1.

C.4.2.2 Data Summary/Results

Experimental data collected during mixing tests of the SRNL 4PJM test stand are presented in this subsection. In support of the design parameter scale law testing program, the primary focus of these tests was determining time-to-mix data while operating the PJMs under scaled constant volume conditions in both Laponite RD and kaolin-bentonite simulants.

Although Test Exception 24590-WTP-TEF-RT-03-059[(a)] requested mixing tests at an aspect ratio of 1.6 to ensure satisfactory performance of the capacitance level probes and PJM pressure transmitters, the maximum tank level for the 4PJM test stand was limited to 25 inches. Once again, at tank levels above 25 inches the annular clearance between the capacitance probe and PJM top head could be filled with simulant, potentially affecting the level probe calibration and the pressure transmitter penetrations.

Testing was conducted with a Laponite RD simulant at an initial tank level of 25 inches from the bottom. The time sequence to fully mix the tank contents with PJMs operating at a nominal 8 m/s (26.3 ft/sec) nozzle velocity was to be observed. Specific interests in the time to breakthrough at the tank surface, time to achieve movement down the tank wall, and time for simulant to exhibit turbulent motion at the tank wall were identified. However, at a nominal velocity of 26.1 ft/sec, cavern breakthrough did not occur.

The same simulant behavior that occurred in the cavern tests was observed in the mixing tests (refer to subsection C.4.1.2). The only exception was that in the PJM shadow zones, air bubbles at the tank wall ratcheted downward at approximately 0.1875 to 0.25 inch per pulse.

As noted, the initial test run at a nominal velocity of 26.1 ft/sec did not produce a mixing zone that lead to breakthrough. However, observations of mixing at the tank wall were noted during this test run.

(a) Test Exception 24590-WTP-TEF-RT-03-059 to Test Plan WSRC-TR-2003-00363, SRT-RPP-2003-00174 Rev. 0. "Determine Time to Fully Mix Stagnant Laponite Simulant in SRTC 4 PJM One-Eighth Scale Test Platform."

Flow at the tank wall was not turbulent; it translated downward in a ratcheting motion with each discharge pulse. In the PJM shadow zones air bubbles at the tank wall ratcheted downward at approximately 0.125 to 0.1875 inch per pulse. In the regions between the pulse tubes, air bubbles at the tank wall ratcheted downward at approximately 0.3125 to 0.375 inch per pulse.

General observations of mixing were noted during several progressive cavern tests (i.e., the test stand was operating with a steady-state cavern prior to a change in operating parameters that lead to an increased cavern). With the test stand filled with Laponite RD simulant at an initial level of 15.5 inches from the bottom of the tank (0.9 aspect ratio), the PJM test stand operated for approximately 170 minutes, and a fully developed cavern was established. The existing cavern elevation was 7.625 inches maximum to 6.75 inches minimum (data file 031029R4A). Fractures of the simulant surface occurred 4 minutes after adjusting PJM operating conditions. Sheared simulant extruded from a fracture 20 minutes after the test was started and was moving across the top surface with each PJM pulse. This fluidized material emerged from a fracture extending from the north PJM (PJM1) to the east PJM (PJM2) and migrated outward toward the northeast tank wall. At this point approximately 20% of the top surface was covered with fluidized material. At 45 minutes, the cavern reached the top surface adjacent to PJM1 and PJM2, and at this point approximately 30% of the top surface was fluidized. The remaining surface simulant was gelled, with the tank centerline cavern height ranging from 12.75 inches maximum to 12.135 inches minimum. At the southwest tank wall the cavern height ranged from 13.5 inches maximum to 12.63 inches minimum. At 145 minutes, the tank was fully fluidized, although flow at the tank wall was not turbulent; it was translating downward in a ratcheting motion with each discharge pulse. In the PJM shadow zones and the regions between the pulse tubes, air bubbles at the tank wall ratcheted downward at approximately 0.31 to 0.38 inch per pulse.

During another progressive cavern test with the test stand filled with Laponite RD simulant at an initial tank level of 15.5 inches from the bottom of the tank (0.9 aspect ratio), the PJM test stand operated for approximately 245 minutes, and a fully developed cavern was established. The existing cavern elevation was 13 inches maximum to 12 inches minimum, as documented in data file 031104R3A. Fluidized simulant extruded from a fracture 3 minutes after the test was started and was moving across the top surface with each PJM pulse. This sheared material emerged from a fracture extending from the east PJM (PJM2) to the west PJM (PJM4) and migrated outward toward the north tank wall. At 5 minutes approximately 50% of the top surface was covered with fluidized material. At 6 minutes the top surface was completely covered. At 26 minutes the tank was fully fluidized, although flow at the tank wall was not turbulent but was ratcheting downward with each discharge pulse.

Testing with kaolin-bentonite simulant was proposed under Test Exception 24590-WTP-TEF-RT-03-085[(a)] to evaluate mixing characteristics. However, as experienced with other similar opaque simulants (AZ-102), the interior tank wall was coated with a thin layer of simulant that obscured visual observations of mixing conditions. In fact, it was observed during test runs with the kaolin-bentonite simulant that air bubbles at the tank wall did not translate up and down with corresponding PJM operations. There are no visually distinguishable indications between the bulk tank kaolin-bentonite simulant and sheared material emerging on the top surface during system operation. Colorimetric dye techniques were recommended, but given the smaller volume of simulant in the 1/9-scale test stand, the established sampling rates from

(a) Test Exception 24590-WTP-TEF-RT-03-059 to Test Plan WSRC-TR-2003-00363, SRT-RPP-2003-00174 Rev. 0, "Determine Time to Fully Mix Stagnant Laponite Simulant in SRTC 4 PJM One-Eighth Scale Test Platform."

the larger scale test stands would have removed a significant amount of simulant over the duration of an extended test run, potentially biasing the overall mixing results.

Further consideration was given to direct dye injection into the mixing zone upon PJM system startup to visually determine the time to break through at the simulant surface. This was judged a viable option, but experience with the opaque AZ-102 simulant and direct dye injection methods showed that the stagnant boundary layer at the interior tank wall continued to obscure visual determination of simulant movement at the tank wall or determination of a fully mixed tank. SRNL was unable to perform the explicit kaolin-bentonite mixing or cavern tests using the measurement methods proposed in the test exception.[a] Consequently, breakthrough tests were pursued.

C.4.3 Breakthrough Tests

These tests involved incrementally increasing the nozzle discharge velocity under scaled constant volume conditions until the mixing zone (sheared fluid cavern) breaks through the top surface of the simulant in the test tank. Some of the PJM operating conditions during cavern testing created mixing zones that increased in height and led to breakthrough. For comparison purposes, those results are presented in Section C.4.1.

Breakthrough testing presented in this section used a non-Newtonian kaolin-bentonite simulant. The testing was performed with the 4PJM array centered in the test tank and discharging vertically downward. Breakthrough determination of surface motion was performed by visual observation. To ensure consistency with breakthrough determination criteria, SRNL personnel witnessed breakthrough test runs at the APEL. Experimental data consisted of data defining the PJM operations, visual observation of surface motion/overall mixing, and simulant rheology.

C.4.3.1 Test Description

The test description for the breakthrough tests was the same as for the 1PJM cavern test description discussed in subsection C.2.1.1. As a result, only differences will be mentioned. Kaolin-bentonite simulant was transferred into the mixing tank, agitated with a mixer, and recirculated with the mixing tank transfer pump until the tank contents were fully fluidized.

During the testing, system performance and top surface motion were monitored. Breakthrough was defined as having occurred when the PJM system discharge created an upsurge at the surface of the simulant with a secondary ripple and accompanying horizontal motion. When breakthrough conditions were visually evident, system operations were logged to a data file for approximately 25 pulse cycles. Observations of the top surface motion were recorded, and a sheared fluid sample was rheologically characterized.

C.4.3.2 Data Summary and Results

Experimental data collected during breakthrough tests of the SRNL 1/9-scale 4PJM test stand are presented in this subsection. In support of the design parameter scale law testing program, the primary focus of these tests was determining the PJM nozzle velocity (under scaled constant volume conditions) required to establish a mixing zone that would break through the top surface of the simulant in the test tank. Testing was conducted with a kaolin-bentonite simulant at an initial level of 15.5 inches from the bottom of the tank. The system was operated, and PJM operating parameters were adjusted to incrementally increase the nozzle discharge velocity. Results are listed in Table C.12.

Table C.12. SRNL 4PJM Breakthrough Test—Data Summary

Reference Number	Data File Number	Average Velocity (ft/sec)	Drive Time, t_D (s)	Nominal Velocity (ft/sec)	Aspect Ratio	Breakthrough
S-16	031211R1A	22.8	1.20	25.4	0.90	yes

Rheological characterization of the simulant is presented in Table C.13. Total solids for the simulant were determined to be 25.55 wt%. During this breakthrough test, an upsurge was produced in the center of the test tank with horizontal surface motion but no secondary ripple at a nominal discharge velocity of 23.5 ft/sec (drive time (t_D) of 1.3 sec).

Consequently, the nominal nozzle velocity was increased to 25.4 ft/sec (drive time (t_D) of 1.2 sec). At a nominal velocity of 25.4 ft/sec, the 4PJM system created an upsurge at the top surface of the simulant with a secondary ripple and accompanying horizontal motion. Analysis of the data file determined the average discharge velocity to be 22.8 ft/sec.

Tracer particles were added to the center of the tank with the system discharging at a nominal velocity of 25.4 ft/sec, and the number of pulses to move the particles to the outer wall was recorded. The typical particle migrated to the outer wall with a curved travel path ending toward the shadow zone on the back side of a pulse tube. The tracer particle data summary is presented in Table C.14. A schematic plan view of the tank depicting a typical tracer particle travel path is shown in Figure C.6.

Table C.13. SRNL 4PJM Breakthrough Test with Kaolin-Bentonite Simulant—Rheology Data Summary (Constant Volume Tests—Tank Level 15.5 in., 0.9 aspect ratio)

Ref Number	Data File Number	Bingham Plastic Data[(a)]			Power Law Data[(a)]			Herschel-Bulkley Data[(a)]			
		Yield Stress τ_{BP} (Pa)	Consistency η_{BP} (cP)	Fit Factor R^2	PL Consistency K_{PL} (Pa-s^n)	n	Fit Factor R^2	HB Yield Stress τ_{HB} (Pa)	HB Consistency κ_{HB} (Pa-s^b)	HB Exponent b	Fit Factor R^2
S-16	031211 R1A	18.3	21.46	0.993	5.64	0.271	0.931	16.39	0.094	0.793	0.998
(a) All flow curves were fitted on the down curve, and parameters are the average of two flow curves.											

Table C.14. SRNL 4PJM Breakthrough Test—Tracer Particle Data Summary

Number of PJM Discharge Pulses	Radial Distance from Tank Center (in.)	Radial Distance from Tank Center (%)	
0	0.0	0	← Tank Centerline
1	2.0	23	
2	3.8	44	
3	5.3	61	← PJM Pitch Diameter
4	6.8	79	
15	8.6	100	← Outer Wall

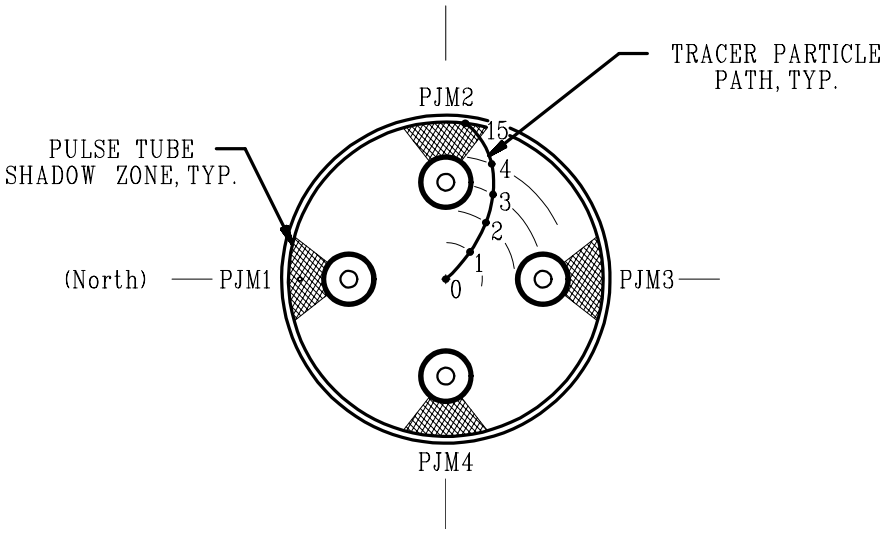

Figure C.6. SRNL 4PJM Test Stand—Schematic of Tracer Particle Path

C.4.4 Velocity Tests

These tests involved operating the PJM system at a discrete nozzle discharge velocity under scaled constant volume conditions while recording the bulk tank level. The intent of this series of tests was to correlate the pulse tube level probe response with changes in the bulk tank level as recorded by laser distance measurement instruments. The discharge velocity of the PJMs was calculated from the change in pulse tube level and change in bulk tank level for comparison.

To record bulk tank level changes, three laser distance measurement instruments were installed above the test tank to measure changes in tank level. These DISTO™ pro^{4}a laser instruments (Art No. 724975) were manufactured by Leica Geosystems AG in Heerbrugg, Switzerland. One instrument was installed above the centerline of the tank, and the other two were installed 2.5 and 1.5 inches from the inside wall in the northeast (far) and southwest (near) quadrants of the tank, respectively. The output from these instruments was recorded to data files during PJM operation.

This testing was performed with the 4PJM array centered in the tank and discharging vertically downward. Velocity tests were conducted at a nominal nozzle discharge velocity of 8 m/s (26.25 ft/sec) and 12 m/s (39.37 ft/sec) using a nominal 5-Pa non-Newtonian kaolin-bentonite simulant and at 8 m/s (26.25 ft/sec), 10 m/s (32.81 ft/sec), and 12 m/s (39.37 ft/sec) using a nominal 30 Pa kaolin-bentonite simulant. Although velocity tests were performed with water, these data files were not analyzed due to the random turbulent upsurge in the center of the test tank with no quantifiable means to measure the affected volume. In addition, the turbulent mixing conditions using water produced ripples and oscillations in the bulk tank level that led to erratic level measurements from the laser instruments. Testing with a non-Newtonian kaolin-bentonite simulant dampened the ripples and oscillations in the bulk tank level. Experimental data defined PJM operations, bulk tank level laser measurements, and simulant rheology.

C.4.4.1 Test Description

This subsection describes a typical velocity test. Kaolin-bentonite simulant was transferred to the mixing tank, agitated with a mixer, and recirculated with the mixing tank transfer pump until the tank contents were fully fluidized.

As previously discussed in the "Data Summary Results" subsections for the cavern and mixing tests, operating parameters were input to the control computer, and the compressed air supply regulator was adjusted to achieve the target velocity and discharge volume. An initial rheology measurement of a baseline sample was taken. Once the system was started, operating parameters were adjusted as needed, and when target conditions were reached system operations and laser distance data were logged to their respective data files for approximately 25 pulse cycles. System performance and top surface motion were monitored throughout the duration of the test. A sample of the sheared simulant solution was collected from the test tank for rheology analysis. Upon completion of the test sequence, the test tank was drained and rinsed clean.

C.4.4.2 Data Summary and Results

Experimental data collected during velocity tests of the SRNL 1/9-scale 4PJM test stand are presented in this subsection. In support of the design parameter scale law testing program, the primary focus of these tests was determining the correlation between the pulse tube level changes measured by the capacitance level probes and the bulk tank level changes measured with laser distance measurement instruments.

Before testing, the tank was water calibrated by filling it with a known mass of water and recording the level read from the scale attached to the clear acrylic tank wall. The pulse tubes were vented to the atmosphere, and water temperature was 24.9°C (76.82°F). Results of this calibration are presented in Table C.15. The tank cross-sectional area is constant for the level range of 6.25 to 25 inches. Water calibration results are plotted in Figures C.7 and C.8. In Figure C.7, the constant cross-sectional area is evident from the linear relationship; this area was determined to be 226 in^2. In Figure C.8, it is shown that the tank required 0.98 gal of simulant per inch of tank level. It was determined that 13.8 gal of simulant was required to fill the test tank to the normal level, 15.5 inches (0.9 aspect ratio).

Velocity testing was conducted with a kaolin-bentonite simulant at an initial tank level of 15.5 inches from the bottom of the tank. The system was operated and PJM operating parameters adjusted to achieve target conditions. Tank level measurements from the three laser instruments were logged to data files. For analysis the data files were converted to Excel spreadsheets. A description of the various column labels used in the Excel spreadsheets is given in Table C.16.

Table C.15. SRNL 4PJM Tank Water Calibration

Weight of Water (kg)	**Tank Water Level** (in.)	**Volume of Water [(a)] at 24.9°C**	
		($in.^3$)	(gal)
17.42	[(b)]	1066.00	4.61
19.44	6.63	1190.02	5.15
37.59	11.56	2300.43	9.96
56.14	16.56	3435.83	14.87

(a) Using weight density of water = 62.247 lb/ft^3.
(b) Water level was below the stainless steel rim of the tank.

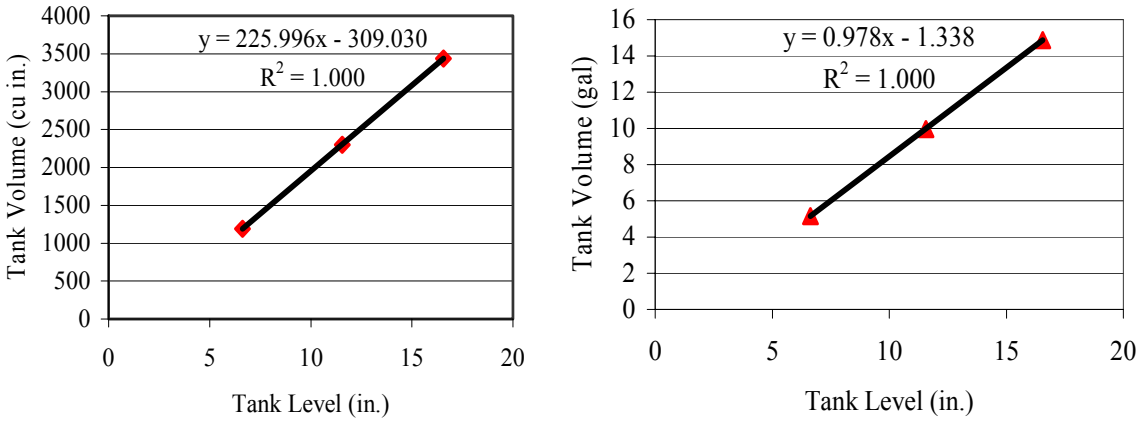

Figure C.7. SRNL 4PJM Tank Level Versus Volume (left, in.^{3}; right, gal)

Table C.16. SRNL 4PJM Laser Measurement Description of the Excel Spreadsheet Columns

Excel Column	Variable Label	Description	Measured Unit
A	Date	Date the experiment was conducted	month/day/year
B	Time	Time when the data were logged	hr:min:sec
C	Time	Time when the data were logged	min:sec
D	Measured value	Level of the liquid in pulse tube 2 (East)	inches

The PJM data files were analyzed to determine the average discharge velocity. The data summary is presented in Table C.17. An Excel spreadsheet corresponding to the data file number listed in this table contains PJM operating conditions and laser measurements. Rheological characterization of the simulant is presented in Table C.18.

The laser measurement data files were analyzed to determine the linear rate of change in tank level during a PJM discharge pulse. Six pulses from each run were analyzed and the average linear rate of change in tank level determined for each laser instrument. Nozzle velocity was determined by multiplying the rate of change in tank level by the ratio of tank area to total nozzle area. Average nozzle velocity measurements were compared by calculating the ratio of average capacitance probe velocity to average laser velocity. The results from this analysis are presented in Tables C.19 through C.23.

Table C.17. SRNL 4PJM Velocity Test—Data Summary

Data File Number	Average Velocity (ft/sec)	Drive Time t_P (s)	Target Nominal Velocity (m/s)	Target Nominal Velocity (ft/sec)	Tank Aspect Ratio	Nominal Target Yield Stress (Pa)
040608R5A	22.12	1.16	8	26.25	0.90	5
040608R6A	26.95	0.77	12	39.37	0.90	5
040610R1A	22.54	1.16	8	26.25	0.90	30
040610R2A	25.31	0.93	10	32.81	0.90	30
040610R3A	27.78	0.77	12	39.37	0.90	30

Table C.18. SRNL 4PJM Velocity Test with Kaolin-Bentonite Simulant—Rheology Data Summary (Constant volume tests—tank level 15.5 in., 0.9 aspect ratio)

Data File Number	Bingham Plastic Data[(a)]			Power Law Data[(a)]			Herschel-Bulkley Data[(a)]			
	Yield Stress τ_{BP} (Pa)	Consistency η_{BP} (cP)	Fit Factor R^2	PL Consistency K_{PL} (Pa-s^n)	n	Fit Factor R^2	HB Yield Stress τ_{HB} (Pa)	HB Consistency κ_{HB} (Pa-s^b)	HB Exponent b	Fit Factor R^2
040608R5A	5.65	20.30	0.993	1.35	0.383	0.987	4.25	0.129	0.715	1.000
040608R6A										
040610R1A	28.1	23.8	0.985	12.6	0.189	0.957	21.1	0.751	0.524	0.998
040610R2A										
040610R3A										

(a) All flow curves were fitted on the down curve and parameters are the average of two flow curves.

Table C.19. SRNL 4PJM Velocity Test—040608R5A Data Summary[(a)]

Pulse Number	Capacitance Probe Nozzle Velocity (ft/sec)					Laser Slope (in./s)			
	PJM1	PJM2	PJM3	PJM4	Average	NE (far)	Center	SW (near)	Average
39	21.22	21.48	22.76	20.92	21.60	0.7758	1.0538	0.7798	0.8698
40	23.16	23.41	23.21	22.82	23.15	0.7684	1.1957	0.7272	0.8971
41	22.92	23.14	22.93	22.62	22.90	0.7786	1.1806	0.7694	0.9095
42	21.81	22.00	21.82	21.49	21.78	0.8051	0.7444	0.7787	0.7761
43	21.47	21.66	21.53	21.19	21.46	0.7978	1.0041	0.5972	0.7997
44	20.99	21.16	21.03	20.76	20.98	0.8020	1.0391	0.7325	0.8579
Average	21.93	22.14	22.21	21.63	**21.98**	0.7880	1.0363	0.7308	0.8517
Average Laser Nozzle Velocity (ft/sec)						21.72	28.57	20.15	**23.48**

(a) Average laser nozzle velocity ratio = 0.936; test run date, June 8, 2004; target velocity, 8 m/s; nominal simulant yield stress, 5 Pa.

Table C.20. SRNL 4PJM Velocity Test—040608R6A Data Summary[(a)]

Pulse Number	**Capacitance Probe Nozzle Velocity** (ft/sec)					**Laser Slope** (in./s)			
	PJM1	PJM2	PJM3	PJM4	Average	NE (far)	Center	SW (near)	Average
35	28.53	26.90	26.82	26.17	27.10	0.5775	2.0943	0.8982	1.1900
36	25.93	26.34	28.43	25.54	26.56	0.8716	1.2860	0.9108	1.0228
37	25.44	25.84	27.92	25.08	26.07	0.7060	1.9743	0.9459	1.2087
38	26.51	26.81	26.75	26.14	26.55	0.6290	2.2125	0.6938	1.1784
39	25.50	25.85	27.86	25.17	26.10	0.4990	1.5892	0.6959	0.9280
40	26.99	27.28	29.30	26.60	27.54	0.7812	1.6567	0.8713	1.1031
Average	26.49	26.50	27.85	25.78	**26.65**	0.6774	1.8022	0.8360	1.1052
Average Laser Nozzle Velocity (ft/sec)						18.67	49.68	23.05	**30.47**
(a) Average laser nozzle velocity ratio = 0.875; test run date, June 8, 2004; target velocity, 12 m/s; nominal simulant yield stress, 5 Pa.									

Table C.21. SRNL 4PJM Velocity Test—040610R1A Data Summary[(a)]

Pulse Number	**Capacitance Probe Nozzle Velocity** (ft/sec)					**Laser Slope** (in./s)			
	PJM1	PJM2	PJM3	PJM4	Average	NE (far)	Center	SW (near)	Average
36	22.78	23.14	23.33	22.52	22.94	0.4891	1.1356	0.5089	0.7112
37	21.94	22.26	22.40	21.66	22.07	0.5995	1.1263	0.4624	0.7294
38	22.61	22.85	23.10	22.34	22.72	0.5750	0.9903	0.5961	0.7205
39	22.61	22.92	23.10	22.33	22.74	0.6633	1.1835	0.6160	0.8209
40	22.67	22.97	22.99	22.34	22.74	0.6862	1.2056	0.5658	0.8192
41	21.85	22.13	22.28	21.56	21.95	0.6426	1.1100	0.5986	0.7837
Average	22.41	22.71	22.86	22.12	**22.53**	0.6093	1.1252	0.5580	0.7641
Average laser nozzle velocity (ft/sec)						16.80	31.02	15.38	**21.07**
(a) Average laser nozzle velocity ratio = 1.069; test run date, June 10, 2004; target velocity, 8 m/s; nominal simulant yield stress, 30 Pa.									

Table C.22. SRNL 4PJM Velocity Test—040610R2A Data Summary[(a)]

Pulse Number	**Capacitance Probe Nozzle Velocity** (ft/sec)					**Laser Slope** (in./s)			
	PJM1	PJM2	PJM3	PJM4	Average	NE (far)	Center	SW (near)	Average
32	26.43	26.80	26.87	26.02	26.53	0.6847	1.4363	0.6713	0.9308
33	24.34	24.71	24.73	24.03	24.45	0.7912	1.6046	0.6565	1.0174
34	25.48	25.89	26.02	25.16	25.64	0.8017	1.3385	0.6712	0.9371
35	24.76	25.07	25.18	24.42	24.86	0.7975	1.1784	0.6674	0.8811
36	26.04	26.40	26.50	25.63	26.14	0.7744	1.4582	0.5961	0.9429
37	26.25	26.63	26.76	25.84	26.37	0.8286	1.3232	0.7301	0.9606
Average	25.55	25.92	26.01	25.18	**25.66**	0.7797	1.3899	0.6654	0.9450
Average Laser Nozzle Velocity (ft/sec)						21.49	38.31	18.34	**26.05**
(a) Average laser nozzle velocity ratio = 0.985; test run date, June 10, 2004; target velocity, 10 m/s; nominal simulant yield stress, 30 Pa.									

Table C.23. SRNL 4PJM Velocity Test—040610R3A Data Summary[(a)]

Pulse Number	**Capacitance Probe Nozzle Velocity** (ft/sec)					**Laser Slope** (in./s)			
	PJM1	PJM2	PJM3	PJM4	Average	NE (far)	Center	SW (near)	Average
33	27.00	27.39	27.74	26.59	27.18	1.1323	1.6957	0.5062	1.1114
34	28.78	29.09	29.60	28.39	28.97	0.8441	1.5111	0.6227	0.9926
35	28.28	28.67	29.21	27.90	28.52	0.5762	1.4004	0.6173	0.8646
36	27.48	27.84	28.20	27.12	27.66	0.8239	1.3104	0.5249	0.8864
37	28.48	26.94	27.33	26.27	27.26	0.9364	1.6627	0.5651	1.0547
38	26.86	27.26	27.73	26.64	27.12	0.8435	1.5447	0.7167	1.0350
Average	27.81	27.86	28.30	27.15	**27.78**	0.8594	1.5208	0.5921	0.9908
Average Laser Nozzle Velocity (ft/sec)						23.69	41.92	16.32	**27.31**
(a) Average laser nozzle velocity ratio = 1.017; test run date, June 10, 2004; target velocity, 12 m/s; nominal simulant yield stress, 30 Pa.									

C.5 Reference

Wilson DA, ML Restivo, HN Guerrero, TJ Steeper, RE Eibling, EK Hansen, TM Jones, and KR Eberl. November 2004. *One-Eighth Scale Pulse Jet Mixer (PJM) - Design Parameters Scale Law Testing.* WSRC-TR-2004-00430 Rev. 0 (SRNL-RPP-2004-00069 Rev. 0), Westinghouse Savannah River Company, Aiken, South Carolina.

Appendix D

Simulant Selection

Appendix D Contents

Figures

Tables

Appendix D

Simulant Selection

Simulant selection for the Waste Treatment Plant (WTP) Pulse Jet Mixer (PJM) Program was accomplished by an aggressive evaluation and testing program. The technical basis for selecting the non-Newtonian simulants is described in WTP-RPT-111, *Non-Newtonian Slurry Simulant Development and Selection for Pulse Jet Mixer Testing* (Poloski et al. 2004). This appendix presents an overview of relevant conclusions from that report and summarizes the target rheological values to which the simulants were designed.

Simulants were required for the two primary stages of the PJM program. The first stage involved verification of a PJM scaling law that would allow results of tests conducted at small scale to be applied to larger-scale systems (the subject of this current report). This step required a transparent simulant so that PJM mixing performance could be observed and measured directly. In this case, shear strength was the dominant rheological parameter affecting PJM performance. For the second stage of the PJM program, scaled prototypic versions of potential full-scale WTP PJM vessels were tested with an opaque particulate simulant designed to match actual pretreated high-level waste (HLW) sludge rheological properties that were identified as significant to PJM performance—yield stress and consistency. The opaque simulant was also used in the scaling tests as an additional means of validating the approach and to gain experience with the simulant prior to the scaled prototype testing.

Because of the scope and magnitude of the PJM test program (many tests with large quantities of simulant at multiple test locations) it was important to identify simulants that were nonhazardous, relatively easy to prepare, rheologically stable, and cost-effective.

D.1 Transparent Simulant Selection

Three transparent simulants were initially evaluated: Laponite RD,[(a)] Carbopol Ulrez-10,[(b)] and xanthan gum (Rhodicare T).[(c)] Cavern heights from single PJM tests in the Applied Process Engineering Laboratory (APEL) test stand at Battelle – Pacific Northwest Division (PNWD) described in Appendix B were found to be much lower for Carbopol and xanthan gum than for Laponite. It was hypothesized that the viscoelastic properties of the Carbopol and xanthan gum significantly altered the turbulent jet structure and, consequently, cavern formation. An additional test with a WTP process simulant was performed to confirm these limitations. Thus, Laponite was chosen as the simulant to confirm PJM scaling laws because it most closely matched the performance of the process simulant. The significant rheological properties for PJM performance during transparent simulant testing are summarized in Table D.1. Target values and actual Laponite simulant values are shown. This table indicates that Laponite meets the objectives for transparent PJM testing.

(a) Southern Clay Products, Inc., Gonzales, Texas, http://www.gelwhite.com/tb/tb21.html
(b) Noveon, Inc., Cleveland, Ohio, http://www.personalcare.noveoninc.com/techdata/pdf/tds225.pdf
(c) Rhodia, Cranbury, New Jersey, http://www.rhodia-hpcii.com/hpcii/product_detail.jsp

Table D.1. Summary of Significant Transparent Simulant Properties for PJM Performance Evaluation

Property	Goal Values	Simulant Values
Shear Strength	30 Pa during normal operation 80 Pa during restart condition	Adjustable in this range based on Laponite and salt concentrations and aging time. With Hanford process water and 16 to 24 hours gel time at ambient temperature, the following correlation applies to 1.5 and 2.5 wt% Laponite. $y = 1.06 x^{4.76}$ (D.1) where y is shear strength (Pa) and x is wt% Laponite, approximately 30 Pa at 1.5 wt% and 80 Pa at 2.5 wt%.

D.2 Transparent Simulant Development

Laponite, selected as the transparent simulant, is a synthetic smectite clay mineral resembling the natural mineral hectorite. Its chemical formula, $Na(Mg,Li)_3Si_4O_{10.5}(OH)_2$, is close to that of hectorite, $Na_{0.3}(Mg,Li)_3Si_4O_{10}(F,OH)_2$, but it has a higher sodium content. Laponite is produced by heat processing of a proprietary gel. Crystallizing the gel produces nanoscale crystals in the form of platelets that are approximately 1 nm thick and 25 nm across, as shown in Figure D.1. When dispersed in water, Laponite forms a transparent slurry. The transparency is a result of the small (colloidal) particle size. The slurry is thixotropic—it flows when subjected to shear stress and is a stable gel at rest. At rest, the positively charged edges of Laponite particles tend to associate themselves with the negatively charged faces, building stable, voluminous aggregates. Under shear stress, the particles are forced to orient themselves perpendicular to the velocity gradient, decreasing their resistance to flow. At rest, electrostatic forces recover the original gel structure. The rheology of Laponite suspensions can be modified by adding ionic salts or organic polymers. For example, adding organic polymers can change the Laponite slurry from a thixotropic to a rheopectic fluid.

As shown in Table D.1, shear strength is the primary design parameter for PJM testing with a transparent simulant. Preliminary rheological testing was done with Laponite to determine the recipe needed to produce shear strength values in the range of 10–100 Pa. Hanford process water was used for this test. The Laponite gel appeared to reach steady-state shear strength in approximately 16 to 24 hours. A plot of shear strength versus concentration for Laponite with a gel time of 16 to 24 hours at ambient temperature is shown in Figure D.2, from which more precise targets could be interpolated. The Laponite recipe chosen for PJM testing based on these data was 1.92 wt% for a target shear strength of approximately 30 Pa.

Many of the PJM test vessels were placed where there was no temperature control and the ambient temperature varied during testing. Because the shear strength samples were in relatively small containers, their temperatures were more readily affected by ambient temperature variations than the contents of the adjacent, larger PJM vessels. Based on data from Speers et al. (1987) on drilling fluids, the potential variation of shear strength due to small temperature differences was expected to be small; however, a sample of Laponite was taken and homogenized, then placed in a water bath at controlled temperature. At various gel times (0 to 50 hours after homogenization), a sample was taken and analyzed for shear strength. This procedure was repeated at three temperatures, 15°, 25°, and 35°C. Results from these runs are shown in Figure D.3. Based on previous experience with shear strength measurements, an error of ±10% was used for the error bars. When these data were fit to a first-order rate model developed by

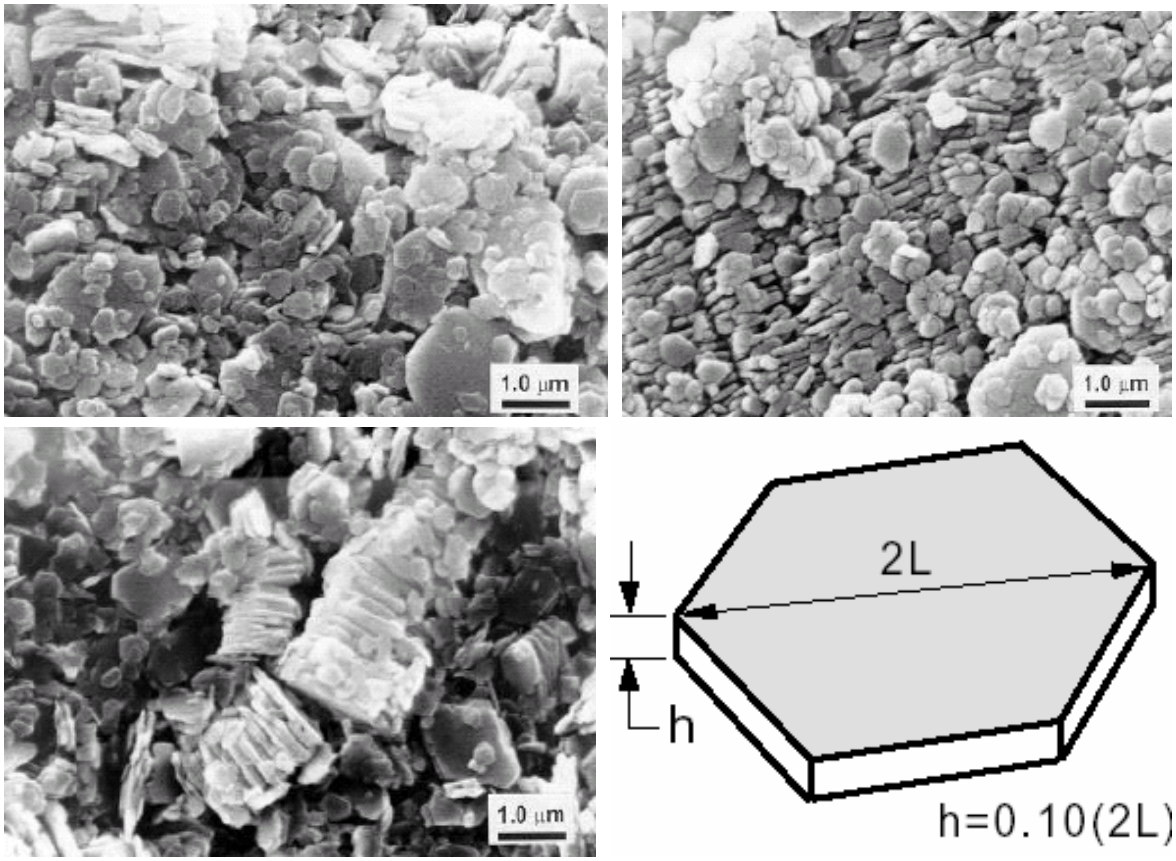

Figure D.1. Micrographs of Laponite Particles

Speers et al. (1987), results indicated that the material did approach steady-state shear strength values by the 16–24 hour gel time with minimal impact due to temperature differences between 15° and 35°C, which exceeded the maximum expected temperature variation during testing.

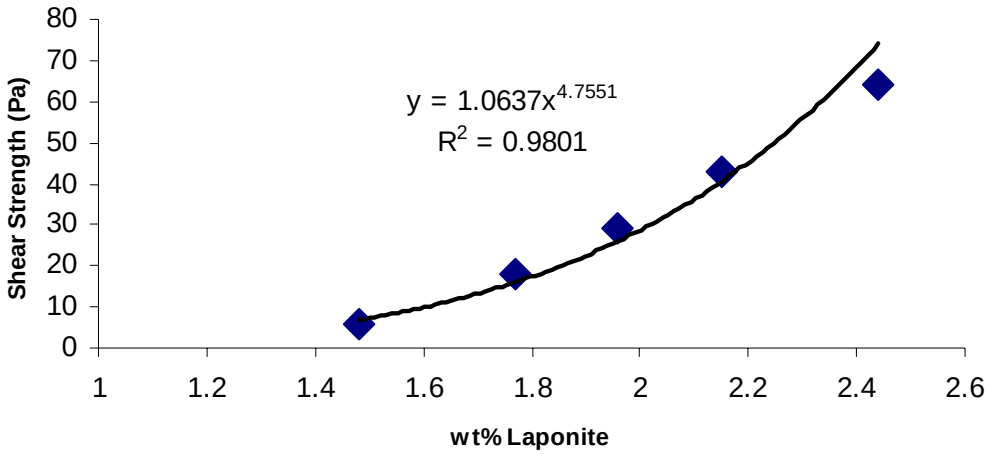

Figure D.2. Laponite RD Shear Strength as a Function of Concentration in Hanford Process Water at Ambient Temperature with a Gel Time of 16–24 hours

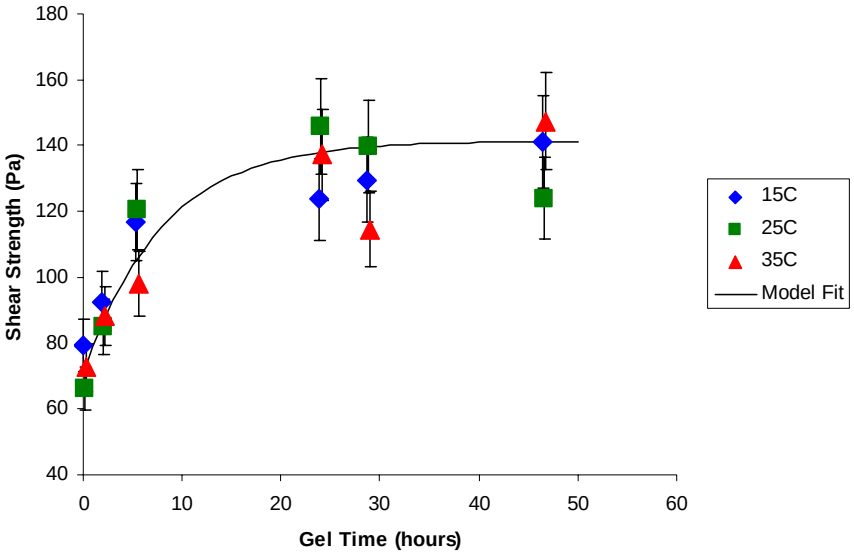

Figure D.3. Laponite Shear Strength as a Function of Temperature and Gel Time

D.3 HLW Sludge Simulant Selection

For the second stage of testing, scaled prototypic versions of potential full-scale WTP PJM vessels were tested with a simulant designed to match actual pretreated HLW sludge rheological properties identified as significant to PJM performance. The simulant was based on a previous Hanford tank retrieval simulant consisting of a mixture of kaolin clay (EPK Feldspar Pulverized)[(a)] and bentonite clay (WYO-Ben Big Horn CH-200)[(b)] in Hanford process water. The recipe calls for a composite of 80% kaolin and 20% bentonite mixed with Hanford water to a loading of approximately 27 wt%. Unlike the transparent Laponite simulant, this clay-based simulant is opaque. A summary of the rheological properties significant to PJM performance during kaolin-bentonite simulant testing is given in Table D.2.

Table D.2. Significant Clay Simulant Properties for PJM Performance and Goal Values

Property	Goal Values	Simulant Values
Density	1200 kg/m^3	1180 kg/m^3 at 27 wt%
Bingham Consistency	30 cP	Adjustable; with Hanford process water at ambient temperature, the following correlation applies between 23 and 27 wt% kaolin-bentonite: $y = 0.005\ x^{2.61}$ (D.2) where y is the consistency (cP) and x is the wt% kaolin-bentonite clay, approximately 30 cP at 27 wt%.
Bingham Yield Stress	30 Pa	Adjustable; with Hanford process water at ambient temperature, the following correlation applies between 23 and 27 wt% kaolin-bentonite: $y = 2.33\times10^{-5}\ x^{4.27}$ (D.3) where y is the yield stress (Pa) and x is the wt% kaolin-bentonite clay, approximately 30 Pa at 27 wt%

(a) Feldspar Corporation, Atlanta, Georgia, http://www.zemex.com/minerals/epk.html
(b) Wyo-Ben, Inc., Billings, Montana, http://www.wyoben.com/z-downloads/product_sheets/bighorn_ch200.pdf

Goal values and actual kaolin-bentonite simulant values are also shown in the table. Data presented in Table D.2 indicates that kaolin-bentonite simulant meets the objectives for PJM testing.

D4 High-Level Waste Sludge Simulant Development

Clay suspensions are used widely in industry and commonly exhibit a shear-thinning pseudoplastic flow. Brownian motion, van der Waals forces, and electrostatic forces determine the interactions among clay particles. The main mode of particle interaction is flocculation, or formation of agglomerates. The agglomerates organize themselves into a three-dimensional structure or coagulated suspension that resists flow. When shear is placed on the structure, it breaks down and the suspension flows. As shear increases agglomerate size decreases, resulting in diminishing viscosity—characteristic of a pseudoplastic fluid. In this manner, interaction between the agglomerates contributes to energy dissipation during viscous flow.

Rassat et al. (2003) developed a simulant for Hanford tank retrieval studies. This was a mixture of 80% kaolin (EPK Feldspar Pulverized) and 20% bentonite (WYO-Ben Big Horn CH-200) powder mixed to various solids concentrations in Hanford process water. This recipe produced a simulant with Bingham plastic properties near the goal of 30 Pa yield stress and 30 cP consistency. The simulant appeared to develop shear strength in the range of 10 to 100 Pa. These properties appeared to occur at a solids loading in the 20 to 30 wt% range.

Consequently, several laboratory-scale samples were prepared using this recipe at various solids concentrations. Flow curves were measured for each sample and a correlation between Bingham consistency, shown in Figure D.4, and Bingham yield stress, shown in Figure D.5, was developed. To achieve the target 30-Pa yield stress, the recipe called for 27 wt% kaolin-bentonite clay. The density of the simulant at 27 wt% is approximately 1180 kg/m^3.

Although not the primary design parameter for an opaque simulant, the shear strength behavior of the kaolin-bentonite simulant was investigated, similar to Laponite. Initial shear-strength-versus-gel-time curves, shown in Figure D.6, indicate that the shear strength of kaolin-bentonite clay developed over a longer period of time than Laponite.

To investigate the effect of temperature on shear strength, a sample of kaolin-bentonite simulant was taken and homogenized, then placed in a water bath at controlled temperature. At various gel times (0 to 100 hr after homogenization), the sample was analyzed for shear strength. This procedure was repeated at 15°, 25°, and 35°C. Results are shown in Figure D.7. Based on previous experience with shear strength measurements, an error of ±10% was used for the error bars. When the data were fit to a first-order rate model applied by Speers et al. (1987) results indicated temperature had a significant effect on shear strength. The shear strength development appeared to increase as temperature increased from 15° to 35°C. If shear strength measurements are required during PJM testing with the kaolin-bentonite samples, steps should be taken to ensure the temperature of the samples is close to the temperature of the bulk vessel.

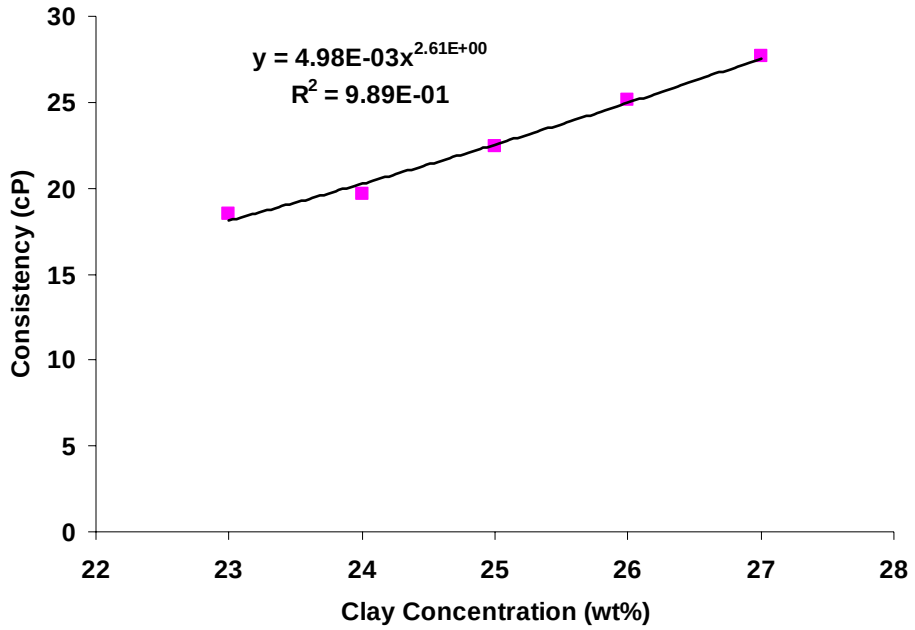

Figure D.4. Correlation Between Bingham Consistency and Kaolin-Bentonite Concentration at Ambient Temperature

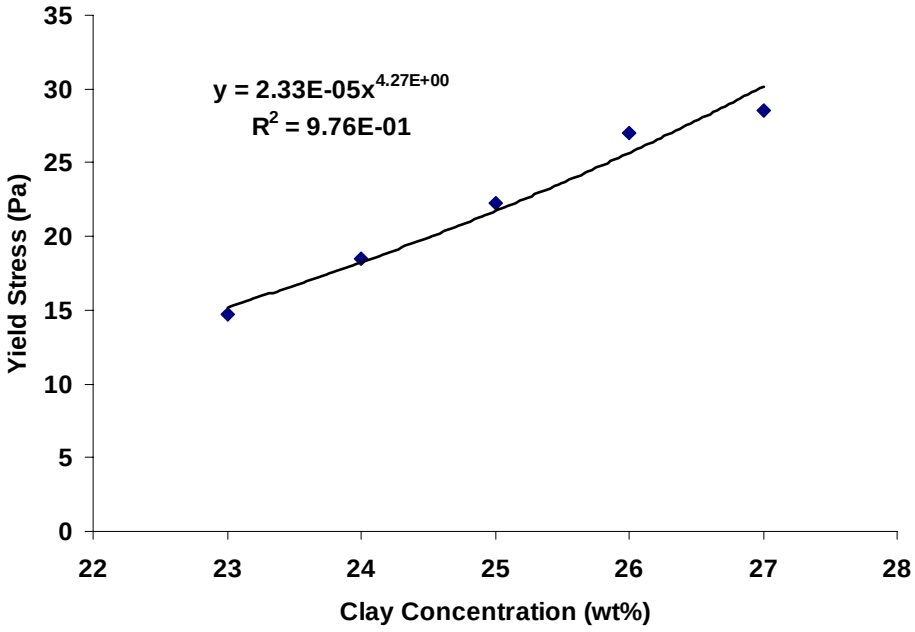

Figure D.5. Correlation Between Bingham Yield Stress and Kaolin-Bentonite Concentration at Ambient Temperature

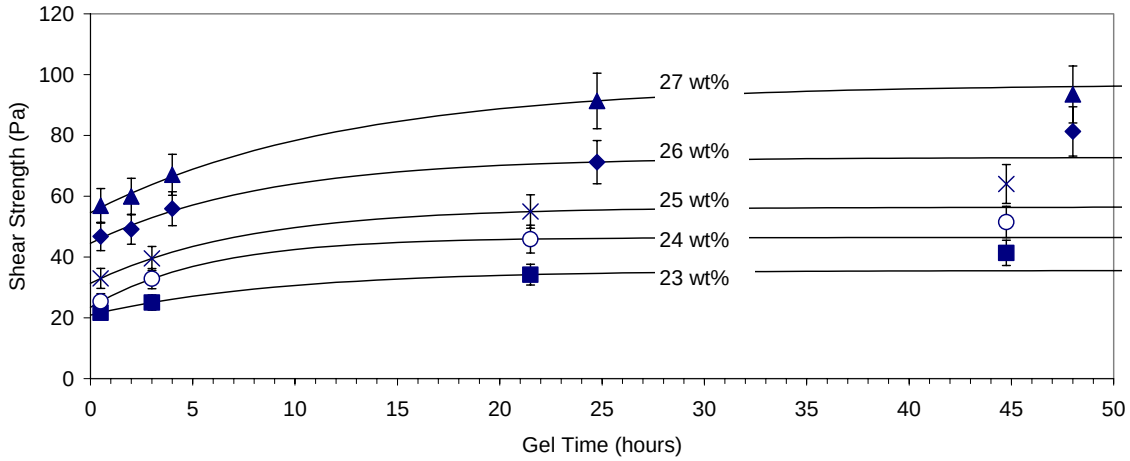

Figure D.6. Shear Strength as a Function of Gel Time for Kaolin-Bentonite Simulant at Various Solids Concentrations at Ambient Temperature

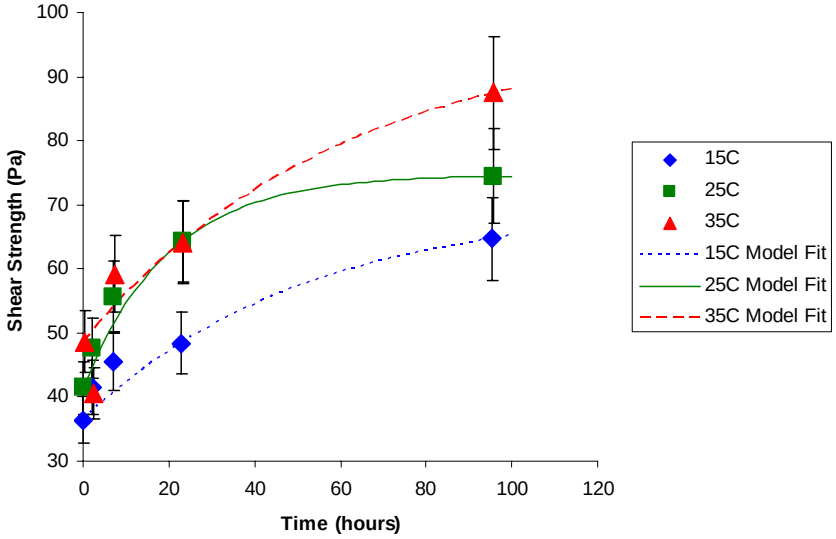

Figure D.7. Kaolin-Bentonite Shear Strength as a Function of Temperature and Gel Time

D.5 References

Poloski AP, PA Meyer, LK Jagoda, and PR Hrma. 2004. *Non-Newtonian Slurry Simulant Development and Selection for Pulse Jet Mixer Testing*. PNWD-3495, Battelle – Pacific Northwest Division, Richland, Washington.

Rassat SD, LM Bagaasen, LA Mahoney, RL Russell, DD Caldwell, and DP Mendoza. 2003. *Physical and Liquid Chemical Simulant Formulations for Transuranic Wastes in Hanford Single-Shell Tanks.* PNNL-14333, Pacific Northwest National Laboratory, Richland Washington.

Speers RA, KR Holme, MA Tung, and WT Williamson. 1987. "Drilling fluid shear stress overshoot behavior." *Rheologica Acta*, Vol. 26, pp. 447-452.

Distribution

No. of Copies

OFFSITE

2 Savannah River National Laboratory

Richard Edwards
Savannah River National Laboratory
Westinghouse SA
Aiken, SC 29808-0001

David A. Wilson
Savannah River National Laboratory
Westinghouse SA
Aiken, SC 29808-0001

No. of Copies

ONSITE

18 Battelle—Pacific Northwest Division

J. A. Bamberger	K7-15
J. M. Bates	K7-15
J. R. Bontha	K6-24
C. W. Enderlin	K7-15
J. A. Fort	K7-15
M. A. Friedrich	K5-16
M. A. Gerber	K2-12
D. E. Kurath	P7-28
P. A. Meyer	K7-15
F. Nigl	K7-15
A. P. Poloski	P7-25
H. D. Smith	K6-24
D. E. Wallace	K6-24
S. T. Yokuda	K7-15
Project Office (2)	P7-28
Information Release (2)	K1-06

5 Bechtel National, Inc.

H. Abodishish	H4-02
S. M. Barnes	H4-02
J. F. Doyle (2)	H4-02
G. L. Smith	H4-02